



UNIWERSYTET ŚLĄSKI
W KATOWICACH

Wydział Nauk Ścisłych i Technicznych
Instytut Chemii

mgr NATALIA SOSZKA

**WPLYW ODDZIAŁYWAŃ MIĘDZYCZĄSTECZKOWYCH NA ZACHOWANIE
ALKOHOLI MONOHYDROKSYLOWYCH W UKŁADACH LITYCH I
MATERIAŁACH NANOPOROWATYCH**

PRACA DOKTORSKA

PROMOTORZY:

dr hab. Barbara Hachuła, prof. UŚ

dr hab. Magdalena Tarnacka, prof. UŚ

Chorzów 2024

*Chciałabym serdecznie podziękować
dr hab. Barbarze Hachule, prof. UŚ
i dr hab. Magdalenie Tarnackiej, prof. UŚ
za wskazanie interesującej tematyki badawczej,
opiekę naukową, ogrom życzliwości, cierpliwości,
poświęcony czas i wsparcie merytoryczne.*

*Panu prof. dr hab. Kamilowi Kamińskiemu –
za okazane wsparcie merytoryczne.*

*Składam serdeczne podziękowania
dr hab. Romanowi Wrzalikowi, prof. UŚ
za nieustanną pomoc, poświęcony czas i wsparcie.*

*Koleżankom z pokoju E/1/4,
dziękuję za każdy wspólnie spędzony dzień,
wiarę we mnie, podnoszenie na duchu
oraz za każdą przeprowadzoną rozmowę*

*Pracę dedykuję Kamilowi,
wiem, że patrzysz z góry i jesteś ze mnie dumny.*



N A R O D O W E C E N T R U M N A U K I

Badania przeprowadzone na potrzeby niniejszej pracy doktorskiej finansowane były w ramach projektu Narodowego Centrum Nauki pt. *„Korelacja między ograniczoną rozmiarowością i oddziaływaniami z powierzchnią i ich wpływ na dynamikę molekularną materiałów ograniczonych przestrzennie dwuwymiarowo. Czy rozmiar zastosowanego ograniczenia przestrzennego ma znaczenie?”* (nr decyzji: 2019/33/B/ST3/00500), którego kierownikiem była dr hab. Magdalena Tarnacka, prof. UŚ

Spis treści

1. WSTĘP.....	6
2. OMÓWIENIE OTRZYMANYCH WYNIKÓW	18
2.1 Jak wprowadzenie do struktury molekularnej alkoholu grup funkcyjnych mogących tworzyć dodatkowe oddziaływania, wpłynie na zachowanie asocjacyjne alkoholi?.....	18
2.2 Jaki wpływ na zdolności asocjacyjne alkoholi ma inkorporacja do układów ograniczonych przestrzennie?	27
2.3. Czy alkohole fenyłowe są w stanie tworzyć nieodwracalnie zaadsorbowaną warstwę molekuł w ograniczeniu przestrzennym?	34
3. PODSUMOWANIE	38
4. TREŚCI ARTYKUŁÓW STANOWIĄCYCH PODSTAWĘ ROZPRAWY DOKTORSKIEJ WRAZ Z OŚWIADCZENIAMI WSPÓŁAUTORÓW.....	41
5. BIBLIOGRAFIA	113

1. WSTĘP

Alkohole to klasa związków organicznych, które stoją w centrum zainteresowania wielu dziedzin nauki, ze względu na ich niezwykle właściwości fizykochemiczne, a także z powodu dużego znaczenia w przemyśle. Wspomniane własności są wynikiem obecności w ich strukturze grupy hydroksylowej (-OH), która połączona jest z atomem węgla o hybrydyzacji sp^3 . Jej obecność sprawia, iż alkohole cechują się możliwością tworzenia specyficznych oddziaływań międzycząsteczkowych, a mianowicie – wiązań wodorowych.

Wiązanie wodorowe to rodzaj oddziaływania międzycząsteczkowego, w którym atom wodoru grupy protonodonorowej oddziałuje z wolną parą elektronową atomu akceptora. Możliwość tworzenia oddziaływania wynika z faktu, iż wiązanie kowalencyjne grupy protonodonorowej jest spolaryzowane – atom wodoru staje się centrum ładunku dodatniego, w związku z czym możliwe jest „przyciąganie” elektronów grupy akceptorowej (**Rysunek 1**).



Rysunek 1. Schemat wiązania wodorowego.

Wiązanie wodorowe jest typem specyficznego oddziaływania, co wynika z pewnych uwarunkowań, m.in. wymienionych wcześniej warunków polaryzacji wiązania kowalencyjnego grupy X-H oraz dysponowania wolną parą elektronową przez atom Y. Dodatkowo konieczne jest, aby atomy X i Y posiadały silnie elektroujemny charakter, dlatego rolę donorów protonów odgrywają najczęściej grupy -OH, -NH, -SH, czy -XH (X = atom fluorowca), a akceptorami protonu są atomy takie jak: F, O, N, S, X, a także molekuly posiadające w swojej strukturze wiązania wielokrotne (podwójne, potrójne, czy układy aromatyczne). Co więcej, atomy X i Y muszą posiadać małe promienie kowalencyjne, gdyż konieczne jest zbliżenie się do siebie grupy X-H i atomu Y na dostatecznie małe odległości.

Istnieje wiele sposobów klasyfikacji omawianych oddziaływań. Rozpatrując różnice w elektroujemnościach atomów X i Y, wiązania wodorowe możemy podzielić na symetryczne lub asymetryczne (w zależności od odpowiednio braku lub występowania różnic w elektroujemnościach atomów) [1]. Dodatkowo, w zależności od tego, z iloma atomami połączony jest atom wodoru wyróżniamy wiązania dwucentrowe, trzycentrowe, a nawet czterocentrowe [2]. Natomiast jednym z najbardziej popularnych i najczęściej stosowanych kryterium jest siła tworzącego się wiązania wodorowego. Możemy wyróżnić zatem (*i*) silne

wiązania wodorowe, ich energia jest większa niż 15 kcal mol^{-1} , (ii) oddziaływania średniej mocy – w zakresie energii $4\text{--}15 \text{ kcal mol}^{-1}$, oraz (iii) słabe wiązania wodorowe o sile mniejszej niż 4 kcal mol^{-1} [3]. Specyficzność wiązania wodorowego może prowadzić do zmian występujących w wiązaniu X-H, co przejawiać się będzie odmienną charakterystyką spektralną. Z tego powodu wiązania te dzielimy na konwencjonalne wiązania wodorowe, w których obserwuje się przesunięcie częstości drgań rozciągających grupy X-H w kierunku niższych wartości liczb falowych, tzw. *red shift*. Efekt ten wynika z wydłużenia i osłabienia wiązania i dotyczy klasycznych wiązań wodorowych. Do odwrotnej sytuacji dochodzi w przypadku niekonwencjonalnych wiązań wodorowych, gdzie częstość pasma pochodzącego od drgań rozciągających X-H przesuwa się ku wyższym wartościom (*blue shift*) [4].

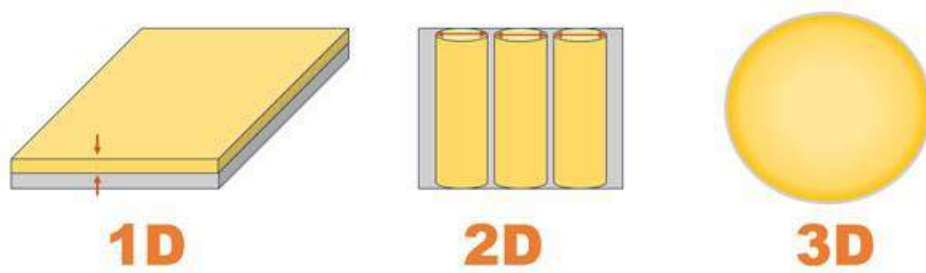
Możliwość tworzenia wiązań wodorowych przez cząsteczki alkoholu sprawia, iż związki te ulegają procesowi asocjacji, w którym molekuly łączą się ze sobą, tworząc asocjaty/agregaty. Należy wspomnieć, że alkohole nie są jedynymi związkami asocjacyjnymi. Zjawisku temu ulega także m.in. woda, kwasy karboksylowe, aminy, czy amidy. Na sam proces asocjacji wpływ może mieć wiele czynników, np. struktura molekularna związków asocjujących [5–8], temperatura [9–12], ciśnienie [12–16] czy dodatek rozpuszczalników [17–19]. Natomiast alkohole są interesującym przykładem, gdyż możemy je rozpatrywać jako molekuly amfifilowe posiadające polarną (grupa hydroksylowa, -OH) i niepolarną (łańcuch alifatyczny, układ aromatyczny) część w swoich strukturach. Dlatego też, modyfikacja ich struktury polegająca na zmianie długości łańcucha alifatycznego, liczby czy położenia grup hydroksylowych, przyłączenia innych grup funkcyjnych prowadzi do zmian w tworzących się oddziaływaniach specyficznych. Jako przykład mogą posłużyć tu długołańcuchowe alkohole, w których tworzące się oddziaływania dyspersyjne mogą „konkurować” z wiązaniami wodorowymi [20]. Modyfikacja struktury cząsteczek powoduje, że powstające asocjaty przyjmują różne kształty i rozmiary. Związane wodorowo agregaty mogą tworzyć struktury łańcuchowe, micelowe [21–23], a nawet, mogą występować w postaci zamkniętych pętli, czy pierścieni [24]. Dodatkowo, zmieniając rzędowość alkoholu (np. w przypadku butanoli) zauważalny jest spadek stopnia asocjacji spowodowany rosnącą zawadą steryczną [25]. Podobny efekt obserwowalny jest dla halogenowych pochodnych etanolu, gdzie podstawienie w strukturze alkoholu atomów wodoru atomami chloru powoduje mniejszą zdolność do łączenia się cząsteczek w agregaty [26]. Ponadto, na zmniejszenie stopnia asocjacji wpływa nie tylko ilość przyłączonych atomów halogenów, ale także, jak wskazują ostatnie badania spektroskopowe, to, który fluorowiec został przyłączony [27].

Interesującym wydaje się także być badanie jak na zachowanie asocjacyjne alkoholi będzie wpływać możliwość tworzenia przez molekuly oddziaływań innych niż wiązania wodorowe. Wśród oddziaływań międzycząsteczkowych, poza wiązaniami wodorowymi, wyróżniamy także oddziaływania uniwersalne (van der Waalsa), związane z istnieniem trwałych momentów dipolowych molekuł, jak i z ich polaryzowalnością. Wyróżnia się więc oddziaływania typu *i*) dipol – dipol lub dipol – ładunek (oddziaływania orientacyjne), *ii*) trwałych momentów dipolowych z indukowanymi momentami dipolowymi (oddziaływania polaryzacyjne) oraz *iii*) chwilowych (nietrwałych) momentów dipolowych, tj. oddziaływania typu dipol indukowany – dipol indukowany (oddziaływania dyspersyjne) [28,29]. W przypadku prostych alkoholi monohydroksylowych, wzrost długości łańcucha alifatycznego powoduje osłabienie procesu asocjacji, co związane jest z rosnącym znaczeniem oddziaływań dyspersyjnych [20]. Co więcej, jak pokazują badania alkoholi rozpuszczonych w rozpuszczalnikach niepolarnych, przy niskich stężeniach alkoholi (gdy wartość ułamka molowego alkoholu była mniejsza niż 0,05), w układach dominują oddziaływania dyspersyjne, a alkohole występują w postaci monomerów [30]. Warto także wspomnieć o związkach aromatycznych, które mogą tworzyć oddziaływania dyspersyjne pomiędzy elektronami π , tzw. oddziaływania π -stacking, które nierzadko stoją za ich zdolnością tych układów do samoorganizacji [31]. Ciekawych obserwacji dostarczyły badania alkoholowego analogu naftalenu – 1-naftolu. Pierwsze eksperymenty wskazały na łączenie się molekuł poprzez wiązania wodorowe oraz π -stackingi. Natomiast, najnowsze badania sugerują, iż dimery 1-naftolu tworzą się poprzez częściowe nakładanie się na siebie pierścieni aromatycznych, co prowadzi do tworzenia oddziaływań typu π - π , ale nie obserwuje się wiązań wodorowych pomiędzy jednostkami [32].

W kontekście wspomnianych wyników badań intrygujące wydają się więc alkohole aromatyczne, które posiadają w swojej strukturze zarówno grupę hydroksylową jak i pierścień aromatyczny, co skutkuje możliwością obserwowania mnogości oddziaływań międzycząsteczkowych. Co zaskakujące, ta grupa związków posiada stosunkowo ubogą literaturę w odniesieniu do ich zdolności asocjacyjnych, która dodatkowo, udziela sprzecznych informacji na temat uporządkowania strukturalnego, tzn. badania dielektryczne wskazują albo na brak agregacji cząsteczek alkoholu [33], lub na możliwość ich tworzenia [34–36]. Dlatego też w niniejszej pracy doktorskiej głównie skupiono się na scharakteryzowaniu zachowania asocjacyjnego prostych alkoholi monohydroksylowych zawierających grupę fenylową, (nazwane później alkoholami fenyłowymi) wykorzystując szereg metod badawczych.

Obecnie, większość badań procesu asocjacji alkoholi przeprowadza się dla materiałów litych (ang. *bulk*). Natomiast na tworzące się oddziaływania i zachowanie asocjacyjne substancji można także wpływać stosując geometryczne ograniczenie przestrzenne. Badania z wykorzystaniem takich układów pozwalają na rozszerzenie dotychczasowej wiedzy na temat zjawiska asocjacji.

Materiały ograniczone przestrzennie to układy o nanometrowych rozmiarach, i często unikalnych właściwościach. Znajdują one zastosowanie między innymi w przemyśle farmaceutycznym jako nowe nośniki leków [37–39], czy w układach elektronicznych [40,41]. Jednym z kluczowych czynników charakteryzujących ograniczenie przestrzenne jest geometria układów, dlatego też dzielimy je na układy ograniczone jedno- (1D), dwu- (2D) lub trójwymiarowo (3D) (**Rysunek 2**).

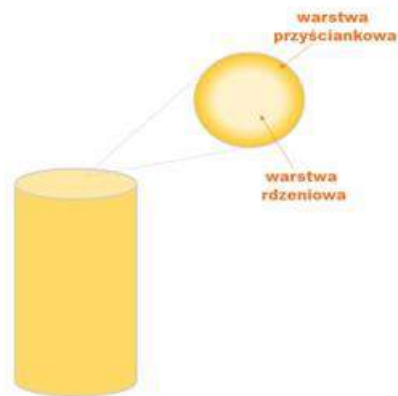


Rysunek 2. Podział ograniczenia przestrzennego ze względu na jego geometrię.

W pierwszym przypadku, substancja ograniczona jest w jednym kierunku, z . Typowym przykładem ograniczenia 1D są tzw. cienkie warstwy (ang. *thin films*). W układach ograniczonych przestrzennie dwuwymiarowo, badany materiał ograniczony jest w dwóch kierunkach, x i y , m.in. poprzez wprowadzenie substancji do membran posiadających w swoich strukturach pory o nanometrycznych średnicach. Gdy materiał jest ograniczony w trzech kierunkach, x , y i z , mówimy o ograniczeniu przestrzennym trójwymiarowym, którego przykładem mogą być nanocząstki.

Ważnym aspektem ograniczenia przestrzennego jest jego wpływ na zachowanie substancji, co rozpatruje się w oparciu o dwa główne efekty [42–51]. Pierwszym z nich jest rozmiarowość (ang. *finite size*), czyli wspomniana wcześniej geometria układu ograniczającego, a także, w przypadku nanoukładów 2D, średnica nanoporów. Drugim ważnym czynnikiem są efekty powierzchniowe (ang. *surface effects*), wynikające z możliwości tworzenia się oddziaływań pomiędzy elementem ograniczającym a „uwięzionym” materiałem. Warto nadmienić, że w przypadku mezoporów, specyfika układu (ścianki matrycy) zmienia dynamikę infiltrowanej

substancji, staje się ona silnie niejednorodna, co prowadzi do powstania dwóch warstw molekuł, zgodnie z modelem dwuwarstwowym [52] (**Rysunek 3**).



Rysunek 3. Schematyczne przedstawienie modelu dwóch warstw w membranie krzemowej.

Molekuły zlokalizowane w centrum kanału, stanowią tzw. warstwę rdzenia (ang. *core layer*). Są to cząsteczki, które oddziałują ze sobą i charakteryzują się szybszą dynamiką. Natomiast frakcja molekuł znajdujących się w bezpośrednim sąsiedztwie ścianek matrycy, czyli warstwa przysciankowa (ang. *interfacial layer*), ze względu na możliwość występowania oddziaływań substancja – por, posiada zmniejszoną mobilność. Słuszność tego konceptu potwierdza występowanie zjawiska podwójnego zeszklenia. Podczas gdy materiał lity posiada przejście szkliste w temperaturze T_g , wprowadzenie go do matrycy porowatej powoduje, że obserwujemy zjawisko zeszklenia w temperaturach poniżej i powyżej T_g materiału litego ($T_{g\ bulk}$). W temperaturze niższej niż $T_{g\ bulk}$ obserwuje się witrifikację molekuł znajdujących się w rdzeniu pora ($T_{g\ core}$), natomiast powyżej $T_{g\ bulk}$ dochodzi do zeszklenia cząsteczek związanych w powierzchnią ścianek pora ($T_{g\ interfacial}$) [52]. Co więcej, badania przeprowadzone dla polimerów w warunkach jednowymiarowego ograniczenia wykazały interesujące zjawisko, tj. T_g może wzrastać lub maleć w porównaniu do $T_{g\ bulk}$, a nawet zaobserwować można brak wpływu ograniczenia na tę temperaturę [53–60]. Fenomen ten dyskutowano w kontekście zastosowanego substratu lub oddziaływań typu polimer – powierzchnia substratu.

Interesującym przypadkiem cieczy asocjującej, której właściwości drastycznie zmieniają się w ograniczeniu przestrzennym jest woda. Ogólnie, „zamknięcie” substancji w porach silnie wpływa na przejścia fazowe. W kontekście wody, jej infiltracja do krzemionkowych matryc nanoporowatych umożliwiła obniżenie temperatury topnienia nawet o 50 K, w zależności od

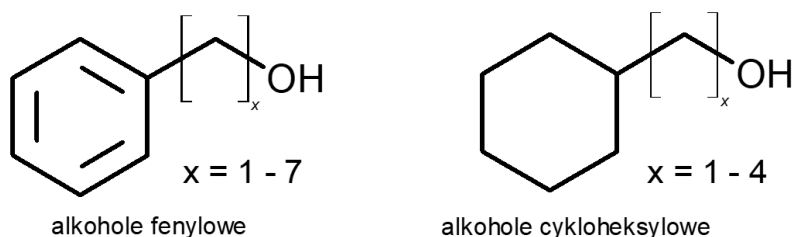
średnicy zastosowanych porów. W związku z tym, woda może być termodynamicznie stabilna znacznie poniżej temperatury nukleacji ($T = 231 \text{ K}$) [61], a tym samym, pory mogą zostać wykorzystane jako „próbówki” do badania właściwości cieczy przechłodzonej. Przy dalszym obniżaniu temperatury obserwowano krystalizację wody. Co ciekawe, w ograniczeniu przestrzennym woda krystalizuje w układzie regularnym, inaczej niż w warunkach normalnego ciśnienia, gdzie krystalizacja zachodzi w układzie heksagonalnym [62]. W przypadku wody zaobserwowano także zjawisko tworzenia się dwóch frakcji molekuł. Struktura i dynamika molekuł warstwy rdzeniowej jest podobna do makroskopowej wody, natomiast cząsteczki znajdujące się w pobliżu ścianek materiału ograniczającego, okazały się być bardzo zniekształcone pod względem tworzącej się sieci wiązań wodorowych, a zatem zostało naruszone ich uporządkowanie strukturalne. Poza tym, dynamika frakcji przyściankowej silnie zależała od modyfikacji powierzchni materiału; w hydrofilowych porach była ona wolniejsza w porównaniu do tej z bardziej hydrofobowymi membranami czy molekułami warstwy rdzeniowej. Zauważalna była nawet całkowita immobilizacja frakcji przyściankowej, podczas gdy frakcja cząsteczek rdzenia wciąż wykazywała dynamikę podobną do materiału litego [63].

Kolejną interesującą grupą związków są alkohole, które w odróżnieniu od wody, w niskich temperaturach nie ulegają krystalizacji, a wykazują zjawisko przejścia szklistego. Jedną z pierwszych prac poświęconych badaniom alkoholi w ograniczeniu przestrzennym skupiła się zachowaniu *tert*-butanolu w matrycach krzemowych typu MCM-41 z użyciem techniki rozpraszania neutronów. Zaobserwowano, iż tzw. *pre-pik* (ang. *pre-peak*) powiązany z uporządkowaniem średniego zasięgu (a zatem można sugerować, że związany także z pewną strukturą supramolekularną) jest nieobecny na dyfraktogramach alkoholu ograniczonego przestrzennie. Świadczyło to o zahamowaniu procesu asocjacji w nanoskali [64]. Jednakże, dalsze badania strukturalne wsparte symulacjami komputerowymi wskazały, że *tert*-butanol ulega asocjacji w ograniczeniu przestrzennym, a brak obecności *pre-piku* na dyfraktogramach może wynikać z efektu objętości wyłączonej lub ze wzajemnych korelacji matryca – ciecz. Co więcej, oddziaływania por – alkohol zauważalne były także w membranach o charakterze hydrofobowym [65,66]. Innym, intensywnie badanym alkoholem, jest 2-etylo-1-heksanol. Uzyskane dane dielektryczne dla alkoholu wprowadzonego do membran porowatych ujawniły spadek amplitudy procesu Debye’a w ograniczeniu przestrzennym w odniesieniu do substancji litej, co zostało zinterpretowane jako zmiana w stopniu asocjacji. Dodatkowo, zauważono zmiany w strukturze molekularnej, tzn. naruszone zostało dalekozasięgowe upakowanie cząsteczek w wyniku reorganizowania się molekuł oraz interakcji z otoczeniem [67]. Intrygujące są także wyniki badań przeprowadzonych dla alkoholi monohydroksylowych

różniących się położeniem grupy hydroksylowej w strukturze związku (1-propanol, 2-etylo-1-heksanol oraz 4-metylo-3-heptanol), opisujące wpływ ograniczenia przestrzennego na dynamikę wspomnianych związków. Dla każdego z nich obserwowano przyspieszenie procesów relaksacyjnych, niezależnie od struktury. Co więcej, ograniczenie przestrzenne wpływało na liczbę molekuł tworzących struktury supramolekularną, tj. w membranach porowatych struktury te składały się z mniejszej liczby cząsteczek. Oszacowując temperatury zeszklenia dla otrzymanych związków, największy spadek zauważalny był dla 4-metylo-3-heptanolu (zmiana o 23 K w stosunku do substancji litej). Tym samym stwierdzono, że ograniczenie przestrzenne ma największy wpływ na 4-metylo-3-heptanol i powiązано to ze strukturą tworzących się asocjatyw, bowiem w tym związku dominują struktury pierścieniowe (ang. *ring-like*) [68]. Warto również wspomnieć o badaniach przeprowadzonych dla serii alkoholi fenylowych wprowadzonych do porów glinowych. Są to jak dotąd jedyne badania poświęcone tym związkom wprowadzonym do mezoporów. W eksperymencie wykorzystano membrany o stałych średnicach porów ($d = 10$ oraz 40 nm) i tzw. modulowane pory o zmiennej średnicy porów ($d = 19, 28$ nm). W toku badań zaobserwowano, że membrany te wpływają na ciecze w odmienny sposób. Powszechnie opisywane dla infiltrowanych cieczy zjawisko podwójnego przejścia szklistego nie było wykrywalne w przypadku alkoholi w modulowanych matrycach, a tym samym dynamika dominującego procesu relaksacyjnego była podobna do tej obserwowanej w materiale litym. Co więcej, zarówno dla inkorporowanych jak i litych próbek widma dielektryczne zdominowane były przez jeden wyraźny proces relaksacji, który w przypadku materiałów litych przybierał charakter relaksacji Debye'a. Nie obserwowano żadnych dodatkowych procesów relaksacyjnych (np. relaksacji strukturalnej α lub procesów związanych z dynamiką cząsteczek oddziaływujących ze ściankami materiału) dla materiałów infiltrowanych w nanoporach. Stwierdzono także, że zastosowanie modulowanych materiałów miało większy wpływ na asocjację alkoholi [69].

Raportowane, tak odmiennie właściwości, dla ograniczonych przestrzennie cieczy asocjujących stanowiły inspirację do podjęcia badań przeprowadzonych na potrzeby niniejszej pracy doktorskiej. W celu zbadania wpływu oddziaływań międzycząsteczkowych alkoholi monohydroksylowych na ich zachowanie w materiałach litych i ograniczeniu przestrzennym przebadano dwie grupy alkoholi, tj. alkohole fenyłowe (AF) oraz alkohole cykloheksylowe (AC). Wybrane substancje charakteryzowały się obecnością pierścienia aromatycznego lub cykloheksylowego w swoich strukturach molekularnych. Wśród badanych alkoholi fenylowych znalazły się: alkohol benzyłowy, 2-fenylo-1-etanol, 3-fenylo-1-propanol, 4-fenylo-1-butanol, 5-fenylo-1-pentanol oraz 7-fenylo-1-heptanol. Natomiast badane w niniejszej pracy doktorskiej

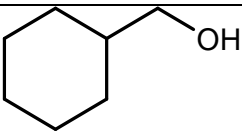
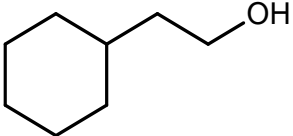
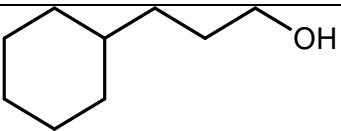
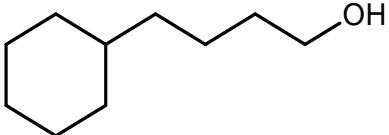
alkohole cykloheksylowe to: 1-cykloheksylometanol, 2-cykloheksylo-1-etanol, 3-cykloheksylo-1-propanol i 4-cykloheksylo-1-butanol. Wzory strukturalne użytych alkoholi znajdują się na **Rysunku 4**. Nazwy oraz skróty użytych substancji podane są w **Tabeli 1**. Wszystkie substancje charakteryzowały się czystością >98% i zostały zakupione w firmie Sigma Aldrich. W celu oczyszczenia próbek z wilgoci zastosowano proces liofilizacji (wymrażania w ciekłym azocie) z użyciem linii Schlenka.



Rysunek 4. Struktury chemiczne badanych alkoholi monohydroksylowych.

Tabela 1. Wzory strukturalne, nazwy oraz skróty alkoholi monohydroksylowych.

Wzór strukturalny	Nazwa	Skrót
Alkohole fenylowe		
	Alkohol benzylový	AB
	2-fenýlo-1-etanol	2F1E
	3-fenýlo-1-propanol	3F1P
	4-fenýlo-1-butanol	4F1B
	5-fenýlo-1-propanol	5F1P
	7-fenýlo-1-heptanol	7F1H

Alkohole cykloheksylowe (cykliczne)		
	Cykloheksylometanol	CM
	2-cykloheksylo-1- etanol	2C1E
	3-cykloheksylo-1- propanol	3C1P
	4-cykloheksylo-1- butanol	4C1B

Do badania wpływu ograniczenia przestrzennego wykorzystano natywne oraz silanizowane matryce krzemowe o średnicy porów 4 nm. Natywne membrany (**Rysunek 5**) zostały wykonane stosując metodę elektrochemicznego trawienia. Jako elektrolit zastosowano mieszaninę kwasu fluorowodorowego oraz etanolu w stosunku 1:1, w celu uzyskania średnic porów równych 4-5 nm o porowatości 7-9%. Uzyskane w ten sposób matryce miały grubość $50 \pm 5 \mu\text{m}$.



Rysunek 5. Fotografia przedstawiająca natywny por krzemowy o średnicy $d = 4$ nm.

Aby otrzymać silanizowane membrany krzemowe, natywne mezopory zostały zanurzone w roztworze metoksytrimetylosilanu ($CH_3OSi(CH_3)_3$) i heksanu (w stosunku 1:1). Mieszanina została podgrzana do temperatury 323 K i pozostawiona na 72 h, w wyniku czego dochodziło do wymiany grup hydroksylowych znajdujących się na powierzchni porów na grupy metoksyłowe ($-OCH_3$). Tak przygotowane matryce posiadały bardziej hydrofobowy charakter.

Aby wprowadzić alkohol do matrycy zastosowano następujący protokół. W pierwszej kolejności, puste membrany zostały wygrzewane w wysokiej próżni (10^{-5} mbar) w temperaturze 373 K przez 24 godziny w celu usunięcia wszelkich lotnych zanieczyszczeń. Następnie matryca została umieszczona w kolbce zawierającej alkohol. Taki układ utrzymywano w temperaturze $T = 313$ K (dla AC) i $T = 323$ K (dla AF) w próżni (10^{-2} bar) przez czas jednej godziny w celu wypełnienia się porów wybranym alkoholem. Po zakończonej infiltracji nadmiar próbki z powierzchni membran został usunięty, stosując chusteczki bezpyłowe.

W celu zbadania i określenia wpływu oddziaływań międzycząsteczkowych na zachowanie asocjujące alkoholi wykorzystano szereg metod eksperymentalnych, pozwalających na kompleksowe spojrzenie na badany problem badawczy. Dlatego też zastosowano metodę spektroskopii w podczerwieni (IR), spektroskopii Ramana, szerokopasmowej spektroskopii dielektrycznej (BDS), różnicowej kalorymetrii skaningowej (DSC), dyfrakcji rentgenowskiej (XRD) oraz metodę badania kątów zwilżania.

Celem niniejszej rozprawy doktorskiej był poznanie wpływu oddziaływań międzycząsteczkowych (wiązań wodorowych) na zachowanie alkoholi monohydroksylowych

w materiałach litych jak i w ograniczeniu przestrzennym, a w szczególności próba odpowiedzi na następujące pytania:

- A. Jak wprowadzenie do struktury molekularnej alkoholu grup funkcyjnych mogących tworzyć dodatkowe oddziaływania, wpłynie na zachowanie asocjacyjne alkoholi?
- B. Jaki wpływ na zdolności asocjacyjne alkoholi ma inkorporacja do układów ograniczonych przestrzennie?
- C. Czy alkohole fenylowe są w stanie tworzyć nieodwracalnie zaadsorbowaną warstwę molekuł w ograniczeniu przestrzennym?

Rezultaty przeprowadzonych badań zostały opublikowane w międzynarodowych czasopismach naukowych z listy filadelfijskiej:

- P1. N. Soszka, B. Hachuła, M. Tarnacka, E. Kamińska, J. Grelska, K. Jurkiewicz, M. Geppert-Rybczyńska, R. Wrzalik, K. Grzybowska, S. Pawlus, M. Paluch, K. Kamiński, **The Impact of the Length of Alkyl Chain on the Behavior of Benzyl Alcohol Homologues – the Interplay between Dispersive and Hydrogen Bond Interactions.** *Phys. Chem. Chem. Phys.* **2021**, 23 (41), 23796 – 23807.
- P2. N. Soszka, B. Hachuła, M. Tarnacka, J. Grelska, K. Jurkiewicz, M. Geppert – Rybczyńska, R. Wrzalik, K. Grzybowska, S. Pawlus, M. Paluch, K. Kamiński, **Aromaticity Effect on Supramolecular Aggregation. Aromatic vs. Cyclic Monohydroxy Alcohols.** *Spectrochim. Acta – Part A Mol. Biomol. Spectrosc.* **2022**, 276, 121235.
- P3. N. Soszka, M. Tarnacka, B. Hachuła, M. Geppert – Rybczyńska, K. Prusik, K. Kamiński, **The Impact of Interface Modification on the Behavior of Phenyl Alcohols within Silica Templates.** *J. Phys. Chem. C*, **2024**, (doi: 10.1021/acs.jpcc.3c08084)
- P4. N. Soszka, M. Tarnacka, B. Hachuła, P. Włodarczyk, R. Wrzalik, M. Hreczka, M. Paluch, K. Kamiński, **The Existence of Strongly Bonded Layer in Associating Liquids within Silica Pores – the Spectral and Molecular Dynamics Study.** *Nanoscale*, **2024**, 16, 6636-6647

Treści powyższych publikacji stanowiących podstawę niniejszej pracy doktorskiej są załączone w **Rozdziale 4**. Wyniki uzyskane w trakcie trwania doktoratu zostały zaprezentowane na konferencjach naukowych:

1. European Meeting on Physical Organic Chemistry „Chemistry in a Confined Space” (2021), Karpacz, Polska, poster „The impact of nanoscale confinement on the behavior of associating materials”
2. XV Kopernikańskie Seminarium Doktoranckie (2022), Toruń, Polska, wystąpienie ustne „Wpływ aromatyczności na asocjację alkoholi monohydroksylowych”
3. 2nd Global Summit on Nanotechnology and Materials Science (2023), Fiano Romano, Rzym, Włochy, poster „Spectroscopic evidence of irreversibly adsorbed layer in 2D geometrical confinement – the case of monohydroxy alcohols”

Ponadto jestem współautorką 4 artykułów naukowych, które nie zostały włączone do rozprawy doktorskiej:

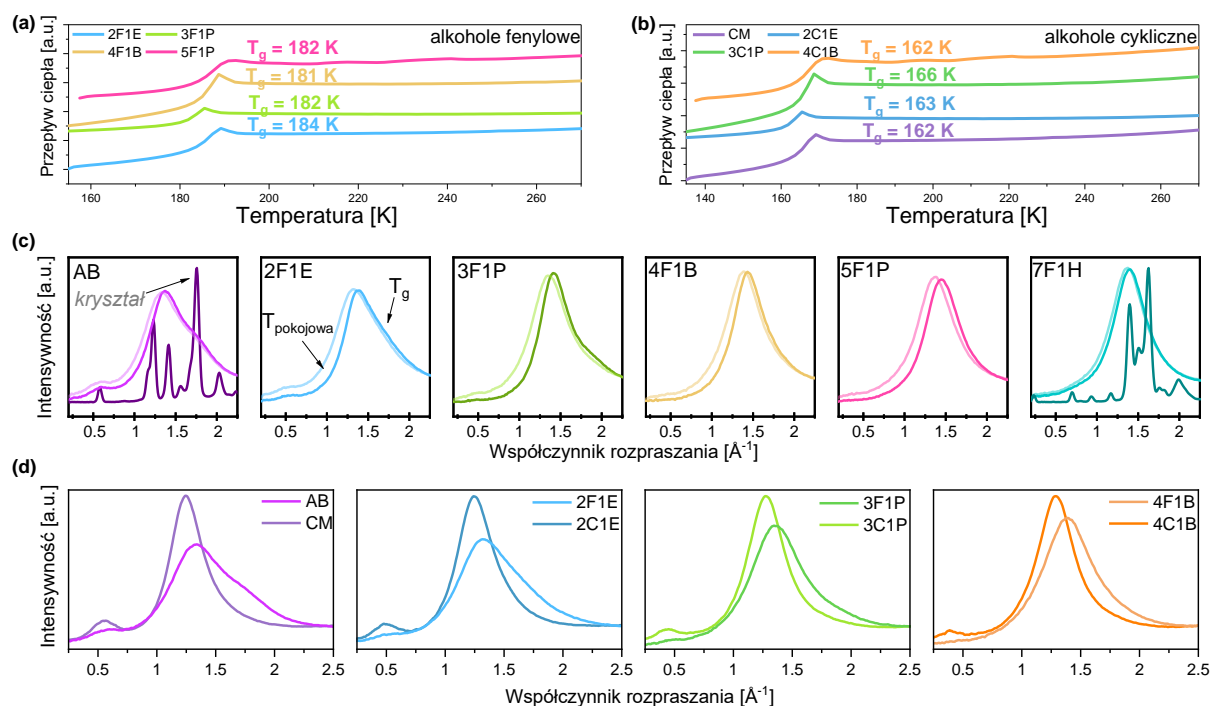
1. **N. Soszka**, B. Hachuła, M. Tarnacka, E. Kamińska, S. Pawlus, K. Kamiński, M. Paluch, Is a Dissociation Process Underlying the Molecular Origin of the Debye Process in Monohydroxy Alcohols?, *J. Phys. Chem. B*, **2021**, 125 (11), 2960 – 2967
2. B. Hachuła, J. Grelska, **N. Soszka**, K. Jurkiewicz, A. Nowok, A. Szeremeta, S. Pawlus, M. Paluch, K. Kamiński, Systematic Studies on the Dynamics, Intermolecular Interactions and Local Structure in the Alkyl and Phenyl Substituted Butanol Isomers. *J. Mol. Liq.*, 2022, 346, 117098
3. A. Minecka, M. Tarnacka, **N. Soszka**, B. Hachuła, K. Kamiński, E. Kamińska, Studying the Intermolecular Interactions, Structural Dynamics, and Non-Equilibrium Kinetics of Clinidipine Infiltrated into Alumina and Silica Pores. *Langmuir*, 2022, 39 (1), 533 – 544
4. K. Łucak, A. Szeremeta, R. Wrzalik, J. Grelska, K. Jurkiewicz, **N. Soszka**, B. Hachuła, D. Kramarczyk, K. Grzybowska, B. Yao, K. Kamiński, S. Pawlus, Experimental and Computational Approach to Studying Supramolecular Structures in Propanol and Its Halogen Derivatives. *J. Phys. Chem. B*, **2023**, 127 (42), 9102 – 9110

2. OMÓWIENIE OTRZYMANYCH WYNIKÓW

2.1 Jak wprowadzenie do struktury molekularnej alkoholu grup funkcyjnych mogących tworzyć dodatkowe oddziaływania, wpłynie na zachowanie asocjacyjne alkoholi?

Jak wspomiano w części teoretycznej, modyfikacja struktury chemicznej alkoholu może wpływać na jego zdolności asocjacyjne chociażby poprzez powstawanie nowych oddziaływań. Pierwszym celem niniejszej pracy doktorskiej było przeanalizowanie wpływu długości łańcucha alifatycznego oraz aromatyczności na zachowanie asocjacyjne molekuł poprzez zbadanie serii alkoholi fenylowych (**Tabela 1**), oraz porównanie ich właściwości z odpowiadającymi im alkoholami cykloheksylowymi.

Badania kalorymetryczne AF wskazują na możliwość witrifikacji czterech z sześciu badanych związków. Dwa z nich, tj. alkohol benzytowy oraz 7-fenyl-1-heptanol ulegały krystalizacji. Jak widać na **Rysunku 6a** do przejścia szklanego AF dochodzi w porównywalnych temperaturach ($T_g \sim 182$ K), dlatego też można stwierdzić, iż wydłużanie łańcucha węglowodorowego nie wpływa znacząco na możliwość zeszklenia tych alkoholi. Podobnymi wynikami charakteryzują się alkohole cykliczne (**Rys. 6b**). Temperatury przejścia szklanego AC są niższe niż odpowiadających im AF, co sugeruje wpływ przyłączonego do struktury pierścienia na temperaturę przejścia szklanego alkoholi.

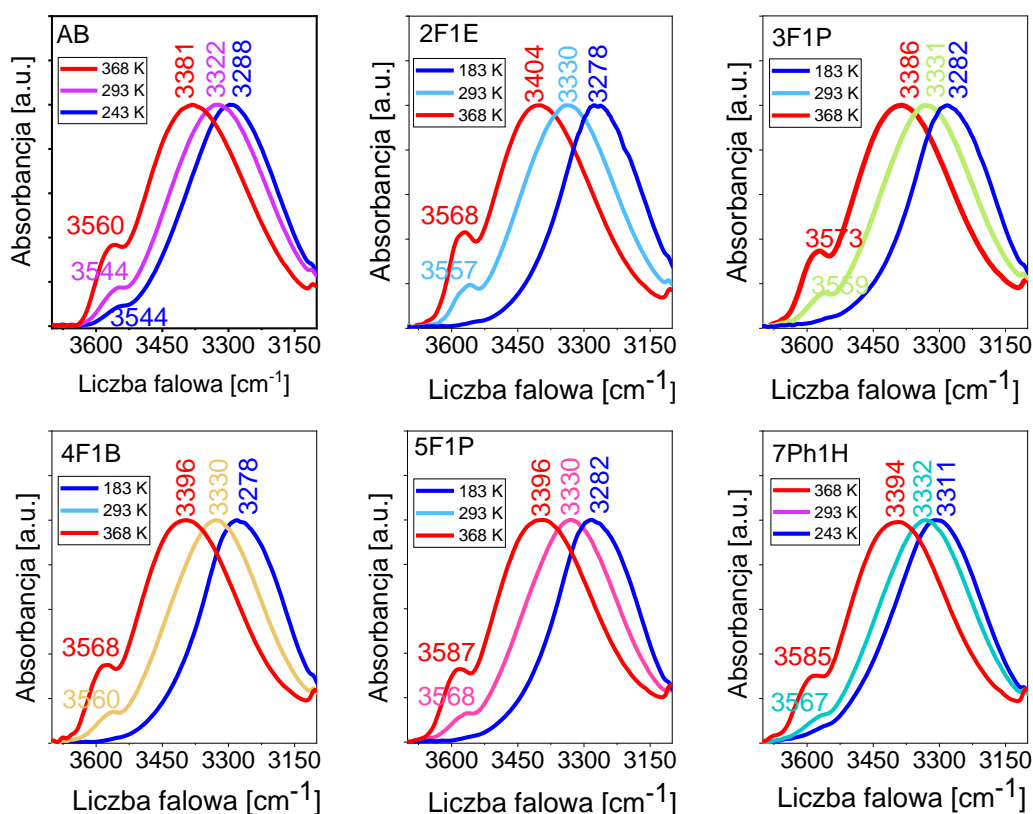


Rysunek 6. (a, b) Termogramy zarejestrowane podczas chłodzenia z szybkością 10 K/min dla AF oraz AC. (c) Dyfraktogramy zarejestrowane w temperaturze pokojowej oraz temperaturze zeszklenia AF. (d) Porównanie dyfraktogramów AF i AC w temperaturze pokojowej.

Informację o właściwościach strukturalnych badanych związków uzyskano dzięki badaniom dyfrakcyjnym. Zarówno dyfraktogramy AF jak i AC charakteryzują się obecnością dwóch pików, tj. typowym dla cieczy amorficznej „halo” oraz tzw. *pre-pikiem* zlokalizowanym w niższym zakresie wektora rozpraszania (Q) (**Rys. 6c,d**). Pochodzenie *pre-piku* dyskutowane jest w kontekście powstawania uporządkowania średniego zasięgu wynikającego z tworzenia się zasocjowanych struktur [70,71]. W przypadku AB oraz 7F1H zaprezentowano również dyfraktogramy krystalicznych próbek. Analiza obrazów dyfrakcyjnych uzyskanych dla AF wskazuje na zmiany zachodzące w strukturach badanych alkoholi wraz z wydłużaniem się łańcucha alifatycznego. Intensywność wspomnianego *pre-piku* maleje dla „dłuższych” alkoholi, co pozornie może świadczyć o słabszej asocjacji molekuł. Co więcej, z wydłużaniem łańcucha węglowodorowego główny pik staje się bardziej symetryczny (jego szerokość maleje) oraz obserwowany jest wzrost amplitudy tego piku, świadczący o wzroście lokalnego uporządkowania cząsteczek. Porównując dyfraktogramy AF z tymi otrzymanymi dla AC widoczne są wyraźne różnice w zarejestrowanych obrazach dyfrakcyjnych, tj. główny pik w przypadku AF jest szerszy, charakteryzuje się mniejszą intensywnością oraz przesunięciem w stronę wyższych wartości wektora rozpraszania, Q .

Dodatkowo, *pre-pik* jest mniej intensywny w przypadku AF. Te różnice sugerują, iż wprowadzenie aromatyczności wprowadza większą heterogeniczność do struktury międzycząsteczkowej. Asymetryczny kształt głównego pasma AF wynika z nakładania się na siebie dwóch składowych (dwóch preferowanych ułożeń molekuł), tj. ułożenia spowodowanego tworzeniem się wiązań wodorowych $O - H \cdots O$, oraz istnienia dodatkowych oddziaływań π , w których bierze udział pierścień aromatyczny.

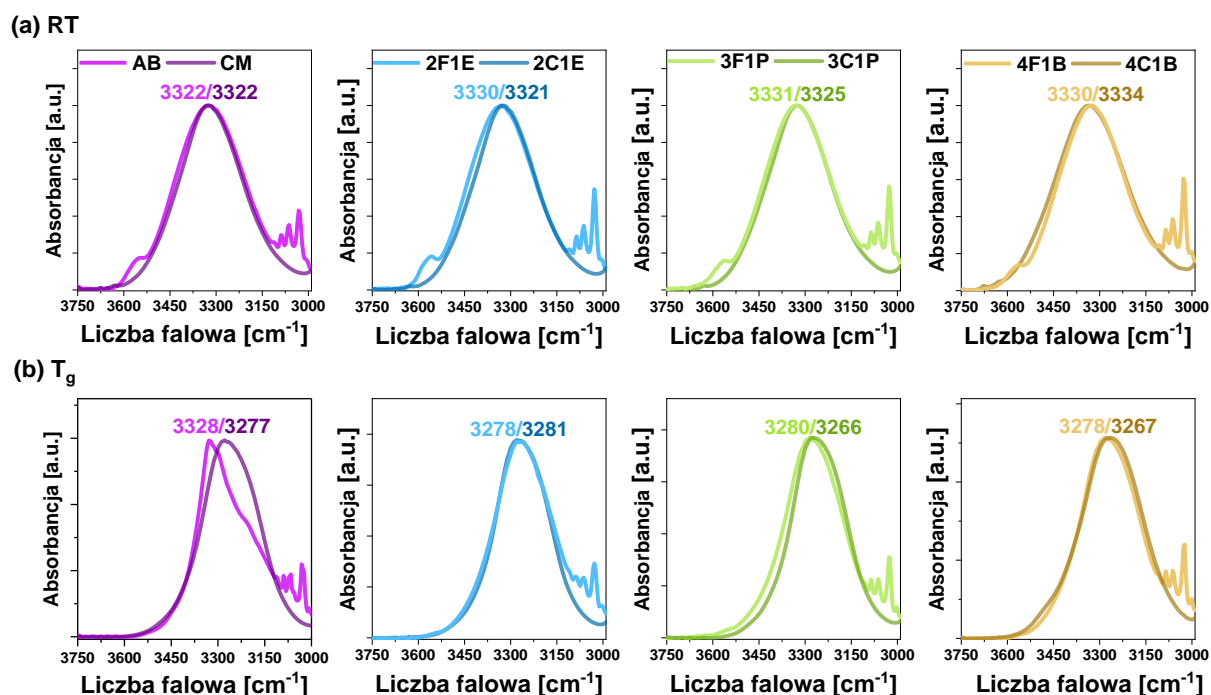
Aby w pełni uzyskać informację o stopniu zasocjowania molekuł, zostały wykonane pomiary metodą spektroskopii w podczerwieni. Należy w tym miejscu wspomnieć, iż jest to jedna z najczulszych metod, która pozwala obserwować zachodzące zmiany w asocjacji molekuł, szczególnie pod kątem wiązań wodorowych, poprzez śledzenie zmian występujących na pasmach odpowiadających drganiom grup hydroksylowych (ν_{OH}). W pierwszym kroku zarejestrowano temperaturową zależność parametrów spektralnych pasm ν_{OH} na zachowanie asocjacyjne alkoholi. Na **Rysunku 7** przedstawione zostały widma w podczerwieni w zakresie spektralnym $3750 - 3100 \text{ cm}^{-1}$ zarejestrowane w trzech temperaturach: 368 K, 293 K oraz 183 K. Pasma o małej intensywności zlokalizowane w zakresie spektralnym $3570 - 3540 \text{ cm}^{-1}$ odpowiada drganiom rozciągającym wolnych (niezwiązanych) grup hydroksylowych, $\nu_{OH \text{ free}}$, natomiast szerokie pasmo z maksimum znajdującym się przy $\sim 3300 \text{ cm}^{-1}$ związane jest z drganiami rozciągającymi grup OH powiązanych ze sobą wiązaniami wodorowymi, $\nu_{OH \text{ assoc}}$. Te same pasma obserwuje się w przypadku AC, jednakże intensywność pasma $\nu_{OH \text{ free}}$ jest dużo niższa w porównaniu z AF. Stąd, porównując tylko strukturę subtelną pasm, można wnioskować o lepszej asocjacji AC w porównaniu do AF. Co więcej, zmiana temperatury powoduje zmianę w stopniu asocjacji molekuł AF, co widoczne jest poprzez zmiany intensywności pasm $\nu_{OH \text{ free}}$ i $\nu_{OH \text{ assoc}}$. Wraz z obniżaniem temperatury obserwuje się zmniejszenie intensywności pasma $\nu_{OH \text{ free}}$ oraz wzrost intensywności pasma $\nu_{OH \text{ assoc}}$. Dowodzi to o zachodzących zmianach w agregacji cząsteczek. W niższych temperaturach liczbie molekuł uczestniczących w tworzeniu wiązań wodorowych rośnie, a tym samym wzrasta stopień asocjacji.



Rysunek 7. Widma w podczerwieni AF przedstawione w zakresie spektralnym 3750 – 3100 cm^{-1} w trzech temperaturach: 368 K, 293K oraz 183 K. W przypadku AB oraz 7F1H zaprezentowano widma zarejestrowane przed krystalizacją alkoholi ($T = 243$ K).

Podobne zachowanie występuje w przypadku AC (**Rys. 8**). Analiza częstości pasm $\nu_{OH\text{ assoc}}$ w temperaturze pokojowej wskazuje na niewielkie różnice w sile tworzących się wiązań wodorowych – pasma charakteryzują się porównywalnymi wartościami liczb falowych. Wyjątkiem jest tutaj alkohol benzylowy, którego maksimum pasma $\nu_{OH\text{ assoc}}$ jest najniższe ze wszystkich badanych alkoholi ($\nu = 3322\text{ cm}^{-1}$). Interesujących obserwacji dostarczyły pomiary alkoholi w niższych temperaturach. Jak widać na **Rys. 8b** w temperaturze zeszklenia alkohole z parzystą liczbą grup $-CH_2$ w łańcuchu posiadają mniejsze wartości liczb falowych pasma ν_{OH} w porównaniu z alkoholami z nieparzystą liczbą grup $-CH_2$. Świadczy to o zmianach w sile wiązań wodorowych, tj. w „parzystych” alkoholach (2F1E, 4F1B) dochodzi do tworzenia silniejszych wiązań wodorowych niż w alkoholach „nieparzystych”. Porównując częstości pasm AF z AC widać, iż w temperaturze pokojowej obie grupy alkoholi posiadają porównywalne wartości liczb falowych pasma ν_{OH} , co świadczy o podobnej sile tworzących

się wiązań wodorowych. Natomiast, podczas obniżania temperatury, dochodzi do zauważalnej różnicy w położeniu pasm, tj. częstości pasm dla AC są mniejsze, co świadczy o różnicach w sile wiązań wodorowych. Dodatkowo, z analizy szerokości połówkowej pasm $\nu_{OH\ assoc}$ można uzyskać informacje o stopniu homo/heterogeniczności w dystrybucji sił wiązań wodorowych. Zwężenie pasm $\nu_{OH\ assoc}$ AF występujące przy obniżaniu temperatury wskazuje na bardziej homogeniczną sieć wiązań wodorowych w niskich temperaturach. Co interesujące, w temperaturze pokojowej obserwowany jest spadek szerokości pasma od AB do 3F1P, a następnie jego wzrost dla alkoholi z dłuższymi łańcuchami alifatycznymi. Wskazuje to na zmiany w organizacji wiązań wodorowych przechodząc od „krótszych” alkoholi do „dłuższych”. Dodatkowo, pasma $\nu_{OH\ assoc}$ AF są szersze w porównaniu do pasm $\nu_{OH\ assoc}$ AC, a więc w przypadku AF występuje większa heterogeniczność w dystrybucji tworzących się oddziaływań. Co więcej, poszerzenie pasma, podobnie jak w przypadku pomiarów dyfrakcyjnych, może wskazywać na występowanie dodatkowych oddziaływań międzycząsteczkowych, m.in. oddziaływań $OH \cdots \pi$.



Rysunek 8. Porównanie widm w podczerwieni w zakresie spektralnym 3750 – 3000 cm⁻¹ AF i AC w temperaturze (a) pokojowej oraz (b) przejścia szklistego.

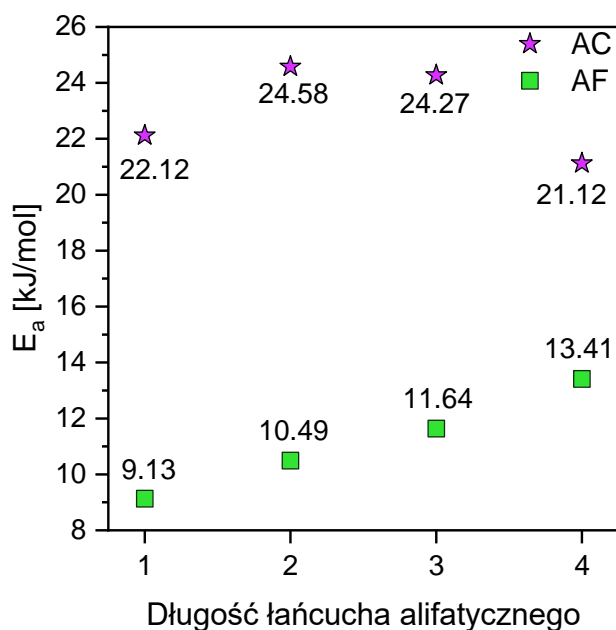
Co ciekawe, porównując widma w podczerwieni dla wszystkich AF w temperaturze pokojowej widać spadek intensywności pasma $\nu_{OH\ free}$ wraz z wydłużaniem łańcucha alifatycznego, co świadczy o większym stopniu asocjacji molekuł. Ten interesujący trend,

przeciwny do tego, który obserwuje się w przypadku prostych alkoholi alifatycznych [20], spowodowany jest lepszą separacją pierścienia aromatycznego od grupy hydroksylowej. Z tego powodu, można także stwierdzić, iż pierścień ten pełni rolę zawady sterycznej w badanych alkoholach. Dodatkowo, dla obu grup alkoholi obliczono wartość energii aktywacji procesu dysocjacji (E_a), według poniższego wzoru, która mówi o sile jaką należałoby dostarczyć do cząsteczek, aby rozerwać wiązanie wodorowe [72].

$$\ln K = \frac{A_{free}}{A_{assoc}} = -\frac{E_a}{RT} + \frac{\Delta S}{R} \quad (1)$$

K – stała równowagi; A_{free} – intensywność integralna pasma $\nu_{OH\ free}$; A_{assoc} – intensywność integralna pasma $\nu_{OH\ assoc}$; E_a – energia aktywacji procesu dysocjacji; R – stała gazowa; T – temperatura; ΔS – entalpia procesu dysocjacji

Jak widać na **rysunku 9** wraz ze wzrostem długości łańcucha alifatycznego w AF rośnie wartość wspomnianej energii. Zgadza się to z informacją o stopniu asocjacji molekuł – dłuższe alkohole charakteryzują się większym stopniem agregacji. Dodatkowo, na wyższe wartości E_a może wpływać większa giętkość łańcucha, co wpływało na konformację i upakowanie molekuł. Natomiast w przypadku AC, ich wartości E_a są dwukrotnie większe niż odpowiadające im AF. Może wynikać to z większej elastyczności pierścienia cykloheksylowego, który może występować w różnych konfiguracjach (m.in. konformacji łódkowej lub krzeselkowej), co prowadzi do większej stabilizacji wiązań wodorowych, i tym samym nie obserwuje się liniowego trendu wzrostu energii ze wzrostem łańcucha w przypadku AC.



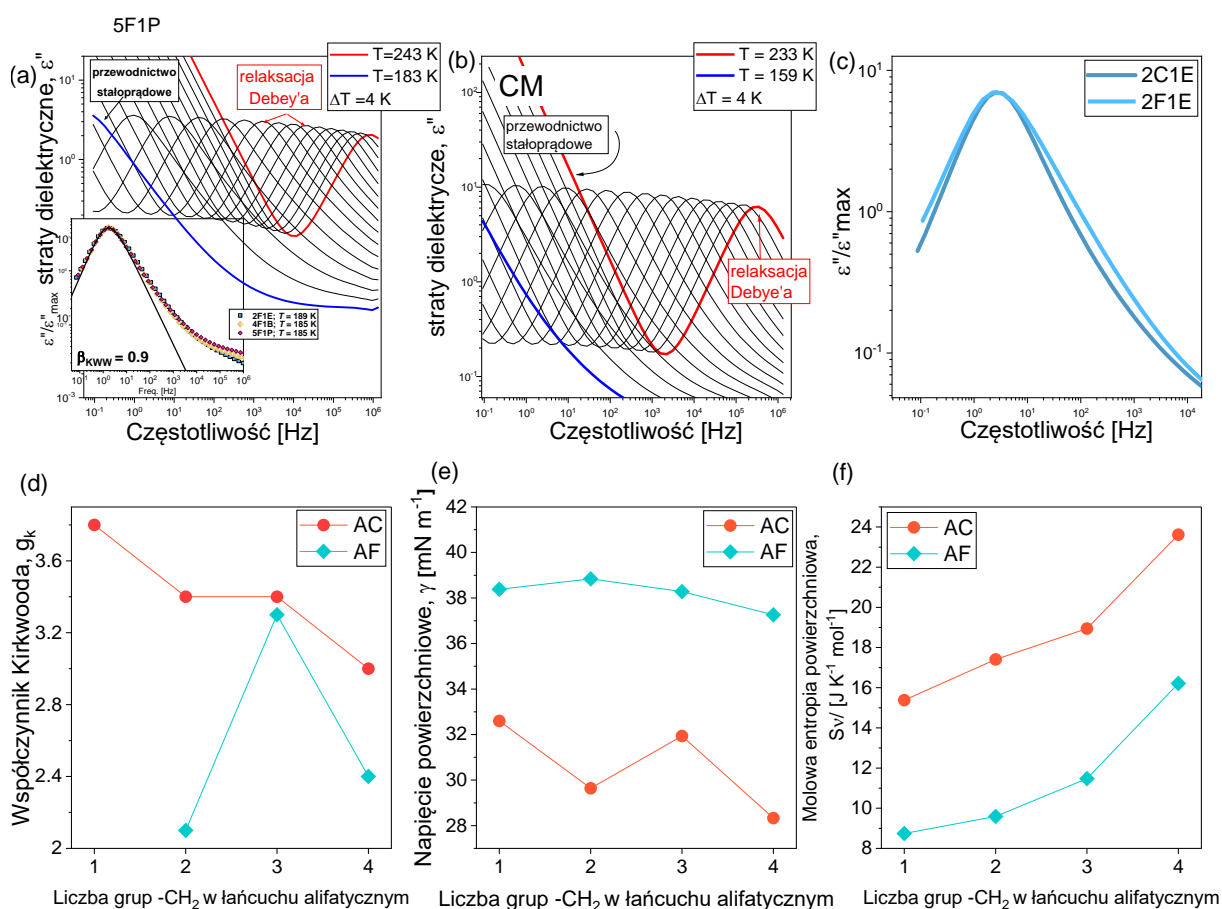
Rysunek 9. Wartości energii aktywacji procesu dysocjacji dla alkoholi fenylowych i cykloheksylowych.

W celu uzyskania pełnego obrazu zachowań asocjacyjnych alkoholi przeprowadzono także pomiary dielektryczne, wykorzystując metodę szerokopasmowej spektroskopii dielektrycznej. Przedstawione na **Rysunku 9a,b** widma strat dielektrycznych zarówno AF jak i AC ujawniły, poza przewodnictwem stałoprądowym, jeden dominujący proces/tryb relaksacji. Otrzymany parametr β_{KWW} (poprzez dopasowanie pasm za pomocą funkcji Kohlrauscha-Williamsa-Wattsa [73,74]) w obu przypadkach posiada wartości $\sim 0,9$, co świadczy, iż obserwowana relaksacja to proces Debye'a, charakterystyczny dla alkoholi monohydroksylowych, związany z dynamiką struktur supramolekularnych [72]. Co więcej, porównanie widm strat dielektrycznych AF i AC ujawnia poszerzenie pasma w przypadku aromatycznych alkoholi (**Rys. 9c**). Wynikać to może z różnic w populacji wiązań wodorowych, głównie pod względem ich heterogenicznej natury. Dodatkowo, otrzymane wartości współczynnika korelacji Kirkwooda (g_k) [75], mówiącym o wzajemnej korelacji sąsiadujących ze sobą dipoli charakteryzowały się wartościami większymi od 1.

$$g_k = \frac{9k_B \varepsilon_0 M T (\varepsilon_s - \varepsilon_\infty) (2\varepsilon_s + \varepsilon_\infty)}{\rho N_A \mu^2 \varepsilon_s (\varepsilon_\infty + 2)^2} \quad (2)$$

k_B – stała Boltzmana; M – masa molowa; T – temperatura; ρ – gęstość; N_A – liczba Avogadro; μ – moment dipolowy; ε_0 – przenikalność elektryczna próżni; ε_s – przenikalność statyczna; ε_∞ – przenikalność wysokoczęstotliwościowa

Dodatni parametr, wskazuje na tendencję do ustawienia się molekuł w określonym kierunku, sugerując pewne uporządkowanie, natomiast ujemny parametr g_k mówi o braku uporządkowania lub o losowości w orientacji molekularnej. Co więcej, wartości g_k rosną wraz z obniżaniem temperatury. W przypadku AF, obserwowane są niemonotoniczne zmiany wartości g_k wraz z wydłużaniem łańcucha, zarówno w temperaturze 225 K jak i w temperaturze bliskiej przejściu fazowemu ($T_g + 10$ K), co sugeruje występowanie konkurencyjnych do wiązań wodorowych oddziaływań niepolarnych części cząsteczki (oddziaływania dyspersyjne). Odmienne zachowanie wykazują AC, gdzie wraz z wydłużeniem łańcucha węglowodorowego następował spadek wartości g_k .



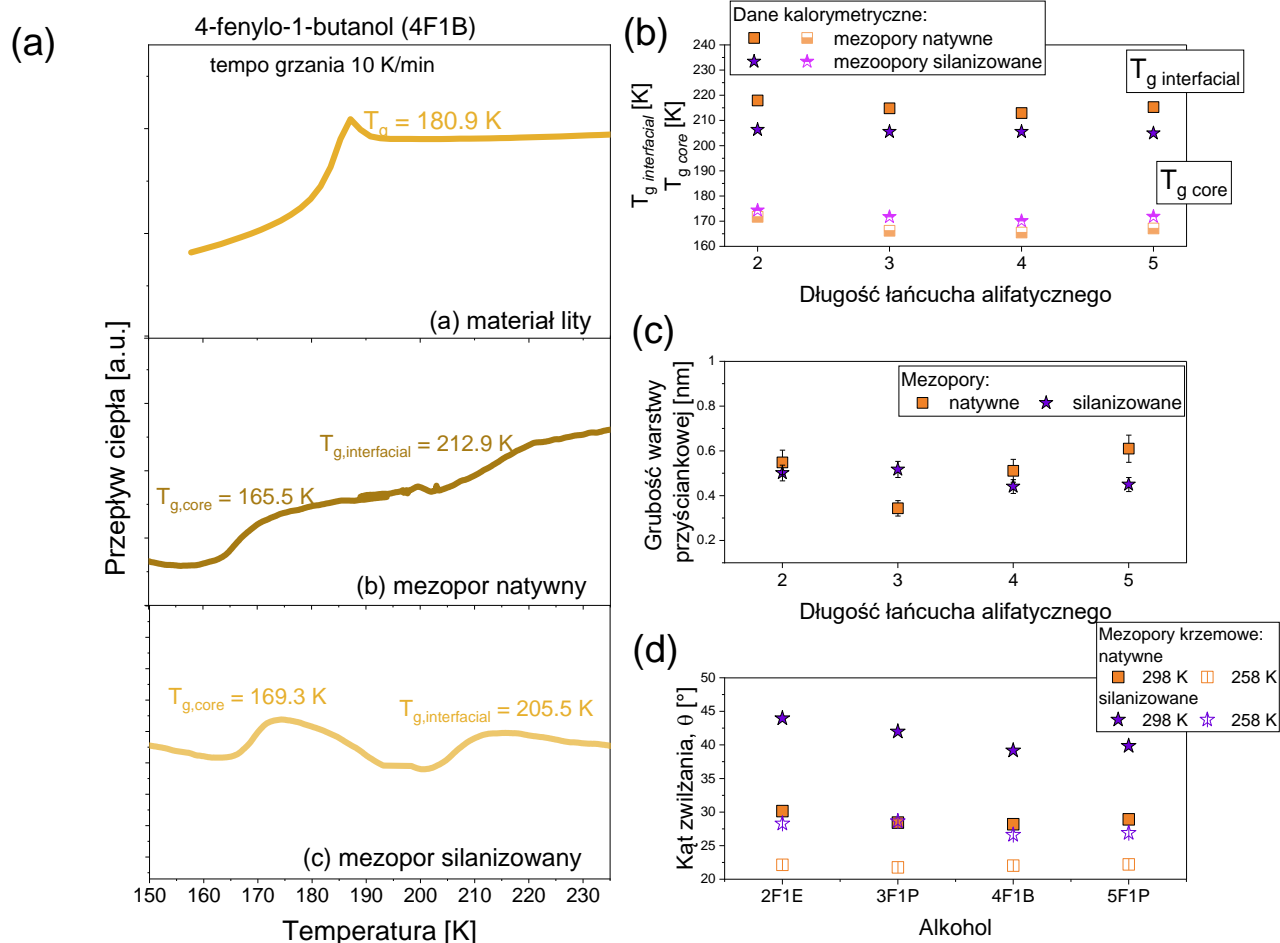
Rysunek 9. (a) Widma strat dielektrycznych dla 5F1P. We wstawce porównanie szerokości pasm AF oraz dopasowanie widma funkcją Kohlrausa-Williamsa-Wattsa. (b) Widma strat dielektrycznych cykloheksylometanolu. (c) Porównanie widm dielektrycznych 2F1E oraz 2C1E. (d) Zależność współczynnika Kirkwooda w zależności od długości łańcucha alifatycznego badanych alkoholi. (e) Napięcie powierzchniowe badanych AF i AC. (f) Molowa entropia powierzchniowa badanych AF i AC.

Ostatni etap charakterystyki substancji litych polegał na zbadaniu warstw powierzchniowych alkoholi. Wartości napięcia powierzchniowego AF oscylują w granicach 39 – 37 $mN m^{-1}$, podczas gdy dla AC ich wartości wynoszą znajdując się w przedziale 28 – 33 $mN m^{-1}$ (**Rys. 9e**). Dodatkowo, molowa entropia powierzchniowa (S_v), będąca miarą entropii powierzchni kuli zawierającej 1 mol cząsteczek, w przypadku AF rośnie wraz z wydłużaniem łańcucha, co sugeruje, iż cząsteczki mogą tworzyć na powierzchni mono-warstwę molekuł połączonych wiązaniami wodorowymi. W przypadku AC, posiadają one wartości S_v większe niż ich aromatyczne odpowiedniki (**Rys. 9f**). Wyższe wartości sygnalizują większy wpływ pierścienia cykloheksylowego na warstwę powierzchniową molekuł.

2.2 Jaki wpływ na zdolności asocjacyjne alkoholi ma inkorporacja do układów ograniczonych przestrzennie?

Zgodnie z obecnym stanem wiedzy substancje wprowadzone do materiałów ograniczających przestrzennie często wykazują inne właściwości fizykochemiczne w porównaniu z makroskopowymi próbkami. Dlatego też, po scharakteryzowaniu materiałów litych, przeprowadzone zostały badania alkoholi fenylowych (od 2F1E do 5F1P) infiltrowanych do mezoporowatych membran wykonanych z tlenku krzemu(IV) o średnicy porów (d) równych 5 nm.

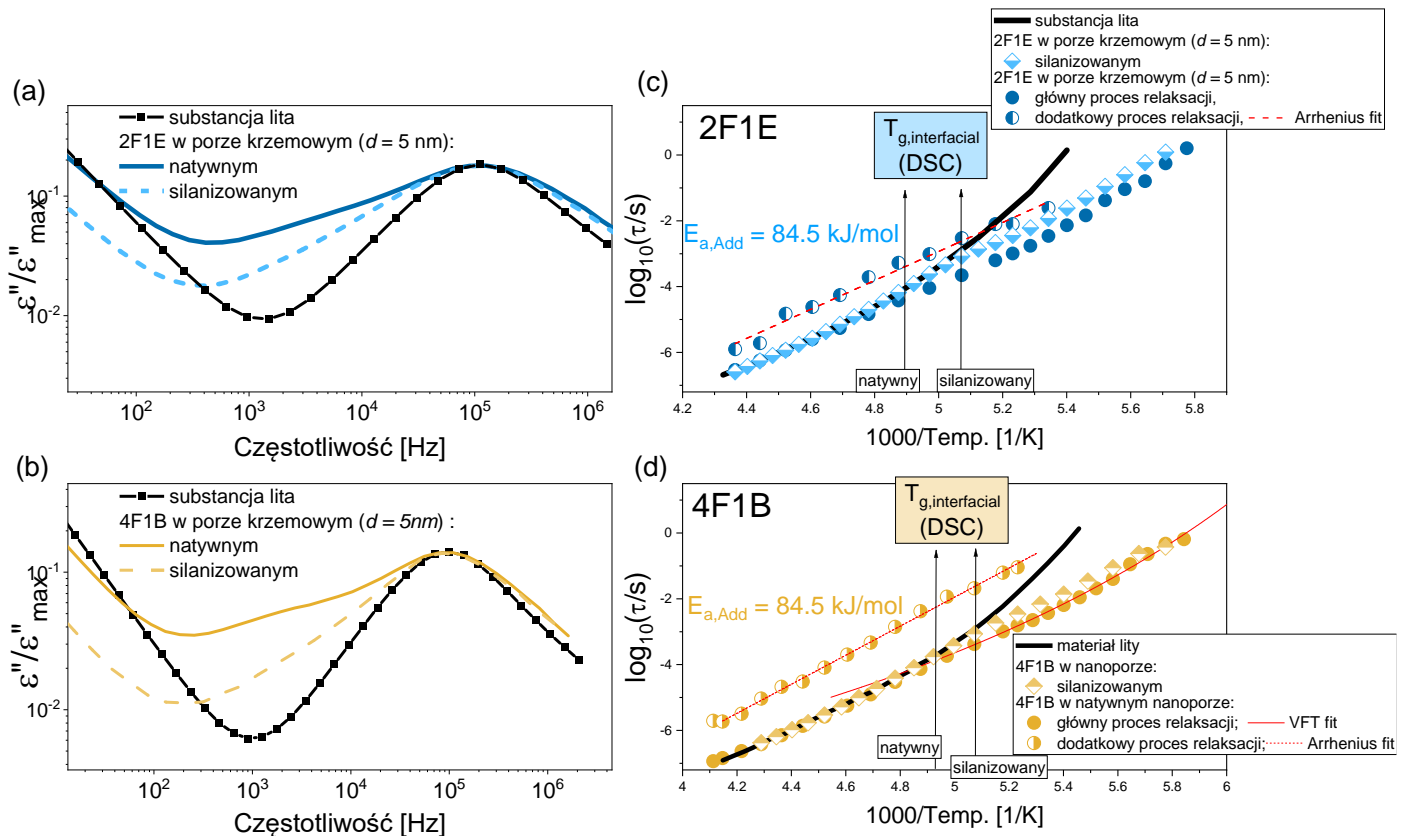
Interesujące wyniki otrzymano z badań kalorymetrycznych, a mianowicie, materiały lite charakteryzują się obecnością jednego procesu przejścia szklistego. Natomiast w matrycach porowatych (natywnych oraz silanizowanych), jak widać na **Rysunku 10a**, dla 4F1B zaobserwowano dwa przejścia szkliste, zlokalizowane w temperaturach powyżej ($T_{g,interfacial}$) i poniżej ($T_{g,core}$) temperatury T_g układu litego. Ten sam efekt obserwowany jest w pozostałych badanych alkoholach fenylowych (**Rys. 10b**). Zgodnie z modelem dwuwarstwowym, związane jest to z obecnością dwóch warstw molekuł – warstwy rdzeniowej oraz przyściankowej. Co więcej, wykorzystując prosty model matematyczny, zakładający bezpośrednią proporcjonalność między pojemnością cieplną a liczbą cząsteczek, możliwe jest oszacowanie grubości warstwy przyściankowej, która wynosi $\sim 0,5$ nm, zarówno w natywnych jak i silanizowanych membranach (**Rys. 10c**). Obserwację dwóch procesów zeszklenia oraz podobnej grubości warstwy przyściankowej można powiązać ze zwilżalnością powierzchni mezoporów przez aromatyczne alkohole. Otrzymane kąty zwilżania (θ), pokazane na **Rysunku 10d** wskazują, iż układy silanizowane posiadają wyższe wartości θ w porównaniu do ich natywnych odpowiedników, natomiast zarówno dla silanizowanych jak i natywnych membran wartości $\theta < 90^\circ$. Dodatkowo, zwilżalność powierzchni jest lepsza w niższych temperaturach (otrzymywane wartości θ były mniejsze niż w temperaturze pokojowej).



Rysunek 10. (a) Termogramy zarejestrowane dla 4F1B jako materiału litego oraz w natywnych i silanizowanych mezoporach krzemionkowych. (b) Wartości temperatur zeszklenia dla wszystkich badanych alkoholi fenylowych. (c) Grubość warstwy przyściankowej dla badanych alkoholi fenylowych. (d) Kąty zwilżania otrzymane dla alkoholi fenylowych w mezoporach natywnych i silanizowanych w dwóch temperaturach: 298 K i 258 K.

Śledząc dynamikę molekularną badanych układów, co interesująco, na widmach strat dielektrycznych dla alkoholi ograniczonych w natywnych mezoporach, obserwuje się obecność, poza przewodnictwem stałoprądowym, dwóch procesów relaksacyjnych (**Rys. 11 a,b**). Występowanie dodatkowego procesu relaksacyjnego może być związane z dynamiką molekuł warstwy przyściankowej (ang. *interfacial proces*). Efekt ten jest słabiej widoczny w przypadku matryc silanizowanych, natomiast bazując na wynikach kalorymetrycznych, również w matrycach silanizowanych zakłada się obecność molekuł tej warstwy. Co więcej, w porównaniu do materiałów litych, pasmo pochodzące od dominującego procesu relaksacji jest poszerzone, co świadczy o większej heterogeniczności ruchliwości molekuł po wprowadzeniu do materiału ograniczającego, wynikającego z dodatkowych

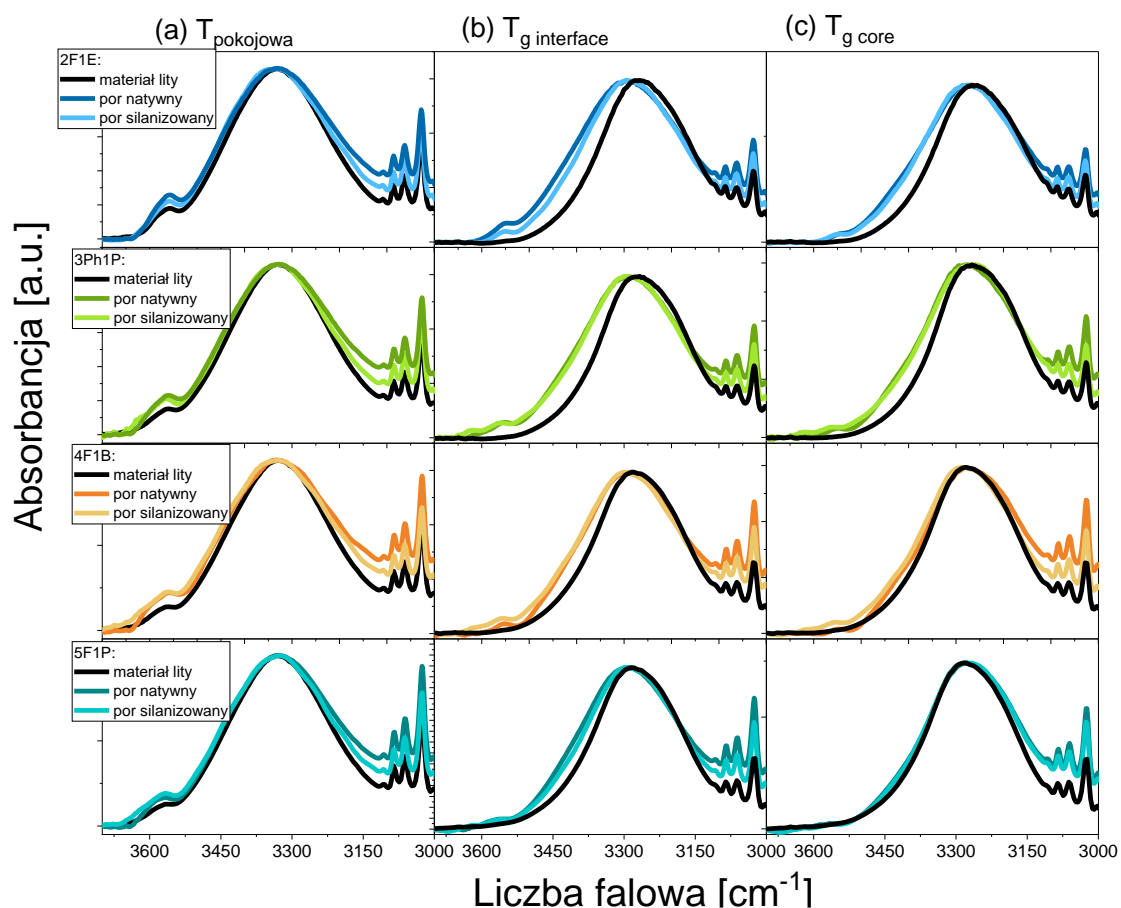
oddziaływań. By uzyskać dodatkowe informacje wynikające z pomiarów dielektrycznych, określono temperaturową zależność czasów relaksacji obserwowanych pików – dominującego (τ_{dom}) oraz dodatkowego (τ_{add}). Na przedstawionych na **Rys. 11 c,d** mapach relaksacji obserwuje się odchylenie czasów relaksacji τ_{dom} próbek ograniczonych przestrzennie w porównaniu z materiałem litym, zarówno w membranach natywnych, jak i silanizowanych. Temperatura, w której dochodzi do odchylenia, odpowiada temperaturze przejścia szklistego warstwy przyściankowej, ustalonej na podstawie pomiarów kalorymetrycznych, co oznacza, że powodem obserwowanego odchylenia może być wityfikacja cząsteczek znajdujących się w pobliżu ścianek porów. Obserwując zachowanie $\tau_{dom}(T)$, jego odchylenie nie odpowiada zachowaniu wolniejszego procesu relaksacji dielektrycznej występującej dla materiałów ograniczonych przestrzennie. Sugerowane jest więc, iż związana jest ona ze zmianami zachodzącymi w sieci wiązań wodorowych.



Rysunek 11. (a,b) Widma strat dielektrycznych dla wybranych AF. (c,d) Zależności temperaturowe czasów relaksacji wybranych AF przedstawione w funkcji $1000/Temp.$

Aby to sprawdzić, przeprowadzone zostały badania za pomocą spektroskopii w podczerwieni. **Rysunek 12** przedstawia widma w podczerwieni w zakresie spektralnych 3700

– 3000 cm^{-1} alkoholi litych i ograniczonych przestrzennie. Na podstawie pomiarów w szerokim zakresie temperaturowym możliwe było ocenienie wpływu temperatury na dynamikę ograniczonych przestrzennie alkoholi. Wraz z obniżeniem temperatury obserwowane jest przesunięcie częstości pasma $\nu_{OH\ assoc}$ w stronę niższych liczb falowych zarówno w porach, jak i materiałach litych. Efekt ten, wskazuje na wyraźne wzmocnienie tworzących się wiązań wodorowych po ochłodzeniu układów. Co więcej, w obu grupach układów intensywność pasma $\nu_{OH\ free}$ maleje wraz z obniżeniem temperatury, wskazując na wyższy stopień asocjacji molekuł. Analizując wpływ ograniczenia przestrzennego w temperaturze pokojowej (**Rys. 12**) zauważalne są zmiany głównie w intensywności pasma $\nu_{OH\ free}$ oraz szerokości pasma $\nu_{OH\ assoc}$, co mówi odpowiednio o zmniejszeniu stopnia asocjacji w mezoporach oraz większej heterogeniczności wśród molekuł tworzących wiązania wodorowe. Jak można zauważyć, większe zmiany na widmach IR zauważalne są dla próbek wprowadzonych do natywnych krzemowych membran, co można powiązać z silniejszym wpływem oddziaływań alkohol – por warstwy przyściankowej na zachowanie asocjacyjne AF. Obniżanie temperatury powoduje dalsze zmiany. Widoczne są przesunięcia częstości pasm $\nu_{OH\ assoc}$, tj. ograniczone geometrycznie AF charakteryzują się większymi wartościami liczb falowych w porównaniu do materiałów litych (**Tabela 2**). Wskazuje to na osłabienie wiązań wodorowych. Wciąż obserwowalne na widmach są pasma $\nu_{OH\ free}$ dla alkoholi w porach, tym samym, ograniczenie przestrzenne hamuje asocjację, obserwowalną dla materiałów litych. Interesujące są także zmiany w szerokości połówkowej pasm – widma infiltrowanych alkoholi cechują się znacznym ich poszerzeniem w stosunku do alkoholi litych. Największe odchylenia w szerokości występują po stronie lewego ramienia pasma ν_{OH} , w zakresie spektralnym utożsamianym ze „słabszymi” wiązaniami wodorowymi, co może wskazywać na obecność dodatkowego wkładu od cząsteczek słabiej związanych. Dekonwolucja pasma ν_{OH} za pomocą funkcji Gaussa wymaga użycia dwóch składowych w przypadku materiału litego, a dla infiltrowanych alkoholi – trzech. Dodatkowy wkład zlokalizowany został w zakresie wyższych częstości, co sugeruje istnienie dodatkowych, słabszych oddziaływań międzycząsteczkowych.

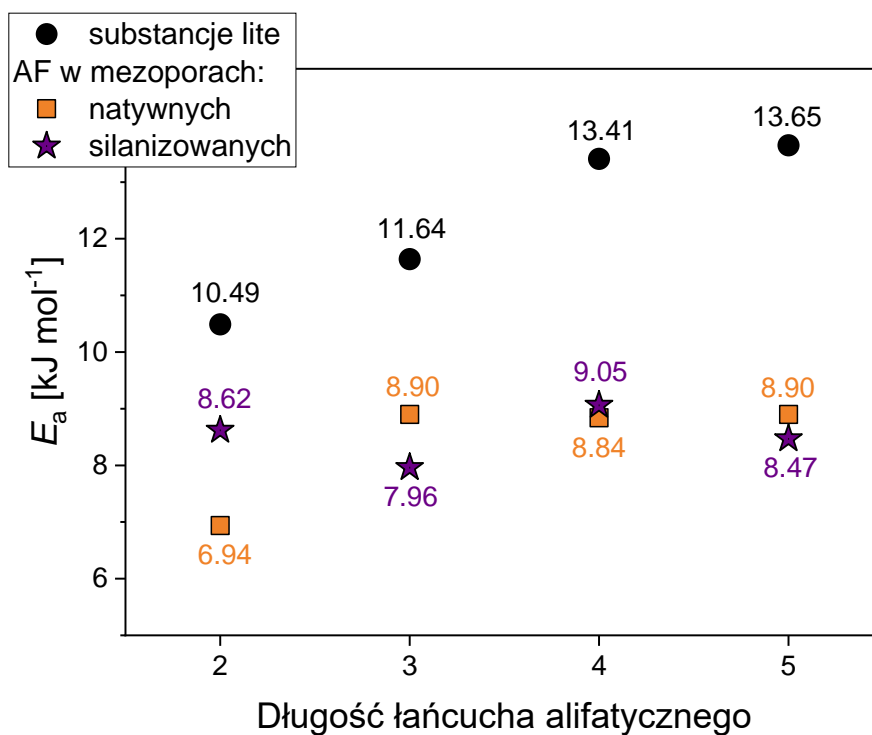


Rysunek 12. Widma w podczerwieni w zakresie spektralnym $3750 - 3000 \text{ cm}^{-1}$ zarejestrowane dla AF jako materiałów litych oraz wprowadzonych do natywnych i silanizowanych mezoporów krzemowych ($d = 5 \text{ nm}$). Widma zarejestrowane są w temperaturze (a) pokojowej, (b) temperaturze zeszklenia warstwy przyściankowej oraz (c) temperaturze zeszklenia warstwy rdzeniowej.

Tabela 2. Wartości liczb falowych pasma $\nu_{OH\ assoc}$ dla AF jako materiałów litych oraz w ograniczeniu przestrzennym.

Alkohol	$\nu_{OH\ assoc}$ [cm ⁻¹] w T _{pokojowej}	$\nu_{OH\ assoc}$ [cm ⁻¹] w T _g interfacial	$\nu_{OH\ assoc}$ [cm ⁻¹] w T _g core
materiał lity			
2F1E	3330	3285	3262
3F1P	3331	3285	3268
4F1B	3330	3287	3274
5F1P	3330	3293	3280
natywne membrany krzemowe			
2F1E	3329	3291	3273
3F1P	3328	3291	3279
4F1B	3333	3286	3272
5F1P	3327	3298	3274
silanizowane membrany krzemowe			
2F1E	3337	3291	3277
3F1P	3329	3288	3263
4F1B	3328	3297	3285
5F1P	3326	3294	3282

Oszacowując energię aktywacji procesu dysocjacji (E_a) zachodzącego w membranach krzemionkowych, otrzymane energie charakteryzują się mniejszymi wartościami w porównaniu do materiałów litych ($E_a \sim 7 - 9$ kJ mol⁻¹ dla mezoporów vs $E_a \sim 10 - 14$ kJ mol⁻¹ dla materiałów litych), (**Rysunek 13**). Zmiana wartości wskazuje na istotny wpływ ograniczenia przestrzennego na oddziaływania między molekułami. W rezultacie, aby rozerwać wiązanie wodorowe utworzone w membranach należy dostarczyć mniej energii niż dla próbki makroskopowej. Fakt ten dobrze koresponduje z niższym stopniem asocjacji infiltrowanych alkoholi w porównaniu z materiałami litymi. Co więcej, zauważony liniowy wzrost energii wraz z wydłużaniem łańcucha alifatycznego w układach litych nie jest obserwowany w membranach krzemionkowych, gdzie dla każdego alkoholu energie procesu asocjacji przyjmują podobne wartości.



Rysunek 13. Wartości energii aktywacji procesu dysocjacji dla AF inkorporowanych do natywnych i silanizowanych membran krzemowych, jak i dla materiałów litych.

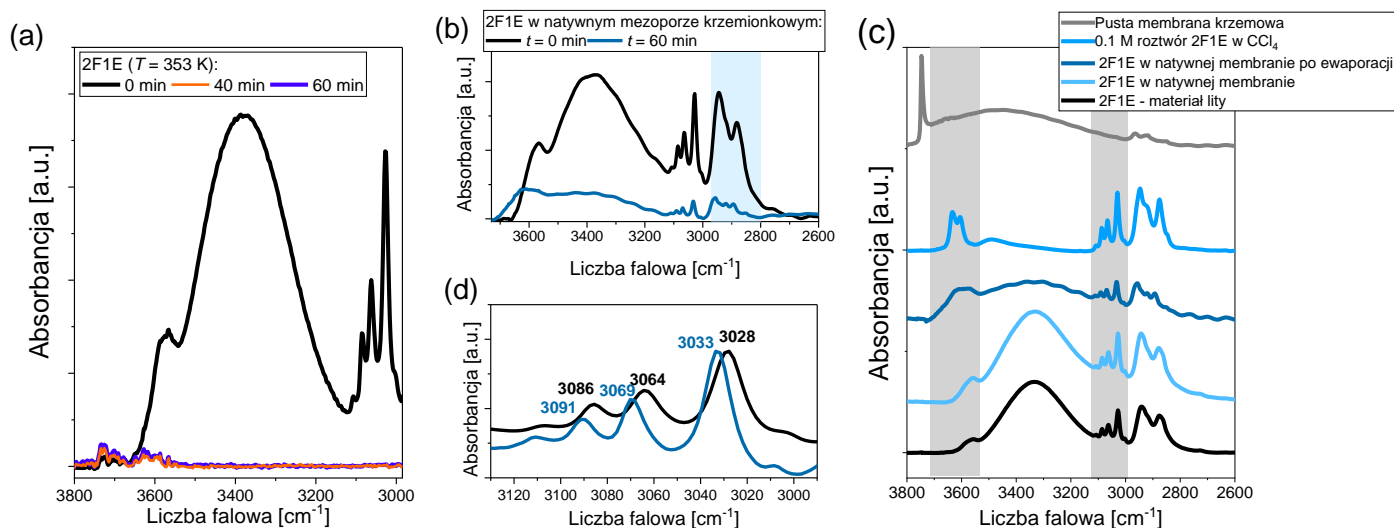
2.3. Czy alkohole fenylowe są w stanie tworzyć nieodwracalnie zaadsorbowaną warstwę molekuł w ograniczeniu przestrzennym?

Zauważone w widmach IR niewielkie zmiany w strukturze subtelnej pasma $\nu_{OH\ assoc}$ w temperaturze pokojowej, opisane w podrozdziale 2.2., skłoniły do rozmyślań nad pochodzeniem tego efektu. Możliwym jest, iż w warunkach normalnych, ograniczenie przestrzenne nie wpływa znacząco na zachowanie asocjacyjne alkoholi, lub, co także prawdopodobne, obraz spektralny obserwowany w widmach IR zdominowany jest przez molekuly warstwy rdzeniowej. Dlatego też, by zweryfikować powyższe hipotezy, przeprowadzono badania polegające na odparowaniu alkoholu (2F1E, 3F1P) z wnętrza porów. Podczas infiltrowania substancji, molekuly znajdujące się w pobliżu ścianek materiału ograniczającego przestrzennie, silnie oddziałują z grupami funkcyjnymi znajdującymi się na powierzchni tych ścianek, tworząc warstwę przyściankową. Przeprowadzone dotychczas na materiałach ograniczonych 1D badania związane z wymywaniem substancji za pomocą rozpuszczalnika, w celu „odsłonięcia” zaadsorbowanych molekuł pokazują, iż tworząca się warstwa jest nieodwracalnie związana z podłożem. Powstaje więc tzw. nieodwracalnie zaadsorbowana warstwa (ang. *irreversibly adsorbed layer, IAL*) [76–79].

W przypadku poniższych badań zastosowano procedurę odparowania próbek, który trwała 1 godzinę. Zastosowana skala czasowa eksperymentu zweryfikowana została poprzez ewaporację próbek litych, dla których parowanie następowało po 40 minutach (**Rys. 14a**). Zachodzące zmiany podczas odparowywania śledzone były poprzez pomiary w podczerwieni, a dodatkowo, przeprowadzone zostały symulacje dynamiki molekularnej.

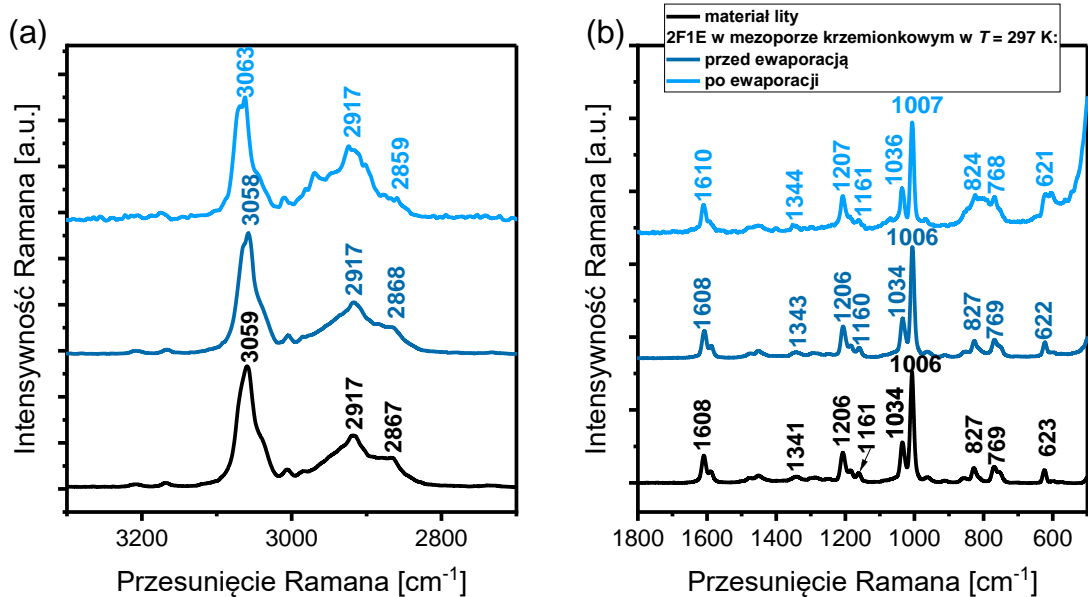
Jak można zauważyć na **Rys. 14a** alkohol całkowicie odparowuje po 40 minutach. Natomiast po przeprowadzonym godzinnym odparowywaniu, infiltrowany do natywnych i silanizowanych porów, alkohol nadal pozostaje w membranach, o czym świadczą przedstawione widma IR (**Rys. 14b**). Co więcej, zarejestrowane po odparowywaniu widma nie wykazują obecności ostrego pików przy $\sim 3750\text{ cm}^{-1}$ (pochodzącego od wolnych grup OH ugrupowania Si-OH), co wyraźnie wskazuje na obecność molekuł alkoholi w matrycach krzemionkowych (**Rys. 14c**). To samo zachowanie obserwowane jest także w przypadku inkorporowanych alkoholi do membran o średnicy $d = 8\text{ nm}$. Zatem, obserwowalne na widmach IR zmiany wynikają z powstawania warstwy molekuł silnie związanych ze ściankami porów. Co interesujące, dochodzi do zmiany w strukturze subtelnej pasma ν_{OH} – jest ono wyraźnie poszerzone, posiada małą intensywność, a pasmo $\nu_{OH\ free}$ dodatkowo jest przesunięte w stronę wyższych częstotliwości. Porównując widma po ewaporacji z widmami alkoholi rozpuszczonych w

CCl_4 , można stwierdzić, iż jeśli nawet po odparowaniu w mezoporach pozostały zasocjowane molekuly, to na wielkość takiego agregatu przypadają 2-3 molekuly, podobnie jak w przypadku rozcieńzonego alkoholu. Co więcej, złożony charakter pasma ν_{OH} odparowanych próbek dostarcza dowodów, by sądzić, że na granicy faz por – alkohol występuje szereg specyficznych wiązań wodorowych, np. $\text{O-H}\cdots\text{O}$ czy $\text{O-H}\cdots\pi$.



Rysunek 14. (a) Widma w podczerwieni 2F1E zarejestrowane w trakcie odparowania próbki, (b) Widma w podczerwieni 2F1E w natywnym porze krzemionkowym zarejestrowane w 353 K przed i po ewaporacji, (c) Porównanie widm w podczerwieni 2F1E jako materiału litego, rozcieńzonego w CCl_4 oraz infiltrowanego do natywnego pora krzemionkowego, (d) Widmo w podczerwieni w zakresie spektralnym drgań rozciągających CH aromatic zarejestrowane przed i po procesie odparowania.

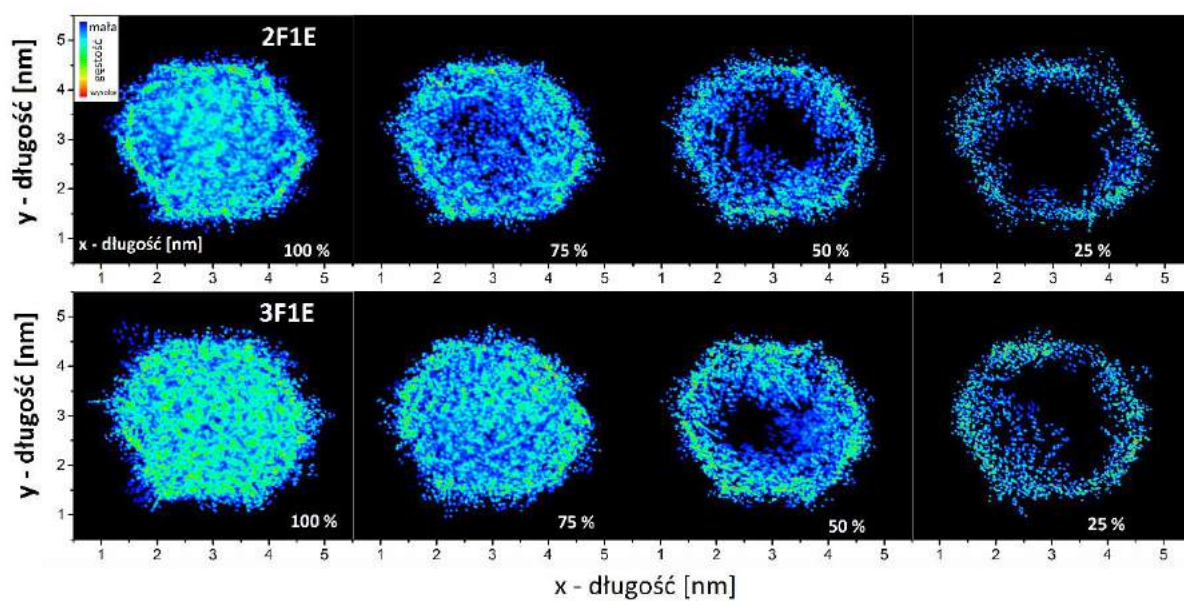
Co interesujące, zauważalne są także zmiany w zakresie spektralnym odpowiadającym drganiom rozciągającym grup CH pierścienia aromatycznego ($\nu_{CH \text{ aromatic}}$) (**Rysunek 14d**). Obserwuje się przesunięcie pasm w kierunku wyższych liczb falowych. Wskazywać to może na zmiany konformacyjne wynikające z procesu adsorpcji lub na występowanie dodatkowych oddziaływań typu π . Aby ustalić mechanizm adsorpcji molekuł zmierzone zostały widma Ramana przed i po procesie odparowania (**Rysunek 15**). Pasma $\nu_{CH \text{ aromatic}}$ (zlokalizowane przy 3058 cm^{-1}) uległo przesunięciu do częstości 3063 cm^{-1} po godzinnych odparowywaniu. Co więcej, struktura subtelna pasma odpowiadającego drganiom rozciągającym grup $\text{C}=\text{C}$ położonego przy częstości 1610 cm^{-1} także była widoczna po ewaporacji. Dodatkowo, nie obserwowano nowych pasm na widmie Ramana po przeprowadzeniu eksperymentu, co oznacza, że w badanych układach dochodziło do adsorpcji fizycznej. Ponadto, pomiary Ramana wskazują na zachodzące zmiany strukturalne/konformacyjne.



Rysunek 15. Widma Ramana 2F1E jako materiału litego i wprowadzonego do natywnej membrany krzemowej zarejestrowane przed i po procesie ewaporacji w zakresie przesunięcia Ramana (a) 3300 – 2700 cm^{-1} oraz (b) 1800 – 500 cm^{-1} .

Przeprowadzone badania w podczerwieni zostały wsparte symulacjami dynamiki molekularnej. Początkowe symulacje wskazały, iż gęstość infiltrowanego alkoholu jest o około 30% niższa niż alkoholu litego ($0,67 \text{ g} \cdot \text{cm}^{-3}$ i $1 \text{ g} \cdot \text{cm}^{-3}$, odpowiednio). Następnie, zmniejszając gęstość alkoholu ze 100% do kolejno 75%, 50% i 25% odtworzono proces odparowania próbki. W symulacjach wyraźnie widać, że zmniejszenie ilości cząsteczek alkoholu ze 100% do 25% jest związane z tworzeniem się warstwy alkoholu na wewnętrznej powierzchni matrycy krzemionkowej (**Rysunek 16**). Dodatkowo, zbadany został wpływ średnicy porów na tworzenie się IAL poprzez symulacje przeprowadzone na membranach o średnicy $d = 8 \text{ nm}$. Eliminacja cząsteczek alkoholu z wnętrza nanoporów prowadzi do powstania takiej samej warstwy jak w przypadku porów o średnicy $d = 4 \text{ nm}$. W ramach badania rozkładu dystrybucji asocjatów obserwuje się tworzenie się najsilniejszych asocjatów (pod względem siły wiązań wodorowych) w układach litych, a najsłabszych w ograniczeniu $d = 4 \text{ nm}$. Co więcej dystrybucja agregatów tworzących się poprzez oddziaływania alkohol – alkohol w ograniczeniu przestrzennym jest podobna do tej w układzie litym, natomiast średni rozmiar klastrów jest mniejszy w mezoporach w porównaniu do substancji litej. Wynik ten dobrze koreluje z badaniami w podczerwieni, gdzie obserwowalna była niewielka zmiana w pozycji pasma ν_{OH} pomiędzy układem litym a porami. Porównano także ilość asocjatów całej populacji próbki (tj. biorąc po uwagę obie frakcje molekuł) w zależności od gęstości alkoholu w

mezoporach (100% i 50%). W obu przypadkach 2F1E cechuje się większą ilością agregatów niż 3F1P. Natomiast, gdy kryterium porównania są wiązania wodorowe występujące w warstwie rdzeniowej, ilość wolnych grup hydroksylowych jest wyższa w ograniczeniu dla obu alkoholi w porównaniu do układów litych. Ta zależność dobrze odpowiada zmianom widocznym na widmach IR, gdzie intensywność pasma $\nu_{OH\ free}$ jest wyższa dla inkorporowanych alkoholi niż dla substancji litych.



Rysunek 16. Rozkład gęstości AF w matrycy porowatej przy założeniu gęstości, odpowiednio 100, 75, 50 oraz 25%.

Dodatkowo, za pomocą obliczeń z wykorzystaniem teorii funkcjonału gęstości (DFT) oszacowana została energia oddziaływań alkohol – alkohol oraz alkohol – por. Energia wiązania wodorowego warstwy przyściankowej jest większa niż energia warstwy rdzeniowej, ale tylko wtedy, gdy por jest grupą protonodonorową, a alkohol grupą protonoakceptorową wiązania wodorowego. Wtedy energię oddziaływań wynoszą $E_{int,SiOH} = 45,3 \text{ kJ mol}^{-1}$ oraz $E_{int,SiO_2H_2} = 50,2 \text{ kJ mol}^{-1}$. Oznacza to, że z energetycznego punktu widzenia, takie oddziaływania są najstabilniejsze. Biorąc pod uwagę zmiany pasma $\nu_{CH\ aromatic}$ obserwowane w widmach IR i Ramana, została obliczona także energia możliwych oddziaływań typu π - π , tj. oddziaływań typu *sandwich* oraz *T-shape*, których wartości wynosiły odpowiednio $E_{int,sandwich} = 26,8 \text{ kJ mol}^{-1}$ i $E_{int,T-shape} = 16,4 \text{ kJ mol}^{-1}$. Symulacje potwierdziły występowanie oddziaływań typu π , które posiadały mniejsze wartości energii niż wiązania wodorowe, a dodatkowo stabilizowały energetycznie tworzącą się warstwę zaadsorbowanych molekuł.

3. PODSUMOWANIE

Niniejszy cykl publikacji dostarcza nowych informacji na temat asocjacji alkoholi monohydroksylowych, w tym przypadku alkoholi fenylowych oraz cykloheksylowych poprzez analizę wpływu zmian w strukturze chemicznej, oddziaływań międzycząsteczkowych, temperatury, zawady sterycznej, czy wykorzystania ograniczenia geometrycznego. Dodatkowo, podjęty został temat zjawiska nieodwracalnie tworzącej się warstwy, do tej pory opisywanej w przypadku układów ograniczonych przestrzennie jedno- lub trójwymiarowo.

Jak pokazały przeprowadzone systematyczne badania przy użyciu różnych technik eksperymentalnych, długość łańcucha alifatycznego może wpływać na asocjację alkoholi fenylowych. Wyniki pokazują, iż wraz ze wzrostem grup metylenowych w łańcuchu, występują nieliniowe zmiany we właściwościach strukturalnych, spektroskopowych, termicznych, dielektrycznych i powierzchniowych badanych układów. Co interesujące, skrajne wartości tych właściwości obserwowano dla alkoholi w środku serii długości łańcucha, co wskazuje na znaczącą zmianę w mechanizmie asocjacji molekuł. Najbardziej jednolity pod względem sił wiązań wodorowych był 3F1P (porównanie szerokości pasm ν_{OH}), a następnie obserwowano wzrost heterogeniczności dla dalszych układów, co wskazuje na znaczący wpływ oddziaływań dyspersyjnych, co dodatkowo potwierdziły badania dielektryczne. Niewątpliwie rolę w asocjacji cząsteczek odgrywała także odległość grupy hydroksylowej od pierścienia aromatycznego. Jak wskazują rosnące z wydłużeniem łańcucha alkilowego wartości stopnia asocjacji oraz energii aktywacji procesu dysocjacji, molekuły „dłuższych” alkohole lepiej ze sobą oddziałują (asocjują).

Porównanie zachowania alkoholi aromatycznych z ich cykloheksylowymi odpowiednikami wskazały na znaczące różnice między dwiema grupami alkoholi ujawniając różnice w strukturach tworzących się wiązań wodorowych. Badania strukturalne, spektroskopowe oraz dielektryczne sugerują, że zamiana pierścienia aromatycznego na cykloheksylowy prowadzi do znaczących różnic w sile i populacji tworzących wiązań wodorowych – cykliczne alkohole lepiej asocjują. Ogólnie ujmując, przeprowadzone badania, przyczyniły się do lepszego zrozumienia asocjacji materiałów i korelacji między wiązaniem wodorowym a strukturą chemiczną.

W kolejnym etapie, wprowadzono alkohole fenyłowe w natywne i silanizowane krzemionkowe mezopory ($d = 5$ nm) celem określenia wpływu ograniczenia przestrzennego, a w szczególności jak oddziaływania międzycząsteczkowe wpływają na zachowanie badanych układów. Jak się okazało, dochodziło do zmian w procesie asocjacji molekuł w porównaniu do materiałów litych. Alkohole fenyłowe w mezoporach charakteryzowały się obecnością dwóch

przejsć szklistych. Co interesujące, ujawnił się dodatkowy proces relaksacji, szczególnie zauważalny w przypadku dłuższych łańcuchów alifatycznych, którego pochodzenie molekularne pozostaje niejasne. Widoczna całkowita asocjacja w przypadku układów litych została zahamowana w krzemionkowych matrycach, a obliczone wartości energii asocjacji były niższe niż ich lite odpowiedniki. Obserwowane zmiany tłumaczone zostały tworzeniem dodatkowej warstwy międzyfazowej, wpływającej na zachowanie alkoholi. Odkrycia te, przyczyniły się do zwiększenia naszej świadomości na temat asocjacji cieczy w ograniczeniu przestrzennym.

Ostatni etap prac skupił się na badaniach nierozdzielnie zaadsorbowanej warstwy molekuł alkoholi fenylowych w krzemowych matrycach porowatych. W wyniku przeprowadzenia procesu odparowania, monitorowanego za pomocą spektroskopii w podczerwieni, udało się usunąć z układu molekuły warstwy rdzeniowej, tym samym ujawniając warstwę przyściankową. Uzyskane "szczątkowe" widmo IR w wysokim zakresie liczb falowych charakteryzowało się nową subtelną strukturą w porównaniu do tej w alkoholach litych i ograniczonych przestrzenie. Zaobserwowane zmiany sugerowały różnice w ułożeniu zarówno wolnych, jak i związanych grup OH, co wynikało z tworzenia się warstwy cząsteczek zaadsorbowanych na ściankach porów. Eksperymentalne wyniki zostały potwierdzone przez symulacje dynamiki molekularnej, które także wskazywały na tworzenie się silnie zaadsorbowanej warstwy tworzącej się poprzez wiązania wodorowej, dodatkowo stabilizowanej przez oddziaływania π - π . Nowatorskie podejście pozwoliło nam na odkrycie silnie związanych warstw cząsteczek alkoholi w membranach porowatych charakteryzujących się podobnymi właściwościami do warstw badanych w cienkich warstwach czy nanocząstkach krzemowych.

Podsumowując, niniejsza rozprawa doktorska dostarcza nowych i interesujących danych dotyczących asocjacji alkoholi monohydrosyloowych. Zawartej w niej wyniki są interesujące, a mianowicie, skupiają się na słabo badanej grupie alkoholi, tj. alkoholi fenylowych, dla których dotychczasowa wiedza o asocjacji tych molekuł dostarcza sprzecznych informacji. Praca doktorska pokazuje jak wiele czynników wpływa na możliwość agregacji cząsteczek. Ważnym aspektem jest wskazanie wpływu długości łańcucha oraz zawady sterycznej. Co istotne, dynamika ograniczonych przestrzenie alkoholi różniła się od materiałów litych, a szczególnym osiągnięciem jest eksperymentalne potwierdzenie tworzenia się nieodwracalnie zaadsorbowanej warstwy dla materiałów w ograniczeniu 2D. Przeprowadzone badania są niezwykle ważne z punktu widzenia rozszerzenia naszej wiedzy o oddziaływaniach międzycząsteczkowych, zjawiska asocjacji i wpływu ograniczenia przestrzennego, a

dodatkowo mogą wspomóc badania istotne z punktu widzenia projektowania nowych materiałów.

4. TREŚCI ARTYKUŁÓW STANOWIĄCYCH PODSTAWĘ ROZPRAWY DOKTORSKIEJ WRAZ Z OŚWIADCZENIAMI WSPÓŁAUTORÓW

P1. The Impact of the Length of Alkyl Chain on the Behavior of Benzyl Alcohol Homologues – the Interplay between Dispersive and Hydrogen Bond Interactions

Autorzy: N. Soszka, B. Hachuła, M. Tarnacka, E. Kamińska, J. Grelska, K. Jurkiewicz, M. Geppert-Rybczyńska, R. Wrzalik, K. Grzybowska, S. Pawlus, M. Paluch, K. Kamiński

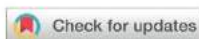
Referencja: *Phys. Chem. Chem. Phys.* 2021, 23 (41), 23796 – 23807

DOI: 10.1039/D1CP02802B

Impact Factor czasopisma: 3.945

Liczba punktów ministerialnych MNiSW czasopisma: 100

Mój udział polegał na przygotowaniu próbek, wykonaniu pomiarów IR i analizie wyników, dyskusji wyników, współtworzenia manuskryptu (przeprowadzenie przeglądu literaturowego, przygotowanie tekstu manuskryptu i rysunków, opis wyników i sformułowanie wniosków), formułowaniu odpowiedzi na uwagi recenzentów oraz korekcie manuskryptu po otrzymanych recenzjach.

Cite this: *Phys. Chem. Chem. Phys.*,
2021, 23, 23796

The impact of the length of alkyl chain on the behavior of benzyl alcohol homologues – the interplay between dispersive and hydrogen bond interactions†

N. Soszka,^{ab} B. Hachuta,^{ab*} M. Tarnacka,^{bc} E. Kamińska,^{bd} J. Grelska,^{bc}
K. Jurkiewicz,^{bc} M. Geppert-Rybczyńska,^a R. Wrzalik,^{bc} K. Grzybowska,^{bc}
S. Pawlus,^{bc} M. Paluch^{bc} and K. Kamiński^{bc}

In this work, we examined the effect of the length of alkyl chain attached to the benzene ring on the self-assembling phenomena for a series of phenyl alcohol (PhA) derivatives, from phenylmethanol (benzyl alcohol) to 7-phenyl-1-heptanol, by means of X-Ray Diffraction (XRD), Differential Scanning Calorimetry (DSC), Fourier Transform Infrared (FTIR) spectroscopy, and Broadband Dielectric Spectroscopy (BDS) methods. XRD data in the reciprocal and real spaces showed a gradual increase in the local order with the elongation of the alkyl chain. However, the position and full width at half maximum of the main diffraction peak exhibited a non-systematic behavior. To better understand this fact, PhAs were subjected to FTIR spectroscopic studies. These investigations revealed that the association degree and the activation energy of dissociation increase as the alkyl chain length grows. On the other hand, BDS data showed a non-monotonic variation in the Kirkwood correlation factor with increasing length of the alkyl chain, indicating a competition between interactions of the non-polar and polar parts of the molecules in the studied PhAs. Finally, it was also found that the molar surface entropy for PhAs increases with the number of methylene groups, approaching values reported for alkanes, which indicates suppression of the surface order for PhAs with a long alkyl chain. This variability of the various parameters as a function of the length of the side chain shows that the interplay between soft interactions has a strong impact on the local structure and intra and intermolecular dynamics of the studied PhAs.

Received 21st June 2021,
Accepted 27th September 2021

DOI: 10.1039/d1cp02802b

rsc.li/pccp

Introduction

In nature, there are few fundamental noncovalent molecular bonds: (i) the purely electrostatic Coulomb ones occurring in ionic systems, (ii) hydrogen bonding, and (iii) van der Waals interactions, in which electrostatic forces also play an important role. The character of the interactions has a strong influence on

the physicochemical properties of a given system, as well as on their self-association ability. In fact, in some particular systems, having characteristic structural motifs – such as coupled aromatic rings, long aliphatic chains or functional hydroxyl, amine, carbonyl, and thiol moieties, molecules tend to organize in supramolecular clusters due to the interactions that are of hydrophilic (polar units) or hydrophobic (aromatic rings, aliphatic chains) nature. In many compounds, the competition between these interactions has a significant impact on the mechanism of a wide variety of processes, including micelle formation, vesicles, and bilayer organization, or protein folding.^{1–4} It was found that the contributions of the hydrophobic interactions (HIs) in driving important processes, like the double-helix formation of DNA and the aqueous dissolution of cellulose, are dominating, whereas the net contribution from H-bonds (HBs) is small.⁵ There are numerous other processes in various chemical disciplines, which also depend strongly on HIs, *i.e.*, complexation, surfactant aggregation, coagulation, and chemical reactivity (HIs induce significant rate enhancements, including the

^a Institute of Chemistry, University of Silesia in Katowice, Szkolna 9
40-006 Katowice, Poland. E-mail: barbara.hachula@us.edu.pl

^b August Chełkowski Institute of Physics, University of Silesia in Katowice,
75 Pałku Piechoty 1, 41-500 Chorzów, Poland

^c Silesian Center for Education and Interdisciplinary Research, 75 Pałku Piechoty
1a, 41-500 Chorzów, Poland

^d Department of Pharmacognosy and Phytochemistry, Faculty of Pharmaceutical
Sciences in Sosnowiec, Medical University of Silesia in Katowice, Jagiellońska 4,
41-200 Sosnowiec, Poland

† Electronic supplementary information (ESI) available: Additional figures and tables, including the results of density, refractive index, and surface tension measurements, together with additional FTIR and CHelpG charge analysis. See DOI: 10.1039/d1cp02802b

Diels–Alder reaction, 1,3-dipolar cycloaddition, and the Claisen rearrangement).^{6,7}

Amphiphilic compounds, containing both hydrophobic and hydrophilic components, are model systems for studying the subtle interplay between both fundamental types of intermolecular interactions.⁸ This class of materials is well represented by the alcohols since they contain both a polar head (hydroxyl) group, which mainly determines the dipole moment of a molecule, and a non-polar part in the form of hydrophobic hydrocarbon structures. Thus, the self-assembly properties of alcohols can be tuned by choice of a specific hydrophobic skeleton (one or more alkyl chains differing in length and/or branching, the aromatic/non-aromatic ring substituents), and the number of hydroxyl moieties. By controlling the molecular structure of the hydrophobic and hydrophilic units, one can modify the interplay between HBs and HIs, and, consequently, molecules of alcohols can associate into nanoassemblies with various sizes and morphologies. According to ref. 9, the degree of self-association of aliphatic 1-alcohols, from methanol to 1-decanol, decreases with an increase in the chain length because of the growing meaning of the interactions between them. It was found that these kinds of forces for butyl alcohol and higher 1-alcohols are more important than the O–H···O–H interactions. As a result, methanol, ethanol, and 1-propanol have unlimited miscibility with water, whereas 1-butanol and higher 1-alcohols are characterized by much lower solubility in this solvent. What is more, *ab initio* molecular dynamics simulations revealed that the HB's geometry, arising from intermolecular O–H···O interactions in liquid monohydroxy alcohols, shows little change with an increase in the size of the alkyl group.¹⁰ In contrast, the departures in the H–O···O angle from linearity are seen with the increase in the alkyl chain, going from methanol to pentanol, in the crystalline state. Thus, it is interesting whether modifying the alcohol by introducing a hydrophobic phenyl group(s) into its backbone and side-chain can influence the architecture of the nanoassociates.

One can find many papers devoted to the understanding of the steric hindrance of the phenyl moiety on the self-association of alcohols, in which two opposite concepts are presented. On the one hand, it is reported that the steric effect significantly prevents the formation of an H-bonded network, hindering the association of molecules in the liquid phase.^{11–14} On the other hand, Böhmer *et al.* showed that HBs are not generally suppressed by the steric hindrance of the phenyl ring, but rather the equilibrium of the ring and chain-like structures is shifted towards the ring-like ones as the phenyl ring and the hydroxyl group get closer to each other.¹⁵ Our previous paper revealed a relationship between the self-association ability of butanol isomers (aliphatic and their phenyl counterparts) and their molecular geometry (the hydroxyl group location within the carbon skeleton).¹⁶ Based on the diffraction and spectroscopic results, we detected a clear difference in the dynamic and static properties between primary and secondary alcohols, independent of the steric hindrance posed by the phenyl moiety. What is important, there are no works on the effect of the chain length on the H-bonding interactions of phenyl alcohols (PhAs). To systematically examine how the H-bond

network of PhAs is affected by the increasing size of the hydrophobic group, linear (primary) monohydroxy alcohols, from phenylmethanol (benzyl alcohol) to 7-phenyl-1-heptanol, were investigated. The studied alcohols have the same hydrophilic O–H group located at the end of the alkyl chain, but the length of the hydrophobic alkyl chain increases from one to seven carbon atoms. Among the large variety of experimental techniques used to study HIs and HBs, four different methods were used to investigate the self-assembling process occurring in these PhAs, *i.e.*, X-Ray Diffraction (XRD), Differential Scanning Calorimetry (DSC), Fourier Transform Infrared (FTIR) spectroscopy, and Broadband Dielectric Spectroscopy (BDS). Moreover, the properties of the surface layers of these PhAs were analyzed using the pendant drop method.

Materials and methods

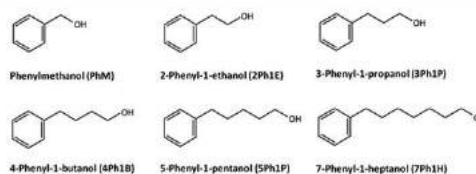
The PhAs ($C_nH_{2n+1}OH$, $n = 1–5, 7$) under investigation, with a purity higher than 98%, were purchased from Sigma-Aldrich. Prior to use, the alcohols were dehydrated to remove water by freezing them in liquid nitrogen. The chemical structures of the studied alcohols are shown in Scheme 1.

Broadband dielectric spectroscopy (BDS)

BDS measurements were carried out on heating after fast quenching of the liquid state in a wide range of temperatures (173–303 K) and frequencies (10^{-1} – 10^6 Hz) using a Novocontrol spectrometer, equipped with an Alpha Impedance Analyzer with an active sample cell and Quatro Cryosystem. The samples were placed between two stainless-steel electrodes (diameter: 15 mm, gap: 0.1 mm) and mounted inside a cryostat. During the measurement, each sample was maintained under a dry nitrogen gas flow. The temperature was controlled with Quatro Cryosystem using a nitrogen gas cryostat, with a stability better than 0.1 K.

Differential scanning calorimetry (DSC)

Calorimetric measurements were carried out using Mettler-Toledo DSC apparatus equipped with a liquid nitrogen cooling accessory and an HSS8 ceramic sensor (heat flux sensor with 120 thermocouples). Temperature and enthalpy calibrations were performed by using indium and zinc standards. The sample was prepared in an open aluminum crucible (40 μ L) outside the DSC apparatus. Samples were scanned at various temperatures at a constant heating rate of 10 K min^{-1} .



Scheme 1 The chemical structures of the PhAs under investigation.

X-ray diffraction (XRD)

XRD measurements were carried out on a Rigaku Denki D/Max Rapid II diffractometer equipped with a rotating Ag anode, an incident beam graphite (002) monochromator, and a 2D imaging plate detector. The system operates in Debye–Sherrer geometry. All PhAs were measured at room temperature (293 K), and additionally, 2Ph1E, 3Ph1P, 4Ph1B and 5Ph1P at the glass transition temperature, T_g , whereas PhM and 7Ph1H were measured at temperatures just before (223 and 253 K, respectively) and after crystallization (213 and 243 K, respectively). The temperature was controlled by Oxford Cryostream Plus and Compact Cooler. The collected two-dimensional diffraction patterns were corrected for background and converted into one-dimensional intensity data versus the scattering vector, according to the formula: $Q = 4\pi(\sin \theta)/\lambda$, where 2θ is the scattering angle and the wavelength of the incident beam, λ , is equal to 0.56 Å. The low- Q XRD data in the range of 1.1–1.55 Å⁻¹ were fitted with pseudo-Voigt functions to determine the main diffraction peak positions, and full widths at half maximum, FWHMs. Then the $I(Q)$ intensity functions obtained at 293 K for each sample were corrected for polarization, absorption, incoherent Compton scattering, and normalized to the electron units and transformed to the structure factor $S(Q) = \frac{I_{\text{coh}}(Q) - (\langle f(Q)^2 \rangle - \langle f(Q) \rangle^2)}{\langle f(Q) \rangle^2}$, where: $I_{\text{coh}}(Q)$ is the coherently scattered intensity normalized to electron units, $\langle f(Q)^2 \rangle = \sum_{i=1}^n c_i f(Q)_i^2$, $\langle f(Q) \rangle = \sum_{i=1}^n c_i f(Q)_i$, c_i and $f(Q)_i$ are the concentration and the atomic scattering factor of the i -th atomic species, respectively, and n is the number of atomic species in the sample. Finally, the diffraction data in reciprocal space were converted to a real space representation in the form of the atomic pair distribution function $\text{PDF}(r) = \frac{2}{\pi} \int_0^{Q_{\text{max}}} Q[S(Q) - 1]W(Q)\sin(Qr)dQ$, where Q_{max} indicates the maximum value of Q achieved in the experiment (here $Q_{\text{max}} = 20 \text{ \AA}^{-1}$) and $W(Q) = \sin(\pi Q/Q_{\text{max}})/(\pi Q/Q_{\text{max}})$ is the Lorech function used to minimize truncation oscillations.

Fourier transform infrared (FTIR) spectroscopy

FTIR spectroscopy measurements were carried out using a Thermo Scientific Nicolet iS50 spectrometer in two temperature ranges: 173–373 K for 2Ph1E, 3Ph1P, 4Ph1B, and 5Ph1P, and 243–373 K for PhM and 7Ph1H due to their crystallization. The frequency region included 4000–400 cm⁻¹. Each spectrum was an average of 16 scans recorded at a resolution of 2 cm⁻¹. The temperature-dependent FTIR measurements were performed using a Linkam THMS 600 stage, which controls the temperature with the accuracy of ±0.1 K. The spectra were collected applying the rate of 5 K min⁻¹. PhAs were placed between the two CaF₂ windows, separated by the 5 μm thick spacer to maintain the desired thickness and the constant geometry. To execute the deconvolution process of the OH stretching vibration bands, MagicPlot software was utilized (version 2.9.3, MagicPlot Systems LLC, Saint Petersburg, Russia).

The deconvolution turned out to be a three-step process. First, a band occurring between 4000–3150 cm⁻¹ was fitted using two Gaussian functions to obtain values for the total intensity of the associated OH groups. Second, the fitted band was subtracted from the original spectrum to then conduct the fitting for the non-bonded OH moieties in the range 3700–3500 cm⁻¹, also using the Gaussian function.

Surface tension measurements

Density (necessary for surface tension measurements by the pendant drop method) was measured by means of an Anton Paar DMA 5000M densimeter. The standard uncertainties are $u(p) = 1 \times 10^{-2}$ MPa and $u(T) = 0.01$ K, and the combined expanded uncertainty of the density is $u(\rho) = 5 \times 10^{-4}$ g cm⁻³ (at 0.95 confidence level ($k \approx 2$)). These measurements were performed in the temperature range $T = 283.15$ – 323.15 K, with a step of 10 K and at 298.15 K in order to find the density at temperatures below 273.15 K but above the melting point of any liquid. However, for 7Ph1H the density values for surface tension measurements were estimated based on the literature value at 293 K (0.9619 g cm⁻³) (0.9584 g cm⁻³ at 298.15 K, 0.9689 g cm⁻³ at 283.15 K and 0.9796 g cm⁻³ at 267.85 K).¹⁷ The density of all substances is presented in Fig. S1a (see the ESI†). The surface tension was measured with the DSA (Drop Shape Analyzer) 100S Krüss Tensiometer (with Advance Software) using the pendant drop method. The instrumental details and experimental procedures have been described previously.^{18,19} The temperature range was 298.2–266.6 K with variable steps, and the number of experimental T points was from 3 to 6. The general uncertainty of the method was 0.2 mN m⁻¹, but in our case, the standard deviation of the mean value (from 7–10 points) was below 0.5 mN m⁻¹. Taking into account the instrument standard uncertainty and the standard uncertainties in pressure, $u(p) = 1 \times 10^{-2}$ MPa, temperature and $u(T) = 0.1$ K and density, $u(\rho) = 5 \times 10^{-4}$ g cm⁻³, the average combined expanded uncertainty $u(\gamma)$ (at the 0.95 level of confidence, $k = 2$) was also at this level.

Refractive index measurements

The refractive index measurements, n , of the studied liquids were carried out using a Mettler Toledo refractometer RM40 in the temperature range 293–343 K. The temperature stability controlled with the aid of a built-in Peltier thermostat was better than 0.1 K. The light source is a light-emitting diode, the beam of which passes through a polarization filter, an interference filter (589 nm), and various lenses before it reaches the sample *via* the sapphire prism characterized by high thermal conductivity. The measurements of n were performed with a resolution of 0.0001. Values of n measured at 303 K are listed in Table 1; on the other hand, their temperature dependences are presented in Fig. S1b (ESI†). Note that the values of n used to calculate the Kirkwood factor at $T_g + 10$ K were estimated according to the linear fit of the measured data shown in Fig. S1b (ESI†).

Density functional theory (DFT) computations

The quantum chemical charges were calculated using the Mulliken population analysis and the CHelpG potential based

Table 1 Molar mass (M) of the examined PhAs, glass transition temperature (T_g , determined from calorimetric and dielectric measurements), as well as values of the stretched exponent (β_{KWW}), dipole moment (μ , obtained from DFT calculations), refractive index (n , measured at 303 K), and the Kirkwood factor (g_k , calculated at 225 K and at $T = T_g + 10$ K)

Sample	M [g mol ⁻¹]	$T_{g,\text{DSC}}$ [K]	$T_{g,\text{DSC}}$ [K] for $\log_{10}\tau = 100$ s	β_{KWW}	g_k at $T_g + 10$ K	g_k at 225 K	μ [D]	n at 303 K
PhM	108.14	—	—	—	—	2	1.393	1.536
2Ph1E	122.16	184 ± 1	180 ± 1	0.80 ± 0.1	3.25	2.8	1.597	1.529
3Ph1P ¹⁵	136.19	182 ± 1	179 ± 1	~0.95 ± 0.1	3.3	3	1.725	1.523
4Ph1B ¹⁹	150.22	181 ± 1	177 ± 1	0.91 ± 0.1	2.4	2.1	1.576	1.517
5Ph1P	164.24	182 ± 1	174 ± 1	0.90 ± 0.1	1.5	1.3	1.734	1.512
7Ph1H	192.30	—	—	—	—	—	1.544	1.504

method with the Gaussian09 package using the standard B3LYP/6-311G(d) model with the Opt = Tight option.²⁰

Results and discussion

To gain access to the structural behavior of the studied PhAs containing the phenyl group and differentiated in terms of the alkyl chain length, their XRD patterns were collected at two different temperatures (see Fig. 1a). PhM crystallized at ~215 K on cooling at a rate of ~5 K min⁻¹. It has already been reported in the literature that PhM crystallizes in a monoclinic $P2_1$ space group and forms double molecular chains bonded by a strong O-H...O hydrogen bond along the c -axis and a surrogate C-H... π interaction along the b -axis in the crystalline phase.²¹ Interestingly, the shape of the XRD data for the liquid PhM at 293 and 223 K resembles a broadened pattern of the crystalline phase (see the bottom panel in Fig. 1a). One can see the main amorphous halo at ~1.3 Å⁻¹, but also a weak pre-peak at ~0.6 Å⁻¹ and a shoulder at ~1.7 Å⁻¹. The pre-peak may

correspond to the residue of the (001) reflection of the crystalline phase while the shoulder appears at the position of the (012), (003) and (11-1) Bragg peaks for the crystal. It is also worth mentioning that the appearance of a pre-peak at a low scattering vector range in various alcohols is generally interpreted as the existence of clusters of molecules self-assembled *via* HBs, leading to the medium-range order.^{22,23} Therefore, it can be assumed that liquid PhM inherits to some extent the intermolecular arrangement and the H-bonding motif from its crystalline phase, forming supramolecular clusters.

Interestingly, the diffraction data of other alcohols show that as the alkyl chain gets longer, the pre-peak vanishes and the amplitude of the main peak increases. Moreover, the right-side shoulder also disappears, and the shape of the main peak becomes more symmetrical. For 4Ph1B and other alcohols with longer chain lengths, the XRD patterns look typical for 'ordinary' liquids, with only one diffuse amorphous halo. At lower temperatures, diffractograms for all samples shift towards higher Q -values, which is a classic temperature effect. 7Ph1E crystallized on cooling at ~243 K (see the upper panel in Fig. 1a). However, the behavior of

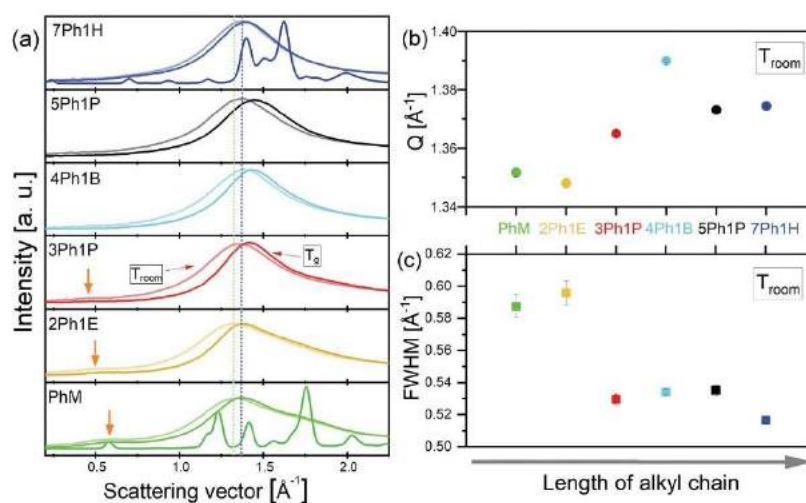


Fig. 1 XRD patterns of the studied PhAs at room and lower temperatures (a). The changes in the main peak position, Q , (b) and the full width at half maximum, FWHM, (c) at 293 K as a function of the alkyl chain length of the PhAs.

7Ph1E is different when compared to PhM as the shape of the diffraction pattern for 7Ph1E in the liquid phase does not resemble that registered for the crystal.

As for the interesting pre-peak feature being a fingerprint of supramolecular clusters in alcohols, we observe, in fact, a very weak bump only for PhAs with short alkyl tails up to $n = 3$. In the literature, the behavior of the pre-peak intensity as a function of alkyl chain length is intensively investigated for various series of compounds. However, usually the opposite trend is observed, namely an increase of the pre-peak amplitude with elongation of the alkyl chain, e.g., for monohydroxy alcohols and diols,^{24,25} as well as ionic liquids.^{26–28} In the case of the former group of compounds, it was explained that it arose due to the better chain-like association of molecules and the increase in the size of chain-like clusters with increasing alkyl chain length. However, in the case of diols it was possible to separate out the pre-peak feature only in the theoretical scattering function from computer simulations, while in experimental diffraction data, the pre- and main peaks were smeared into a single feature. Therefore, based on only cursory experimental diffraction data, it is difficult to tell if specific clusters can appear and describe them quantitatively. The pre-peak is a complex feature arising due to interplay between correlations and anti-correlations of the atom–atom structure factors and its behavior cannot be understood without a model-based investigation. It was nicely presented by Požar *et al.*²² for a series of linear $\text{OH}(\text{CH}_2)_n\text{CH}_3$ alkanols from methanol to 1-nonanol. They showed that for longer alkanols, the alkyl tails are strongly anti-correlated with the head OH groups, influenced by the ordering of the alkyl tail groups and the micro-segregation, contributing negatively to the

pre-peak. Therefore, the absence of the pre-peak in the experimental XRD data for the studied herein PhAs with long alkyl tails does not mean they exhibit no supramolecular ordering. Požar *et al.*²² also noticed a crossover phenomenon for $n = 4$ as a direct consequence of increasing the flexibility of alkyl tails with increasing their length and cancellation of atom–atom contributions to the total structure factor, evidenced as the increase in the pre-peak intensity up to $n = 4$ and then the decrease with the elongation of the alkyl tail.

Here the analysis of the pre-peak parameters is not feasible due to its very low amplitude. However, following the position and the FWHM of the main diffraction peak for data measured at 293 K, presented in Fig. 1b and c, we can also notice that they behave in a non-systematic way with the elongation of the alkyl chain. In turn, the amplitude of the main peak increases systematically, which can be more clearly seen from the comparison of the structure factors shown in Fig. 2a. The increase of the local intermolecular order as a function of the alkyl chain's length is also witnessed by the increase of the amplitude of the PDF(r) peaks, as can be seen in Fig. 2b. To provide more information on the supramolecular structuring in these PhAs, further FTIR and BDS studies were carried out.

Moreover, using the FTIR absorption technique, we have studied the perturbation of the H-bonded supramolecular network in PhAs due to the hydrophobic effects arising from the side chain. We performed studies in a wide range of temperatures (see all the spectra in Fig. S2 in the ESI†). A comparison of the FTIR spectra in the OH and CH stretching frequency ranges, collected at $T_{368\text{K}}$, $T_{293\text{K}}$ and T_{room} , is shown in Fig. 3. At $\sim 3300\text{ cm}^{-1}$ the broad band corresponding to the stretching

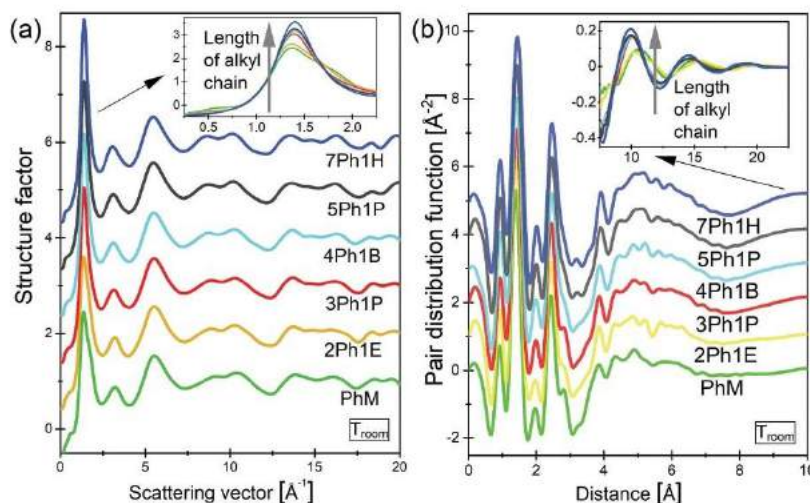


Fig. 2 Structure factors of the studied PhAs at room temperature (a); the data is rounded-up by a value of 1 for clarity. The inset shows the comparison of the main peak region. The corresponding atomic pair distribution functions for the short-range correlations are shown in (b); the data is rounded-up by a value of 1 for clarity. The inset shows a longer range of intermolecular correlations.

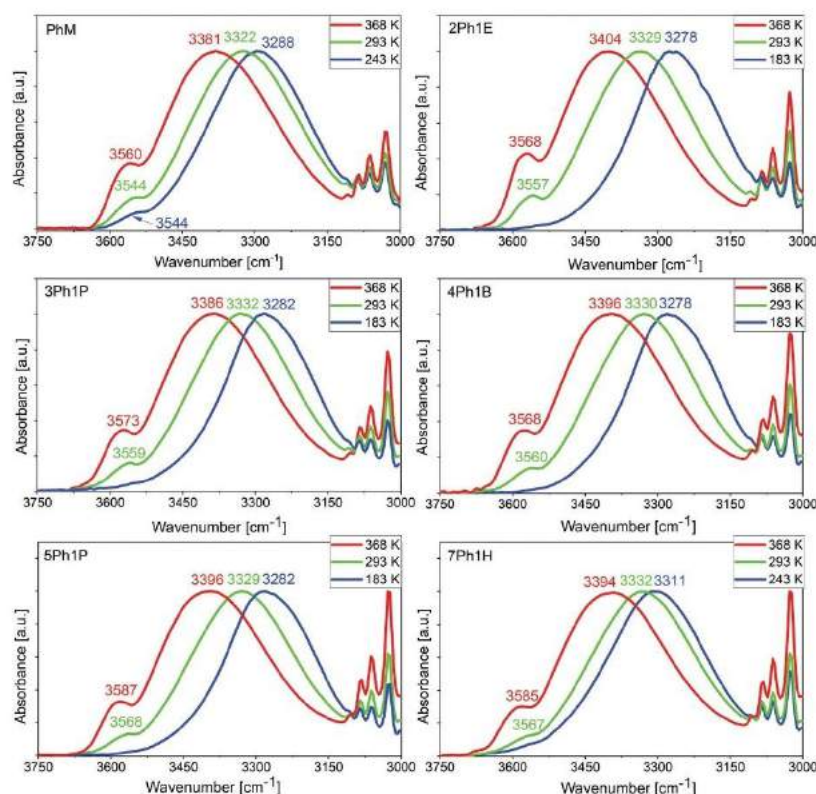


Fig. 3 Infrared spectra of PhAs in the 3750–3000 cm^{-1} frequency range, measured at 368 K (red line), 293 K (green line), and 183 K (blue line); for PhM and 7Ph1H, the blue line indicates the temperature of 243 K (just before crystallization). The presented spectra were normalized to the intensity maximum of the OH band.

vibration of H-bonded OH groups ($\nu_{\text{OH,assoc}}$) can be observed. Additionally, the peak of small intensity at $\sim 3570\text{--}3540\text{ cm}^{-1}$ is detected. It is assigned to the non-H-bonded OH groups ($\nu_{\text{OH,free}}$), which was also confirmed by measuring the IR spectra of PhAs in various organic solvents (Fig. S3, ESI†). The bands located in the 3150–2750 cm^{-1} region are related to the stretching vibrations of the CH groups (Fig. S4 and S5; please see the ESI† for more details). Our results clearly show that with the increase of temperature the $\nu_{\text{OH,assoc}}$ band intensity, corresponding to the population of H-bonded OH moieties, decreases. At the same time, the intensity of the $\nu_{\text{OH,free}}$ band increases. This behavior indicates that at higher temperatures, the concentration of non-H-bonded molecules grows at the expense of H-bonded species. On the other hand, the lowering of temperature causes a red-shift of the OH band's wavenumber. This fact is connected to a decrease in the distance between O and H atoms, leading to strengthening of the O–H...O intermolecular bonds. Moreover, the integral

intensity of the $\nu_{\text{OH,assoc}}$ band grows during cooling, which is related to the increase in the number/amount of HBs. Additionally, the FWHM of the $\nu_{\text{OH,assoc}}$ decreases during the temperature drop, revealing that the H-bond network becomes more homogeneous. As mentioned before, PhM and 7Ph1H crystallize at lower temperatures. The spectral profiles of the ν_{OH} band recorded for them in the liquid and solid states are compared and discussed in the ESI† (Fig. S6).

Analyzing the spectral parameters of the OH band, one can presume that at $T_{293\text{K}}$ PhM creates the strongest HBs, based on the smaller value of the $\nu_{\text{OH,assoc}}$ band position ($\sim 3322\text{ cm}^{-1}$), while the strength of the HBs for the other PhAs is smaller ($\nu_{\text{OH,assoc}} \sim 3330\text{ cm}^{-1}$) and appears to be independent of the chain length. At T_g the alcohols with an even number of alkyl groups in the chain (2Ph1E, 4Ph1B) exhibit stronger HBs than those with an odd number (3Ph1P, 5Ph1P). This phenomenon, called “the odd–even effect”, describing an alternative alteration of material structures and/or properties depending on the odd/

even number of structural units in a molecule, is well-known in chemistry, physics, biology, and materials science.²⁰ Moreover, at T_g no sign of the $\nu_{\text{OH,free}}$ band is detected in all PhAs.

As can be seen from Table S1 (in the ESI[†]), the FWHM value of the $\nu_{\text{OH,assoc}}$ band at 293 K first decreases with the elongation of the alkyl chain from PhM to 3Ph1P, and then starts to increase to 7Ph1H. In detail, PhM at $T_{293\text{K}}$, and also at $T_{368\text{K}}$, has the broadest $\nu_{\text{OH,assoc}}$ band. Therefore, one can deduce that the close location of the OH group to the phenyl ring (the most significant steric hindrance) may be responsible for the biggest diversity and distribution of the HBs. On the other hand, 3Ph1P is characterized by the narrowest $\nu_{\text{OH,assoc}}$ band, indicating the greatest homogeneity of HBs in terms of the strength with respect to other PhAs. This suggests a change in the hydrogen bonding organization, going from short to longer alkyl chain PhAs.

For better insight into the behavior of the self-assembling PhAs during temperature changes, analysis of the integral intensity of the $\nu_{\text{OH,assoc}}$ and $\nu_{\text{OH,free}}$ bands at $T_{293\text{K}}$ and $T_{368\text{K}}$ was performed (Fig. 4a and b). It turned out that the longer the aliphatic chain, the more capable of the association the PhA is. The estimated percentage values of non-H-bonded hydroxyl moieties are presented in Table S1 (ESI[†]). PhM and 2Ph1E show the highest intensity of the $\nu_{\text{OH,free}}$ band, while the $\nu_{\text{OH,free}}$ band of 7Ph1H is characterized by the lowest intensity, indicating the smallest amount of non-H-bonded OH groups. This finding is in sharp contrast to aliphatic alcohols, where the degree of association *via* HBs decreases with the alkyl chain elongation due to the growing impact of dispersive interactions.⁹

Furthermore, we determined the activation enthalpy, E_a , for the dissociation process of PhAs to recognize how the chain-lengths of the PhAs modulate the hydrogen bond formation. A procedure for the calculations of the dissociation of alcohols is described, in detail, in the ESI[†]. It was found that E_a increases with the elongation of the aliphatic chain in PhAs from $\sim 9 \text{ kJ mol}^{-1}$ for PhM to $\sim 14 \text{ kJ mol}^{-1}$ for 7Ph1B (Fig. S7, S8 and Table S2, ESI[†]). This means that more energy is required to break the intermolecular interactions between molecules with a longer alkyl chain. This fact may be connected with the alkyl chain flexibility, which can influence the molecular

conformation, packing, and intermolecular interactions (the supporting C-H $\cdots\pi$, O-H $\cdots\pi$ and/or C-H \cdots O interactions) of the studied alcohols. On the other hand, the steric hindrance of the phenyl ring inhibits the formation of HBs between OH groups when the distance between them is small, *e.g.*, as in PhM. However, as the length of the aliphatic chain grows, the distance between the phenyl ring and OH unit increases, which allows the self-association of PhAs to a larger degree. This fact is consistent with the FTIR results since PhM exhibits the most prominent vibrational band related to non-associated OH groups, whereas for 7Ph1H this peak is the lowest.

Moreover, the FTIR study of PhAs dissolved in tetrachloride carbon (CCl_4) solutions was performed to examine the average number of H-bonded molecules in the supramolecular assemblies, n . As determined, the n value for the PhAs is equal to about 2-3, suggesting that the alcohol molecules associate as small aggregates, *i.e.*, in dimer or trimer forms (Fig. S9, ESI[†]).

Aside from these investigations, we also carried out additional Mulliken and CHelpG charges. The obtained calculated values of these charges are shown in Fig. S10 and Table S3 (ESI[†]).

We also measured the surface tension, γ , and calculated the surface entropy, S^s , as well as molar surface entropy, S_v . The estimated values of S^s , S_v , and γ at different temperatures are presented in Fig. S11-S14 and listed in Table S4 (ESI[†]). As found, the variation of γ for all investigated substances at 298.2 K does not exceed 2 mN m^{-1} . Thus, it is similar to alkyl alcohols, from methanol to 1-heptanol,^{30,31} but the direction of the changes in γ with the length of the alkyl chain in PhAs is reciprocal to those known for alkyl alcohols, namely PhAs with a longer alkyl chain are accompanied by a lower γ . However, the highest value of γ appears again for 2Ph1E which correlates with the findings from other methods. It should also be noted that the numerical values of γ for PhAs are almost two times higher than for alkyl alcohols³⁰ and higher than for benzene (28.18 mN m^{-1} at 298.15 K)³² (Fig. S12, ESI[†]). It seems that γ for PhAs resembles rather that obtained for phenol (40.50 mN m^{-1} at 301.15 K).³³ Much more interesting is the temperature dependence of γ , which can be used to calculate the S^s ($S^s = -\left(\frac{\partial \gamma}{\partial T}\right)_p$, $\text{mN m}^{-1} \text{ K}^{-1}$) and S_v ($S_v = -8.45 \cdot V_m^{2/3}$).

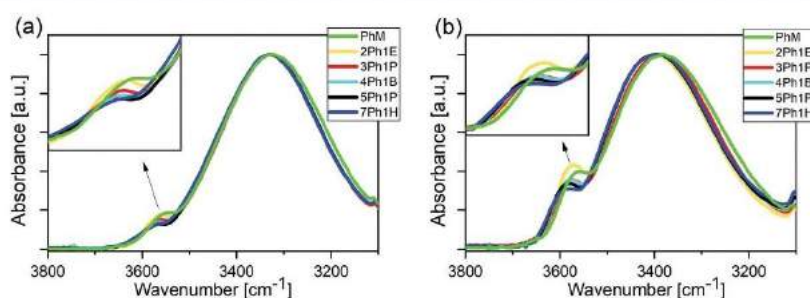


Fig. 4 FTIR spectra of the studied PhAs at (a) 293 K and (b) 368 K. The insets in panels (a) and (b) show enlargements of the stretching vibration band of non-bonded OH groups. The spectra were normalized to the OH stretching vibration intensity peak.

$\left(-\frac{\partial \gamma}{\partial T}\right)_p$, $\text{J K}^{-1} \text{mol}^{-1}$). The thermodynamic justification and interpretation of these quantities are given in detail in ref. 34–36. Both quantities given above are often discussed in relation to the surface order, but the molar surface entropy, S_s , being a measure of the entropy of the surface of a sphere containing 1 mole of molecules, can also be interpreted in terms of possible interactions, like hydrogen bonds.³⁸ The most probable value for many organic substances is around $20 \text{ J K}^{-1} \text{mol}^{-1}$ (in the presence of HBs), as for most of them, the primarily quantum effects derived from London dispersion forces are the most dominant in surface tension.³⁸ However, for alkyl alcohols (and here for PhAs), especially for short-chain representatives, S_s are lower which can indicate that the surface molecules of these substances are ordered similarly as in the bulk. What is more, it is suggested that molecules in these systems can be bunched together in a monolayer in the surface and hydrogen-bonded to the surface by their hydroxyl groups. This situation is opposed to alkanes having large S_s , suggesting their weak mutual attraction³⁸ and a loss in order on surface formation. For comparison, S_s for benzene is $21.81 \text{ J K}^{-1} \text{mol}^{-1}$, but for water it is $8.8 \text{ J K}^{-1} \text{mol}^{-1}$.³⁸ As observed, the S_s^a of PhAs increases with the elongation of the alkyl chain, whereas the S_s^a behavior for alkyl alcohols is the opposite. In this way, the S_s^a of 5Ph1P and 1-pentanol, as well as 7Ph1H and 1-heptanol, are very close (see Fig. S13, ESI†). The S_s value for PhAs and alkyl alcohols increases with the number of methylene groups and has similar values, which supports the idea of similarity between these two homologous series, despite the phenyl moiety in PhAs [Fig. S14, ESI†].

After XRD, FTIR, and γ investigations, we carried out BDS measurements to characterize the molecular dynamics of the PhAs systems. It is worth mentioning that the BDS experiment was not possible to perform for two PhAs, *i.e.*, PhM and 7Ph1H, due to their strong crystallization tendencies upon cooling. Representative dielectric loss spectra collected at temperatures higher than T_g for 2Ph1E and 5Ph1P are illustrated in Fig. 5. As can be observed, except for the dc-conductivity, one dominant relaxation mode, which shifts toward lower frequencies with decreasing temperature, can be detected in the presented spectra. Note that a similar scenario occurs in 3Ph1P¹⁵ and 4Ph1B.³⁰

In the inset of Fig. 5b, we have compared the dielectric spectra of 2Ph1E, 4Ph1B, and 5Ph1P, taken at the indicated T near T_g ($f_D \sim 5 \text{ Hz}$). At first sight, one can find that the shape of the peak is the same, regardless of the length of the alkyl chain in the considered PhAs. Indeed, by fitting the data to the one-sided Fourier transform of the Kohlrausch–Williams–Watts (KWW) function:^{37,38}

$$\Phi_{\text{KWW}}(t) = \exp[-(t/\tau)^{\beta_{\text{KWW}}}] \quad (1)$$

we determined the same stretched exponent, $\beta_{\text{KWW}} \sim 0.90$, for the studied alcohols (see Table 1). Note that the β_{KWW} reported in the literature for 5Ph1P (~ 0.95) is very similar to this value.¹⁵ Fitting of the KWW function to the dielectric data clearly indicated that the main process observed in the loss spectra of PhAs reveals the Debye-like (D) character ($\beta_{\text{KWW}} \approx 1$). This observation remains in agreement with recent reports on similar systems bearing a phenyl moiety in the structure. The small deviation of the loss peak from the Debye response is

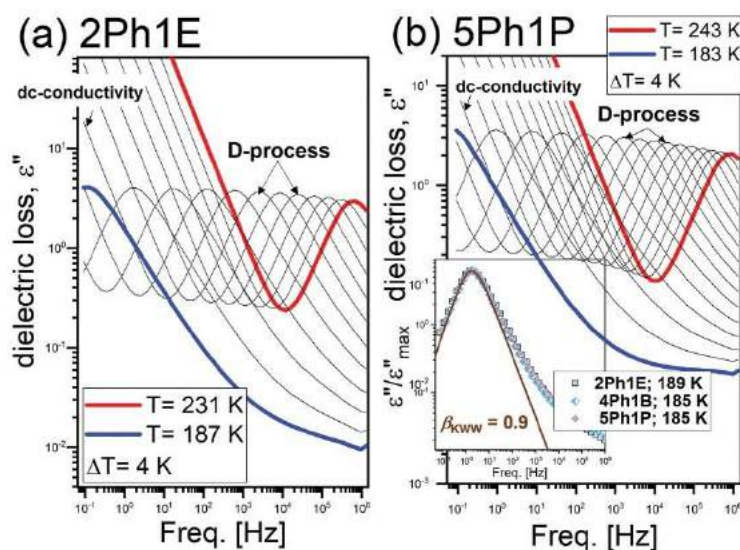


Fig. 5 Dielectric loss spectra of (a) 2Ph1E and (b) 5Ph1P measured above their glass transition temperatures. The inset of panel (b) shows the comparison of dielectric loss spectra at a constant τ_D near T_g .

discussed in the context of its heterogeneous nature. According to Böhmer *et al.*¹⁵ and Jurkiewicz *et al.*,³⁹ the structural and much more intense Debye processes contribute to the observed loss peak. However, due to the similar timescale of both processes in the loss spectra, only one relaxation peak is visible. As a consequence of this, we will refer to this peak as Debye-like in this paper.

Subsequently, to obtain relaxation times of the D-like process, τ_D , the loss spectra shown in Fig. 5 were analyzed with the use of the Havriliak–Negami (HN) function:⁴⁰

$$\tilde{\epsilon}(\omega) = \frac{\sigma_{DC}}{\epsilon_0 \omega} + \frac{\Delta\epsilon}{[1 + (i\omega\tau_{HN})^{\alpha_{HN}}]^{\gamma_{HN}}}, \quad (2)$$

where σ_{DC} is the dc-conductivity, ϵ_0 is the vacuum permittivity, ω is the angular frequency ($\omega = 2\pi f$), $\Delta\epsilon$ is the dielectric strength, and α_{HN} and γ_{HN} are shape parameters, while τ_{HN} is the HN relaxation time, which can be used to determine τ_D via the formula given in ref. 26. Note that due to such close proximity of the Debye and structural relaxation process resulting in the stretched exponent parameter equal to $\beta_{RWW} = 0.90$, the fitting procedure was performed using only one HN function, as the application of an additional mode provided unreliable and non-monotonic variation of the fitting parameters with the temperature for the structural process. This is why we skipped this kind of analysis of the dielectric data. The temperature dependences of $\log_{10}\tau_D$ for 2Ph1E and 5Ph1P, together with the same data taken from the literature for 3Ph1P¹⁵ and 4Ph1B,²¹ are presented in Fig. 6a. From fitting these curves to the

Vogel–Fulcher–Tammann (VFT) equation:⁴⁰

$$\tau_D = \tau_{VFT} \exp\left(\frac{D_T T_0}{T - T_0}\right), \quad (3)$$

where τ_{VFT} is the relaxation time at finite temperature, D_T is the strength parameter, while T_0 is the temperature, where τ_D goes to infinity; we calculated the glass transition temperature, T_g (defined as T at which $\log_{10}\tau_D = 2$). The obtained values are given in Table 1. As can be noted, they are similar to each other (the difference between T_g of the first (2Ph1E) and the last (5Ph1P) alcohol is equal to 6 K). Based on the above, one can conclude that the elongation of the alkyl chain in the studied PhAs does not significantly affect the glass transition temperature. It should be noted that additional calorimetric measurements carried out on 2Ph1E, 3Ph1P, 4Ph1B, and 5Ph1P (see Fig. 6c and Table 1) confirmed the results of the dielectric studies unambiguously. Note that the values of $T_{g,DSC}$ (changing in the range 181–184 K), were a few Kelvins higher than those determined from BDS investigations ($T_{g,BDS}$). This results from the fact that the position of the structural relaxation is probably slightly shifted compared to dominating the Debye process.

Finally, to answer the question of whether there is any variation in the local molecular arrangement in the studied alcohols, we calculated the Kirkwood correlation factor (g_k). For this purpose, the following equation was applied:⁴¹

$$g_k = \frac{9k_B\epsilon_0 MT(\epsilon_s - \epsilon_\infty)(2\epsilon_s + \epsilon_\infty)}{\rho N_A \mu^2 \epsilon_s (\epsilon_\infty + 2)^2} \quad (4)$$

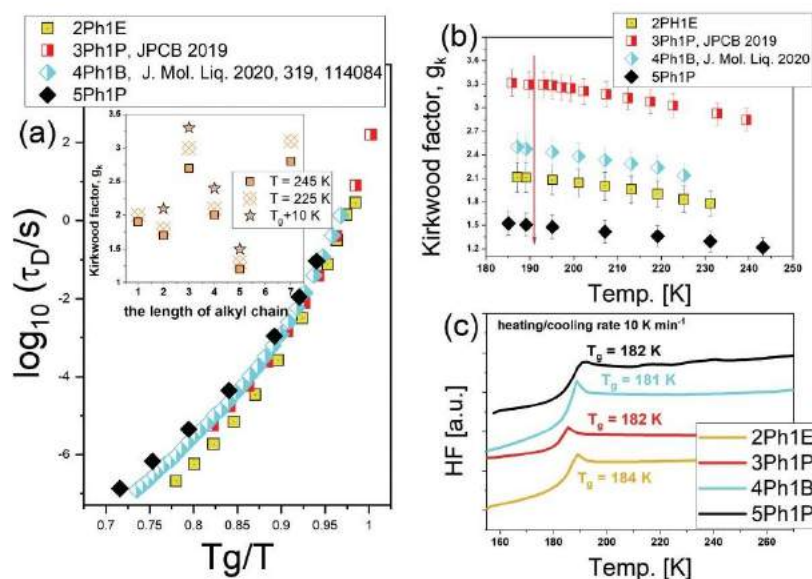


Fig. 6 (a) Temperature dependences of the Debye relaxation times, τ_D , determined for the examined PhAs, plotted as a function of T_g/T . (b) Temperature dependences of the Kirkwood factor, g_k , together with error bars. (c) DSC thermograms collected for the indicated PhAs. The inset in panel (a) shows the values of g_k , determined at the indicated temperature conditions plotted as a function of the length of the alkyl chain of the examined PhAs.

where k_B is the Boltzmann constant ($\sim 1.38 \times 10^{-23} \text{ m}^2 \text{ kg s}^{-2} \text{ K}^{-1}$), M is the molar mass, ρ is the density, N_A is Avogadro's number ($\sim 6.022 \times 10^{23}$), μ is the molecular dipole moment determined from density functional theory (DFT) computations, and ϵ_s and ϵ_∞ are the static permittivity and permittivity at infinite frequencies, respectively (the values of ϵ_s were taken from the BDS data, while ϵ_∞ was estimated from refractive index (RI) measurements).

The temperature dependences of the g_K parameter for four examined alcohols (data for 3Ph1P and 4Ph1B were taken from ref. 15 and 39, respectively) are presented in Fig. 6b. It can be seen that in each case g_K increases with lowering T , which is similar to the behavior reported for various phenyl propanols,¹⁵ phenyl butanols,³⁹ as well as isomers of butanol.¹² Another interesting finding is that there is a non-systematic variation in g_K with the increasing length of the alkyl chain in the structure of PhAs at T_g . It is clearly visible that g_K is the highest for 3Ph1P. Further chain elongation leads to a decrease in this parameter. Additionally, we also estimated the Kirkwood factor at higher

temperatures, 245 and 225 K for PhM and 7Ph1H (they were still liquids at these conditions), and compared them to other systems (see the inset to panel (a) in Fig. 6). The values of g_K calculated at 225 K and at $T = T_g + 10$ K have been collected in Table 1. It was found that there is a non-monotonic change in this parameter as the length of the alkyl chain grows. This strongly indicates that there is a competition between the interactions of the non-polar and polar parts of the molecules in the studied PhAs. For the heptanol homologue (7Ph1H), the dispersive interactions prevail over hydrogen ones, while in smaller alcohols, either the interactions are comparable, or the latter forces are dominant.

Finally, the increasing alkyl chain effectively modifies the structural, thermal, spectroscopic, dielectric, and surface properties. To better illustrate the alternation of different parameters described within this paper, we plotted them against the number of carbon atoms in the side chain. Fig. 7 clearly demonstrates that the consistent, non-monotonic trends in the analyzed properties as a function of the alkyl

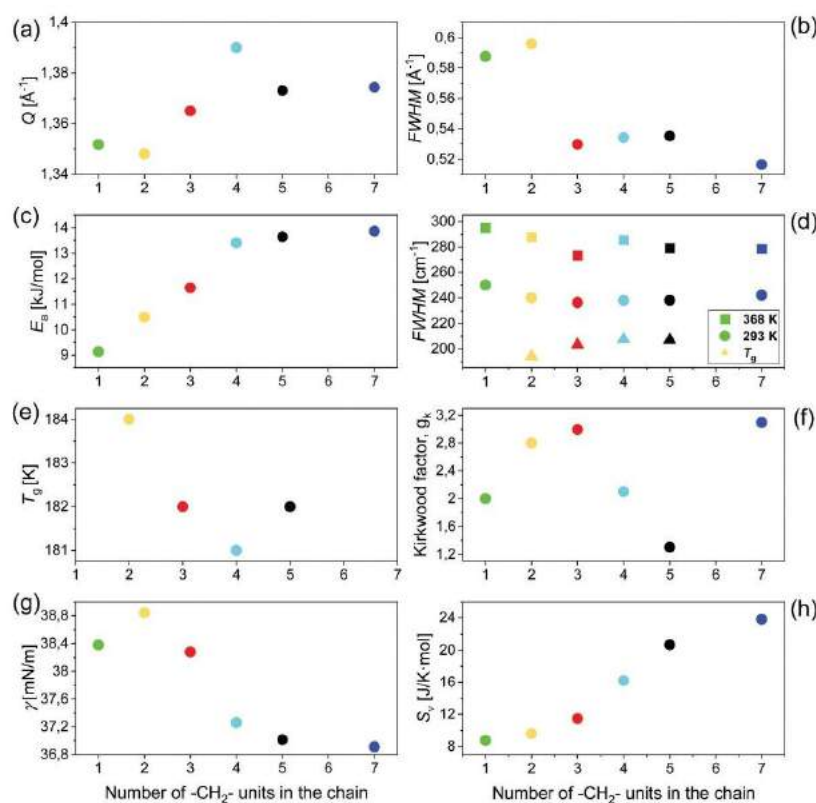


Fig. 7 The effect of the alkyl chain length on (a and b) structural, (c and d) infrared, (e) thermal, (f) dielectric, and (g and h) surface (298 K) parameters for the studied PhAs.

chain length were obtained for the studied PhAs. Interestingly, the alcohols located more or less in the middle of the series (2Ph1E/3Ph1M/4Ph1B) exhibit the highest values of d (the nearest-neighbour correlation distance), T_g (the glass transition temperature), g_K (the Kirkwood factor) as well as the greatest Q position and the lowest value of the FWHM of the ν_{OH} band. We attribute this effect to the differences in the supramolecular self-assembly, structural order, and HB patterns, going from short- to long-chain PhAs, resulting from the interplay between the dispersive and H-bonding interactions. The other origin of this effect is the chain flexibility of PhAs due to a larger number of methylene groups and the formation of other weak interactions between the molecules. What is more, some discussed parameters (the $\nu_{OH,assoc}$ band position; CHelpG atomic charges) also slightly follow the "odd-even" effect related to the number of carbons in the alkyl chain. In general, our work illustrates that HBs can be effectively formed in the series of PhAs differing in the alkyl chain length, irrespectively of the steric effect of the benzene ring, and the association is primarily governed by the chemical nature of apolar chains.

Conclusions

In summary, comprehensive systematic studies assessing the interrelation between the chain length and the self-assembling process of PhAs have been conducted using different experimental methods. It was found that as the number of methylene groups in the carbon side chain increases, non-monotonic changes in the structural (the position and width of the main diffraction peak), thermal (the glass transition temperature), spectroscopic (the ν_{OH} bandwidth), dielectric (the Kirkwood correlation factor) and surface (the surface tension, the surface entropy, the molar surface entropy) properties are observed. Surprisingly, extreme values of these parameters are reported for PhAs from the middle of the series (2Ph1E, 3Ph1P). This indicates a strong change in the assembling mechanism going from shorter to longer PhAs. Moreover, with increasing chain length, the contribution of dispersive forces to the association is more significant. From the analysis of the diffraction data, it is clearly seen that the short-range intermolecular order increases as the alkyl chain length grows. Moreover, the analysis of the dependencies of the position and FWHM of the main diffraction peak as a function of increasing alkyl chain length shows a crossover for PhAs located in the middle of the series (3Ph1P/4Ph1B). This phenomenon is also reflected in the FWHM values of the $\nu_{OH,assoc}$ band, which change non-monotonically with the length of the alkyl chain, namely firstly decreasing from PhM to 3Ph1P, and then increasing to 7Ph1H. This suggests a greater homogeneity of HBs in terms of strength for 3Ph1P with respect to other PhAs. Moreover, the FTIR data reveal that the association degree of PhAs and the activation enthalpy of their dissociation increase as the alkyl chain length grows. Thus, PhAs associate better the further the OH group is located in relation to the phenyl ring. Moreover, there is a non-monotonic change in the Kirkwood correlation factor as the length of the alkyl chain

extends; namely, it is the highest for 3Ph1P, and further chain elongation leads to a decrease in this parameter. Also, the surface tension, the surface entropy, as well as the molar surface entropy exhibit an alternative for PhAs with a shorter alkyl chain. Thus, in the present work, it has been found that when the length of the alkyl chain is extended, the interplay between dispersive and HB interactions increases. These findings provide new physical insights into the association-property relation of PhAs.

Conflicts of interest

The authors declare no competing financial interests.

Acknowledgements

B. H., J. G., K. J., K. K., and S. P. are thankful for the Polish National Science Centre's financial support within the OPUS project (Dec. no. UMO-2019/35/B/ST3/02670). M. T., M. P., and N. S. are thankful for the financial support from the Polish National Science Centre within the OPUS project (Dec. no. 2019/33/B/ST3/00500). This research was supported in part by PL-Grid Infrastructure.

References

- 1 B. Widom, P. Bhimalapurama and K. Koga, *Phys. Chem. Chem. Phys.*, 2003, **5**, 3085–3093.
- 2 A. L. Lomize, I. D. Pogozheva, M. A. Lomize and H. I. Mosberg, *BMC Struct. Biol.*, 2007, **7**, 44.
- 3 M. Schauerl, M. Podewitz, B. J. Waldner and K. R. Lied, *J. Chem. Theory Comput.*, 2016, **12**(9), 4600–4610.
- 4 E. E. Meyer, K. J. Rosenberg and J. Israelachvili, *Proc. Natl. Acad. Sci. U. S. A.*, 2006, **103**, 15739–15746.
- 5 B. Lindman, B. Medronho, L. Alves, M. Norgren and L. Nordenskiöld, *Quart. Rev. Biophys.*, 2021, **54**, e3.
- 6 S. Otto and J. B. F. N. Engberts, *Org. Biomol. Chem.*, 2003, **1**, 2809–2820.
- 7 M. Bogunia and M. Makowski, *J. Phys. Chem. B*, 2020, **124**(46), 10326–10336.
- 8 D. Lombardo, M. A. Kiselev, S. Magazù and P. Calandra, *Adv. Condensed Matter Phys.*, 2015, 151683.
- 9 M. Kwaśniewicz and M. A. Czarnecki, *Appl. Spectrosc.*, 2018, **72**(2), 288–296.
- 10 A. Jindal and S. Vasudevan, *Phys. Chem. Chem. Phys.*, 2020, **22**, 6690–6697.
- 11 S. Pérez-Casas, R. Moreno-Esparza, M. Costas and D. Patterson, *J. Chem. Soc., Faraday Trans.*, 1991, **87**, 1745–1750.
- 12 O. E. Kalinovskaya, J. K. Vij and G. P. Johari, *J. Phys. Chem. A*, 2001, **105**, 5061–5070.
- 13 G. P. Johari, O. E. Kalinovskaya and J. K. Vij, *J. Chem. Phys.*, 2001, **114**, 4634.
- 14 A. Nowok, M. Dułski, J. Grelska, A. Z. Szeremeta, K. Jurkiewicz, K. Grzybowska, M. Musiał and S. Pawlus, *J. Phys. Chem. Lett.*, 2021, **12**(8), 2142–2147.

- 15 T. Böhmer, J. P. Gabriel, T. Richter, F. Pabst and T. Blochowicz, *J. Phys. Chem. B*, 2019, **123**, 10959–10966.
- 16 B. Hachula, J. Greliska, N. Soszka, K. Jurkiewicz, A. Nowok, A. Z. Szeremeta, S. Pawlus, M. Paluch and K. Kaminski, *J. Mol. Liq.*, 2021, 117098.
- 17 N. Fischer, *Zh. Obshch. Khim.*, 1950, **20**, 1114–1118.
- 18 A. Wandschneider, J. K. Lehmann and A. Heintz, *J. Chem. Eng. Data*, 2008, **53**, 596–599.
- 19 J. Feder-Kubis, M. Geppert-Rybczynska, M. Musiał, E. Talik and A. Guzik, *Colloids Surf., A*, 2017, **529**, 725–732.
- 20 M. J. Frisch, G. W. Trucks, H. B. Schlegel, G. E. Scuseria, M. A. Robb, J. R. Cheeseman, G. Scalmani, V. Barone, B. Mennucci, G. A. Petersson, H. Nakatsuji, M. Caricato, X. Li, H. P. Hratchian, A. F. Izmaylov, J. Bloino, G. Zheng, J. L. Sonnenberg, M. Hada, M. Ehara, K. Toyota, R. Fukuda, J. Hasegawa, M. Ishida, T. Nakajima, Y. Honda, O. Kitao, H. Nakai, T. Vreven, J. A. Jr. Montgomery, J. E. Peralta, F. Ogliaro, M. Bearpark, J. J. Heyd, E. Brothers, K. N. Kudin, V. N. Staroverov, R. Kobayashi, J. Normand, K. Raghavachari, A. Rendell, J. C. Burant, S. S. Iyengar, J. Tomasi, M. Cossi, N. Rega, J. M. Millam, M. Klene, J. E. Knox, J. B. Cross, V. Bakken, C. Adamo, J. Jaramillo, R. Gomperts, R. E. Stratmann, O. Yazyev, A. J. Austin, R. Cammi, C. Pomelli, J. W. Ochterski, R. L. Martin, K. Morokuma, V. G. Zakrzewski, G. A. Voth, P. Salvador, J. J. Dannenberg, S. Dapprich, A. D. Daniels, Ö. Farkas, J. B. Foresman, J. V. Ortiz, J. Cioslowski and D. J. Fox, *Gaussian 09*, Gaussian, Inc., Wallingford CT, 2009.
- 21 S. K. Nayak, R. Sathishkumar and T. G. Row, *CrystEngComm*, 2010, **12**(10), 3112–3118.
- 22 M. Pozar, J. Bolle, C. Sternemann and A. Perera, *J. Phys. Chem. B*, 2020, **124**(38), 8358–8371.
- 23 A. Ghoufi, *J. Phys. Chem. B*, 2020, **124**, 11501–11509.
- 24 M. Požar and A. Perera, *Chem. Phys. Lett.*, 2017, **671**, 37–43.
- 25 M. Tomšič, A. Jamnik, G. Fritz-Popovski, O. Glatter and L. Vlček, *J. Phys. Chem. B*, 2007, **111**, 1738–1751.
- 26 H. Liu and S. J. Paddison, *Macromolecules*, 2017, **50**, 2889–2895.
- 27 A. Triolo, O. Russina, H. J. Bleif and E. Di Cola, *J. Phys. Chem. B*, 2007, **111**, 4641–4644.
- 28 J. N. A. Canongia Lopes and A. A. H. Pádua, *J. Phys. Chem. B*, 2006, **110**, 3330–3335.
- 29 F. Tao and S. L. Bernasek, *Chem. Rev.*, 2007, **107**, 1408–1453.
- 30 G. Vázquez, E. Alvarez and J. M. Navaza, *J. Chem. Eng. Data*, 1995, **40**, 611–614.
- 31 Y. V. Efremov, *Zh. Fiz. Khim.*, 1966, **40**, 1240–1247.
- 32 R. K. Wanchoo, J. Narayan, G. K. Raina and V. K. Rattan, *Chem. Eng. Commun.*, 1989, **81**, 145–156.
- 33 R. B. Badachhape, M. K. Gharpurey and A. B. Biswas, *J. Chem. Eng. Data*, 1965, **10**, 143–145.
- 34 J. Lyklema, *Colloids Surf., A*, 2001, **186**, 11–16.
- 35 R. T. Myers, *J. Colloid Interface Sci.*, 2004, **274**, 229–236.
- 36 L. Glasser, *J. Chem. Thermodyn.*, 2021, **157**, 106391.
- 37 G. Williams and D. C. Watts, *Trans. Faraday Soc.*, 1970, **66**, 80–85.
- 38 R. Kohlrausch, *Ann. Phys.*, 1847, **72**, 353–405.
- 39 K. Jurkiewicz, S. Kołodziej, B. Hachula, K. Grzybowska, M. Musiał, J. Greliska, R. Bielas, A. Talik, S. Pawlus, K. Kamiński and M. Paluch, *J. Mol. Liq.*, 2020, **319**, 114084.
- 40 F. Kremer and A. Schönhal, *Broadband Dielectric Spectroscopy*, Springer, Berlin, 2003.
- 41 J. G. Kirkwood, *J. Chem. Phys.*, 1939, **7**, 911–919.
- 42 W. Dannhauser and R. H. Cole, *J. Chem. Phys.*, 1955, **23**, 1762–1766.

P2. Aromaticity Effect on Supramolecular Aggregation. Aromatic vs. Cyclic Monohydroxy Alcohols

Autorzy: N. Soszka, B. Hachuła, M. Tarnacka, J. Grelska, K. Jurkiewicz, M. Geppert – Rybczyńska, R. Wrzalik, K. Grzybowska, S. Pawlus, M. Paluch, K. Kamiński

Referencja: *Spectrochim. Acta – Part A Mol. Biomol. Spectrosc.* **2022**, 276, 121235

DOI: 10.1016/j.saa.2022.121235

Impact Factor czasopisma: 4.831

Liczba punktów ministerialnych MNiSW czasopisma: 140

Mój udział polegał na przygotowaniu próbek, wykonaniu pomiarów IR i analizie wyników, dyskusji wyników, współtworzenia manuskryptu (przeprowadzenie przeglądu literaturowego, przygotowanie tekstu manuskryptu i rysunków, opis wyników i sformułowanie wniosków), formułowaniu odpowiedzi na uwagi recenzentów oraz korekcie manuskryptu po otrzymanych recenzjach.



Aromaticity effect on supramolecular aggregation. Aromatic vs. cyclic monohydroxy alcohols



N. Soszka^{a,b}, B. Hachuła^{a,*}, M. Tarnacka^b, J. Grelska^b, K. Jurkiewicz^b, M. Geppert-Rybczyńska^a, R. Wrzałik^b, K. Grzybowska^b, S. Pawlus^b, M. Paluch^b, K. Kamiński^b

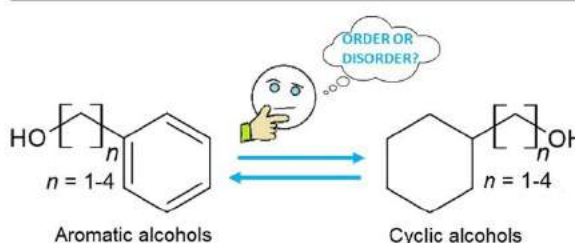
^aInstitute of Chemistry, Faculty of Science and Technology, University of Silesia in Katowice, Szkolna 9, 40-006 Katowice, Poland

^bInstitute of Physics, Faculty of Science and Technology, University of Silesia in Katowice, 75 Pułku Piechoty 1, 41-500 Chorzów, Poland

HIGHLIGHTS

- A comprehensive study on self-aggregation of monohydroxy alcohols (MAs).
- Impact of phenyl and cyclohexyl ring on the aggregation of MAs.
- Aromaticity affects the self-assembly of MAs.
- Phenyl ring introduces more heterogeneity in the organization of molecules than the cyclic one.

GRAPHICAL ABSTRACT



ARTICLE INFO

Article history:

Received 14 January 2022

Received in revised form 30 March 2022

Accepted 2 April 2022

Available online 6 April 2022

Keywords:

Self-association
Steric hindrance
Phenyl alcohols
Cyclohexyl alcohols
Aromaticity

ABSTRACT

In this paper, the steric hindrance effect related to the presence of either a cyclic or aromatic ring on the self-association process in the series of monohydroxy alcohols (MAs), from cyclohexanemethanol to 4-cyclohexyl-1-butanol and from benzyl alcohol to 4-phenyl-1-butanol, was studied using X-Ray Diffraction (XRD), Differential Scanning Calorimetry (DSC), Fourier Transform Infrared (FTIR) spectroscopy, Broadband Dielectric Spectroscopy (BDS) and the Pendant Drop (PD) methods. Based on FTIR results, it was shown that phenyl alcohol (PhA) and cyclohexyl alcohol (CA) derivatives reveal substantial differences in the association degree, the activation energy of dissociation, and the homogeneity of supramolecular nanoassociates suggesting that the phenyl ring exerts a stronger steric impact on the self-assembly of molecules than cyclohexyl one. Additionally, XRD data revealed that phenyl moiety introduces more heterogeneity in the organization of molecules compared to the cyclic one. The changes in the self-association process of alcohols were also reflected in differences in the molecular dynamics of the H-bonded aggregates, as well as in the Kirkwood factor, defining the long-range correlation between dipoles, which were slightly higher for CAs with respect to those determined for PhAs. Unexpectedly it was also found that the surface layers of PhAs were more organized than those formed by CAs. Thus, these findings provided insight into the impact of aromaticity on the self-assembly process, H-bonding pattern, supramolecular structure, and intermolecular dynamics of the studied alcohols.

© 2022 The Authors. Published by Elsevier B.V. This is an open access article under the CC BY-NC-ND license (<http://creativecommons.org/licenses/by-nc-nd/4.0/>).

1. Introduction

Aromaticity is one of the most important concept in chemistry, which allows the structural understanding of molecular stability and unusual reactivity of certain carbon-based molecules. This

* Corresponding author.

E-mail address: barbara.hachula@us.edu.pl (B. Hachuła).

<https://doi.org/10.1016/j.saa.2022.121235>

1386-1425/© 2022 The Authors. Published by Elsevier B.V.

This is an open access article under the CC BY-NC-ND license (<http://creativecommons.org/licenses/by-nc-nd/4.0/>).

unique property is strongly connected with the presence of the delocalized π electrons in the system. Importantly, interactions involving aromatic rings, such as aromatic $\pi - \pi$ stacking, stabilize the supramolecular architecture, ensure the stability of molecules/biomolecules, participate in biorecognition processes, and are a topic of considerable interest in crystal/material engineering [1–12]. These non-covalent forces play an especially important role in self-assembly at the supramolecular level as the aromatic rings can interact in different ways (stacked arrangement, edge- or point-to-face, T-shaped conformation), generating various supramolecular architectures. Such nanostructures can also be affected by halogen substituents which form halogen bonding synths competing with these molecular contacts.

Aromatic rings, due to their rigidity and planar geometry, can distort the specific attractive interactions, including hydrogen bonds (HBs), and affect the self-assembly of amphiphilic compounds, such as alcohols. In the case of aryl alcohols, the bulky aromatic moiety can be a source of competitive $\pi \cdots \pi$, C–H $\cdots \pi$ and/or O–H $\cdots \pi$ contacts. Many experimental and theoretical investigations focused on the competition between these different interactions that can occur in complexes of substituted aromatic alcohols (phenol and ethynylbenzene [13], phenol₂ [14] and *p*-cresol₂ [15] homodimers; anisole \cdots phenol [16], 7-azaindole \cdots phenol [17] or *p*-aminophenol \cdots *p*-cresol heterodimers [18]), especially to characterize the stabilization driving forces of π -stacked and HB dimers [19–21]. On the other hand, the papers devoted to the subject of intra- and/or intermolecular interactions in neat aryl alcohols mainly focused on the study of steric hindrance effect and π electrons on self-assembling phenomena in the liquid phase [22–32]. Firstly, Johari et al. [23] showed that the steric hindrance from the phenyl group in 1-phenyl-1-propanol reduces the extent of intermolecular H-bonding as the Debye-type relaxation process vanishes in this system. Then, the other authors reported that the aromatic ring only affects the supramolecular architecture of associating compounds, i.e., the equilibrium of the ring and chain-like H-bonded structures depends on the mutual distance of the phenyl ring and the hydroxyl group [26]. Recent work from Nowok and al. [31] also demonstrated that the phenyl ring exerts a much stronger effect on the self-organization of alcohol molecules via the O–H \cdots O scheme than any other type of steric hindrance, leading to a significant decline in the size and concentration of the H-bonded clusters.

In view of the above, it is worth adding that our previous experimental studies of intermolecular interactions in phenyl alcohols also shed new light on the supramolecular self-assembly, structural order, and HB patterns in aromatic systems [33,34]. We reported that HBs could be effectively formed in the series of phenyl alcohols differing in the alkyl chain length, irrespectively of the steric effect of the benzene ring [34]. What is more, their association was primarily governed by the chemical nature of apolar chains. In the case of phenyl derivatives of butyl alcohols, the major factor deciding about the association and nanoordering in self-assemblies was the location of the OH functional group in relation to the carbon skeleton, while the steric hindrance or length of the alkyl side chain does not have a significant influence on the H-bond formation [33]. Thus, our studies signified the modulation of H-bonded alcohol properties and the nanoscale aggregation through aromaticity and persuaded us to extend the study further to other H-bonded compounds having different structural and electronic properties, i.e., cyclic alcohols. This class of alcohols is expected to form H-bonds more easily than their aromatic derivatives due to the high flexibility of the cyclic ring allowing the molecule to acquire open configurations where the hydroxyl group is more exposed and hence more available for H-bonding [22]. In contrast, for phenols, the rigidity of the aromatic ring imposes a

unique conformation characterized by the coplanarity of the hydroxyl group and the aromatic ring [22].

Inspired by these results, in this study, we evaluated the influence of the various degree of steric hindrance of the hydroxyl group, aromatic versus non-aromatic, on the self-association ability of alcohols. Moreover, we also analyzed the impact of the length of the alkyl chain on the self-assembling process of non-aromatic cyclic alcohol homologous. To the best of our knowledge, this is the first systematic study on the supramolecular self-assembly of cyclic alcohols in the literature. As all of the lower-order cyclic alcohols form a plastic crystal, until now, they have been mainly investigated for studying glass transition phenomena [35–39]. To deeper examine the steric effects on the H-bond formation in alcohols, we have studied the structural, thermal, and spectroscopic properties of four phenyl alcohols (PhAs; from benzyl alcohol to 4-phenyl-1-butanol) and their cyclohexyl analogs (CAs; from cyclohexanemethanol to 4-cyclohexyl-1-butanol; Scheme 1) using Broadband Dielectric Spectroscopy (BDS), Infrared (IR) Spectroscopy, Differential Scanning Calorimetry (DSC), and X-Ray Diffraction (XRD) techniques. Moreover, the properties of the surface layer were investigated using the pendant drop (PD) method.

2. Materials and methods

Cyclic alcohols (cyclohexanemethanol (CM), 2-cyclohexyl-1-ethanol (2C1E), 3-cyclohexyl-1-propanol (3C1P), 4-cyclohexyl-1-butanol (4C1B)) and their phenyl counterparts (benzyl alcohol (BA), 2-phenyl-1-ethanol (2Ph1E), 3-phenyl-1-propanol (3Ph1P), 4-phenyl-1-butanol (4Ph1B)) under investigation (purity > 98%) were purchased from Sigma-Aldrich. Before use, all alcohols were dried under a stream of liquid nitrogen. The chemical structures of the studied alcohols are presented in Scheme 1.

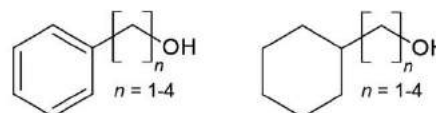
2.1. Broadband dielectric spectroscopy (BDS)

BDS measurements were carried out on heating after a fast quenching of the liquid state in a wide range of temperatures (159–303 K) and frequencies (10^{-1} – 10^6 Hz) using Novocontrol spectrometer, equipped with Alpha Impedance Analyzer with an active sample cell and Quatro Cryosystem. The samples were placed between two stainless-steel electrodes (diameter: 15 mm, gap: 0.1 mm) and mounted inside a cryostat. During the measurement, each sample was maintained under dry nitrogen gas flow. The temperature was controlled by Quatro Cryosystem using a nitrogen gas cryostat, with stability better than 0.1 K.

The collected dielectric spectra were analyzed by the superposition of Havriliak-Negami (HN) function with the dc-conductivity term [40] to determine the relaxation times of the Debye process, τ_D :

$$\epsilon''(\omega) = \frac{\sigma_{dc}}{\epsilon_0 \omega} + \frac{\Delta\epsilon}{[1 + (\omega\tau_{HN})^{\alpha_{HN}}]^{\beta_{HN}}} \quad (1)$$

where α_{HN} and β_{HN} are the shape parameters representing the symmetric and asymmetric broadening of given relaxation peaks, $\Delta\epsilon$ is the dielectric relaxation strength, τ_{HN} is the HN relaxation time, ϵ_0 is



Scheme 1. The chemical structures of (left) aromatic (phenyl) and (right) cyclic (cyclohexyl) alcohols under investigation.

the vacuum permittivity, and ω is an angular frequency ($\omega = 2\pi f$). Note that all τ_D were estimated from τ_{HN} accordingly to the equation given in Ref. [41].

Additionally, the stretching parameter β_{KWW} , which is usually used to describe the Full Width at Half Maximum (FWHM) of the α -loss peaks, has been determined from the α_{HN} and β_{HN} parameters from the following equation [42]:

$$\alpha_{HN}\beta_{HN} = \beta_{KWW}^{1.23} \quad (2)$$

It was found that $\beta_{KWW} \sim 0.91$ – 0.96 (see Table 1). Note that the fitting procedure was performed using only one HN function, as the application of additional mode was unreliable, and the fitting parameters of the second HN function changed non-monotonically with the temperature. Alternatively, the value of the stretched exponent, β_{KWW} , was determined from the fitting of chosen spectra to the one-sided Fourier transform of the Kohlrausch-Williams-Watts (KWW) function [43,44].

To determine the glass transition temperatures of all studied CAs, the estimated τ_D were fitted by the Vogel-Fulcher-Tammann (VFT) equation [45–47]:

$$\tau_D = \tau_\infty \exp\left(\frac{D_T T_0}{T - T_0}\right) \quad (3)$$

where τ_∞ , D_T and T_0 are the fitting parameters. Note that T_g is defined as a temperature at which $\tau_D = 100$ s.

2.2. Refractive index measurements

The refractive index, n , measurements of the studied liquids were carried out using the Mettler Toledo refractometer RM40 in the temperature range 293–343 K. The temperature stability controlled with the aid of a built-in Peltier thermostat was better than 0.1 K. The light source is a light-emitting diode, the beam of which passes through a polarization filter, an interference filter (589 nm), and various lenses before it reaches the sample via the sapphire prism characterized by high thermal conductivity. The measurements of n were performed with a resolution of 0.0001. The determined values are presented in Fig. S1 (please see the Supplementary Material (SM) file). Note that the values of n parameter used to calculate the Kirkwood correlation factor (g_k) at $T = T_g + 10$ K were estimated according to the linear fit of the measured data.

2.3. Differential Scanning Calorimetry (DSC)

Calorimetric measurements were carried out by Mettler-Toledo DSC apparatus equipped with a liquid nitrogen cooling accessory and an HSS8 ceramic sensor (heat flux sensor with 120 thermocouples). Temperature and enthalpy calibrations were performed by using indium and zinc standards. The sample was prepared in an open aluminum crucible (40 μ L) outside the DSC apparatus. Samples were scanned at various temperatures at a constant heating rate of 10 K min^{-1} .

Table 1

Molar mass [M] of examined CAs, glass transition temperature (T_g , determined from calorimetric and dielectric measurements), as well as values of the stretched exponent (β_{KWW}), the Kirkwood factor (g_k , calculated at $T = T_g + 10$ K), dipole moment (μ , obtained from DFT calculations), and the refractive index (n , measured at 303 K).

Sample	M [g mol ⁻¹]	$T_{g, DSC}$ [K]	T_g [K] for $\tau_D = 100$ s	β_{KWW}	g_k at $T_g + 10$ K	μ [D]	n at 303 K
CM	108.14	162 \pm 2	157 \pm 2	0.96 \pm 0.1	3.8	1.523	1.460
2C1E	122.16	163 \pm 2	159 \pm 2	0.95 \pm 0.1	3.4	1.613	1.461
3C1P	136.19	166 \pm 2	160 \pm 2	0.94 \pm 0.1	3.4	1.537	1.462
4C1B	150.22	162 \pm 2	162 \pm 2	0.91 \pm 0.1	2.9	1.652	1.463

2.4. X-ray diffraction (XRD) scattering

The wide-angle XRD patterns were collected using a Rigaku Denki D/MAX Rapid II-R diffractometer equipped with a rotating Ag anode, a graphite (002) monochromator, and an image plate detector in the Debye-Scherrer geometry. The wavelength of the incident beam, λ , was 0.5608 Å. The beamwidth at the sample was 0.3 mm. Each sample was measured at room temperature of around 293 K and around the glass transition temperature, in transmission geometry, in borosilicate glass capillaries having 1.5 mm in diameter and 0.01 mm of wall thickness. The temperature was controlled using Oxford Cryostream 800 cooler. The total X-ray scattering data were collected in the range of the scattering vector $Q = \frac{4\pi \sin \theta}{\lambda}$ (where 2θ is the scattering angle) of 0.25–20 Å⁻¹ and corrected for background. A comparison of the X-ray scattering data for CAs and PhAs in the full-measured Q range of 0.25–20 Å⁻¹ is shown in the SM file in Fig. S2.

2.5. Fourier transform infrared (FTIR) spectroscopy

FTIR spectra were recorded using a Thermo Scientific Nicolet iS50 spectrometer with a resolution of 2 cm⁻¹ (16 scans) in the spectral range of 400–4000 cm⁻¹. The spectrometer was equipped with a Linkam THMS 600 heating/cooling stage (Linkam Scientific Instruments Ltd., Surrey, UK) which allowed us to execute the temperature measurements in the range 373–93 K for CM, 368–133 K for 2C1E, 3C1P, and 4C1B applying the rate of 5 K min^{-1} . The spectra were collected every 5 K in transmission mode. To obtain samples of uniform thickness and absorbance value, a liquid cell with two CaF₂ windows separated by the 6 μ m thick Mylar spacer was used. Throughout the experiment, liquid nitrogen was passed through the spectrometer to avoid atmospheric H₂O and CO₂ bands in the spectrum. Moreover, FTIR spectra of alcohol solutions in carbon tetrachloride (CCl₄) were also collected in the frequency range 400–4000 cm⁻¹ using a transmission solution cell with KBr windows and a path length of 1.03 mm. The solutions were prepared by serial dilution of a 0.1 M solution down to 0.0001 M. A total of 16 scans with a spectral resolution of 2 cm⁻¹ were averaged for each sample. The MagicPlotPro software (version 2.9.3, MagicPlot Systems LLC, Saint Petersburg, Russia) was used to perform the deconvolution process of the OH stretching bands, enabling the determination of activation enthalpy for cyclic alcohol dissociation. The step-by-step process of the OH stretching band decomposition was described in our previous work [33] and in the SM file.

2.6. Surface tension measurements

The density of the investigated CAs was measured using Anton Paar DMA 5000 M densimeter. Condition for these measurements has been previously described in the previous paper [34] (the standard uncertainties are $u(p) = 1 \cdot 10^{-2}$ MPa and $u(T) = 0.01$ K, and the combined expanded uncertainty of the density is $u(\rho) = 5 \cdot 10^{-4}$ g cm⁻³ (at 0.95 confidence level ($k \approx 2$)). The temperature range for density measurements was $T = (283.15$ – $323.15)$ K, with a step of 10 K and at 298.15 K. Based on density

temperature dependence, it was possible to calculate density at lower temperatures necessary for surface tension measurements and the calculation of Kirkwood factor, g_p . The density of CAs and PhAs [34] was presented in Fig. S3. This comparison shows that the density of CAs is significantly lower than that of PhAs.

The surface tension was measured using the pendant drop method with the Drop Shape Analyzer DSA 100S – the Krüss Tensiometer (equipped with Advance Software). The instrumental description as well as all procedures have been described previously [34,48,49]. The general T range was (298.2–267.6) K with variable steps at a minimum of 4 temperatures. The general uncertainty of the method was 0.2 mN m^{-1} , but in our case, the standard deviation of the mean value was for three first homologues below 0.6 mN m^{-1} and only for 4-cyclohexyl-1-butanol at 273.2 K was around 1 mN m^{-1} . Based on the instrument standard uncertainty and the standard uncertainties in pressure, $u(p) = 1 \cdot 10^{-2} \text{ MPa}$, temperature and $u(T) = 0.1 \text{ K}$ and density, $u(\rho) = 5 \cdot 10^{-4} \text{ g cm}^{-3}$, the average combined expanded uncertainty $u(\gamma)$ (at 0.95 level of confidence, $k = 2$) was not worse than 1 mN m^{-1} . The surface tension of CAs is presented in Fig. 5 (a), whereas a comparison of γ with those of PhAs [34] and aliphatic alcohols (AAs) [50,51] at $T = 298.2 \text{ K}$, is drawn in Fig. 5(b). Moreover, in Fig. 5(c) and 5(d), the surface entropy ($S^s = -(\frac{\partial \gamma}{\partial T})_p$, $10^{-3} \text{ mN m}^{-1} \text{ K}^{-1}$) and the molar surface entropy ($S_v = -8.45 \cdot V_m^{2/3} \cdot (-\frac{\partial \gamma}{\partial T})_p$, $\text{J K}^{-1} \text{ mol}^{-1}$, where V_m is the molar volume) are presented, respectively. These quantities are calculated based on the temperature dependence of surface tension. Fig. 5 includes also S^s and S_v of PhAs³⁴, AAs and alkanes [50–52].

2.7. Density functional theory (DFT) computations

Density functional theory (DFT) calculations using the B3LYP functional, combined with the 6-311+G(2d,p) basis set, were performed within the Gaussian09 software package [53]. The geometries of benzene and benzyl alcohol dimers were optimized with the Opt = Tight option. The counterpoise method was used to correct the interaction energies (ΔE_{BSSE}) for the basis set superposition error (BSSE) [54].

3. Results and discussion

At first, we start our investigation with the calorimetric measurements in order to reveal all possible phase transitions in the studied materials. The recorded DSC curves are shown in Fig. 1 (a). As illustrated, all samples exhibit one pronounced jump in their heat capacity related to the glass transitions located at 162–166 K, defined as the glass transition temperature, T_g . Interestingly, the estimated T_g s are basically independent of the alkyl chain length in the examined CAs, revealing no molecular mass, M , dependence, see Fig. 1(a) and Table 1. In this context, one can recall recent studies on the series of non-aromatic MAs, which revealed that their T_g increases with M [31,55]. However, it should be highlighted that those reports considered various MAs isomers of more complex chemical structure, whereas herein, we focused only on cyclohexyl-substituted MAs characterized by linear structure and a different number of $-\text{CH}_2-$ groups (see Scheme 1), in contrast to the previous investigations [31]. Nevertheless, one can mention that the values of T_g s determined for examined CAs are significantly lower when compared to the ones reported previously for their aromatic counterparts, phenyl-substituted MAs (PhAs). Note that T_g s of PhAs change in range of 181–184 K [26,27,34] (see Fig. 6 (a)). In this context, one can assume that the examined CAs are characterized by T_g s comparable rather to the aliphatic alcohols than PhAs. This implies that the aromaticity

of the side group has a significant impact on the glass transition temperature of MAs.

Taking all of those observations into account, we wonder if the varying length of the alkyl chain of CAs would affect the molecular dynamics of these compounds and how it would be different compared to their aromatic counterparts. Thus, we performed additional dielectric measurements. Representative dielectric loss spectra measured for two selected CAs, cyclohexanemethanol (CM) and 4-cyclohexyl-1-butanol (4C1B), are shown in Fig. 1(b, c). As illustrated, one can distinguish two dielectric processes, dc conductivity (at lower frequencies) and Debye like, D , process (at high frequencies), see Fig. 1(b, c). Both of them shift toward lower frequencies with decreasing temperature. Note that the value of the stretched exponent, β_{KWW} , reaches ~ 0.91 – 0.96 (all values are listed in Table 1; β_{KWW} was determined from the shape parameters of the Havriliak-Negami (HN) function with an additional conductivity term [40] used to fit recorded loss spectra – details are shown in the Experimental section). These values clearly confirmed that the dominant process observed in Fig. 1(b, c) for all examined CAs has the Debye-like character ($\beta_{\text{KWW}} \approx 1$). At this point one can also mention that the determined values of β_{KWW} parameter for CAs are comparable to those previously reported for their aromatic counterparts, where $\beta_{\text{KWW}} \sim 0.90$ – 0.95 [26,27,34]. One can recall that the presence of the exponential decay of the electric polarization (D -relaxation), characterized by a single time constant, is considered as a characteristic feature for some associating liquids, including MAs having hydroxyl unit (s) attached to the terminal carbon [56]. Note that often for those materials, the Debye mode dominates the recorded dielectric response [57,58], resulting in that the structural α -relaxation is reflected only as an excess wing on the D -peak's high-frequency flank. It should be mentioned that although the molecular mechanism of the Debye relaxation remains a puzzle [59–63], recently, this unique dielectric mode has been generally discussed in terms of the variation of the formed hydrogen bonds, including migration of defects through the H-bonded network [27], dissociation process [64] or the transition from the ring to the linear architecture of supramolecular structures as deduced from dielectric measurements carried out in the nonlinear regime [65]. Therefore, by analyzing the shape, the dielectric strength, $\Delta\epsilon$, and the relaxation times, τ , of D -process, one can gain some indirect insights into the population and behavior of H-bonds and morphology of associates.

In the inset of Fig. 1(b), we plotted the dielectric loss spectra measured for all studied CAs and characterized by the same relaxation times of the Debye like process, τ_D (representative loss spectra were arbitrarily shifted vertically to superpose at maximum). Interestingly, we observed a broadening of the distribution of relaxation times with the length of the alkyl chain of studied materials. It might imply some variation in the H-bonded structures formed by examined series of CAs due to an increasing alkyl chain (an increasing molecular mass). Surprisingly, a comparison of loss spectra of 2C1E (non-aromatic MA) and 2Ph1E (aromatic MA) superposed at constant τ_D also shows that there are some differences between both classes of MA. As shown, the distribution of relaxation times of PhAs is slightly broader when compared to their non-aromatic counterparts; see the insert in Fig. 1(c). This broadening might arise due to a different timescale between the structural (α) and D modes [26,27] (or alternatively due to the varying dielectric strength of both modes), as a result of the variation within the population of HB between both classes of materials (especially in terms of its heterogeneous nature). The differences in the behavior of the HB population arose due to variation in the chemical structure of examined MA will be investigated further by means of IR spectroscopy in the latter part of the manuscript.

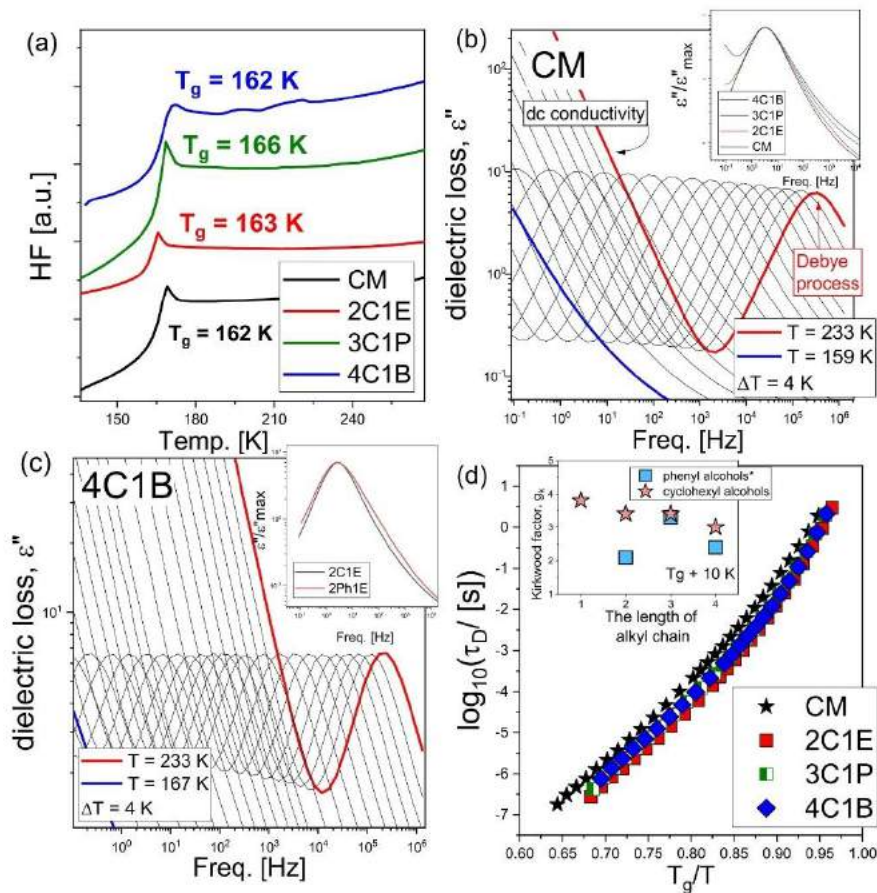


Fig. 1. (a) DSC thermograms collected for indicated CAs. (b, c) Dielectric loss spectra of CM and 4C1B were measured above their glass transition temperatures. The insets of panels (b) and (c) show the comparison of dielectric loss measured spectra at constant τ_D near T_g of all examined CAs and the comparison between 2Ph1E and 2C1E, respectively. (d) Temperature dependences of the relaxation times of Debye-like process, τ_D , determined for the examined CAs, plotted as a function of T_g/T . As the inset in panel (d), values of the Kirkwood factor, g_K , determined at $T_g + 10K$ plotted as a function of the length of the alkyl chain of examined CAs. *Data for PhAs were taken from Ref. [34].

Furthermore, we determined the values of glass transition temperature from the dielectric data. In Fig. 1(d), we have shown the relaxation times of the Debye like mode, τ_D , plotted as a function of T_g/T . Note that all τ_D were determined from fits of recorded loss spectra to the HN function with an additional conductivity term [40] (see **Experimental section**). The obtained $\tau_D(T)$ -dependences were further fitted to the Vogel-Fulcher-Tammann (VFT) equation in order to determine the values of T_g 's of examined compounds (see **Experimental section**). All estimated values of T_g (defined as T at which $\tau_D = 100$ s) are added in Table 1. As it can be seen, T_g 's determined from $\tau_D(T)$ -dependences are a few degrees lower (0–6 K) than those obtained from calorimetric studies. Note that this might be due to the different heating rates applied in both techniques.

Taking advantage of performed dielectric measurements, we calculated the Kirkwood correlation factor (g_K), which provides useful information about the variation in the local molecular

arrangement in the studied CAs. The g_K parameter was estimated as follow [66]:

$$g_K = \frac{9k_B \epsilon_0 M T (\epsilon_s - \epsilon_\infty)(2\epsilon_s + \epsilon_\infty)}{\rho N_A \mu^2 \epsilon_s (\epsilon_\infty + 2)^2} \quad (4)$$

where: k_B is the Boltzmann constant ($\sim 1.38 \times 10^{-23}$ m² kg s⁻² K⁻¹), N_A is Avogadro's number ($\sim 6.022 \times 10^{23}$), ρ is density, μ is molecular dipole moment determined from Density Functional Theory (DFT) computations, whereas ϵ_s and ϵ_∞ are static permittivity and permittivity at infinite frequencies, respectively. Note that the ϵ_s parameter was taken from BDS data, while the ϵ_∞ one was estimated from refractive index (n) measurements (where $\epsilon_\infty = n^2$, the temperature dependence of n is shown in Fig. S1). The temperature dependences of g_K parameter are presented in Fig. S4, whereas those calculated at $T = T_g + 10K$ are shown in the inset in Fig. 1(d) and Fig. 5(b). As illustrated, $g_K \sim 3-4$ for all examined CAs in the whole range of experimental data. Moreover, g_K increases upon

cooling, as was previously reported for various aromatic alcohols [26,27,34] as well as aliphatic MA, i.e., isomers of butanol [67]. One can recall that taking into account the Dannhauser approach, the value of $g_K > 1$ indicates cross-correlation between chain-like aggregates in self-assembling systems [67–69]. However, it should be mentioned that the value of g_K decreases with the elongation of the length of the alkyl chain in the structure of CAs. Note that the highest and the lowest value of g_K were reached for CM and 4C1B, respectively (see the inset in Fig. 1(d)). This might indicate that an increasing alkyl chain (and therefore molecular weight) of CAs disturbs the formation of chain-like self-assemblies. Nevertheless, it should be highlighted that the linear decrease of g_K as a function of an increasing number of $-CH_2-$ groups observed for CAs is opposite to the one observed for PhAs. As reported, g_K determined for phenyl-substituted MA revealed a clearly non-monotonic variation with the increasing length of the alkyl group, where the maximum (the highest value of g_K) was noticed for 3Ph1P [34]. Therefore, one can assume that there are some significant differences in the strength and population of self-assemblies formed by either aromatic or non-aromatic alcohols. To follow, in detail, differences in the behavior of HBs arose due to variation in the chemical structure of examined MA, further FTIR studies were performed.

To shed light on the dynamics of hydrogen bonds (HBs) in alcohols and to better understand/recognize the influence of the aromatic ring on the assembling phenomenon, special attention was paid to FTIR spectra of CAs and their phenyl analogs in the OH stretching (ν_{OH}) vibrational region. It should be noted that the impact of the length of the alkyl side chain on the behavior of benzyl alcohol homologues was studied in detail in our previous paper [34]. The representative FTIR spectra for CAs at selected temperatures (the room temperature, RT = 293 K, and T_g) in the region of 3750–2990 cm^{-1} are presented in Fig. 2. Characteristic peaks, appearing at ~ 3330 cm^{-1} and 3629 cm^{-1} at RT, are assigned to the stretching vibration of the hydrogen-bonded (ν_{OH}^{HB}) and non-hydrogen-bonded 'free' (ν_{OH}^{free}) hydroxyl groups, respectively. The band assignment of the last one is additionally confirmed by the measurements of solutions of CAs in various non-polar solvents (cyclohexane, carbon tetrachloride (CCl_4), benzene) (Fig. S5 in the SM file). Based on Fig. S5, one can also see that the type of solvent influences the self-assembly process of alcohols under investigation. In addition, the association of CAs in CCl_4 depends on the alkyl chain length, i.e., the ν_{OH}^{HB} band profile changes with the elongation of the chain length (the different intensity ratio of peaks at

ca. 3490 cm^{-1} and 3350 cm^{-1}). On the other hand, for diluted solutions of CAs in cyclohexane and benzene, the lengthening of the side chain does not vary the spectral properties of ν_{OH}^{HB} band. As presented in Table S1, up to the $x = 3$ (where x is the number of CH_2 units in the hydrocarbon side chain), the frequencies of ν_{OH}^{HB} band at 293 K are comparable (these data were obtained from the band deconvolution of FTIR spectra with the use of Gaussian–Lorentzian functions in OMNIC software; Fig. S6 in the SM file), implying a similar strength of HBs in these systems. On the other hand, the value of ν_{OH}^{HB} frequency for 4C1B deviates from the others, i.e., HBs between 4C1B molecules are slightly weaker than for shorter CAs. With the decreasing of temperature, the red-shift of ν_{OH}^{HB} bands is observed which indicates the weakening of the OH-bonds due to the formation of stronger HBs. Interestingly, when comparing the frequencies of the ν_{OH}^{HB} signals of CAs in both temperatures, it is seen that the intermolecular interactions in 4C1B are the weakest among all CAs at RT, but the situation changes at T_g when they become the strongest ones. Moreover, on cooling, the ν_{OH}^{free} band disappears confirming nearly complete/total association of CA molecules at T_g . On the other hand, the estimation/calculations of the non-bonded OH moieties' percentages in CAs at RT (Fig. S8(a)) shows that the population of the H-bonded OH groups decreases, while that of the free OH increases (from 0.54% to 1.05%) with the elongation of the chain length. Such a small fraction of non-associated (monomeric) molecules was also identified in aliphatic alcohols (<2% in methanol and even less in other alcohols) [70]. Therefore, the degree of self-association of CAs slightly decreases with the increase in the side chain length. A similar spectral effect was detected for aliphatic 1-alcohols in the liquid phase by Kwaśniewicz and Czarnecki [71].

Next, an analysis of the bandwidth of OH stretching vibration measured by the full width at half maximum, $FWHM$, was conducted. Herein it should be stressed that $FWHMs$ of the ν_{OH}^{HB} bands were obtained as parameters from the curve fitting using Gaussian–Lorentzian functions in OMNIC software (see Fig. S6). It can be clearly seen that $FWHM$ values are essentially similar for the first three CAs at RT. However, it considerably changes in the case of 4C1B, i.e., $FWHM$ is greater than for the others (ca. 30 cm^{-1}) at RT. This indicates that the most heterogeneous aggregates in terms of HB strength are formed in 4C1B. Therefore, one can state that the length of the alkyl side chain starts to affect the distribution of H-bonded networks significantly for longer cyclic alcohols, i.e., when the $x = 4$. Such behavior may suggest the competition

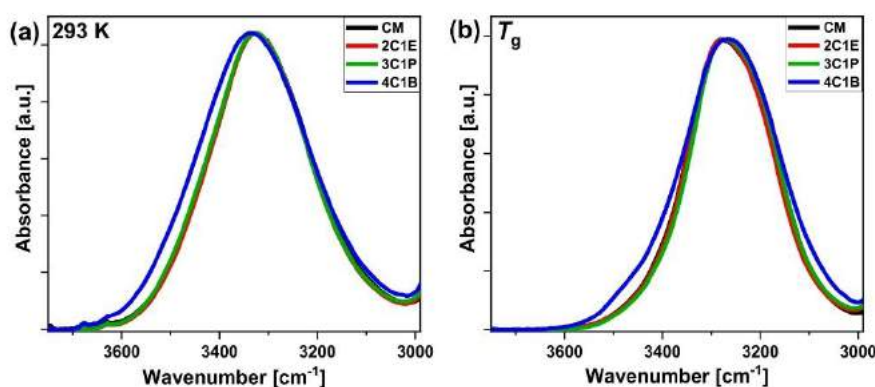


Fig. 2. FTIR spectra of CAs in the frequency range 3750–2990 cm^{-1} measured at (a) 293 K and (b) T_g . The spectra were normalized to the maximum intensity of OH stretching vibration.

between the dispersive and HB interactions as the length of alkyl units increases. At T_g , *FWHMs* generally take smaller values suggesting that more ordered and homogeneous supramolecular nanoassociates are formed (Table S1).

Further, to discuss/reveal the role of aromaticity in alcohol self-assembly, the spectral properties of CAs and PhAs were compared. FTIR spectra of both CAs and PhAs in the range 3750–3000 cm^{-1} at RT and T_g are presented in Fig. 3. At first glance, the clear difference in the amount of non-bonded OH moieties is visible for the studied alcohols at 293 K, that is, the intensity of $\nu_{\text{OH}}^{\text{free}}$ is much higher in the spectra of aromatic alcohols compared to the cyclic ones (Fig. 3(a)). It indicates that the aromatic ring indeed acts as a steric hindrance and prevents molecules from forming HB aggregates to a greater extent compared to CAs. As can be seen from Table S1, the shortest alcohols, CA and BA, are characterized by the strongest interactions at RT (the lowest frequency of the $\nu_{\text{OH}}^{\text{HB}}$ band). For CAs, the HB strength decreases with an elongation of the chain length at RT. Interestingly, the same effect was observed for neat aliphatic 1-alcohols, i.e., the hydrogen bonding weakens with the chain length increase [71]. It is of note that the opposite trend is observed for CAs at T_g . In the case of PhAs, a non-monotonic change in HB strength, as the length of the alkyl chain grows, occurs at both temperatures (the weakest HB interactions for 2Ph1E at RT and 3Ph1P at T_g). This irregular spectral variation for PhAs indicates a strong change in the assembling mechanism going from shorter to longer PhAs resulting from an interplay between dispersive and HB interactions [34]. Similar behavior was detected in the case of protic ionic liquids (PILs), in which the lengthening of the cation alkyl chain leads to well-defined self-assembled nanostructures in which the polar and apolar domains were better segregated [72]. Nanostructure in PILs results from electrostatic and H-bonding attractions between charged groups leading to the formation of polar domains. Cation alkyl groups are repelled from these regions and forced to cluster together into apolar regions.

An analysis of the *FWHMs* of studied alcohols at both temperatures clearly shows that the shorter PhAs (up to the $x = 3$) have a broader ν_{OH} bands than CAs, which suggests the existence of additional interactions involving aromatic rings apart from the typical $\text{O} - \text{H} \cdots \text{O}$ contacts. The existence of such competitive type of H-bonds, $\text{O} - \text{H} \cdots \pi$, was also suggested by DFT calculations ($\text{O} - \text{H} \cdots \text{O}$ ($\Delta E_{\text{BSSE}} = -5.67 \text{ kcal} \cdot \text{mol}^{-1}$) vs. $\text{O} - \text{H} \cdots \pi$ ($\Delta E_{\text{BSSE}} = -2.06 \text{ kcal} \cdot \text{mol}^{-1}$); Fig. S7). Interestingly, there is a reverse rela-

tionship for butanols, i.e., *FWHM* of 4C1B is considerably greater than 4Ph1B. Therefore, it can be concluded that HBs of shorter CAs ($x = 1-3$) are more homogeneous (the interactions are similar in strength) than those of PhAs. This property also changes with the chain length for PhAs, i.e., their $\nu_{\text{OH}}^{\text{HB}}$ bands at RT narrow with the elongation of the alkyl chain. The opposite is true at a lower temperature (T_g).

Further, we performed the calculations of the activation enthalpy (E_a) for the dissociation of CAs using the van't Hoff equation, according to the procedure described in our previous work, and compared them with the values obtained for PhAs [34]. Fig. S8(b) shows that CAs exhibit a non-monotonic relationship between E_a values and the number of CH_2 units in the side chain, i.e., the maximum value of E_a occurs for 2C1E (24.58 $\text{kJ} \cdot \text{mol}^{-1}$). In contrast, a clear increase in the E_a values with a chain extension is observed for PhAs. What is more, the E_a values of CAs are much higher than those of phenyl derivatives ($\sim 10 \text{ kJ} \cdot \text{mol}^{-1}$). It might be related to the higher flexibility of cyclohexyl ring, for which much more comfortable conformations can be adapted, resulting in an increased HB stabilization. It should also be mentioned that the average enthalpies of H-bonding for methanol, ethanol, propan-1-ol, propan-2-ol, butan-1-ol, hexan-1-ol and octan-1-ol in the liquid phase are in the range from -15.1 to $-17.7 \text{ kJ} \cdot \text{mol}^{-1}$ [70]. Thus, these values are between those obtained for CAs and PhAs. We also determined the average number of molecules in H-bonded aggregates of CAs based on the investigation of alcohols in dilute CCl_4 solution using the method described in the SM file. As presented in Table S2, CAs form the supramolecular assemblies (n) containing 3 or 4 H-bonded molecules, whereas the n equals 3 for PhAs. Consequently, at RT the trimers and tetramers dominate in CAs.

Based on the performed FTIR studies, we observed that the elimination of aromaticity in the examined monohydroxy alcohols, made by a simple substitution of phenyl ring by non-aromatic cyclohexyl one, leads to some pronounced difference in the strength and the population of formed hydrogen bonds network. To support these observations concerning the differences in the HB distribution in the studied materials as an effect of side group aromaticity, further structural studies were performed.

The differences in the supramolecular structure between the studied alcohols are also revealed in the X-ray diffraction (scattering) patterns. Fig. 4 (a) shows the comparison of the scattering data

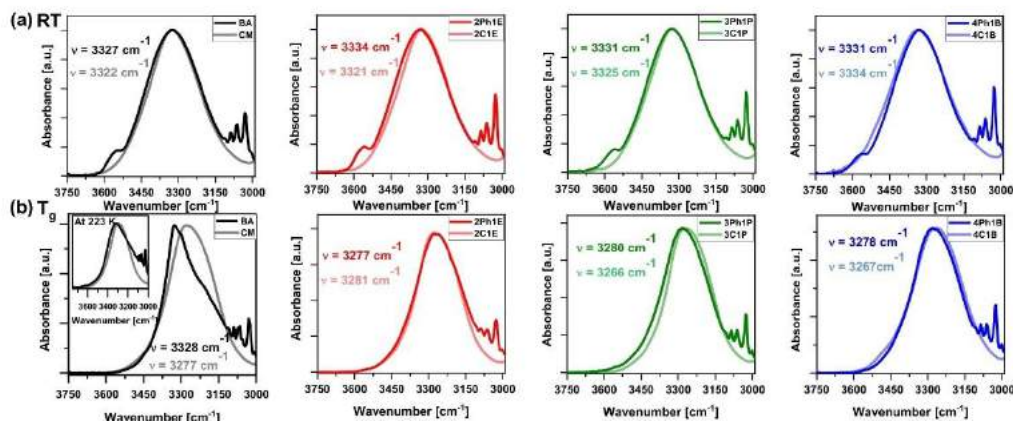


Fig. 3. Comparison of CAs and PhAs at (a) 293 K and (b) T_g in the spectral range of 3750–2990 cm^{-1} . The inset shows the $\nu_{\text{OH}}^{\text{free}}$ bands at 223 K (at temperature just before crystallization of BA). The spectra were normalized with respect to the absorbance maximum of the OH stretching vibration peak.

in the low- Q range up to 2.5 \AA^{-1} for the four pairs of cyclic alcohols and their phenyl analogues, as a function of alkyl chain length looking from left to right. The diffractograms for CAs in this range are characterized by two features related to the intermolecular structure: the main peak around 1.25 \AA^{-1} and the pre-peak around 0.5 \AA^{-1} . The origin of the pre-peak in alcohols has been discussed in many papers [73–76] and explained based on the computer simulations as arising due to structural correlations between OH groups as a consequence of the association of molecules by HBs. One can see that the intensity of the pre-peak decreases, the width increases, while its position shifts towards lower Q values with the elongation of the chain for CAs. It means that the correlation distances move towards greater values and the total intermolecular correlations weaken on this length scale for longer CAs. Since the correlations in the pre-peak region for alcohols are mainly due to OH groups, it indicates a weakening of the association of CAs via HBs with the increase in the chain length.

The X-ray scattering data for PhAs show clear differences compared to their cyclic analogs: (i) the main peak is much wider, less-intense, asymmetric and shifted towards higher Q values, (ii) the pre-peak is damped. In fact, the pre-peak is clearly visible only for the shortest PhA – BA. With the increase of the chain length, the pre-peak is suppressed. A similar tendency was observed for CAs. For the 4Ph1B, the pre-peak completely disappears. It means that the supramolecular correlations on the medium-range scale are missing, or the partial atomic correlations cancel each other out. The explanation of this phenomenon may be possible based on the computer simulations. Nevertheless, such a difference in the scattering patterns between the cyclic and aromatic alcohols suggests that the aromaticity introduces more heterogeneity into the intermolecular structure. This is also confirmed by the behavior of the main peak related to the short-range intermolecular correlations. It is clearly seen that the main peak is more asymmetric and its *FWHM* is much wider for aromatic alcohols than for cyclic counterparts. The asymmetry of the main peak suggests that it is composed of two overlapping components. That would indicate two preferred arrangements of molecules. It would be possible when the phenyl ring stacking occurs. The presence of two competitive organization of molecules, via the π -related interactions and H-bonding, would introduce two different periodic lengths, i.e. a lar-

ger distance between molecules (comparable to the intermolecular distance in CAs) as well as a smaller distance related to the phenyl ring stacking. Therefore, the short-range structure of PhAs can be considered more heterogeneous than CAs. The differences in the position and full-width at half maximum of the main diffraction peak for CAs and PhAs are presented in Fig. 4 (a,b).

Fig. 4(b) shows the XRD patterns for the studied alcohols measured at temperatures around T_g . BA crystallized at this condition. For the other alcohols, the positions of the main peak shift towards higher Q values (smaller distances) with the temperature drop. This is the standard temperature effect. The *FWHM* values also behave as standard – decrease for lower temperatures, indicating an increase in the degree of structural order and coherence length.

To obtain more information about the behavior of alcohols differentiated in terms of the side groups (aromatic or non-aromatic), we also measured their surface tension, γ , and calculated the surface entropy, S^s , as well as molar surface entropy, S_p , which is supposed to allow us to distinguish these materials according to the intermolecular forces. The estimated values of S^s , S_p , and γ at different temperatures are shown in Fig. 5 and are listed in Table S3. It can be noticed that previously, for PhAs [34], longer alkyl chain homologues had lower surface tension, which was reciprocal to the behavior of γ in homologues series of AAs [50,51] (Fig. 5(b)). In this work, the surface tension of CAs at 298.2 K changes irregularly with the lengthening of the alkyl chain (Fig. 5(a)). Moreover, the γ values of CAs are between the surface tension of AAs and PhAs (Fig. 5(b)). The more detailed interpretation of S^s and S_p is given in refs. [52,77,78]. However, it should be noticed that both entropies are interpreted in terms of the surface order [78]. It can also be added that S_p , similarly like molar surface energy, concerns the sphere of volume, which consists of 1 mol of molecules. The most common value of S_p for many organic substances is around $20 \text{ J K}^{-1} \text{ mol}^{-1}$, due to the primarily quantum effects derived from London dispersion forces, which is the most dominant in surface tension [78]. This is also characteristic of alkanes having large molar surface entropy due to their weak mutual attraction [78]. However, as it was reported earlier [34,52], for AAs and PhAs, especially for shorter homologues S_p can achieve lower values (see Fig. 5(d)). The molar surface entropy below $20 \text{ J K}^{-1} \text{ mol}^{-1}$ was also observed for water ($8.8 \text{ J K}^{-1} \text{ mol}^{-1}$

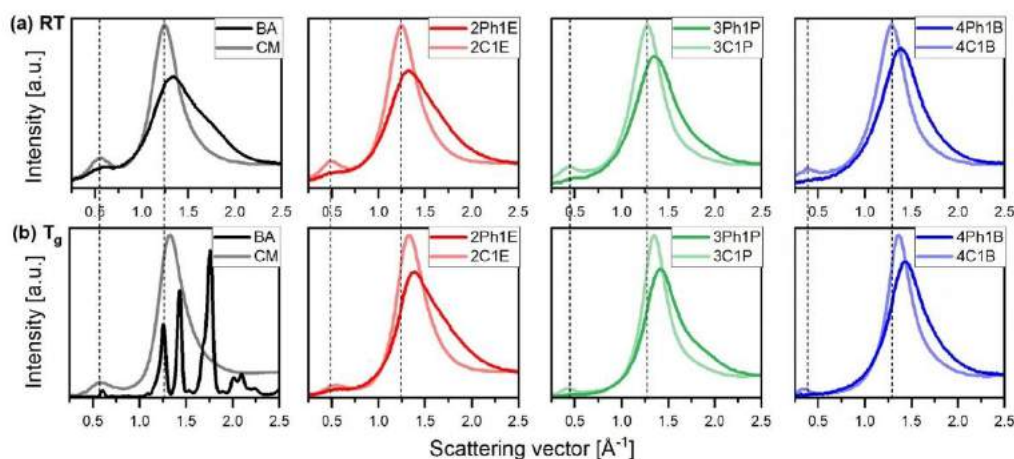


Fig. 4. Comparison of XRD data for CAs and PhAs at (a) 293 K and (b) T_g in the low- Q range of $0.25\text{--}2.5 \text{ \AA}^{-1}$. The data for PhAs were normalized to the maximum of the main peak, while the data for each CA were normalized to the high- Q range ($5\text{--}20 \text{ \AA}^{-1}$) of the corresponding PHA.

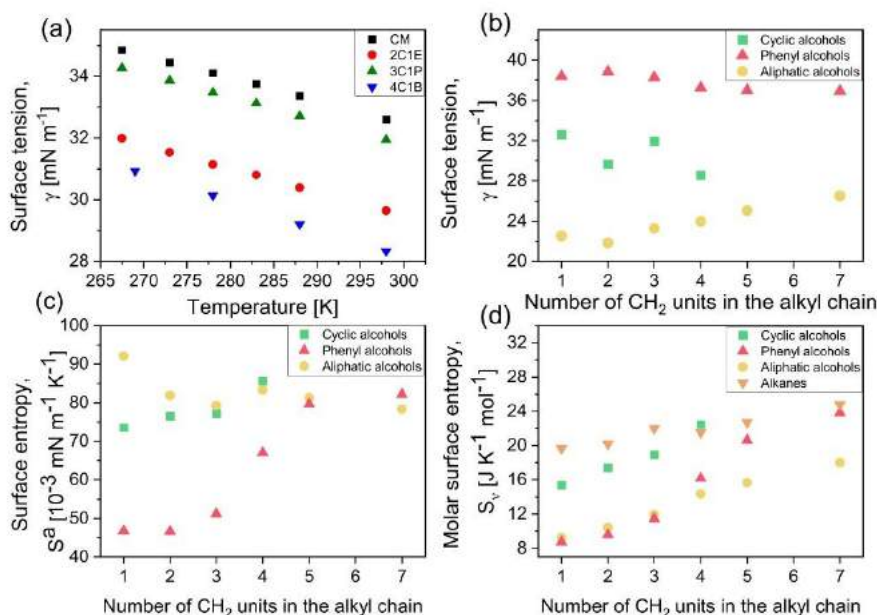


Fig. 5. (a) Surface tension of CAs at different temperatures T . (b) Comparison of surface tension of CAs with γ of PhAs³⁴ and aliphatic alcohols [50,51] at $T=298.2$ K. (c) Surface entropy ($S^a = -(\frac{\partial \gamma}{\partial T})_p, 10^{-3} \text{ mN m}^{-1} \text{ K}^{-1}$) of CAs compared with S^a of PhAs³⁴ and aliphatic alcohols [50,51]. (d) Molar surface entropy ($S_v = -8.45 \cdot V_m^{2/3} \cdot (\frac{\partial \gamma}{\partial T})_p, \text{ J K}^{-1} \text{ mol}^{-1}$) of CAs compared with S_v of PhAs³⁴, aliphatic alcohols and alkanes [52].

[77]), which can be attributed to a similar order of molecules on the surface and in bulk. This is presumably possible due to the monolayer present on the surface created by hydrogen-bonded hydroxyl groups, which are bound to the surface. From Fig. 5(d), it is seen that the molar surface entropy of CAs resembles rather S_v of alkanes than AAs. It is maybe not very surprising when S_v of cyclohexane is $23 \text{ J K}^{-1} \text{ mol}^{-1}$ (calculated based on data from Vargaftik [79]), whereas for toluene $18 \text{ J K}^{-1} \text{ mol}^{-1}$ (calculated based on data from Badachhape [80]) and for benzene: $21.81 \text{ J K}^{-1} \text{ mol}^{-1}$ [78]. Relatively high S_v values of CAs show that the influence of cyclohexane on the surface properties of these substances is very strong. At the same time, the surface entropy (Fig. 5(c)) of CAs, calculated directly from the temperature dependence of surface tension, shows the similarity to S^a of AAs with the exception of CM. It can be added that the surface entropy, S^a , of CAs increases with the lengthening of the alkyl chain, like for PhAs, whereas the S^a behaviour for AAs is quite the opposite (see Fig. 5(c)). From the inspection of Fig. 5(b) and 5(c) (surface tension and surface entropy), it is obvious that the surface of CAs is ordered like for AAs, to a larger extent than it was for PhAs. This is despite the presence of cyclohexane in the molecule - a kind of steric hindrance for the creation of hydrogen bonds. To sum up, taking into account S^a - CAs seem to be closer to AAs, whereas the normalized parameter, S_v shows the real influence of the cyclohexane of the surface layer order of CAs, which seem to be similar to alkanes (Fig. 5(c) and (d)).

In order to fully recognize the effect of the aromatic substituent in examined MAs on the H-bonding properties, the plots of different studied parameters versus the side alkyl chain length of associating liquids were constructed and presented in Fig. 6. An interesting correlation between the Kirkwood factor and the side alkyl chain length is observed. Generally, PhAs exhibit the non-

monotonic behavior of g_{H} as the number of CH₂ units in the chain varies, whereas this factor decreases as the length of the side alkyl chain increases in CAs. Moreover, the T_{B} values for CAs are lower than those for PhAs, resembling aliphatic alcohols. FTIR results show that the replacement of a flexible cyclic ring with a rigid aromatic one modifies the spectral parameters of the ν_{OH} band. It is manifested by the changes in the intensity, the full width at half maximum, the wavenumber of the OH stretching vibration band, and the activation enthalpy for the dissociation process. FTIR data also showed that the aromatic moiety leads to larger spatial heterogeneity in H-bond strength for shorter PhAs (BA, 2C1E) compared to CAs, whereas for longer ones, there is a change in this trend. The E_a values suggested that the OH energy is sensitive to the H-bonding environment, i.e., PhAs exhibit much lower E_a values than CAs. However, in the case of PhAs, the E_a value increases with elongation of side alkyl chain length, while the non-monotonic dependence of this parameter is observed for CAs. What is more, the FWHM values of the $\nu_{\text{OH}}^{\text{HB}}$ band of PhAs at 293 K decreases with the elongation of the alkyl chain, which may indicate a gradual disappearance of the O-H... π interactions (suggested by DFT calculations). It also indicates that the steric hindrance of the bulky phenyl groups in the proximity of the OH group of PhAs occur, in which aromatic rings act as intermolecular "spacers/inhibitors" for H-bonding formation. X-ray scattering data reveal damping of the pre-peak as well as broadening of the main peak and decrease in its intensity for PhAs in comparison to CAs. These features suggest that the intermolecular structure of PhAs is more complex than CAs. This is evidenced by the asymmetric shape of the main diffraction peak as well as the shift of its position towards greater Q values (shorter correlation distances) for PhAs compared to CAs. It is also seen that with the elongation of the alkyl chain, the values of the correlation distances increase.

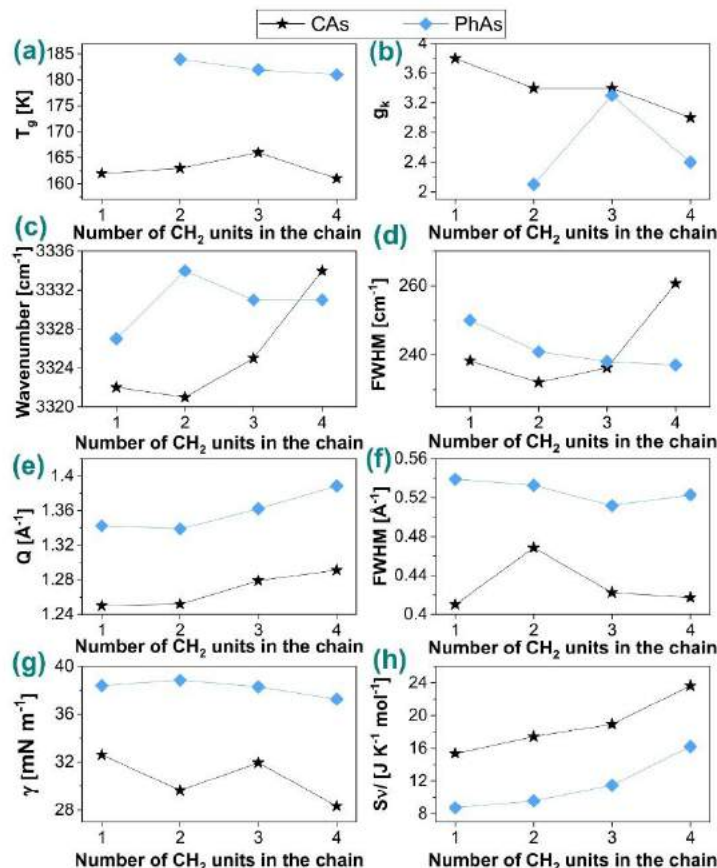


Fig. 6. The effect of aromaticity and the alkyl chain length on (a) thermal, (b) dielectric (at $T_g + 10$ K) (c, d) infrared, (e, f) diffraction, and (g, h) surface data for the studied CAs and PhAs at $T = 298$ K (the error bars are within the experimental points).

Thus, we can conclude that for longer-chained alcohols, there is a weakening of the association process. In addition, the surface tension of the studied alcohols decreases with increasing alkyl chain length, with the effect of odd-even in CAs. The values of surface entropy and molar surface entropy of CAs are higher than those of corresponding PhAs, which may be due to the slightly stronger hydrogen bonding in CAs. It should be noticed that, at first glance, the surface properties of the studied MAs (the γ , S^0 , and S_v) are in apparent contradiction with the structural, thermal, and spectroscopic results. A possible reason for this is the lack of compensation of specific actions on the surface, as some molecules only come into contact with the surface. Thus, the surface effects do not have to correlate with the processes occurring in bulk.

4. Conclusions

In this paper, we probe the influence of aromaticity on the associating behavior of a series of non-aromatic monohydroxy alcohols and their aromatic counterparts by means of various experimental techniques, infrared and dielectric spectroscopy, X-ray diffraction

and differential scanning calorimetry. Additionally, the surface tension measurements were performed, and calculations on surface entropy and molar surface entropy were made. It was found that both groups of alcohol differ in the glass transition temperature, Kirkwood factor, and the distribution of relaxation times, which indirectly imply differences in the population of hydrogen-bonding structures formed by those materials. This assumption is confirmed by IR measurements, which reveal the changes in the intensity, the full width at half maximum and wavenumber of the OH stretching vibration bandwidth, and furthermore the activation enthalpy for the dissociation. Moreover, the examined CAs form the supramolecular assemblies (n) containing 3 or 4 H-bonded molecules, whereas the n equals 3 for PhAs. This simply indicates that the elimination of aromaticity in the examined monohydroxy alcohols, made by a simple substitution of phenyl ring by non-aromatic cyclohexyl one, leads to some pronounced difference in the strength and the population of formed hydrogen bonds network. Also, performed XRD analysis indicated a difference in the molecular packing between both classes of materials, CAs and PhAs, as the nano-clusters created in PhAs are characterized by higher disorder between molecules. Interestingly, all

results revealed that the introduction of aromaticity in the structure of monohydroxy alcohols influences the ability of these alcohols to build a hydrogen bond network and spatial organization. We believe that the presented data allow a better understanding of the behavior of self-assembling materials and the correlation between HB and chemical structure.

CRedit authorship contribution statement

N. Soszka: Writing – original draft, Investigation, Formal analysis, Visualization. **B. Hachula:** Writing – original draft, Formal analysis, Methodology, Conceptualization. **M. Tarnacka:** Investigation, Formal analysis, Funding acquisition. **J. Grelska:** Investigation. **K. Jurkiewicz:** Investigation, Formal analysis. **M. Geppert-Rybczyńska:** Investigation, Formal analysis. **R. Wrzałik:** Investigation. **K. Grzybowska:** Investigation. **S. Pawlus:** Investigation, Funding acquisition. **M. Paluch:** Supervision. **K. Kamiński:** Methodology, Supervision.

Declaration of Competing Interest

The authors declare the following financial interests/personal relationships which may be considered as potential competing interests: Magdalena Tarnacka reports financial support was provided by National Science Centre Poland. Natalia Soszka reports financial support was provided by National Science Centre Poland. Barbara Hachula reports financial support was provided by National Science Centre Poland. Joanna Grelska reports financial support was provided by National Science Centre Poland. Karolina Jurkiewicz reports financial support was provided by National Science Centre Poland. Kamil Kamiński reports financial support was provided by National Science Centre Poland. Sebastian Pawlus reports financial support was provided by National Science Centre Poland.

Acknowledgement

M.T., and N.S. are thankful for financial support from the Polish National Science Centre within the OPUS project (Dec. no 2019/33/B/ST3/00500). B.H., J.G., K.J., K.K., and S.P. are thankful for the Polish National Science Centre's financial support within the OPUS project (Dec. no UMO-2019/35/B/ST3/02670). This research was supported in part by PLGrid Infrastructure.

Appendix A. Supplementary material

The Supporting Material file is available free of charge at <http://pubs.acs.org>. It contains additional figures and tables, including the results of refractive index, density, the FTIR spectra of CAs and their solutions in CCl₄ as well as the comparison of XRD data for CAs and PhAs at 293 K and T_g. Supplementary data to this article can be found online at <https://doi.org/10.1016/j.saa.2022.121235>.

References

- [1] E.A. Meyer, R.K. Castellano, F. Diederich, Interactions with aromatic rings in chemical and biological recognition, *Angew. Chem. Int. Ed.* 42 (2003) 1210–1250, <https://doi.org/10.1002/anie.200322285>.
- [2] W.R. Zhuang, Y. Wang, P.F. Cui, L. Xing, J. Lee, D. Kim, H.L. Jiang, Y.K. Oh, Applications of π - π stacking interactions in the design of drug-delivery systems, *J. Control. Release* 294 (2019) 311–326, <https://doi.org/10.1016/j.jconrel.2018.12.014>.
- [3] T. Chen, M. Li, J. Liu, π - π Stacking Interaction: A Nondestructive and Facile Means in Material Engineering for Bioapplications, *Cryst. Growth Des.* 18 (2018) 2765–2783, <https://doi.org/10.1021/acs.cgd.7b01503>.
- [4] Z.F. Yao, J.Y. Wang, J. Pei, Control of π - π Stacking via Crystal Engineering in Organic Conjugated Small Molecule Crystals, *Cryst. Growth Des.* 18 (2018) 7–15, <https://doi.org/10.1021/acs.cgd.7b01385>.
- [5] A. Banerjee, A. Saha, B.K. Saha, Understanding the Behavior of π - π Interactions in Crystal Structures in Light of Geometry Corrected Statistical Analysis: Similarities and Differences with the Theoretical Models, *Cryst. Growth Des.* 19 (2019) 2245–2252, <https://doi.org/10.1021/acs.cgd.8b01857>.
- [6] D. Sharada, V.G. Saraswata, B.K. Saha, Steering the Host Network from Cage to Channel by π - π Interactions among the Guest Molecules, *Cryst. Growth Des.* 18 (2018) 3719–3723, <https://doi.org/10.1021/acs.cgd.8b00487>.
- [7] P. Bora, B. Saikia, B. Sarma, Regulation of π - π Stacking Interactions in Small Molecule Cocrystals and/or Salts for Physicochemical Property Modulation, *Cryst. Growth Des.* 18 (2018) 1448–1458, <https://doi.org/10.1021/acs.cgd.7b01377>.
- [8] J.H. Deng, J. Luo, Y.L. Mao, S. Lai, Y.N. Gong, D.C. Zhong, T.B. Lu, π - π stacking interactions: Non-negligible forces for stabilizing porous supramolecular frameworks, *Sci. Adv.* 6 (2020) 1–9, <https://doi.org/10.1126/sciadv.aax9976>.
- [9] C.R. Martinez, B.L. Iverson, Rethinking the term “ π -stacking”, *Chem. Sci.* 3 (2012) 2191–2201, <https://doi.org/10.1039/c2sc20045g>.
- [10] T.F. Headen, C.A. Howard, N.T. Skipper, M.A. Wilkinson, D.T. Bowron, A.K. Soper, Structure of π - π Interactions in aromatic liquids, *J. Am. Chem. Soc.* 132 (2010) 5735–5742, <https://doi.org/10.1021/ja909084a>.
- [11] A.R. Nekoei, M. Vatanparast, π -Hydrogen bonding and aromaticity: A systematic interplay study, *Phys. Chem. Chem. Phys.* 21 (2019) 623–630, <https://doi.org/10.1039/c8cp07003b>.
- [12] H.W. Roesky, M. Andruh, The interplay of coordinative, hydrogen bonding and π - π stacking interactions in sustaining supramolecular solid-state architectures: A study case of bis(4-pyridyl) and bis(4-pyridyl-N-oxide) tectons, *Coord. Chem. Rev.* 236 (3–2) (2003) 91–119.
- [13] D. Vojta, M. Vazdar, The study of hydrogen bonding and π - π interactions in phenol-ethylbenzene complex by IR spectroscopy, *Spectrochim. Acta A* 132 (2014) 6–14, <https://doi.org/10.1016/j.saa.2014.04.149>.
- [14] R. Brause, M. Santa, M. Schmitt, K. Kleinermanns, Determination of the geometry change of the phenol dimer upon electronic excitation, *ChemPhysChem* 8 (2007) 1394–1401, <https://doi.org/10.1002/cphc.200700127>.
- [15] S. Yan, L.H. Spangler, Intermolecular modes of S1 p-cresol dimer; information concerning structure and dynamics, *J. Phys. Chem.* 95 (1991) 3915–3918, <https://doi.org/10.1021/j100163a007>.
- [16] G. Pietrapzeria, M. Pasquini, F. Mazzoni, G. Piani, M. Becucci, M. Biczysko, D. Michalski, J. Bloino, V. Barone, Noncovalent interactions in the gas phase: The anisole-phenol complex, *J. Phys. Chem. A* 115 (2011) 9603–9611, <https://doi.org/10.1021/jp200444a>.
- [17] M.C. Capello, M. Broquier, C. Dedonder-Lardeux, C. Jouvett, G.A. Pino, Fast excited state dynamics in the isolated 7-azaindole-phenol H-bonded complex, *J. Chem. Phys.* 138 (2013) 054304, <https://doi.org/10.1063/1.4789426>.
- [18] M.C. Capello, F.J. Hernández, M. Broquier, C. Dedonder-Lardeux, C. Jouvett, G.A. Pino, Hydrogen bonds vs. π -stacking interactions in the p-aminophenol-p-cresol dimer: An experimental and theoretical study, *Phys. Chem. Chem. Phys.* 18 (2016) 31260–31267, <https://doi.org/10.1039/c6cp06352g>.
- [19] K. Müller-Dethlefs, P. Hobza, Noncovalent Interactions: A Challenge for Experiment and Theory, *Chem. Rev.* 100 (2000) 143–167, <https://doi.org/10.1021/cr9900331>.
- [20] I. Ali, S. Sharma, B. Bezbaruah, Quantum Mechanical study on the π - π stacking interaction and change in conformation of phenolic systems with different intermolecular rotations, *Comput. Chem. Phys.* 06 (04) (2018) 71–86.
- [21] A. Olasz, P. Mignon, F. De Proft, T. Veszprémi, P. Geerlings, Effect of the π - π Stacking interaction on the acidity of phenol, *Chem. Phys. Lett.* 407 (2005) 504–509, <https://doi.org/10.1016/j.cplett.2005.03.145>.
- [22] S. Pérez-Casas, R. Moreno-Esparza, M. Costas, D. Patterson, Effect of steric hindrance and π electrons on alcohol self-association, *J. Chem. Soc. Faraday Trans. 87* (1991) 1745–1750, <https://doi.org/10.1039/FT9918701745>.
- [23] G.P. Johari, O.E. Kalinovskaya, J.K. Vij, Effects of induced steric hindrance on the dielectric behavior and H bonding in the supercooled liquid and vitreous alcohol, *J. Chem. Phys.* 114 (2001) 4634–4642, <https://doi.org/10.1063/1.1346635>.
- [24] K. Shin-ya, H. Sugeta, S. Shin, Y. Hamada, Y. Katsumoto, K. Ohno, Absolute configuration and conformation analysis of 1-phenylethanol by matrix-isolation infrared and vibrational circular dichroism spectroscopy combined with density functional theory calculation, *J. Phys. Chem. A* 111 (2007) 8598–8605, <https://doi.org/10.1021/jp068448v>.
- [25] M. Mons, E.G. Robertson, J.P. Simons, Intra- and Intermolecular π -Type Hydrogen Bonding in Aryl Alcohols: UV and IR-UV Ion Dip Spectroscopy, *J. Phys. Chem. A* 104 (2000) 1430–1437, <https://doi.org/10.1021/jp993178k>.
- [26] T.T. Böhmer, J.P. Gabriel, T. Richter, F. Pabst, T. Blochowicz, Influence of Molecular Architecture on the Dynamics of H-Bonded Supramolecular Structures in Phenyl-Propanols, *J. Phys. Chem. B* 123 (2019) 10959–10966, <https://doi.org/10.1021/acs.jpcc.9b07768>.
- [27] K. Jurkiewicz, S. Kolodziej, B. Hachula, K. Grzybowska, M. Musiał, J. Grelska, R. Bielas, A. Talić, S. Pawlus, K. Kamiński, M. Paluch, Interplay between structural static and dynamical parameters as a key factor to understand peculiar behaviour of associated liquids, *J. Mol. Liq.* 319 (2020) 114084, <https://doi.org/10.1016/j.molliq.2020.114084>.
- [28] S. Kolodziej, J. Knapik-Kowalczyk, K. Grzybowska, A. Nowok, S. Pawlus, Essential meaning of high pressure measurements in discerning the properties of monohydroxy alcohols with a single phenyl group, *J. Mol. Liq.* 305 (2020) 112863, <https://doi.org/10.1016/j.molliq.2020.112863>.
- [29] A. Nowok, K. Jurkiewicz, M. Dulski, H. Hellwig, J.G. Malecki, K. Grzybowska, J. Grelska, S. Pawlus, Influence of molecular geometry on the formation, architecture and dynamics of H-bonded supramolecular associates in 1-

- phenyl alcohols, *J. Mol. Liq.* 326 (2021) 115349, <https://doi.org/10.1016/j.molliq.2021.115349>.
- [30] A. Nowok, M. Dulski, K. Jurkiewicz, J. Grelska, A.Z. Szeremeta, K. Grzybowska, S. Pawlus, Molecular stiffness and aromatic ring position – crucial structural factors in the self-assembly processes of phenyl alcohols, *J. Mol. Liq.* (2021) 116426, <https://doi.org/10.1016/j.molliq.2021.116426>.
- [31] A. Nowok, M. Dulski, J. Grelska, A.Z. Szeremeta, K. Jurkiewicz, K. Grzybowska, M. Musiał, S. Pawlus, Phenyl Ring: A Steric Hindrance or a Source of Different Hydrogen Bonding Patterns in Self-Organizing Systems? *J. Phys. Chem. Lett.* 12 (2021) 2142–2147, <https://doi.org/10.1021/acs.jpclett.1c00186>.
- [32] J.P. Gabriel, E. Thoms, R. Richert, High electric fields elucidate the hydrogen-bonded structures in 1-phenyl-1-propanol, *J. Mol. Liq.* 330 (2021) 115626, <https://doi.org/10.1016/j.molliq.2021.115626>.
- [33] B. Hachuła, J. Grelska, N. Soszka, K. Jurkiewicz, A. Nowok, A.Z. Szeremeta, S. Pawlus, M. Paluch, K. Kaminski, Systematic studies on the dynamics, intermolecular interactions and local structure in the alkyl and phenyl substituted butanol isomers, *J. Mol. Liq.* (2021) 117098, <https://doi.org/10.1016/j.molliq.2021.117098>.
- [34] N. Soszka, B. Hachuła, M. Tarnačka, E. Ozimina-Kamiska, J. Grelska, K. Jurkiewicz, M. Geppert-Rybczyńska, R. Wrzałka, K.A. Grzybowska, S. Pawlus, M. Paluch, K. Kaminski, The impact of the length of alkyl chain on the behavior of benzyl alcohol homologous. The interplay between dispersive and hydrogen bond interaction, *Phys. Chem. Chem. Phys.* 23 (2021) 23796–23807, <https://doi.org/10.1039/D1CP02802B>.
- [35] S. Mustafa, L.A. Dissado, R.M. Hill, Structure and Dipole Relaxation Mechanisms in the Cyclic Alcohols Cyclopentanol to Cyclo-octanol, *J. Chem. Soc. Faraday Trans. 79* (1983) 369–417, <https://doi.org/10.1039/F29837900369>.
- [36] M. Tyagi, S.S.N. Murthy, Study of the nature of glass transitions in the plastic crystalline phases of cyclo-octanol, cycloheptanol, cyanoadamantane and cis-1,2-dimethylcyclohexane, *J. Chem. Phys.* 114 (2001) 3640–3652, <https://doi.org/10.1063/1.1342811>.
- [37] M.P. Nighil Nath, M.K. Sulaiman, M.S. Thayyil, Thermal & dielectric spectroscopic investigation on orientationally disordered crystal-cyclobutanol, *Mater. Today Proc.* 18 (2019) 1620–1626, <https://doi.org/10.1016/j.matpr.2019.05.256>.
- [38] R. Brand, P. Lunkenheimer, A. Loidl, Relaxations and fast dynamics of the plastic crystal cyclo-octanol investigated by broadband dielectric spectroscopy, *Phys. Rev. B – Condens. Matter Phys.* 56 (1997) R5713–R5716, <https://doi.org/10.1103/PhysRevB.56.R5713>.
- [39] R. Brand, P. Lunkenheimer, A. Loidl, Relaxation dynamics in plastic crystals, *J. Chem. Phys.* 116 (2002) 10386–10401, <https://doi.org/10.1063/1.1477186>.
- [40] S. Havriliak, S. Negami, A complex plane analysis of α -dispersions in some polymer systems, *J. Polym. Sci. Part C Polym. Symp.* 14 (1966) 99–117, <https://doi.org/10.1002/polc.5070140111>.
- [41] F. Kremer, A. Schönhals (Eds.), *Broadband Dielectric Spectroscopy*, Springer, Berlin, 2003.
- [42] F. Alvarez, A. Alegria, J. Colmenero, Relationship between the time-domain Kohlrausch-Williams-Watts and frequency-domain Havriliak-Negami relaxation functions, *Phys. Rev. B.* 44 (1991) 7306–7312, <https://doi.org/10.1103/PhysRevB.44.7306>.
- [43] G. Williams, D.C. Watts, Non-symmetrical dielectric relaxation behaviour arising from a simple empirical decay function, *Trans. Faraday Soc.* 66 (1970) 80–85, <https://doi.org/10.1039/TF9706600080>.
- [44] R. Kohlrausch, Ueber das Dellmann'sche Elektrometer, *Ann. Phys.* 72 (1847) 353–405, <https://doi.org/10.1002/andp.18471481102>.
- [45] H. Vogel, Das temperaturabhängigkeitsgesetz der viskosität von flüssigkeiten, *J. Phys. Z.* 22 (1921) 645–646.
- [46] G.S. Fulcher, Analysis of Recent Measurements of the Viscosity of Glasses, *J. Am. Ceram. Soc.* 8 (1925) 339–355, <https://doi.org/10.1111/j.1151-2916.1925.tb16731.x>.
- [47] G. Tammann, W. Hesse, Die abhängigkeit der viskosität von der temperatur bei unterkühlten flüssigkeiten, *Z. Anorg. Allg. Chem.* 156 (1926) 245–257, <https://doi.org/10.1002/zaac.19261560121>.
- [48] A. Wandschneider, J.K. Lehmann, A. Heintz, Surface Tension and Density of Pure Ionic Liquids and Some Binary Mixtures with 1-Propanol and 1-Butanol, *J. Chem. Eng. Data.* 53 (2008) 596–599, <https://doi.org/10.1021/jc700621d>.
- [49] J. Feder-Kubis, M. Geppert-Rybczyńska, M. Musiał, E. Talić, A. Guzik, Exploring the surface activity of a homologues series of functionalized ionic liquids with a natural chiral substituent: (-)-menthol in a cation, *Colloids Surf. A Physicochem. Eng. Asp.* 529 (2017) 725–732, <https://doi.org/10.1016/j.colsurfa.2017.06.040>.
- [50] G. Vázquez, E. Alvarez, J.M. Navaza, Surface tension of alcohol + water from 20 to 50 °C, *J. Chem. Eng. Data* 40 (1995) 611–614, <https://doi.org/10.1021/jc00019a016>.
- [51] Y.V. Efremov, Density, surface tension, saturation vapor pressure, and critical parameters of alcohols, *Zh. Fiz. Khim.* 40 (1996) 1240–1247.
- [52] R.T. Myers, True molar surface energy and alignment of surface molecules, *J. Colloid Interface Sci.* 274 (2004) 229–236, <https://doi.org/10.1016/j.jcis.2003.12.048>.
- [53] Gaussian 09, Revision A.02, M.J. Frisch, G.W. Trucks, H.B. Schlegel, G.E. Scuseria, M.A. Robb, J.R. Cheeseman, G. Scalmani, V. Barone, G.A. Petersson, H. Nakatsuji, X. Li, M. Caricato, A. Marenich, J. Bloino, B.G. Janesko, R. Gomperts, B. Mennucci, H.P. Hratchian, J.V. Ortiz, A.F. Izmaylov, J.L. Sonnenberg, D. Williams-Young, F. Ding, F. Lipparini, F. Egidi, J. Goings, B. Peng, A. Petrone, T. Henderson, D. Ranasinghe, V.G. Zakrzewski, J. Gao, N. Rega, G. Zheng, W. Liang, M. Hada, M. Ehara, K. Toyota, R. Fukuda, J. Hasegawa, M. Ishida, T. Nakajima, Y. Honda, O. Kitao, H. Nakai, T. Vreven, K. Throssell, J.A. Montgomery, Jr., J.E. Peralta, F. Ogliaro, M. Bearpark, J.J. Heyd, E. Brothers, K.N. Kudin, V.N. Staroverov, T. Keith, R. Kobayashi, J. Normand, K. Raghavachari, A. Rendell, J.C. Burant, S.S. Iyengar, J. Tomasi, M. Cossi, J.M. Millam, M. Klene, C. Adamo, R. Cammi, J.W. Ochterski, R.L. Martin, K. Morokuma, O. Farkas, J.B. Foresman, D.J. Fox, Gaussian, Inc., Wallingford CT, 2016.
- [54] S.F. Boys, F. Bernardi, *Mol. Phys.* 19 (1970) 553–566, <https://doi.org/10.1080/00268977000101561>.
- [55] V.N. Novikov, E.A. Rössler, Correlation between glass transition temperature and molecular mass in non-polymeric and polymer glass formers, *Polymer* 54 (2013) 6987–6991, <https://doi.org/10.1016/j.polymer.2013.11.002>.
- [56] R. Böhmer, C. Gainaru, R. Richert, Structure and dynamics of monohydroxy alcohols—Milestones towards their microscopic understanding, 100 years after Debye, *Phys. Rep.* 545 (2014) 125–195, <https://doi.org/10.1016/j.physrep.2014.07.005>.
- [57] M. Wikarek, S. Pawlus, S.N. Tripathy, A. Szulc, M. Paluch, How different molecular architectures influence the dynamics of H-bonded structures in glass-forming monohydroxy alcohols, *J. Phys. Chem. B* 120 (2016) 5744–5752, <https://doi.org/10.1021/acs.jpcc.6b01458>.
- [58] T. Böning, J. Lueg, J. Bolle, C. Sternemann, C. Gainaru, M. Tolan, R. Böhmer, Connecting structurally and dynamically detected signatures of supramolecular Debye liquids, *J. Chem. Phys.* 147 (2017) 234501, <https://doi.org/10.1063/1.4986866>.
- [59] L.M. Wang, R. Richert, Dynamics of glass-forming liquids. IX. Structural versus dielectric relaxation in monohydroxy alcohols, *J. Chem. Phys.* 121 (2004) 11170–11176, <https://doi.org/10.1063/1.1811072>.
- [60] C. Brot, M. Magar, Comment on “dispersion at millimeter wavelengths in methyl and ethyl alcohols”, *J. Chem. Phys.* 39 (1963) 841–842, <https://doi.org/10.1063/1.1734336>.
- [61] O.E. Kalinovskaya, J.K. Vij, The exponential dielectric relaxation dynamics in a secondary alcohol's supercooled liquid and glassy states, *J. Chem. Phys.* 112 (2000) 3262–3266, <https://doi.org/10.1063/1.480909>.
- [62] V.V. Levin, Y.D. Feldman, Dipole relaxation in normal aliphatic alcohols, *Chem. Phys. Lett.* 87 (1983) 162–164, [https://doi.org/10.1016/0009-2614\(82\)83579-3](https://doi.org/10.1016/0009-2614(82)83579-3).
- [63] P.M. Déjardin, S.V. Titov, Y. Cornaton, Linear complex susceptibility of long-range interacting dipoles with thermal agitation and weak external ac fields, *Phys. Rev. B.* 99 (2019) 1–14, <https://doi.org/10.1103/PhysRevB.99.024304>.
- [64] N. Soszka, B. Hachuła, M. Tarnačka, E. Kaminska, S. Pawlus, K. Kaminski, M. Paluch, Is a Dissociation Process Underlying the Molecular Origin of the Debye Process in Monohydroxy Alcohols?, *J. Phys. Chem. B.* 125 (2021) 2960–2967, <https://doi.org/10.1021/acs.jpcc.0c10970>.
- [65] L.P. Singh, R. Richert, Watching hydrogen-bonded structures in an alcohol convert from rings to chains, *Phys. Rev. Lett.* 109 (2012) 1–5, <https://doi.org/10.1103/PhysRevLett.109.167802>.
- [66] J.G. Kirkwood, The dielectric polarization of polar liquids, *J. Chem. Phys.* 7 (1939) 911–919, <https://doi.org/10.1063/1.1750343>.
- [67] W. Dannhauser, R.H. Cole, Dielectric properties of liquid butyl alcohols, *J. Chem. Phys.* 23 (1955) 1762–1766, <https://doi.org/10.1063/1.1740576>.
- [68] W. Dannhauser, Dielectric study of intermolecular association in isomeric octyl alcohols, *J. Chem. Phys.* 48 (1968) 1911–1917, <https://doi.org/10.1063/1.1668989>.
- [69] C.P. Johari, W. Dannhauser, Dielectric study of the pressure dependence of intermolecular association in isomeric octyl alcohols, *J. Chem. Phys.* 48 (1968) 5114–5122, <https://doi.org/10.1063/1.1668182>.
- [70] B.N. Solomonov, V.B. Novikov, M.A. Varfolomeev, A.E. Klimovitskii, Calorimetric determination of hydrogen-bonding enthalpy for neat aliphatic alcohols, *J. Phys. Org. Chem.* 18 (2005) 1132–1137, <https://doi.org/10.1002/poc.977>.
- [71] M. Kwaśniewicz, M.A. Czarnecki, The Effect of Chain Length on Mid-Infrared and Near-Infrared Spectra of Aliphatic 1-Alcohols, *Appl. Spectrosc.* 72 (2018) 288–296, <https://doi.org/10.1177/0003702817732253>.
- [72] R. Hayes, S. Imberti, G.G. Warr, R. Atkin, Effect of cation alkyl chain length and anion type on protic ionic liquid nanostructure, *J. Phys. Chem. C* 118 (2014) 13998–14008, <https://doi.org/10.1021/jp503429k>.
- [73] A.K. Karmakar, P.S.R. Krishna, R.N. Joarder, On the structure function of liquid alcohols at small wave numbers and signature of hydrogen-bonded clusters in the liquid state, *Phys. Lett. Sect. A Gen. At. Solid State Phys.* 253 (3–4) (1999) 207–210.
- [74] A. Perera, F. Sokolić, L. Zoranić, Microstructure of neat alcohols, *Phys. Rev. E – Stat. Nonlinear. Soft Matter Phys.* 75 (2007) 1–4, <https://doi.org/10.1103/PhysRevE.75.060502>.
- [75] L. Almásy, A.I. Kuklin, M. Požar, A. Baptista, A. Perera, Microscopic origin of the scattering pre-peak in aqueous propylamine mixtures: X-ray and neutron experiments: Versus simulations, *Phys. Chem. Chem. Phys.* 21 (2019) 9317–9325, <https://doi.org/10.1039/c9cp01137d>.
- [76] A. Ghoufi, Molecular origin of the prepeak in the structure factor of alcohols, *J. Phys. Chem. B.* 124 (2020) 11501–11509, <https://doi.org/10.1021/acs.jpcc.0c09302>.

- [77] J. Lyklema, A discussion on surface excess entropies, *Colloids Surfaces A Physicochem. Eng. Asp.* 186 (2001) 11–16, [https://doi.org/10.1016/S0927-7757\(01\)00477-0](https://doi.org/10.1016/S0927-7757(01)00477-0).
- [78] L. Glasser, Volume-based thermodynamics of organic liquids: Surface tension and the Eötvös equation, *J. Chem. Thermodyn.* 157 (2021) 106391, <https://doi.org/10.1016/j.jct.2021.106391>.
- [79] N.B. Vargaftik, *Thermophysical Properties of Gases and Liquids, A Reference Book*, Nauka, Moscow, 1972.
- [80] R.B. Badachape, M.K. Charpurey, A.B. Biswas, Density and surface tension of phenol, (mono-, di- and tri-)chlorophenols, salol, and (o- and m-) chloronitrobenzenes, *J. Chem. Eng. Data* 10 (1965) 43–145, <https://doi.org/10.1021/jc60025a022>.

P3. The Impact of Interface Modification on the Behavior of Phenyl Alcohols within Silica Templates

Autorzy: N. Soszka, M. Tarnacka, B. Hachuła, M. Geppert – Rybczyńska, K. Prusik, K. Kamiński

Referencja: *J. Phys. Chem. C*, 2024,

DOI: 10.1021/acs.jpcc.3c08084

Impact Factor czasopisma: 3.7

Liczba punktów ministerialnych MNiSW czasopisma: 140

Mój udział polegał na przygotowaniu próbek materiałów litych i infiltrowanych do matryc krzemowych, wykonaniu pomiarów IR i analizie wyników, dyskusji wyników, współtworzenia manuskryptu (przeprowadzenie przeglądu literaturowego, przygotowanie tekstu manuskryptu i rysunków, opis wyników i sformułowanie wniosków), formułowaniu odpowiedzi na uwagi recenzentów oraz korekcie manuskryptu po otrzymanych recenzjach.

Impact of Interface Modification on the Behavior of Phenyl Alcohols within Silica Templates

Natalia Soszka, Magdalena Tarnacka,* Barbara Hachula, Monika Geppert-Rybczyńska, Krystian Prusik, and Kamil Kamiński

Cite This: <https://doi.org/10.1021/acs.jpcc.3c08084>

Read Online

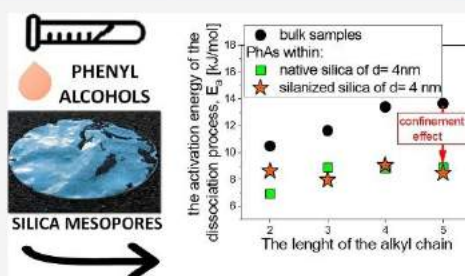
ACCESS |

Metrics & More

Article Recommendations

Supporting Information

ABSTRACT: Herein, thermal and dynamical properties, as well as host–guest intermolecular interactions, and the wettability of a series of monohydroxy phenyl-substituted alcohols (PhAs) infiltrated into native and silanized silica mesopores (of pore diameter, $d \sim 5$ nm) were investigated by means of dielectric and infrared (IR) spectroscopy, differential scanning calorimetry, and contact angle measurements. Calorimetric data showed the occurrence of the two glass transition temperatures, T_g . Importantly, around the one detected at higher temperatures ($T_{g,interfacial}$), a strong deviation in the temperature evolution of the relaxation time of the main process was observed for all systems. Moreover, an additional mode unrelated to the mobility of the interfacial layer and core molecules was revealed. One can suppose that it could be connected to either the slow Arrhenius process (SAP, previously reported for the polymer thin films) or the mobility of hydrogen-bonded structures. Further, IR investigations showed that the applied nanoconfinement had little impact on the strength of the hydrogen bonds (HBs), but it influenced the HBs' distribution (including the 'new' population of HBs) and the degree of association. Additionally, for the first time, we calculated the activation energy values of the dissociation process for PhAs in mesopores, which turned out to be lower with respect to those estimated for bulk samples. Thus, our research clearly showed the impact of the spatial geometrical restriction on the association process in alcohols having significant steric hindrance.



1. INTRODUCTION

Geometric nanoconfinement is a versatile platform for modifying the structural and dynamic properties of soft matter systems, making them highly relevant for nanoscale applications. Previous investigations have revealed that materials adjacent to a solid and near-surface can exhibit interfacial regions of reduced density,^{1–3} interfacial freezing,^{4–6} interfacial melting,^{7–10} molecular layering,^{11–14} molecular orientation,¹⁵ or specific lateral molecular arrangements.¹⁶ Consequently, significant deviations in their properties, such as flow and intermolecular entanglements, local chain mobility, glass transition temperature, diffusion, tautomerization, or crystallization, are noted when compared to bulk samples.^{17–28} Due to these facts, confined systems hold promise for diverse industrial applications, including nanolithography, lubrication, paints, surface treatments, and elastic membranes.

Among many types of nanostructures, silica mesoporous materials, such as MCM-41 or SBA-15, possess the O–H groups (silanol groups ($\equiv\text{Si}-\text{OH}$)) inside pores that can easily interact through H-bonds with lattice oxygen. To successfully tailor these materials for nanotechnology applications, the membrane characteristic is often adjusted by altering the pore diameter or surface properties. The latter includes

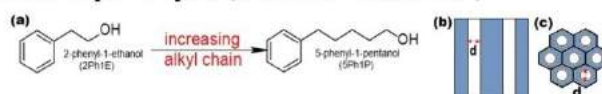
postsynthesis modifications, typically involving silanizing agents like methoxytrimethylsilane, trimethyl chloride,²⁹ mercaptopropyltrimethoxysilane,³⁰ hexamethyldisilazane,³¹ or chlorotrimethylsilane,³² which change the surface of the silica from hydrophilic to hydrophobic by replacing the O–H groups with organic groups via O–Si–C covalent bonds. This alteration affects the pore structure, which determines the nature of host–guest interactions. To illustrate that, one can refer to the studies on water in hydrophilic and hydrophobic nanochannels. In the former case, IR spectroscopy revealed a predominant icelike structure because of comparable strong interactions between the water molecules and the pore wall (interfacial interactions),²⁹ while for the latter one, water behaved more liquid-like (bulk-like), as water molecules interacted less with the silica surface (fewer interaction sites at the pore wall) and more with each other.³³ Similar trends

Received: December 11, 2023

Revised: March 25, 2024

Accepted: March 25, 2024

Scheme 1. (a) Chemical Structures of Investigated Phenyl Alcohols and the Schematic Structure of (b) the Cross-Section and (c) the Top of Applied Silica Mesopore Templates (d Denotes the Pore Diameter)



were also observed for aliphatic mono- and polyhydroxy alcohols^{31,34} infiltrated into nanopores, where hydrophobization of the silica surface hinders H-bonds between the pore wall and the guest molecules, making the dynamics of the confined liquid more bulk-like.³¹ The effects related to the reduction of surface interactions were also seen for hydroxyl-terminated polymers infiltrated into modulated anodic alumina (AAO) templates.³⁵ In this case, the factor responsible for the disturbance of the interaction at the polymer–membrane interface was the roughness of applied nanotemplates. Importantly, similar results were also reported for PhAs infiltrated within mesoporous anodic aluminum oxide (AAO) membranes having constant and varying pore diameters ($d = 10\text{--}40$ nm). Samples within ordinary AAO templates revealed a pronounced confinement effect on the glass transition temperature, T_g , and the structural relaxation process, whereas alcohols in the latter templates showed a bulklike behavior in the whole range of studied temperatures.³⁶ Herein, one can also mention the papers where authors explored the impact of the position of the hydroxyl group (primary, secondary, tertiary) in the molecular skeleton of monohydroxy alcohol (MA) being nanospatially restricted on their supramolecular organization and molecular dynamics.^{37–40}

In this paper, we investigated the effect of surface interactions on the behavior of a series of phenyl-substituted monohydroxy alcohols (PhAs) from ethanol to pentanol (see their chemical structure in Scheme 1(a)) incorporated into mesoporous (un)treated silica templates by means of broadband dielectric spectroscopy (BDS), differential scanning calorimetry (DSC), and Fourier transform infrared (FTIR) spectroscopy. The applied silica mesopores are composed of uniaxial nanochannels (open from both sides) with a defined pore size (see Scheme 1(b,c)). The characterization of the produced membranes was made by using scanning electron microscopy (SEM, see Figure S1). The mean diameter of the mesopores, d , was determined as $\lambda \sim 5$ nm.

2. MATERIALS AND METHODS

2.1. Materials. 2-Phenyl-1-ethanol (2Ph1E), 3-phenyl-1-propanol (3Ph1P), 4-phenyl-1-butanol (4Ph1B), and 5-phenyl-1-pentanol (5Ph1P) with a purity higher than 98% were supplied by Sigma-Aldrich. Their chemical structures are shown in Scheme 1(a). The native and silanized silica mesopores of pore diameter, $d \sim 5$ nm (Scheme 1(b,c)), were produced by the electrochemical etching of silicon wafers and subsequent thermal oxidation. Details about the fabrication of silica templates and their further modification are presented in the Supporting Information, SI file.^{41,42} The characterization of the produced membranes was made by using scanning electron microscopy (SEM).

2.2. Sample Preparations. Prior to filling, the silica membrane was dried in an oven at $T = 373$ K under vacuum in order to remove any volatile impurities from the nanochannels, and alcohols were subjected to freezing in liquid nitrogen to remove water. After cooling, membranes were infiltrated with

alcohols. Then, the alcohol–membrane systems were maintained under vacuum (10^{-2} bar) to allow the liquid to flow inside via capillary forces. The complete filling was obtained by weighing the templates before and after each infiltration to a constant mass. After the infiltration process, the excess of the sample on the surface was removed. The pore diameter of silica nanopores was confirmed by SEM measurements (Figure S1). The filling degree reaches $\sim 90\%$. Note that taking into account the porosity of applied membranes ($\sim 10\%$) together with the cylindrical shape of porous nanochannels (characterized by a pore diameter of $d \sim 5$ nm and length, $l \sim 50$ μm), we calculated the maximum amount of alcohol, which can be infiltrated within the molecules, and we compared this value with the weight of the infiltrated substance.

2.3. Scanning Electron Microscopy (SEM). The pore distribution images were taken by using a JEOL JSM-7100F TTLS LV/EDS field emission scanning electron microscope (SEM). For the SEM observations, samples in the form of small flakes cut from the received sheet were stuck to the sample holder by a carbon conductive tape. Secondary electron images (SEIs) obtained at magnifications ranging from 35 to 500,000 times were collected by an E-T detector at beam accelerating voltages between 2 and 15 kV. The mean diameter of the mesopores, d , was determined as $4.8(\pm 1.1)$ nm. The mesopores were measured by using the ImageJ package. The mean diameter of the mesopores was determined by fitting a log-normal distribution to the experimental data (the histogram in Figure S1(c)). Note that in the case of the modified templates, the silanization process (carried out on the native mesopores) does not affect the mean diameter of the applied mesoporous templates, resulting in a similar SEI as in the case of native membranes.

2.4. Differential Scanning Calorimetry (DSC). Calorimetric measurements were carried out by using a Mettler-Toledo DSC apparatus equipped with a liquid nitrogen cooling accessory and an HSS8 ceramic sensor (a heat flux sensor with 120 thermocouples). Temperature and enthalpy calibrations were performed using indium and zinc standards. The sample was prepared in an open aluminum crucible (40 μL) outside of the DSC apparatus. Samples were scanned at various temperatures at a constant heating rate of 10 K/min.

2.5. Surface Tension and Contact Angle Measurements. The surface tension of liquids, γ_L , and the contact angle, θ , were measured by the drop shape analysis 100S Krüss tensiometer, GmbH Germany, with Advance software. The surface tension, γ_L , was measured with the pendant drop method.^{43–45} The γ_L was measured in the temperature range, $T = 293\text{--}333$ K, with a step of 5 K. For each temperature, several drops of a similar volume (~ 2.5 μL) were equilibrated in an argon atmosphere. The temperature measurement uncertainty was ± 0.1 K, whereas the uncertainty of the surface tension was ± 0.1 mN/m. The contact angle measurements were performed at nine temperatures in the wide temperature range, $T = 263\text{--}298$ K. Thanks to the measuring chamber adopted to work in the wide temperature range with humidity

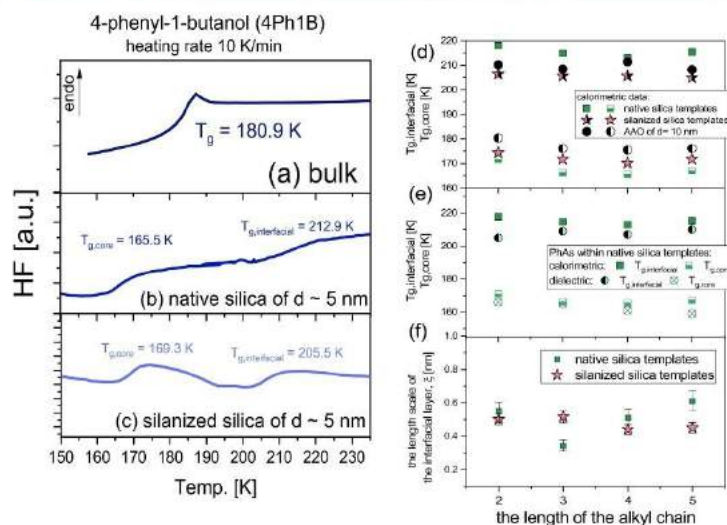


Figure 1. (a–c) DSC thermograms obtained for bulk and confined samples of 4Ph1B. (d) Glass transition temperatures (determined from calorimetric measurements) of all confined samples vs the length of the alkyl chain of the examined PhA. (e) Comparison of the glass transition temperatures obtained from BDS and DSC measurements for all studied infiltrated samples. The uncertainty of T_g determination is ± 2 K for all presented values. (f) Thickness of the interfacial layer (ξ) plotted as a function of the length of the alkyl chain.

control, it was possible to measure the contact angle below the freezing point of water. The contact angle measurements on the solid smooth surfaces have been repeated a dozen or more times. The precision of contact angle measurements was 0.01° , and the estimated uncertainty was not more than $\pm 2^\circ$. For the surface energy (γ_s) estimation of alumina and (native and silanized) silica, some of the following liquids were considered: water, ethylene glycol, diiodomethane, and glycerol. The dispersive and nondispersive parts in the surface tension for these substances were taken from ref 40. The calculated surface energy for native silica was $\gamma_s = 67.6$ mJ/m² with the dominant nondispersive part equaling 66.6 mJ/m². For silanized silica, the respective value was $\gamma_s = 25.3$ mJ/m² with the dominant dispersive part equaling 22.8 mJ/m².⁴⁶ Details are presented in the SI file.

2.6. Broadband Dielectric Spectroscopy (BDS). Measurements were carried out on heating after a fast quenching of the liquid state in a wide range of temperatures (175–243 K) and frequencies (10^{-1} to 10^6 Hz) using a Novocontrol spectrometer equipped with an α impedance analyzer with an active sample cell and a Quatro Cryosystem. Dielectric measurements of bulk samples were performed in a parallel-plate cell (diameter: 15 mm, gap: 0.1 mm), as described in ref 47. Silica membranes filled with studied alcohols were also placed in a similar capacitor (diameter: 10 mm, membrane thickness: 0.05 mm).^{41,42} Nevertheless, the confined samples are heterogeneous dielectrics consisting of a matrix and an investigated compound. Because the applied electric field is parallel to the long pore axes, the equivalent circuit consists of two capacitors composed of $\epsilon_{\text{compound}}^*$ and $\epsilon_{\text{templates}}^*$. Thus, the measured total impedance is related to the individual values through $1/Z_c^* = 1/Z_{\text{compound}}^* + 1/Z_{\text{templates}}^*$ where the contribution of the matrix is marginal. The measured dielectric

spectra were corrected according to the method presented in ref 48.

The normalized α -loss peak for the bulk was fitted to the one-sided Fourier transform of the Kohlrausch–Williams–Watts (KWW) function (the dotted line in Figure 2(c,f))

$$\Phi_{\text{KWW}}(t) = \exp[-(t/\tau_\alpha)^{\beta_{\text{KWW}}}] \quad (1)$$

We found that for bulk PhAs, the fractional exponent, β_{KWW} , which describes the α -relaxation time distribution's nonexponentiality, is equal to 0.9.

In order to obtain relaxation times, τ , the all dielectric data were fitted using the Havriliak–Negami (HN) function⁴⁹

$$\epsilon^*(\omega) = \frac{\sigma_{\text{DC}}}{\epsilon_j \omega} + \epsilon_\infty + \sum_{i=1}^2 \left(\frac{\Delta \epsilon_i}{[1 + (i\omega\tau_{\text{HN},i})^{\alpha_{\text{HN},i}}]^\beta} \right) \quad (2)$$

where σ_{DC} is the dc-conductivity term, ϵ_j is the permittivity of the free space, $\Delta \epsilon$ is the dielectric strength, ω is the angular frequency ($\omega = 2\pi f$), τ_{HN} describes the HN relaxation time, and α_{HN} and β_{HN} are the shape parameters. The subscript i refers to each process. Note that the examples of dielectric spectra collected for the bulk 2Ph1E as well as confined within native silica templates fitted to either a single HN function or two HN functions with the conductivity term, respectively, are shown in Figure S6.

The temperature dependences of the relaxation times (determined for the bulk Debye-like process) were fitted using the Vogel–Fulcher–Tamman (VFT) function^{50–52}

$$\tau = \tau_\infty \exp\left(\frac{B}{T - T_0}\right) \quad (3)$$

where τ_∞ is the relaxation time in the limit of very high temperatures, T_0 is the so-called Vogel temperature, and B is

C

<https://doi.org/10.1021/acs.jpcc.3c08084>
J. Phys. Chem. C XXXX, XXX, XXX–XXX

the activation parameter. T_g s of the bulk samples was determined as the temperature at which $\tau = 100$ s by extrapolating the VFT fits. To determine $T_{g,core}$ for the confined systems, their $\tau_{Dom}(T)$ dependences below $T_{g,interfacial}$ (after the kink) were fitted with either the VFT function or the Arrhenius equation (dependent on the sample)

$$\tau = \tau_{\infty} \exp\left(\frac{E_a}{k_b T}\right) \quad (4)$$

where k_b is the Boltzmann constant, and E_a is the activation energy. $T_{g,core}$ values of the confined PhAs were determined as the temperature at which $\tau = 100$ s by extrapolating either VFT or Arrhenius fits.

2.7. Fourier Transform Infrared (FTIR) Spectroscopy.

The FTIR spectra of bulk and confined samples were recorded on a Nicolet iSSO FTIR spectrometer (Thermo Scientific, Madison, WI) with continuous dry air purging to eliminate carbon dioxide and water vapor. The measurement parameters were set in OMNIC software (Version: 9.6.251, Thermo Scientific) as follows: the spectral resolution of 2 cm^{-1} , 16 scans, a gain of 8, and the spectral region of the collected spectra $4000\text{--}1300 \text{ cm}^{-1}$. Due to the saturation of silica membranes, the region below 1300 cm^{-1} was not analyzed. To monitor the temperature, the Linkam THMS 600 stage was used, which allowed for measurements in the temperature range of $T = 297\text{--}153 \text{ K}$ (with a temperature rate of 4 K/min). Additional purging of the apparatus was applied for 30 min before each measurement. In the first step, the background spectra of an empty pore (Figure S2) were recorded in a wide range of temperatures ($T = 297\text{--}153 \text{ K}$) to eliminate any influence of the template on the spectra of the incorporated alcohol. Infiltrated alcohols were measured under the same conditions as for empty pores, with matching temperature ranges and spectral parameters. The background spectrum of the "empty" pore was automatically subtracted from the measured spectrum. Initial spectral preprocessing, including baseline correction, was performed with the OMNIC program. A simplified scheme for the IR measurements is presented in Scheme S1.

3. RESULTS AND DISCUSSION

Representative DSC curves recorded for bulk 4Ph1B and samples infiltrated into various silica membranes are presented in Figure 1(a–c). Note that representative DSC curves recorded for 2Ph1E and 3Ph1P are shown in Figure S4. All bulk samples exhibit the presence of one glass transition (manifested by a characteristic endothermic jump of the heat capacity). Moreover, T_g s reveal a slight 'odd–even' effect with the change in the molecular weight of alcohol.⁴⁷ Values of the glass transition temperatures determined for nonconfined systems are listed in Table S1. On the other hand, for PhAs incorporated within various silica membranes characterized by a defined pore diameter, $d \sim 5 \text{ nm}$ (see Figure S1), two (double) glass transitions (DGTs, manifested as two endothermic signals) located above and below the bulk T_g were observed. One can stress that herein, the DGT phenomenon was recorded for all examined confined samples, regardless of the length of the alkyl chain of PhAs and the type of templates (native/silanized). It should be noted that the similar scenario was previously reported for a variety of glass formers, including associating materials, infiltrated into various porous templates (silica, alumina, etc.).^{53–58} The presence of

the DGT is assumed to originate from the confinement-induced distribution of interactions within the systems due to the presence of the solid interface, leading to the heterogeneity in terms of molecular dynamics as well as the packing density. Moreover, it can be described by the simple 'two-layer' (or 'core–shell') model,^{55,59} which implies that one can distinguish previously mentioned 'interfacial' molecules of reduced mobility with the glass transition occurring at higher temperatures ($T_{g,interfacial}$), and the particles located at some distance from the interface (more in the middle of the nanochannels) labeled as the 'core' fraction characterized by lower values of the glass transition temperatures ($T_{g,core}$). Importantly, until now, it was assumed that the lack of specific interactions between confined molecules and the interface would result in the absence of a defined interfacial layer. However, recent studies of polar van der Waals liquid, (S)-(–)-4-methoxymethyl-1,3-dioxolan-2-one (labeled as S-methoxy-PC),⁶⁰ incorporated within AAO membranes of different pore sizes and modified surfaces clearly show that it is not the case, and even for the silanized hydrophobic surface, the DGT phenomenon (especially the presence of $T_{g,interfacial}$) can be seen. A similar situation was found in our study, but it seems that the silanization process of the mesoporous templates affects the DSC signal. Values of determined T_g s are presented in Figure 1(d) and Table S1. As shown, $T_{g,interfacial}$ and $T_{g,core}$ decrease slightly ($\Delta T_g \sim 5 \text{ K}$) with the elongation of the alkyl chain for the samples infiltrated into both types of applied templates. Nevertheless, there is a pronounced difference in T_g s between materials infiltrated within either native or silanized silica templates, where the difference between both T_g s (defined as $\Delta T_g = T_{g,interfacial} - T_{g,core}$) is higher for alcohols within the latter pores. This possibly originates from the specific H-bonding interactions between native silica and alcohol, which are strongly reduced in the silanized pores.

Next, in order to quantify the volume of the interfacial layer dependently on the surface interactions, we calculated the length scale of the interfacial layer, ξ , as follows:⁵⁸

$$\xi = \frac{d}{2} \left[1 - \left(1 - \frac{\Delta C_{p,interfacial}}{\Delta C_{p,interfacial} + \Delta C_{p,core}} \right)^{1/2} \right] \quad (5)$$

where ΔC_p s are heat capacity changes at the corresponding T_g (determined from the differences between C_p after and before the detected heat capacity jump). Note that eq 5 was applied under the following conditions: the volume of the material in the surface layer is proportional to the step change of its heat capacity; the density of the confined sample is constant along the pore radius; and the pore is cylindrical. Additionally, it should be highlighted that eq 5 is a simple mathematical model, assuming direct proportionality between the heat capacity and the number of molecules, and it does not take into account any variation in the density, roughness, or curvature of applied templates. This might lead to some overestimation of ξ . The determined values of ξ for all examined samples plotted as a function of the alkyl chain are shown in Figure 1(f). As illustrated, the interfacial layer reaches the length scale of approximately $\xi \sim 0.5 \text{ nm}$ for all samples incorporated into the native or silanized porous template. For comparison, one can mention that for PhAs infiltrated within the AAO membrane of a significantly higher pore size, $d = 10\text{--}40 \text{ nm}$, $\xi \sim 2$ to 7 nm .⁵⁶ Such a high value of ξ seems to indicate up to 10 molecular layers, which might be achieved by

D

<https://doi.org/10.1021/acs.jpcc.3c08084>
J. Phys. Chem. C XXXX, XXX, XXX–XXX

the formation of some associating structure (most likely loosely packed) near or at the interface. Moreover, one can add that for other MAs, i.e., 2-ethyl-1-hexanol, 2-ethyl-1-butanol, and 5-methyl-3-heptanol, infiltrated into native silica templates of comparable pore sizes ($d = 4\text{--}8\text{ nm}$), the length scale of the interfacial layer reaches $\xi \approx 0.5$ to 1.4 nm .⁴⁰

In order to understand why we observe two prominent glass transition temperatures in recorded thermograms and a rather comparable length scale of the interfacial layer in alcohols infiltrated within native and modified silica, we carried out additional measurements of the contact angle, θ ,^{46,62,63} which can be used to quantify wettability. As one can recall, the smaller θ indicates the better spreading out of a liquid drop on the examined surface (and thus, better wettability). Values of determined θ values for all examined PhAs are shown in Table 1 and Figure S3. All of these measurements were carried out on

Table 1. Contact Angle, θ , at 298 and 258 K, as well as the Surface Tension, γ_L

sample	γ_L at 298 K [mN/m] ^a	native silica		silanized silica	
		θ at 298 K [°]	θ at 258 K [°]	θ at 298 K [°]	θ at 258 K [°]
2Ph1E	38.84	30.2	22.2	44.0	28.3
3Ph1P	38.28	28.4	21.8	42.0	28.6
4Ph1B	37.26	28.2	22.0	39.2	26.6
5Ph1P	37.01	28.9	22.2	39.8	26.9

^aValues of γ_L were taken from ref 61.

the planar surfaces, which most likely have different properties than the curved surface of the pore walls (generated during electrochemical etching). Nevertheless, such an approach is well accepted in literature and provides approximated information about the effect of wettability on the dynamics and shift of the glass transition temperature of the confined materials.^{64,65} As can be seen, all materials are characterized by similar contact angles independent of the examined surface; however, in the case of silanized substrates, values of θ are higher, as can be expected due to differences in the surface interactions. Nevertheless, contrary to the expectations, both surfaces can be considered hydrophilic since for all of them, $\theta < 90^\circ$. Therefore, one can state that there is some difference in the wettability of the material located on native and modified silica, but it is not significant. Moreover, it should be pointed out that the contact angle decreases with a lowering temperature, reaching comparable values $\theta \sim 22^\circ$ and $\theta \sim 28^\circ$ for PhAs spread on the respectively native and silanized silica surfaces at $T = 266\text{ K}$ (see Table 1 and Figure S3). That means that at low temperatures, wettability and intermolecular interactions between materials and pore walls are comparable for all systems independent of the applied type of template. Therefore, one might assume that specific H-bonding interactions with pore walls do not play a significant role in the enhancement of the wettability of the PhA in native silica with respect to the samples infiltrated into the silanized template. Nevertheless, a noticeable shift in the $T_{g,interfacial}$ to the higher temperature for the samples infiltrated into former membranes with respect to the modified ones is most likely due to the formation of the strong H-bonds between host and guest molecules, which are not present in the latter system.

Furthermore, we performed comprehensive dielectric measurements. Figure 2(a,b,d,e) illustrate the representative dielectric loss (ϵ'') spectra obtained for 2-phenyl-1-ethanol

(2Ph1E) and 4-phenyl-1-butanol (4Ph1B) incorporated within native and silanized silica templates of $d \sim 5\text{ nm}$. Data for the nonconfined compound are presented as insets in Figure 2(a,d). Dielectric loss spectra recorded for 3Ph1P and 5Ph1P are shown in Figure S5. As shown, the spectra obtained for bulk samples are composed of two relaxation processes, the dc-conductivity at lower frequencies (related to the ion transport) and a prominent relaxation process at higher frequencies that dominates the recorded spectra (characterized by a Kohlrausch–Williams–Watts (KWW) stretched exponent, $\beta_{KWW} \sim 0.90$, suggesting the Debye-like response, see Figure 2(c,f)).⁵¹ Therefore, in this paper, we label this process as a Debye-like (D) one for the macroscale systems. Note that the loss spectra of various MA often exhibit the presence of a prominent Debye-like peak (originating from the formation of associating structures⁶⁶), whereas the structural (α) process (cooperative motions of molecules) often manifests itself as an excess wing on the high-frequency flank of the Debye mode.^{40,42,67,68} Herein, we observed only one prominent symmetric mode, with no sign of any additional process. Therefore, at first, this single dominant relaxation observed in the dielectric response of PhAs was interpreted as a genuine α mode.⁶⁹ However, recent studies on phenyl-substituted alcohols by a combination of BDS with different experimental techniques (i.e., either photon correlation spectroscopy, PCS, or mechanical measurements^{67,70–72}) clearly show that this relaxation observed in the case of PhAs is, in fact, the superposition of the two modes (a slow Debye-like and an α one, resulting from both the cross-correlation between dipole–dipole and self-dipole correlation, respectively) but is observed as only one relaxation peak due to their similar time scale.⁶⁷

Interestingly, in the case of PhAs infiltrated in various silica membranes, one can observe a different scenario. First, for alcohols within native (untreated) templates, the presence of three relaxation processes can be detected (instead of the two modes observed in the bulk). An additional relaxation process emerges in the middle-frequency range on the low-frequency side of the main relaxation peak. Importantly, it becomes more prominent with an increase in the alkyl chain of examined compounds (see Figure 2(c,f)). On the other hand, it is not resolved for alcohols within silanized (treated) templates. Taking those observations into consideration, one can assume that the additional process might be, in fact, related to the motions of the molecules in close proximity to the interface, which strongly interacts with the pore walls (so-called interfacial molecules).^{46,73} Therefore, often this process is denoted as the interfacial one. It is assumed that this mobility is no longer present within materials confined within treated silica templates due to a lack of specific interactions between PhA molecules and the interface as a result of the silanization. However, taking into account the above-mentioned calorimetric data, one can also expect to observe the interfacial process in the case of silanized systems. In this context, one can briefly remind that this process was not previously reported for alcohols incorporated in AAO templates of various pore sizes,³⁶ which was assigned to the difference in the time scale of the mass exchange between interfacial and core molecules and the experiment time.⁷⁴ It is assumed that when the exchange between both fractions is faster than the time of the experiments, the interfacial process can be detected (and absent if not). Thus, one can assume that the lack of a well-resolved additional process of PhAs within silanized mesopores might be related to the differences between the time scale of

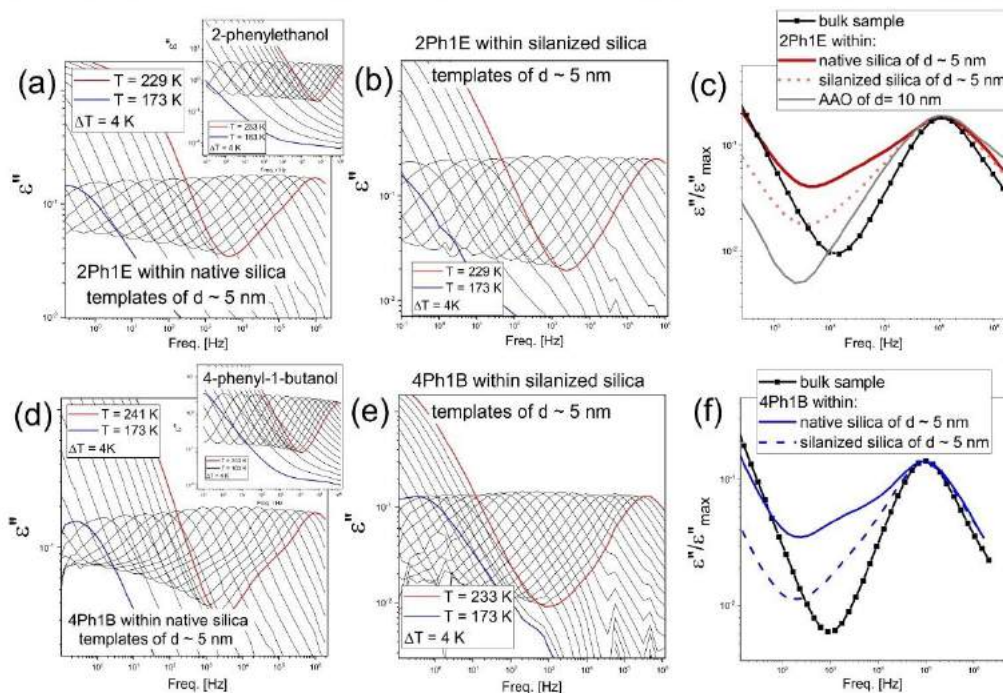


Figure 2. Dielectric loss spectra of (a, b) 2Ph1E and (d, e) 4Ph1B infiltrated within (a, d) native and (b, e) silanized silica templates. The insets in panels (a) and (d) show the dielectric data for the bulk systems. (c, f) Comparison of dielectric loss peaks obtained for all measured samples at $f = 10^5$ Hz.

the mass exchange between interfacial and core molecules and the experiment time when compared to the MAs within native templates.^{74,75}

Figure 2(c,f), representing the shape of the main relaxation process for all examined systems, is shown in comparison to that of the bulk. The presented spectra were shifted to superposed at the same relaxation time as the main relaxation process. As illustrated, the dominant relaxation peak observed for all examined confined systems is broader (especially in the low-frequency region) than those of the bulk sample. This agrees with the previous data reported for PhAs infiltrated within various AAO templates (data for alcohols within AAO membranes of $d = 10$ nm were added). One can mention that this behavior is a common feature of both van der Waals and associating liquids infiltrated into various porous materials (AAO/silica).^{76–77,78} This broadening of the distribution of the relaxation times is often discussed as a result of an increase in the heterogeneity of the molecular mobility observed in the confined systems, most likely induced by the presence of the solid interface (in terms of the introduction of additional interactions within the examined systems).^{73,80} One can add that for associating materials, changes in the hydrogen bond population under confinement might also be taken into consideration.^{67,81} At this point, two issues should be highlighted. First, the observed loss peak under confinement is no longer a Debye-like relaxation; therefore, in the case of confined samples, this mode would be referred to as a

dominant or main relaxation process. Second, the significant broadening of the low-frequency side of the main relaxation peak for PhAs within native silica templates suggests the emerging of a new mode, which might be assigned to the interfacial process as discussed above. However, when examining the spectra collected for PhAs within silanized (treated) templates, one can also see that the interfacial process can be observed as well, but it has a significantly lower amplitude when compared to the materials within native membranes.^{41,42} This might imply that even if the specific interactions at the interface are suppressed due to the performed surface modification, some van der Waals interactions near the surface can still be present, contributing to the formation of the molecule fraction characterized by reduced mobility in the proximity of the more hydrophobic surface. Note that the interfacial process is also affected by the magnitude of the dipole moment libration of immobilized molecules as well as the long-distance correlation between dipoles. Nevertheless, it should be mentioned that up to now, no presence of the interfacial process was reported for materials infiltrated within modified silica templates.^{41,42,82,83} Therefore, the question arises as to the origin of the observed additional relaxation process.

To provide additional information, in the next step, we determined the temperature dependence of the relaxation times, τ , of observed relaxation peaks, the dominant (τ_{Dom}) and additional (τ_{Add}) ones located at high- and middle-frequency

F

<https://doi.org/10.1021/acs.jpcc.3c08084>
J. Phys. Chem. C XXXX, XXX, XXX–XXX

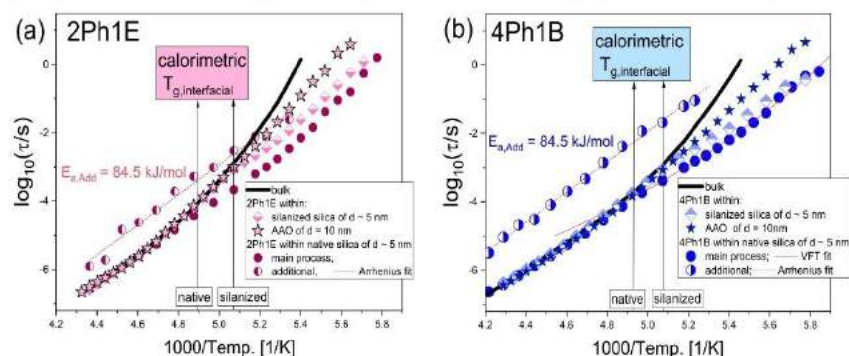


Figure 3. Temperature dependences of the relaxation time (τ) obtained for bulk and confined (a) 2Ph1E and (b) 4Ph1B. For comparison, data for PhAs within AAO templates characterized by $d = 10$ nm are shown (taken from ref 36).

regions, respectively. For that purpose, the dielectric data were fitted using (one or two) Havriliak–Negami (HN) function(s) with an additional dc-conductivity term (see Section 2 and Figure S6).⁸⁴ Determined in this way, relaxation times were plotted versus the inverse temperature and are shown in Figure 3. Data for 3Ph1P and 5Ph1P are shown in Figure S7. As illustrated, there are no differences between the $\tau_{\text{Dom}}(T)$ dependences of examined systems (either bulk or infiltrated) at the 'high-temperature' region, while further cooling revealed a systematic change in the slope of $\tau_{\text{Dom}}(T)$ of infiltrated materials from VFT-like of the bulk characteristic to the more Arrhenius-like at some specific temperature. It should be highlighted that this characteristic 'change in the slope' is a common feature reported for the various systems infiltrated into porous media independent of the applied pore size and the materials the templates are made of (i.e., AAO or silica).^{85,86} Moreover, it should be mentioned that the specific temperature (at which the change in the slope occurs) is reported to strongly depend on the pore size. In fact, the lower the d , the higher is the specific temperature. This deviation of dynamics observed for infiltrated systems was recently assigned to two major effects: (1) changes in the dynamical heterogeneities, ζ , within the glass formers under confinement conditions^{74,86} and (2) the vitrification of the interfacial molecules.^{85,87,88} The former approach implies that the pore size of the applied porous membranes suppresses ζ upon cooling, resulting in the deviation of $\tau(T)$. However, this issue seems to be only valid for the systems characterized by $d \sim \zeta$, where ζ was calculated to approximately $\zeta \sim 2$ to 3 nm.^{74,86,89,90,91} Nevertheless, one can recall that the change of $\tau(T)$ was also reported for the cases where the pore diameter was higher than 18 nm (significantly higher than ζ). Therefore, this phenomenon is often described by considering the vitrification of the interfacial layer (located near the interface). Consequently, below that temperature, the investigated system might be regarded as pseudoisochoric,^{91,92} which results in a change in the temperature dependence of relaxation times of core molecules, which follow $\tau_c(T)$ at constant volume. Hence, the specific temperature (at which the change in the slope occurs) is usually assigned as the glass transition temperature of the interfacial molecules (located in close proximity to the interface and characterized by the 'higher' interfacial interactions and strongly reduced mobility),

$T_{g,\text{interfacial}}$. Note that we also observed a pronounced reduction of the dielectric strength, $\Delta\epsilon$, of the dominant process observed under confinement in comparison to the bulk samples (see Figure S8). One can recall that in the case of associating materials, this behavior might indicate the reduction in the cluster size, association under confinement.³⁵ However, alternatively, this might also suggest that some molecules are "adsorbed" at the interface; therefore, they do not contribute to this mode, leading to a reduction of $\Delta\epsilon$.⁹³

Taking into account the data shown in Figure 3, we draw the attention to three major observations. First, the deviation of $\tau_{\text{Dom}}(T)$ can be observed for all applied types of membranes (native and modified), although the change in $\tau_{\text{Dom}}(T)$ occurs at different conditions (see Table S1). Second, the specific temperature (at which the change in the slope of $\tau_{\text{Dom}}(T)$ occurs) agrees well with $T_{g,\text{interfacial}}$ determined from the calorimetric measurements (see Figure 1(e)). This implies that the vitrification of the interfacial molecules might be responsible for the observed deviation of $\tau_{\text{Dom}}(T)$. Third, it is worthwhile to stress that the temperature at which $\tau_{\text{Dom}}(T)$ deviates from the bulklike behavior does not correspond in any way to the behavior of the slower dielectric relaxation process appearing in the dielectric response of alcohols infiltrated within native silica templates (see Figure 3). Note that the relaxation times of this additional dielectric process reach $\tau_{\text{Add}} \sim 0.01$ – 0.001 s when a change in the slope of the relaxation times of the main dielectric mode occurs. Therefore, taking into account also the results obtained from the calorimetric measurements, i.e., the presence of DGT and the fact that interfacial molecules form an interfacial layer, irrespective of the character of the pore walls, one can indeed assume that the deviation of $\tau_{\text{Dom}}(T)$ originates from the vitrification of the adsorbed molecules in pores. However, the additional dielectric response observed in the loss spectra collected for PhAs within native silica templates of $d \sim 5$ nm (see Figure 1) is most likely not connected to the mobility of the interfacial layer.

Therefore, the question arises about the origin of the observed additional relaxation process. One can mention that the $\tau_{\text{Add}}(T)$ dependence resembles the characteristic of the slow Arrhenius process (SAP) recently observed in the loss spectra collected for the (unequilibrated) polymeric thin films.⁹⁴ This molecular origin seems to be valid, especially

taking into account that the activation energies, E_a , of this process determined for all examined samples reach $E_{a,Add} \sim 70.7\text{--}91.1$ kJ/mol (see Table 2), whereas those of the SAP

Table 2. Activation Energies, $E_{a,Add}$, Calculated from the Arrhenius Equation (Eq 4) for the Additional (Slower) Relaxation Mode Observed in the Dielectric Response of PhAs Incorporated into Native Silica Membranes of $d \sim 5$ nm

	2Ph1E	3Ph1P	4Ph1B	5Ph1P
$E_{a,Add}$ [kJ/mol]	84.5	91.1	84.5	70.7

determined for a series of various polymeric thin films are of the order of $E_{a,SAP} = 100$ kJ/mol. Nevertheless, it should be pointed out that the present data are insufficient to clearly distinguish the origin of the additional dielectric mobility observed for the examined series of PhAs within native silica templates. Therefore, this issue will be explored further within the next projects.

Alternatively, one can assume that this additional dielectric mode can originate from the mobility of "the confinement-induced" associating structures. Note that in the case of the bulk materials, we do not observe any separate mobility related to the structural relaxation but only the presence of a Debye-like process (related to the formation of nanoassociates). In fact, recent studies confirmed that the Debye-like process detected for PhAs is indeed related to the association–dissociation process according to the transient chain model (TCM).⁶⁶ Thus, this additional mobility observed in pores

might be related to the formation of 'new' confinement-induced associating structures. To shed new light on this problem, we performed infrared measurements to monitor the population of hydrogen bonds (HBs) of the studied compounds under confinement. Herein, we focused mostly on monitoring the changes in the H-bonding properties of PhAs, which can be well reflected and visible in the stretching vibration bands of hydroxyl groups located in the wavenumber range from 3700 to 2600 cm^{-1} . In this region, some peaks occur for both bulk and infiltrated PhA samples, namely, the band of weak intensity at ~ 3550 cm^{-1} assigned to the stretching vibrations of the free, nonbonded O–H groups ($\nu_{OH\text{ free}}$), and a broad signal centered at ~ 3330 cm^{-1} associated with the stretching vibrations of H-bonded O–H moieties ($\nu_{OH\text{ assoc}}$). At lower wavenumbers, the peaks related to the stretching vibrations of aromatic (3100–3000 cm^{-1}) and aliphatic (3000–2800 cm^{-1}) C–H groups are observed.

In Figure 4, the IR spectra of bulk and infiltrated samples in the 3700–2600 cm^{-1} spectral range over a wide temperature interval ($T = 297\text{--}153$ K) are shown. One should mention that the H-bonding properties of bulk PhAs were previously detailed in ref 47; hence, in this paper, we mainly analyzed the associating behavior of infiltrated PhAs compared to the bulk ones. As shown in Figure 4, the most significant changes were observed in the ν_{OH} band region, as the position of this band was red-shifted (shifted to lower wavenumbers) with decreasing temperature in both bulk and confined PhAs. Such a spectral behavior clearly indicates the strengthening of H-bonds in these systems upon cooling. The same effect was detected for other primary and secondary monohydroxy

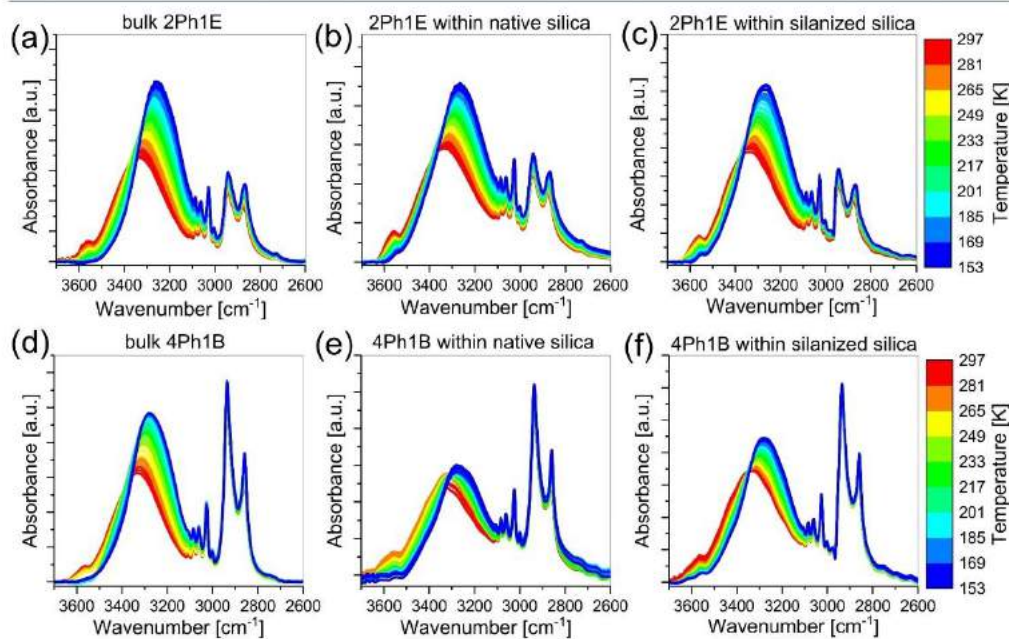


Figure 4. Infrared spectra of 2Ph1E in (a) bulk, (b) native pore, and (c) silanized pore and 4Ph1B in (d) bulk, (e) native pore, and (f) silanized pore in the frequency region 3700–2600 cm^{-1} presented in the temperature range, $T = 297\text{--}153$ K.

H

<https://doi.org/10.1021/acs.jpcc.3c08084>
J. Phys. Chem. C XXXX, XXX, XXX–XXX

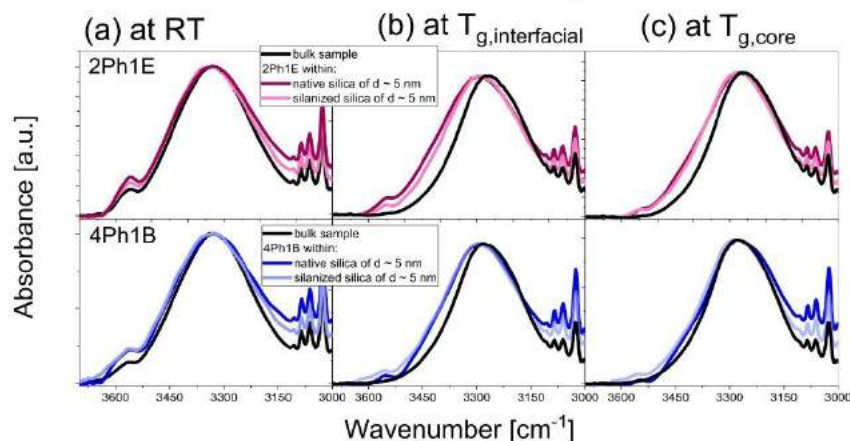


Figure 5. Comparison of FTIR spectra in the frequency region 3720–3000 cm^{-1} for bulk and confined samples of examined PhAs at various chosen temperature conditions: (a) room temperature (RT) and (b, c) calorimetric glass transition temperature of interfacial ($T_{g,\text{interfacial}}$) and core ($T_{g,\text{core}}$) molecules. For the sake of clarity, the spectra were normalized to the OH stretching vibration (ν_{OH}) band.

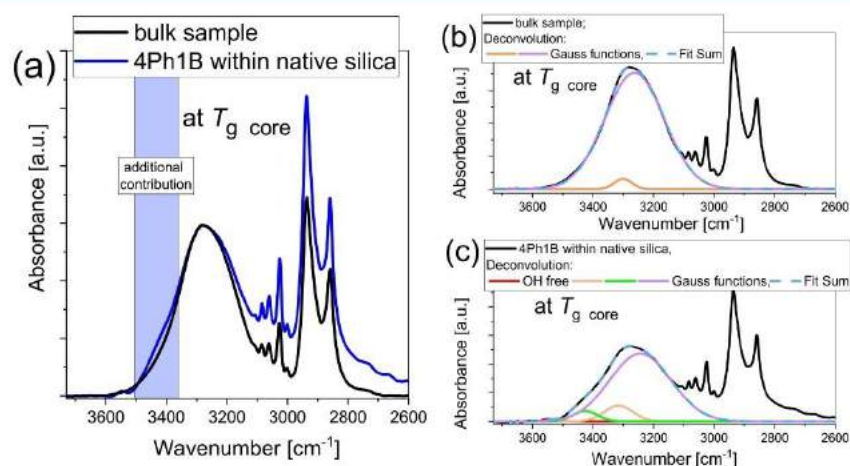


Figure 6. (a) Comparison of the FTIR spectra of bulk 4Ph1B and the sample within native silica mesoporous templates at $T_{g,\text{core}}$. The spectra were normalized to the intensity of the OH band. Deconvolution of the ν_{OH} band of (b) bulk and (c) infiltrated 4Ph1B into the native silica pore at $T_{g,\text{core}}$ using Gauss functions.

alcohols incorporated in silica and alumina mesopores⁴⁰ as well as water confined in periodic mesoporous (organo)silicas.⁹⁵ Furthermore, in both groups of systems, the intensity of the $\nu_{\text{OH free}}$ band decreased as the temperature was lowered/reduced, indicating the higher association degree (larger number of H-bonded MA molecules).

Furthermore, as shown in Figure 5, we compared the FTIR spectra of bulk and confined samples at three temperatures in the 3700–3000 cm^{-1} spectral range. One can see that at RT, the ν_{OH} bands of bulk and confined PhAs exhibit nearly identical shapes, and their positions at the maximum do not differ significantly (see Table S2). Interestingly, the spectroscopic studies conducted for water under confinement showed

that the ν_{OH} band was almost indistinguishable from bulk water,^{17,96} or it was only slightly blue-shifted.⁹⁷ The reported blue shift phenomenon was associated with the poorer H-bond acceptor ability of silica oxygen atoms and thus with the presence of interfacial water molecules.⁹⁷ Moreover, the intensity of the $\nu_{\text{OH free}}$ band was higher for confined PhA samples compared with the bulk. The percentage values of the number/amount of free hydroxyl groups for both bulk and spatially restricted PhAs were calculated and are presented in Figure S9. Details are given in the SI file. It can be noticed that approximately twice as many nonassociated OH groups for MAs under confinement compared to the nonconfined samples is observed, indicating that the association process

of PhAs in geometrical restriction is partly suppressed. These parameter values are similar for both native and silanized silica templates, with slightly higher values for silanized ones, suggesting that functionalizing silica membranes (more hydrophobic) and the overall nanogeometrical restriction led to the presence of more amount of nonbonded OH species in nanopores. What is more, considerable changes in the ν_{OH} bandwidths are detected, i.e., the ν_{OH} bands of MAs in both native and silanized templates are broadened compared to their bulk counterparts. This indicates greater heterogeneity in the distribution of HB aggregates for alcohols under nanoconfinement. At RT, the broadening of this band is more distinct in the lower wavenumber region, suggesting that stronger H-bonds are more affected than weaker ones.

As the temperature decreases, the behavior of the ν_{OH} band resembles that at RT, i.e., the subtle structure of the ν_{OH} band remains, with a weak peak originating from the free hydroxyl groups, suggesting partial association at lower temperatures. As shown, the ν_{OH} peak for MAs in confined samples is shifted to higher wavenumbers, indicating weaker H-bonding interactions in spatial restriction (see Figure 5(b)). Moreover, significant discrepancies between confinement and bulk are observed in the ν_{OH} bandwidth with confined samples having broader bands than bulk samples, especially at lower temperatures. The most prominent difference occurred on the left shoulder of the ν_{OH} band, which might indicate the presence of an additional contribution within the 'weaker H-bonded' OH associate range, much more resolved when compared to the spectra at RT. Note that native silica nanopores exhibit slightly broader ν_{OH} bands compared to silanized membranes. Overall, the widening of the ν_{OH} band follows this order: bulk > silanized pore > native pore, implying a more substantial impact of the hydrophilic environment on the H-bond network of the incorporated PhAs. It should also be mentioned that similar observations were reported for other MAs under confinement, demonstrating that the incorporation of MAs into silica nanomaterials is manifested by the changes in the ν_{OH} peak frequencies and the broadening of the band in the same order as described herein.⁴⁰

To explore the presence of an additional shoulder in the higher frequency region observed for incorporated 4Ph1B (the blue box in Figure 6(a)), we carried out the deconvolution of these spectra recorded at $T_{\text{g,core}}$ in the range of 3600–3000 cm^{-1} . As found, the proper description of the ν_{OH} band of infiltrated 4Ph1B requires the application of three Gaussian curves (see Figure 6(c)), whereas the use of two Gaussian functions is enough to fit the ν_{OH} band of the bulk sample (Figure 6(b)). Interestingly, a new component occurring for the former sample in the higher wavenumber range suggests the existence of additional weak H-bond interactions in the studied system. A similar deconvolution of the ν_{OH} band was presented for water confined in MCM-41 pores. In this case, the region ~ 3350 to 3500 cm^{-1} was assigned to small aggregates of water molecules characterized by different dynamics.⁹⁸ One can also add that the mobility of these 'new' confinement-induced HB interactions, resolved as an additional shoulder in the IR spectra of incorporated PhAs, might contribute to the appearance of the additional relaxation process observed in the loss spectra shown in Figure 2(c,f).

Further, we performed the calculations of the activation energy, E_a , of the dissociation process, using the van't Hoff equation:

$$\ln K = -\frac{E_a}{RT} + \frac{\Delta S}{R} \quad (6)$$

where E_a indicates the activation enthalpy, S is the entropy of the dissociation process, and R is the gas constant. Details of the calculations are shown in the SI file together with the van't Hoff plots for PhAs in native and silanized mesopores, which are presented in Figures S10–14 and Table S3. As can be seen in Figure 7, the estimated values of E_a for PhAs in

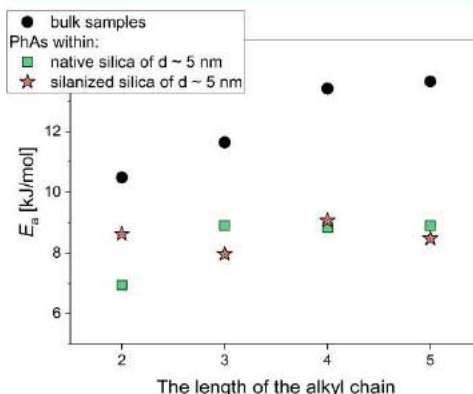


Figure 7. Activation energy of the dissociation, E_a , calculated for bulk PhAs and samples infiltrated into native and silanized silica templates of $d \sim 5 \text{ nm}$.

nanorestriction are lower ($E_a \sim 7$ to 9 kJ/mol) than those in bulk materials (from 10.49 to 13.65 kJ/mol), indicating the significant contribution of weak H-bond interactions occurring in spatially confined geometries compared to the bulk ones in which the stronger HBs dominate. As a result, less energy is required to break these H-bonding interactions in confined samples than in bulk ones. This fact corresponds well with the lower association degree of infiltrated samples relative to that in bulk samples (a slightly smaller number of H-bonded MA molecules relative to free ones under confinement compared to that in bulk samples). Moreover, as the aliphatic chain length increases in bulk alcohols, the dissociation energy tends to rise. However, this trend is not observed in confined samples, where E_a values are comparable (refer to Table 3 for values with errors). It should be mentioned that similar values of this parameter for bulk samples were reported for various aliphatic alcohols, differing in the chain length and the localization of

Table 3. Calculated Activation Energies of Dissociation, E_a , for PhAs Incorporated into Native and Silanized Silica Membranes of $d \sim 5 \text{ nm}$

samples	E_a [kJ/mol]		
	bulk PhAs ^a	PhAs within native silica	PhAs within silanized silica
2Ph1E	10.49 ± 0.28	6.94 ± 0.48	8.62 ± 1.39
3Ph1P	11.64 ± 0.25	8.90 ± 0.52	7.96 ± 1.54
4Ph1B	13.41 ± 0.80	8.84 ± 0.89	9.05 ± 0.74
5Ph1P	13.65 ± 0.43	8.90 ± 0.88	8.47 ± 0.88

^aValues of E_a determined for the bulk samples were taken from ref 61.

J

<https://doi.org/10.1021/acs.jpcc.3c08084>
J. Phys. Chem. C XXXX, XXX, XXX–XXX

the OH groups, with the activation energy of the dissociation process ranging from $E_a = 9\text{--}14$ kJ/mol.⁹⁹ Additionally, the literature shows that the enthalpy required to break HBs in pure water equals $E_a \sim 8$ kJ/mol, and a slightly higher value was calculated for HOD in the D₂O solution and is equal to $E_a \sim 10$ kJ/mol.¹⁰⁰ It should be stressed that, to the best of our knowledge, until now, the values of the activation energy of the dissociation process for systems confined in nanopores have not been determined. Therefore, the values presented herein for PhAs in native and silanized nanomembranes make an important contribution to investigating the impact of nano-restrictive confinement on the behavior of associating materials.

4. CONCLUSIONS

In this paper, we investigated the influence of surface interactions on the associative behavior of phenyl-substituted monohydroxy alcohols. Interestingly, we observed a pronounced deviation of the dominant relaxation process (corresponding to the bulk Debye-like mode) for all examined confined systems occurring at $T_{g(\text{interfacial})}$ independent of the applied type of porous templates. Nevertheless, the dielectric response of PhAs infiltrated within native silica mesopores revealed the presence of an additional relaxation process, particularly pronounced for longer aliphatic chains. Interestingly, it was observed that this additional mobility is most likely not related to vitrification of the interfacial layer, $T_{g(\text{interfacial})}$. Its molecular origin is yet to be clarified. Calorimetric data revealed a double glass transition phenomenon for systems infiltrated in native and modified silica. Moreover, it was found that for both types of membranes, the length of the interfacial layer, ξ , reaches approximately $\xi \sim 0.5$ nm for all PhAs. This suggests that an interfacial layer is formed, irrespective of the character of the pore walls. This observation was explained considering contact angle measurements, which revealed that at low temperatures, all examined PhAs have a similar wettability on both surfaces, $\theta \sim 22$ to 28° . IR measurements showed that the incorporation of PhAs into silica membranes inhibits complete association over the entire temperature range. Moreover, nanogeometrical restriction has a relatively small impact on the H-bonds' strength of infiltrated PhAs, as seen in the ν_{OH} peak position. However, it alters the ν_{OH} bandwidths; i.e., the confined samples are characterized by broader OH bands than those in bulk, indicating greater heterogeneity in the distribution of H-bonded systems in nanoconfinement. Notably, for the first time, we calculated the activation energy values of the dissociation process for confined PhAs, which were lower than those of bulk ones. This result correlates well with the lower association degree of infiltrated PhAs compared to their bulk counterparts, resulting from the spatial restriction. Thus, all experimental methods used consistently confirmed the formation of an additional interfacial layer in infiltrated PhAs in which the alcohol molecules strongly interact with the pore walls. We believe that the presented results offer a better understanding of the processes occurring for associating liquids in nanoconfinement.

■ ASSOCIATED CONTENT

Supporting Information

The Supporting Information is available free of charge at <https://pubs.acs.org/doi/10.1021/acs.jpcc.3c08084>.

It contains additional figures and tables, including figures of SEM pictures of the native silica nanopore, the IR

spectra of 'empty' silica templates, the contact angles measured for examined materials at three different temperatures, and the DSC thermograms for bulk and confined samples. Moreover, it includes the dielectric loss spectra, comparison of the dielectric strength, temperature dependences of relaxation times, the comparison of glass transition temperatures obtained from BDS and DSC measurements, the IR spectra of infiltrated MAs and the percentages of free OH groups, the determination of the degree of association and activation energy of the dissociation process, values of integrated intensities of the ν_{OH} bands, the van't Hoff plots used to calculate the activation energies of dissociation processes, and tables containing glass transition temperatures and wavenumbers of the OH peaks (PDF)

■ AUTHOR INFORMATION

Corresponding Author

Magdalena Tarnacka – August Chelkowski Institute of Physics, University of Silesia in Katowice, 41-500 Chorzów, Poland; orcid.org/0000-0002-9444-3114; Email: magdalena.tarnacka@us.edu.pl

Authors

Natalia Soszka – Institute of Chemistry, University of Silesia in Katowice, 40-006 Katowice, Poland; orcid.org/0000-0001-7774-7450

Barbara Hachula – Institute of Chemistry, University of Silesia in Katowice, 40-006 Katowice, Poland; orcid.org/0000-0001-9886-1076

Monika Geppert-Rybczyńska – Institute of Chemistry, University of Silesia in Katowice, 40-006 Katowice, Poland; orcid.org/0000-0002-7112-9624

Krzysztof Prusik – Institute of Materials Engineering, University of Silesia in Katowice, 41-500 Chorzów, Poland

Kamil Kamiński – August Chelkowski Institute of Physics, University of Silesia in Katowice, 41-500 Chorzów, Poland; orcid.org/0000-0002-5871-0203

Complete contact information is available at: <https://pubs.acs.org/10.1021/acs.jpcc.3c08084>

Notes

The authors declare no competing financial interest.

■ ACKNOWLEDGMENTS

N.S., M.T., and B.H. are thankful for financial support from the Polish National Science Centre (Dec. no 2019/33/B/ST3/00500).

■ REFERENCES

- (1) Mezger, M.; Reichert, H.; Schöder, S.; Okasinski, J.; Schröder, H.; Dosch, H.; Palms, D.; Ralston, J.; Honkimäki, V. High-Resolution in Situ x-Ray Study of the Hydrophobic Gap at the Water-Octadecyl-Trichlorosilane Interface. *Proc. Natl. Acad. Sci. U.S.A.* **2006**, *103* (49), 18401–18404.
- (2) Konovalov, O.; Destri, G. L.; Seec, O. H.; Mezger, M.; Haddad, J.; Deutsch, M.; Checco, A.; Ocko, B. M. Nanoscale Structure of Si/SiO₂/Organics. *ACS Nano* **2014**, *8* (12), 12676–12681, DOI: 10.1021/nn5056223.
- (3) Mezger, M.; Sedlmeier, F.; Horinek, D.; Reichert, H.; Pontoni, D.; Dosch, H. On the Origin of the Hydrophobic Water Gap: An X-

- Ray Reflectivity and MD Simulation Study. *J. Am. Chem. Soc.* **2010**, *132* (19), 6735–6741.
- (4) Ocko, B. M. Smectic-Layer Growth at Solid Interfaces. *Phys. Rev. Lett.* **1990**, *64* (18), 2160–2163.
- (5) Ocko, B. M.; Hlaing, H.; Jepsen, P. N.; Kewalramani, S.; Tkachenko, A.; Pontoni, D.; Reichert, H.; Deutsch, M. Unifying Interfacial Self-Assembly and Surface Freezing. *Phys. Rev. Lett.* **2011**, *106* (13), 16–19.
- (6) Mars, J.; Hou, B.; Weiss, H.; Li, H.; Konovalov, O.; Festersen, S.; Murphy, B. M.; Rütt, U.; Bier, M.; Mezger, M. Surface Induced Smectic Order in Ionic Liquids—an X-Ray Reflectivity Study of [C22C1im]+[NTf2]-. *Phys. Chem. Chem. Phys.* **2017**, *19* (39), 26651–26661.
- (7) Lied, A.; Dosch, H.; Bilgram, J. H. Surface Melting of Ice Ih Single Crystals Revealed by Glancing Angle X-Ray Scattering. *Phys. Rev. Lett.* **1994**, *72* (22), 3554–3557.
- (8) Alejandra Sánchez, M.; Kling, T.; Ishiyama, T.; Van Zadel, M. J.; Bisson, P. J.; Mezger, M.; Jochum, M. N.; Cyran, J. D.; Smit, W. J.; Bakker, H. J.; Shultz, M. J.; Morita, A.; Donadio, D.; Nagata, Y.; Bonn, M.; Backus, E. H. G. Experimental and Theoretical Evidence for Bilayer-Bilayer Surface Melting of Crystalline Ice. *Proc. Natl. Acad. Sci. U.S.A.* **2017**, *114* (2), 227–232.
- (9) Nagata, Y.; Hama, T.; Backus, E. H. G.; Mezger, M.; Bonn, D.; Bonn, M.; Sasaki, G. The Surface of Ice under Equilibrium and Nonequilibrium Conditions. *Acc. Chem. Res.* **2019**, *52* (4), 1006–1015.
- (10) Mezger, M.; Schöder, S.; Reichert, H.; Schröder, H.; Okasinski, J.; Honkimaäki, V.; Ralston, J.; Bilgram, J.; Roth, R.; Dosch, H. Water and Ice in Contact with Octadecyl-Trichlorosilane Functionalized Surfaces: A High Resolution x-Ray Reflectivity Study. *J. Chem. Phys.* **2008**, *128* (24), No. 244705.
- (11) Hulsmann, W. J.; Peters, J. F.; Zwanenburg, M. J.; De Vries, S. A.; Derry, T. E.; Abernathy, D.; Van der Veen, J. F. Layering of a Liquid Metal in Contact with a Hard Wall. *Nature* **1997**, *390* (6658), 379–381.
- (12) Tamam, L.; Pontoni, D.; Hofmann, T.; Ocko, B. M.; Reichert, H.; Deutsch, M. Atomic-Scale Structure of a Liquid Metal-Insulator Interface. *J. Phys. Chem. Lett.* **2010**, *1* (7), 1041–1045.
- (13) Valtiner, M.; Banquy, X.; Kristiansen, K.; Greene, G. W.; Israelachvili, J. N. The Electrochemical Surface Forces Apparatus: The Effect of Surface Roughness, Electrostatic Surface Potentials, and Anodic Oxide Growth on Interaction Forces, and Friction between Dissimilar Surfaces in Aqueous Solutions. *Langmuir* **2012**, *28* (36), 13080–13093.
- (14) Mezger, M.; Schramm, S.; Schröder, H.; Reichert, H.; Deutsch, M.; De Souza, E. J.; Okasinski, J. S.; Ocko, B. M.; Honkimaäki, V.; Dosch, H. Layering of [BMIM]+-Based Ionic Liquids at a Charged Sapphire Interface. *J. Chem. Phys.* **2009**, *131* (9), No. 094701.
- (15) Mezger, M.; Jérôme, B.; Kortright, J. B.; Valvidares, M.; Gullikson, E. M.; Giglia, A.; Mahne, N.; Nannarone, S. Molecular Orientation in Soft Matter Thin Films Studied by Resonant Soft X-Ray Reflectivity. *Phys. Rev. B: Condens. Matter Mater. Phys.* **2011**, *83* (15), No. 155406, DOI: 10.1103/PhysRevB.83.155406.
- (16) Weiss, H.; Cheng, H. W.; Mars, J.; Li, H.; Merola, C.; Renner, F. U.; Honkimaäki, V.; Valtiner, M.; Mezger, M. Structure and Dynamics of Confined Liquids: Challenges and Perspectives for the X-Ray Surface Forces Apparatus. *Langmuir* **2019**, *35* (51), 16679–16692.
- (17) Knight, A. W.; Kalugin, N. G.; Coker, E.; Ilgen, A. G. Water Properties under Nano-Scale Confinement. *Sci. Rep.* **2019**, *9* (1), No. 8246, DOI: 10.1038/s41598-019-44651-z.
- (18) Roth, C. B. Polymers under Nanoconfinement: Where Are We Now in Understanding Local Property Changes? *Chem. Soc. Rev.* **2021**, *50* (14), 8050–8066.
- (19) Zuo, Y.; Zhang, Y.; Huang, R.; Min, Y. The Effect of Nanoconfinement on the Glass Transition Temperature of Ionic Liquids. *Phys. Chem. Chem. Phys.* **2019**, *21* (1), 22–25.
- (20) Grünberg, B.; Emmeler, T.; Gedat, E.; Shenderovich, I.; Findenegg, G. H.; Limbach, H. H.; Bantkowsky, G. Hydrogen Bonding of Water Confined in Mesoporous Silica MCM-41 and SBA-15 Studied by 1H Solid-State NMR. *Chem. - Eur. J.* **2004**, *10* (22), 5689–5696.
- (21) Findenegg, G. H.; Jähnert, S.; Akcakayiran, D.; Schreiber, A. Freezing and Melting of Water Confined in Silica Nanopores. *ChemPhysChem* **2008**, *9* (18), 2651–2659.
- (22) Domin, K.; Chan, K. Y.; Yung, H.; Gubbins, K. E.; Jarek, M.; Sterczynska, A.; Sliwiska-Bartkowiak, M. Structure of Ice in Confinement: Water in Mesoporous Carbons. *J. Chem. Eng. Data* **2016**, *61* (12), 4252–4260.
- (23) Corsetti, F.; Matthews, P.; Artacho, E. Structural and Configurational Properties of Nanoconfined Monolayer Ice from First Principles. *Sci. Rep.* **2016**, *6* (May 2015), No. 18651, DOI: 10.1038/srep18651.
- (24) Mollanen, D. E.; Levinger, N. E.; Fayer, M. D. *Confinement or Properties of the Interface? Dynamics of Nanoscopic Water in Reverse Micelles*, Optics InfoBase Conference Papers, 2007; pp 8942–8948 DOI: 10.1364/Is.2007.ltuc3.
- (25) Rieth, A. J.; Hunter, K. M.; Dincă, M.; Paesani, F. Hydrogen Bonding Structure of Confined Water Templated by a Metal-Organic Framework with Open Metal Sites. *Nat. Commun.* **2019**, *10* (1), No. 4771, DOI: 10.1038/s41467-019-12751-z.
- (26) Beilinson, Y.; Schiller, V.; Regentin, J.; Melillo, J. H.; Greenbaum, A.; Antropova, T.; Cerveny, S.; Vogel, M.; Feldman, Y. The Nature of the Low-Temperature Crossover of Water in Hard Confinement. *J. Phys. Chem. B* **2023**, *127* (22), 5128–5140.
- (27) Brás, A. R.; Fonseca, I. M.; Dionísio, M.; Schönhalz, A.; Affouard, F.; Correia, N. T. Influence of Nanoscale Confinement on the Molecular Mobility of Ibuprofen. *J. Phys. Chem. C* **2014**, *118* (25), 13857–13868.
- (28) Brás, A. R.; Merino, E. G.; Neves, P. D.; Fonseca, I. M.; Dionísio, M.; Schönhalz, A.; Correia, N. T. Amorphous Ibuprofen Confined in Nanostructured Silica Materials: A Dynamical Approach. *J. Phys. Chem. C* **2011**, *115* (11), 4616–4623.
- (29) Weinberger, C.; Zysk, F.; Hartmann, M.; Kaliannan, N. K.; Keil, W.; Kühne, T. D.; Tiemann, M. The Structure of Water in Silica Mesopores – Influence of the Pore Wall Polarity. *Adv. Mater. Interfaces* **2022**, *9* (20), No. 2200245.
- (30) Bauer, F.; Meyer, R.; Bertmer, M.; Naumov, S.; Al-Naji, M.; Wissel, J.; Steinhart, M.; Enke, D. Silanization of Siliceous Materials, Part 3: Modification of Surface Energy and Acid-Base Properties of Silica Nanoparticles Determined by Inverse Gas Chromatography (IGC). *Colloids Surf., A* **2021**, *618*, No. 126472.
- (31) Huwe, A.; Arndt, M.; Kremer, F.; Haggemüller, C.; Behrens, P. Dielectric Investigations of the Molecular Dynamics of Propanediol in Mesoporous Silica Materials. *J. Chem. Phys.* **1997**, *107* (22), 9699–9701.
- (32) Winkler, R.; Tu, W.; Laskowski, L.; Adrjanowicz, K. Effect of Surface Chemistry on the Glass-Transition Dynamics of Poly(Phenyl Methyl Siloxane) Confined in Alumina Nanopores. *Langmuir* **2020**, *36* (26), 7553–7565.
- (33) Weinberger, C.; Zysk, F.; Hartmann, M.; Kaliannan, N. K.; Keil, W.; Kühne, T. D.; Tiemann, M. The Structure of Water in Silica Mesopores – Influence of the Pore Wall Polarity. *Adv. Mater. Interfaces* **2022**, *9* (20), No. 2200245, DOI: 10.1002/admi.202200245.
- (34) Ghoufi, A.; Hureau, I.; Morineau, D.; Renou, R.; Szymczyk, A. Confinement of Tert-Butanol Nanoclusters in Hydrophilic and Hydrophobic Silica Nanopores. *J. Phys. Chem. C* **2013**, *117* (29), 15203–15212.
- (35) Tarnacka, M.; Talik, A.; Kamińska, E.; Geppert-Rybczyńska, M.; Kaminski, K.; Paluch, M. The Impact of Molecular Weight on the Behavior of Poly(Propylene Glycol) Derivatives Confined within Alumina Templates. *Macromolecules* **2019**, *52* (9), 3516–3529.
- (36) Górný, A.; Tarnacka, M.; Zimny, S.; Geppert-Rybczyńska, M.; Brzózka, A.; Sulka, G. D.; Paluch, M.; Kamiński, K. Impact of Nanostructurization of the Pore Walls on the Dynamics of a Series of Phenyl Alcohols Incorporated within Nanoporous Aluminum Oxide Templates. *J. Phys. Chem. C* **2022**, *126* (43), 18475–18489.

- (37) Ghoufi, A.; Hureau, L.; Lefort, R.; Morineau, D. Hydrogen-Bond-Induced Supermolecular Assemblies in a Nanoconfined Tertiary Alcohol. *J. Phys. Chem. C* **2011**, *115* (36), 17761–17767.
- (38) Ananiadou, A.; Papamokos, G.; Steinhart, M.; Floudas, G. Effect of Confinement on the Dynamics of 1-Propanol and Other Monohydroxy Alcohols. *J. Chem. Phys.* **2021**, *155* (18), No. 184504.
- (39) Jansson, H.; Swenson, J. The Slow Dielectric Debye Relaxation of Monoalcohols in Confined Geometries. *J. Chem. Phys.* **2011**, *134* (10), No. 104504.
- (40) Talik, A.; Tarnacka, M.; Geppert-Rybczyńska, M.; Hachula, B.; Bernat, R.; Chirzanowska, A.; Kaminski, K.; Paluch, M. Are Hydrogen Supramolecular Structures Being Suppressed upon Nanoscale Confinement? The Case of Monohydroxy Alcohols. *J. Colloid Interface Sci.* **2020**, *576*, 217–229.
- (41) Iacob, C.; Sangoro, J. R.; Kipnusu, W. K.; Valiullin, R.; Kärger, J.; Kremer, F. Enhanced Charge Transport in Nano-Confined Ionic Liquids. *Soft Matter* **2012**, *8* (2), 289–293.
- (42) Kipnusu, W. K.; Kossack, W.; Iacob, C.; Jasiurkowska, M.; Sangoro, J. R.; Kremer, F. Molecular Order and Dynamics of Tris(2-Ethylhexyl)Phosphate Confined in Uni-Directional Nanopores. *Z. Phys. Chem.* **2012**, *226* (7–8), 797–805.
- (43) Feder-Kubis, J.; Geppert-Rybczyńska, M.; Musiał, M.; Talik, E.; Guzik, A. Exploring the Surface Activity of a Homologues Series of Functionalized Ionic Liquids with a Natural Chiral Substituent: (–)-Menthol in a Cation. *Colloids Surf., A* **2017**, *529*, 725–732.
- (44) Geppert-Rybczyńska, M.; Lehmann, J. K.; Heintz, A. Surface Tensions and the Gibbs Excess Surface Concentration of Binary Mixtures of the Ionic Liquid 1-Ethyl-3-Methylimidazolium Bis-[(Trifluoromethyl) Sulfonyl]Imide with Tetrahydrofuran and Acetonitrile. *J. Chem. Eng. Data* **2011**, *56* (4), 1443–1448.
- (45) Wandschneider, A.; Lehmann, J. K.; Heintz, A. Surface Tension and Density of Pure Ionic Liquids and Some Binary Mixtures with 1-Propanol and 1-Butanol. *J. Chem. Eng. Data* **2008**, *53* (2), 596–599.
- (46) Tarnacka, M.; Geppert-Rybczyńska, M.; Dulski, M.; Grelska, J.; Jurkiewicz, K.; Grzybowska, K.; Kamiński, K.; Paluch, M. Local Structure and Molecular Dynamics of Highly Polar Propylene Carbonate Derivative Infiltrated within Alumina and Silica Porous Templates. *J. Chem. Phys.* **2021**, *154* (6), No. 064701.
- (47) Soszka, N.; Hachula, B.; Tarnacka, M.; Kamińska, E.; Grelska, J.; Jurkiewicz, K.; Geppert-Rybczyńska, M.; Wrzaliak, R.; Grzybowska, K.; Pawlus, S.; et al. The Impact of the Length of Alkyl Chain on the Behavior of Benzyl Alcohol Homologues – the Interplay between Dispersive and Hydrogen Bond Interactions. *Phys. Chem. Chem. Phys.* **2021**, *23* (41), 23796–23807.
- (48) Alexandris, S.; Papadopoulos, P.; Sakellariou, G.; Steinhart, M.; Butt, H. J.; Floudas, G. Interfacial Energy and Glass Temperature of Polymers Confined to Nanoporous Alumina. *Macromolecules* **2016**, *49* (19), 7400–7414.
- (49) Havriliak, S.; Negami, S. A Complex Plane Analysis of α -Dispersions in Some Polymer Systems. *J. Polym. Sci., Part C: Polym. Symp.* **1966**, *14* (1), 99–117.
- (50) Vogel, H. Temperaturabhängigkeitgesetz Der Viskosität von Flüssigkeiten. *J. Phys. Z.* **1921**, *22*, 645–646.
- (51) Fulcher, G. S. Analysis of Recent Measurements of the Viscosity of Glasses. *J. Am. Ceram. Soc.* **1925**, *8*, 339–355.
- (52) Tammann, G.; Hesse, W. Die Abhängigkeit Der Viskosität von Der Temperatur Bei Unterkühlten Flüssigkeiten. *Z. Anorg. Allg. Chem.* **1926**, *156*, 245–257.
- (53) Li, Q.; Simon, S. L. Surface Chemistry Effects on the Reactivity and Properties of Nanoconfined Bisphenol M Dicyanate Ester in Controlled Pore Glass. *Macromolecules* **2009**, *42* (10), 3573–3579.
- (54) Li, L.; Zhou, D.; Huang, D.; Xue, G. Double Glass Transition Temperatures of Poly(Methyl Methacrylate) Confined in Alumina Nanotube Templates. *Macromolecules* **2014**, *47* (1), 297–303.
- (55) Park, J. Y.; McKenna, G. B. Size and Confinement Effects on the Glass Transition Behavior of Polystyrene/o-Terphenyl Polymer Solutions. *Phys. Rev. B: Condens. Matter Mater. Phys.* **2000**, *61* (10), 6667–6676.
- (56) Jackson, C. L.; McKenna, G. B. Vitrification and Crystallization of Organic Liquids Confined to Nanoscale Pores. *Chem. Mater.* **1996**, *8* (8), 2128–2137.
- (57) Cheng, S.; McKenna, G. B. Nanoconfinement Effects on the Glass Transition and Crystallization Behaviors of Nifedipine. *Mol. Pharmaceutics* **2019**, *16* (2), 856–866.
- (58) Jackson, C. L.; McKenna, G. B. The Glass Transition of Organic Liquids Confined to Small Pores. *J. Non-cryst. Solids* **1991**, *131–133* (PART 1), 221–224.
- (59) Kuon, N.; Milischuk, A. A.; Ladanyi, B. M.; Flenner, E. Self-Intermediate Scattering Function Analysis of Supercooled Water Confined in Hydrophilic Silica Nanopores. *J. Chem. Phys.* **2017**, *146* (21), No. 214501.
- (60) Chat, K.; Tu, W.; Laskowski, L.; Adrijanowicz, K. Effect of Surface Modification on the Glass Transition Dynamics of Highly Polar Molecular Liquid S-Methoxy-PC Confined in Anodic Aluminum Oxide Nanopores. *J. Phys. Chem. C* **2019**, *123* (21), 13365–13376.
- (61) Soszka, N.; Hachula, B.; Tarnacka, M.; Kamińska, E.; Grelska, J.; Jurkiewicz, K.; Geppert-Rybczyńska, M.; Wrzaliak, R.; Grzybowska, K.; Pawlus, S.; Paluch, M.; Kamiński, K. The Impact of the Length of Alkyl Chain on the Behavior of Benzyl Alcohol Homologues—the Interplay between Dispersive and Hydrogen Bond Interactions. *Phys. Chem. Chem. Phys.* **2021**, *23* (41), 23796–23807.
- (62) Tarnacka, M.; Kamińska, E.; Paluch, M.; Kamiński, K. New Insights from Nonequilibrium Kinetics Studies on Highly Polar S-Methoxy-PC Infiltrated into Pores. *J. Phys. Chem. Lett.* **2022**, *13* (44), 10464–10470.
- (63) Talik, A.; Tarnacka, M.; Geppert-Rybczyńska, M.; Hachula, B.; Kaminski, K.; Paluch, M. Impact of Confinement on the Dynamics and H-Bonding Pattern in Low-Molecular Weight Poly(Propylene Glycols). *J. Phys. Chem. C* **2020**, *124* (32), 17607–17621.
- (64) Alexandris, S.; Papadopoulos, P.; Sakellariou, G.; Steinhart, M.; Butt, H. J.; Floudas, G. Interfacial Energy and Glass Temperature of Polymers Confined to Nanoporous Alumina. *Macromolecules* **2016**, *49* (19), 7400–7414.
- (65) Politidis, C.; Alexandris, S.; Sakellariou, G.; Steinhart, M.; Floudas, G. Dynamics of Entangled Cis-1,4-Polyisoprene Confined to Nanoporous Alumina. *Macromolecules* **2019**, *52* (11), 4185–4195.
- (66) Gainaru, C.; Meier, R.; Schildmann, S.; Lederle, C.; Hiller, W.; Rössler, E. A.; Böhmer, R. Nuclear-Magnetic-Resonance Measurements Reveal the Origin of the Debye Process in Monohydroxy Alcohols. *Phys. Rev. Lett.* **2010**, *105* (25), No. 258303, DOI: 10.1103/PhysRevLett.105.258303.
- (67) Böhmer, T.; Gabriel, J. P.; Richter, T.; Pabst, F.; Blochowicz, T. Influence of Molecular Architecture on the Dynamics of H-Bonded Supramolecular Structures in Phenyl-Propanols. *J. Phys. Chem. B* **2019**, *123* (51), 10959–10966.
- (68) Büning, T.; Lueg, J.; Bolle, J.; Sternemann, C.; Gainaru, C.; Tolan, M.; Böhmer, R. Connecting Structurally and Dynamically Detected Signatures of Supramolecular Debye Liquids. *J. Chem. Phys.* **2017**, *147* (23), No. 234501.
- (69) Johari, G. P.; Kalinovskaya, O. E.; Vij, J. K. Effects of Induced Steric Hindrance on the Dielectric Behavior and H Bonding in the Supercooled Liquid and Vitreous Alcohol. *J. Chem. Phys.* **2001**, *114* (10), 4634–4642.
- (70) Pabst, F.; Gabriel, J. P.; Böhmer, T.; Weigl, P.; Helbling, A.; Richter, T.; Zourchang, P.; Walther, T.; Blochowicz, T. Generic Structural Relaxation in Supercooled Liquids. *J. Phys. Chem. Lett.* **2021**, *12* (14), 3685–3690.
- (71) Tarnacka, M.; Czaderna-Lekka, A.; Wojnarowska, Z.; Kamiński, K.; Paluch, M. Nature of Dielectric Response of Phenyl Alcohols. *J. Phys. Chem. B* **2023**, *127* (27), 6191–6196.
- (72) Czaderna-Lekka, A.; Tarnacka, M.; Wojnarowska, Z.; Hachula, B.; Paluch, M.; Kamiński, K. On the Relationship between the Debye Process in Dielectric Response and a Dissociation-Association Phenomenon in Phenyl Alcohols. *Phys. Chem. Chem. Phys.* **2023**, *25* (20), 14590–14597.

- (73) He, F.; Wang, L. M.; Richert, R. Dynamics of Supercooled Liquids in the Vicinity of Soft and Hard Interfaces. *Phys. Rev. B: Condens. Matter Mater. Phys.* **2005**, *71* (14), No. 144205, DOI: 10.1103/PhysRevB.71.144205.
- (74) Arndt, M.; Stannarius, R.; Gorbatschow, W.; Kremer, F. Dielectric Investigations of the Dynamic Glass Transition in Nanopores. *Phys. Rev. E* **1996**, *54* (5), 5377–5390.
- (75) Arndt, M.; Stannarius, R.; Groothues, H.; Hempel, E.; Kremer, F. Length Scale of Cooperativity in the Dynamic Glass Transition. *Phys. Rev. Lett.* **1997**, *79* (11), 2077–2080.
- (76) Talik, A.; Tarnacka, M.; Grudzka-Flak, I.; Maksym, P.; Geppert-Rybczyńska, M.; Wolnica, K.; Kamińska, E.; Kamiński, K.; Paluch, M. The Role of Interfacial Energy and Specific Interactions on the Behavior of Poly(Propylene Glycol) Derivatives under 2D Confinement. *Macromolecules* **2018**, *51* (13), 4840–4852.
- (77) Tarnacka, M.; Kamiński, K.; Mapesa, E. U.; Kamińska, E.; Paluch, M. Studies on the Temperature and Time Induced Variation in the Segmental and Chain Dynamics in Poly(Propylene Glycol) Confined at the Nanoscale. *Macromolecules* **2016**, *49* (17), 6678–6686.
- (78) Tarnacka, M.; Wojtyński, M.; Brzózka, A.; Talik, A.; Hachula, B.; Kamińska, E.; Sulka, G. D.; Kamiński, K.; Paluch, M. Unique Behavior of Poly(Propylene Glycols) Confined within Alumina Templates Having a Nanostructured Interface. *Nano Lett.* **2020**, *20* (8), 5714–5719.
- (79) Talik, A.; Tarnacka, M.; Wojtyński, M.; Kamińska, E.; Kamiński, K.; Paluch, M. The Influence of the Nanocurvature on the Surface Interactions and Molecular Dynamics of Model Liquid Confined in Cylindrical Pores. *J. Mol. Liq.* **2020**, *298*, 5549–5556.
- (80) Richert, R.; Yang, M. Surface Induced Glass Transition in a Confined Molecular Liquid. *J. Phys. Chem. B* **2003**, *107* (4), 895–898.
- (81) Soszka, N.; Hachula, B.; Tarnacka, M.; Grelska, J.; Jurkiewicz, K.; Geppert-Rybczyńska, M.; Wrzalił, R.; Grzybowska, K.; Pawlus, S.; Paluch, M.; et al. Aromaticity Effect on Supramolecular Aggregation. Aromatic vs. Cyclic Monohydroxy Alcohols. *Spectrochim. Acta A* **2022**, *276*, No. 121235.
- (82) Jacob, C.; Sangoro, J. R.; Papadopoulos, P.; Schubert, T.; Naumov, S.; Valiullin, R.; Kärger, J.; Kremer, F. Charge Transport and Diffusion of Ionic Liquids in Nanoporous Silica Membranes. *Phys. Chem. Chem. Phys.* **2010**, *12* (41), 13798–13803.
- (83) Jasirukowska-Delaporte, M.; Kossack, W.; Kipnusu, W. K.; Sangoro, J. R.; Jacob, C.; Kremer, F. Glassy Dynamics of Two Poly(Ethylene Glycol) Derivatives in the Bulk and in Nanometric Confinement as Reflected in Its Inter- and Intra-Molecular Interactions. *J. Chem. Phys.* **2018**, *149* (6), No. 064501.
- (84) Kremer, F.; Schönhals, A. *Broadband Dielectric Spectroscopy*; Springer, 2003.
- (85) Adrjanowicz, K.; Kolodziejczyk, K.; Kipnusu, W. K.; Tarnacka, M.; Mapesa, E. U.; Kamińska, E.; Pawlus, S.; Kamiński, K.; Paluch, M. Decoupling between the Interfacial and Core Molecular Dynamics of Salol in 2D Confinement. *J. Phys. Chem. C* **2015**, *119* (25), 14366–14374.
- (86) Uhl, M.; Fischer, J. K. H.; Sippel, P.; Bunzen, H.; Lunkenheimer, P.; Volkmer, D.; Loidl, A. Glycerol Confined in Zeolitic Imidazolate Frameworks: The Temperature-Dependent Cooperativity Length Scale of Glassy Freezing. *J. Chem. Phys.* **2019**, *150* (2), No. 024504.
- (87) Szklarz, G.; Adrjanowicz, K.; Tarnacka, M.; Pionteck, J.; Paluch, M. Confinement-Induced Changes in the Glassy Dynamics and Crystallization Behavior of Supercooled Penofofibrate. *J. Phys. Chem. C* **2018**, *122* (2), 1384–1395.
- (88) Tarnacka, M.; Dulski, M.; Geppert-Rybczyńska, M.; Talik, A.; Kamińska, E.; Kamiński, K.; Paluch, M. Variation in the Molecular Dynamics of DGEBA Confined within AAO Templates above and below the Glass-Transition Temperature. *J. Phys. Chem. C* **2018**, *122* (49), 28033–28044.
- (89) Schönhals, A.; Stauga, R. Broadband Dielectric Study of Anomalous Diffusion in a Poly(Propylene Glycol) Melt Confined to Nanopores. *J. Chem. Phys.* **1998**, *108* (12), 5130–5136.
- (90) Schönhals, A.; Goering, H.; Schick, C. Segmental and Chain Dynamics of Polymers: From the Bulk to the Confined State. *J. Non-cryst. Solids* **2002**, *305* (1–3), 140–149.
- (91) Adrjanowicz, K.; Kamiński, K.; Koperwas, K.; Paluch, M. Negative Pressure Vitrification of the Isochorically Confined Liquid in Nanopores. *Phys. Rev. Lett.* **2015**, *115* (26), No. 265702, DOI: 10.1103/PhysRevLett.115.265702.
- (92) Tarnacka, M.; Kipnusu, W. K.; Kamińska, E.; Pawlus, S.; Kamiński, K.; Paluch, M. The Peculiar Behavior of the Molecular Dynamics of a Glass-Forming Liquid Confined in Native Porous Materials—the Role of Negative Pressure. *Phys. Chem. Chem. Phys.* **2016**, *18* (34), 23709–23714.
- (93) Kipnusu, W. K.; Elsayed, M.; Kossack, W.; Pawlus, S.; Adrjanowicz, K.; Tress, M.; Mapesa, E. U.; Krause-Rehberg, R.; Kamiński, K.; Kremer, F. Confinement for More Space: A Larger Free Volume and Enhanced Glassy Dynamics of 2-Ethyl-1-Hexanol in Nanopores. *J. Phys. Chem. Lett.* **2015**, *6* (18), 3708–3712.
- (94) Song, Z.; Rodríguez-Tinoco, C.; Mathew, A.; Napolitano, S. Fast Equilibration Mechanisms in Disordered Materials Mediated by Slow Liquid Dynamics. *Sci. Adv.* **2022**, *8* (15), No. eabm7154, DOI: 10.1126/sciadv.abm7154.
- (95) Malfait, B.; Moréac, A.; Jani, A.; Lefort, R.; Huber, P.; Fröba, M.; Morineau, D. Structure of Water at Hydrophilic and Hydrophobic Interfaces: Raman Spectroscopy of Water Confined in Periodic Mesoporous (Organo)Silicas. *J. Phys. Chem. C* **2022**, *126* (7), 3520–3531.
- (96) Musat, R.; Renault, J. P.; Candelaresi, M.; Palmer, D. J.; Le Caër, S.; Righini, R.; Pommeret, S. Finite Size Effects on Hydrogen Bonds in Confined Water. *Angew. Chem., Int. Ed.* **2008**, *47* (42), 8033–8035.
- (97) Senanayake, H. S.; Greathouse, J. A.; Ilgen, A. G.; Thompson, W. H. Simulations of the IR and Raman Spectra of Water Confined in Amorphous Silica Slit Pores. *J. Chem. Phys.* **2021**, *154* (10), No. 104503.
- (98) Stefanutti, E.; Bove, L. E.; Alabarse, F. G.; Lelong, G.; Bruni, F.; Ricci, M. A. Vibrational Dynamics of Confined Supercooled Water. *J. Chem. Phys.* **2019**, *150* (22), No. 224504.
- (99) Bauer, S.; Burlafinger, K.; Gainaru, C.; Lunkenheimer, P.; Hiller, W.; Loidl, A.; Böhmner, R. Debye Relaxation and 250 K Anomaly in Glass Forming Monohydroxy Alcohols. *J. Chem. Phys.* **2013**, *138* (9), No. 094505.
- (100) Worley, J. D.; Klotz, I. M. Near-Infrared Spectra of H₂O-D₂O Solutions. *J. Chem. Phys.* **1966**, *45* (8), 2868–2871.

P4. The Existence of Strongly Bonded Layer in Associating Liquids within Silica Pores – the Spectral and Molecular Dynamics Study.

Autorzy: N. Soszka, M. Tarnaacka, B. Hachuła, P. Włodarczyk, R. Wrzalik, M. Hreczka, M. Paluch, K. Kamiński

Referencja: *Nanoscale*, 2024, 16, 6636-6647

DOI: 10.1039/D3NR06187F

Impact Factor czasopisma: 6.7

Liczba punktów ministerialnych MNiSW czasopisma: 140

Mój udział polegał na zaplanowaniu eksperymentu w podczerwieni, przygotowaniu próbek materiałów litych i infiltrowanych do matryc krzemowych, wykonaniu pomiarów IR i analizie wyników, dyskusji wyników, współtworzenia manuskryptu (przeprowadzenie przeglądu literaturowego, przygotowanie tekstu manuskryptu i rysunków, opis wyników i sformułowanie wniosków), formułowaniu odpowiedzi na uwagi recenzentów oraz korekcie manuskryptu po otrzymanych recenzjach.

Cite this: *Nanoscale*, 2024, 16, 6636

The existence of a strongly bonded layer in associating liquids within silica pores – a spectral and molecular dynamics study†

Natalia Soszka,^a Magdalena Tarnacka,^b Barbara Hachuta,^a Patryk Włodarczyk,^c Roman Wrzalik,^b Marek Hreczka,^{c,d} Marian Paluch^b and Kamil Kamiński^b

The properties of confined materials are assumed to be governed by the phenomena occurring at the interface, especially the formation of an irreversible adsorption layer (IAL), which has been widely discussed and detected in the case of thin polymer films and silica nanoparticles. In this paper, we present a novel experimental approach allowing us to reveal the formation of an IAL in two phenyl alcohols infiltrated into various mesoporous silica templates. The proposed methodology (based on evaporation) allowed us to detect the alterations in the OH and aromatic CH stretching vibration bands in infrared spectra, which were considered as evidence of the existence of IAL in constrained systems. Such interpretation was also confirmed by complementary molecular dynamics (MD) simulations that indicated the creation of much stronger hydrogen bonds between alcohols and silanol units than between alcohols themselves. Moreover, computation allowed us to identify additional enormously strong π -stacking interactions between phenyl rings stabilizing the interfacial layer. MD simulations also shed new light on the clustering process of both alcohols under confinement. Simulation and experimental data presented in this paper allowed a much deeper understanding of the processes occurring at the interface-formation of IAL and the association phenomenon at the nanoscale level.

Received 4th December 2023,
Accepted 17th February 2024

DOI: 10.1039/d3nr06187f

rsc.li/nanoscale

1. Introduction

Soft materials under nanometric spatial constraint have attracted over recent years a growing interest from both scientific and industrial perspectives, which arises due to their (often) significantly different behavior from that of their bulk counterparts, just to mention differences in phase transition,^{1,2} dynamics,^{3–5} or the tendency to crystallization.^{6,7} This makes them promising agents in developing a novel generation of drug carriers,^{8–10} sensors,¹¹ coatings,¹² fuel cells,¹³ etc. Changes in basic parameters of confined materials are considered to be an effect of mainly two factors: finite size and

surface effects. However, despite continuing research efforts, the detailed understanding of the confinement effect is yet to be fully addressed (*i.e.*, the contribution of different factors allowing the prediction of the behavior of partially restricted systems).

One can recall that a majority of recent studies suggested the dominant influence of the latter issue (surface effects), which consists of, *e.g.*, interactions^{14,15} (and surface polarity^{16,17}) as well as roughness,^{15,18} curvature¹⁹ and wettability, might be the dominant factor. Nevertheless, it seems that one of the most interesting surface effects affecting/governing the behavior of confined materials is the formation of a fraction of molecules irreversibly adsorbed at the interface of the applied constrained medium (assigned as an irreversibly adsorbed layer, IAL). The occurrence of an IAL was first shown in the case of annealing experiments of capped thin polystyrene films performed by Napolitano and Wübbenhorst.²⁰ The investigation revealed the shift of the segmental relaxation process with time due to the density perturbation leading to the thickening of 'the layer of chains irreversibly adsorbed onto the substrate' (Guiselin brushes) upon annealing, resulting in a change in the glass transition temperature, T_g (even recovery of the bulk-like behavior).^{20–23} It was assumed that

^aInstitute of Chemistry, University of Silesia in Katowice, Szkolna 9, 40-006 Katowice, Poland

^bAugust Chełkowski Institute of Physics, University of Silesia in Katowice, 75 Pułku Piechoty 1a, 41-500 Chorzów, Poland.
E-mail: magdalena.tarnacka@us.edu.pl

^cLukasiewicz Research Network – Institute of Non-Ferrous Metals, Sowinskiego 5, 44-100 Gliwice, Poland

^dDepartment of Mechatronics, Silesian University of Technology, Akademicka 10A, 44-100 Gliwice, Poland

† Electronic supplementary information (ESI) available. See DOI: <https://doi.org/10.1039/d3nr06187f>



the surface coverage increases as the new coming molecules more loosely interact with the surface and are adsorbed by fewer segments forming loops, tails, and trains,^{20,24} depending on the polymer rigidity and, also sometimes, on the interfacial dynamics.²⁵ This was attributed to the formation of a defined IAL of molecules due to a decreasing free volume over time. Those observations also agreed with theoretical studies taking into account various free volume-based models, *i.e.*, free volume diffusion model^{26,27} or a cooperative free volume model,^{28–30} which clearly show that the detected changes in the segmental dynamics and T_g might result from either the diffusion of free volume holes or free volume-dependent segmental relaxation behavior of confined systems, respectively. Herein, it is also worth stressing that the formation of the IAL was also reported in the case of materials cast on silica nanoparticles.^{31–34} Surprisingly, many of the above-mentioned effects observed for various thin polymer films (considered as one-dimensional confinement) are also recognized in higher-dimensional spatially constrained systems such as porous materials (two-dimensional confinement). One can mention the changes in dynamics upon annealing observed for various low,^{35,36} and high-molecular-weight glass^{37,38} formers infiltrated within either silica or anodized aluminum oxide (AAO) porous template characterized by different pore size, $d = 10–160$ nm. It should be also highlighted that in some cases, even the recovery of the bulk-like properties after prolonged annealing were reported.^{39,40} However, despite those similarities between the behavior of thin polymer films and porous materials, we still do not know whether these effects have the

same molecular origin. Up to now, the existence of IAL has been experimentally confirmed only in the case of the former systems; as for the latter, this issue has yet to be addressed. This raises the question of whether it is possible to obtain/extract this layer in membranes, and if formed, whether it is governed by the same physics as in the case of thin films and, thus, is a fundamental feature of spatially confined systems.

Herein, we address some of those questions as we investigated two monohydroxy phenyl-substituted alcohols (PhAs), 2-phenyl-1-ethanol (2Ph1E) and 3-phenyl-1-propanol (3Ph1P, see their chemical structures in Fig. 1), infiltrated into silica mesopores of $d = 4–8$ nm by means of Fourier transform infrared (FTIR) spectroscopy. However, to verify the existence of IAL in porous systems, we propose a slightly different approach in contrast to the Guiselin brushes experiments.^{20,41–43} As porous materials are characterized by highly curved interface when compared to thin films (see Fig. S1 in ESI†), instead of removing the liquid inside the pores by 'washing out', the substances were evaporated from the silica templates. This approach would allow us to avoid the presence of any solvent, which might remain in the system after the procedure. The choice of materials for this study was not accidental. We chose two associating liquids (characterized by a different length of alkyl chain; see Fig. 1), which relatively easily evaporate at ambient pressure. Moreover, in this study, we applied two types of silica membranes, native (of untreated hydrophilic interface) and silanized (of treated hydrophobic interface), to distinguish the role of specific interactions (in this case, hydrogen bonding, H-bonding) in the formation of IAL. The nanoporous silica

Open Access Article. Published on 19 February 2024. Downloaded on 4/4/2024 11:09:40 AM.
This article is licensed under a Creative Commons Attribution 3.0 Unported Licence.

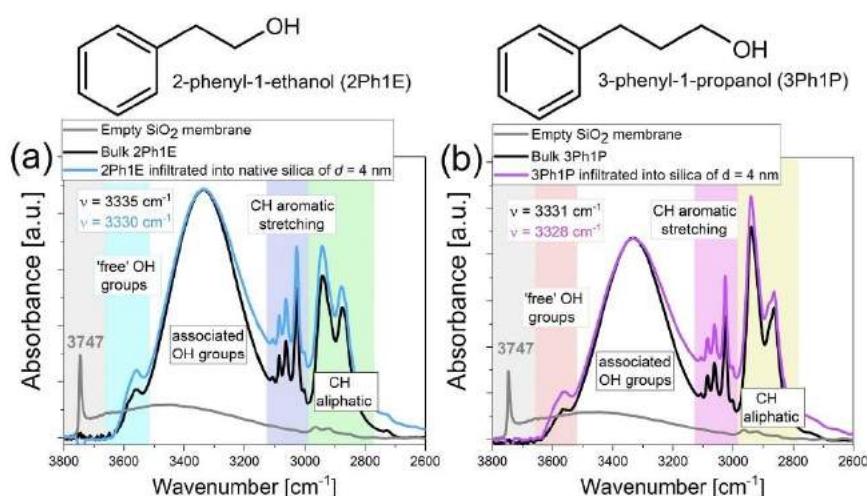


Fig. 1 Infrared spectra of bulk 2Ph1E (a) and 3Ph1P (b) together with those obtained for PhAs infiltrated into native silica templates of $d = 4$ nm measured at $T = 297$ K in the spectral region $3800–2600$ cm^{-1} . The spectra were normalized to the OH stretching vibration peak. Additionally, in each case, a spectrum of empty native silica template is included.

templates were prepared by electrochemical etching of silicon wafers and subsequent thermal oxidation, according to the procedure reported in ref. 44 and 45.

II. Experimental

Materials

2-Phenyl-1-ethanol (2Ph1E) of purity $\geq 98\%$ and 3-phenyl-1-propanol (3Ph1P) of purity 98% were purchased from Sigma Aldrich. Before any experiments, the samples were dried under a stream of liquid nitrogen. The chemical structures of compounds are presented in Fig. 1.

Silica (SiO₂) membranes

Mesoporous silica templates characterized by pore diameter $d = 4\text{--}8$ nm were prepared by electrochemical etching of silicon wafers and subsequent thermal oxidation. For more information, see ref. 45.

Sample preparation

Before filling, SiO₂ membranes were dried in an oven at $T = 373$ K under a vacuum in order to remove any volatile impurities from the nanochannels. After cooling, the templates were placed in a small glass flask containing alcohol. The whole system was maintained for $t = 1.5$ h at $T = 323$ K in a vacuum (10^{-2} bar) to allow infiltration of alcohols into the mesopores. After filling, the excess sample located at the surface of the membrane was removed.

Fourier transform infrared (FTIR) spectroscopy

Temperature- and time-dependent measurements were performed using a Nicolet iS50 spectrometer (Thermo Scientific). Every spectrum was an average of 16 scans collected with a resolution of 2 cm^{-1} . During low-temperature measurements ($T = 297\text{--}153$ K), the bulk of each monohydroxy alcohol (MA) was placed between two CaF₂ windows with $3.5\ \mu\text{m}$ spacers made of polyethylene terephthalate in order to obtain a uniform thickness of samples. The spectra were recorded every 4 K, with a cooling rate of 4 K min^{-1} . Throughout the measurements, liquid nitrogen was passed through the spectrometer to avoid atmospheric H₂O and CO₂ in the spectra. A Linkam heating/cooling stage (Linkam Scientific Instruments Ltd, Surrey, UK) was used to collect the spectra. The annealing spectra of bulk substances were recorded using a GladiATR (Pike Technologies) with a single reflection monolithic diamond. To study the evaporation process, 2Ph1E was measured at $T = 353$ K and 3Ph1P at $T = 363$ K in a time scale of 1 hour. For infiltrated systems, the temperature-dependent experiments were performed in the temperature range $T = 297\text{--}153$ K with the use of a heating/cooling stage, collected every 4 K at a rate of 4 K min^{-1} . As backgrounds, the spectra of empty silica membranes were used in order to obtain data without bands originating from empty pores. The annealing measurements were performed at $T = 353$ K and $T = 363$ K for 2Ph1E and 3Ph1P, respectively. For each system, the sample

was heated up from room temperature to the desired annealing temperature, where spectra were collected every 1 minute for 1 hour.

Raman spectroscopy

The Raman experiment for bulk and infiltrated 2Ph1E was performed using a WITec confocal Raman microscope (CRM alpha 300R) featuring an air-cooled solid-state laser ($\lambda = 532$ nm, $P = 10$ mW). An Olympus LMPlanFI 50 \times objective was chosen. The collected Raman spectra were accumulated by 30 scans with an integration time of 2 s and a resolution of 2 cm^{-1} .

Density functional theory (DFT) calculations

DFT calculations were performed with the ORCA 5.0.4 package.^{46–50} All the geometry optimizations were done with the B97M-D4 functional and 6-31G(2df,2dp) basis set. Energy evaluations were done using hybrid B97 functional with additional D4 corrections and 6-311G(2df,2pd) basis set. The interaction energies were calculated as a difference between the energy of the optimized dimer and the sum of the energy of isolated molecules, according to the following equation:

$$E_{\text{int}} = E_T - \sum_{i=1}^n E_i \quad (1)$$

where E_{int} is the interaction energy, E_T is the total energy of the entire complex, and E_i is the energy of every isolated molecule forming a complex.

Molecular dynamics calculations

Molecular dynamics study was performed with the Gromacs 2023^{51–54} program package. The initial pore structures were modeled in PoreMS software.⁵⁵ Pores with two different sizes were simulated. The length of the pores was equal to 8 nm (12 nm for larger ones), while the inner diameter was equal to 4 nm (8 nm for larger ones). The pore was placed in a box with a length of 12 nm (16 nm for larger ones). On both sides of the pore, there was empty space (2 nm length on each side) prepared for the molecular reservoir. The pore and additional empty space were further filled with alcohol molecules (2Ph1E or 3Ph1P). The initial simulation was done with the isothermal-isobaric ensemble (NPT), where the pressure was set to 1 bar in the z direction and temperature to 293 K (c-rescale mode as barostat and v-rescale mode as thermostat were used). The positions of silica net atoms were frozen in the x and y directions while they were free in the z direction during simulation (which was the direction of applied pressure). The initial simulation time was equal to 5 ns, which was sufficient for density equilibration. In the next step, the pore structure filled with alcohol, without additional space outside the pore (reservoir), was cut and set as the starting configuration for the next production runs. The production runs were done with frozen silica net atom positions and canonical ensemble (NVT) with the v-rescale thermostat type and temperature set to 293 K. The NVT simulation time was equal to 20 ns, which was



sufficient for producing a well-equilibrated system. In all simulations, AMBER force field was used, which is accurate for the silica–organic materials systems.⁵⁶ The bulk systems of 2Ph1E and 3Ph1P were simulated with the NPT ensemble in a cubic box (500 molecules each). The initial structures for bulk simulations were prepared by the Packmol program.⁵⁷ The maps of distribution functions were done with the use of the TRAVIS program^{58–60} for trajectory analysis. Cluster analysis was performed in Gromacs software. The clusters were identified based on the criterion of the distance between the acceptor and donor atoms, which must be below 0.35 nm.

III. Results and discussion

To monitor all changes within the examined materials, we performed FTIR measurements to probe their intermolecular dynamics, where special attention was mainly paid to the bands assigned to the stretching vibrations of (i) the hydroxy (OH) groups that are not involved in intermolecular hydrogen bonds (HBs) (named free OH) ($\nu_{\text{OH free}} \sim 3550 \text{ cm}^{-1}$), (ii) H-bonded OH units ($\nu_{\text{OH bonded}} \sim 3330 \text{ cm}^{-1}$), as well as (iii) the aromatic CH moieties ($\nu_{\text{CH aromatic}} \sim 3100\text{--}3000 \text{ cm}^{-1}$), see Fig. 1. The scope of this article is as follows. At first, we studied the freshly prepared confined materials in comparison to the bulk; then, the evaporation experiments were performed; and at the end, experimental results were compared with the outcome of the molecular dynamics simulations. To our best knowledge, this study is the first one in the literature that reveals/confirms the formation of a layer strongly bonded to the curved surface with properties similar to IAL, which complements our knowledge about this phenomenon, which was mostly studied in case of thin films^{61–65} or nanoparticles.^{66–69}

Fig. 1 shows the FTIR spectra collected for both bulk compounds and MAs infiltrated into the native silica mesopores at room temperature; for comparison, the spectrum of the ‘empty’ native silica membrane is also included. Both MAs, 2Ph1E and 3Ph1P, are characterized by a similar position of the bands assigned to the stretching vibrations of H-bonded OH units (*ca.* 3330 cm^{-1}), while their widths (the full width at half maximum, FWHM) are slightly different ($\text{FWHM}_{2\text{Ph1E}} > \text{FWHM}_{3\text{Ph1P}}$; see Fig. S2†). This indicates that 2Ph1E exhibits a slightly higher heterogeneity in the distribution of HB strength than 3Ph1P.⁷⁰ Interestingly, only a few differences occurred in the investigated systems after the incorporation of the examined PhAs into the silica mesopores (see Fig. S3†). We draw the reader's attention to four of them.

Firstly, a sharp peak at $\sim 3750 \text{ cm}^{-1}$ originating from the stretching vibration of ‘free’ (non-associated) OH (Si-OH) groups in the spectrum of an ‘empty’ native silica membrane is not detected in the spectra of confined MAs (grey line in Fig. 1). This is a clear indication of the effective infiltration of the studied alcohols.

Furthermore, surprisingly, the $\nu_{\text{OH bonded}}$ bands of confined MAs are only slightly blue-shifted (shifted towards higher

wavenumber) relative to the bulk samples, which suggests a shortening of the OH bond lengths correlated with the weakening of the existing HBs. This fact can result from increased steric repulsion between alcohol molecules due to their confinement. One can also mention that the detected blue-shift was widely noticed in the case of other confined MAs, *i.e.*, 2-ethyl-1-hexanol, 2-ethyl-1-butanol, and 5-methyl-3-heptanol,⁷¹ as well as confined water and its isotopic derivatives.^{72–79} In the latter case, the observed spectral effect was explained by the formation of weak H-bonding interactions between OH groups (interfacial water molecules) with the silica oxygen atoms, which exhibit weaker H-bond accepting ability compared to water molecules.⁷⁹

Thirdly, the constrained systems exhibit a larger FWHM of their $\nu_{\text{OH bonded}}$ bands compared to bulk ones, suggesting a greater heterogeneity of the environments experienced by the confined MA molecules. Interestingly, the broadening of these bands in the analyzed spectra is more pronounced in the lower wavenumber region. Therefore, at first glance, it may be assumed that an increase in the $\nu_{\text{OH bonded}}$ bandwidth arises from the presence of OH groups engaged in stronger HBs under confinement.

Lastly, the confined samples show a higher intensity of the $\nu_{\text{OH free}}$ bands compared to bulk samples, which indicates that the confinement affects the association process of MAs and reduces the formation of H-bonded aggregates. It should be highlighted that the same observations were found in the case of MAs incorporated within silanized silica mesopores (see Fig. S4†).

Taking into account the above-mentioned findings, one can assume that, surprisingly, the differences in the strength and the population of HBs occurring in bulk and confined MAs are relatively small despite the application of silica templates characterized by small pore size of $d = 4 \text{ nm}$. Note that the same behavior was also observed in the case of PhAs within silica templates of $d = 8 \text{ nm}$. We assume that this interesting behavior might be a result of two scenarios: (i) the mean size of the nanoaggregates formed by the examined MAs is not affected by the spatial restriction^{80–82} or (ii) the recorded signal is dominated by the ‘core’ molecules, which are characterized by bulk-like properties.^{83–85} In this context, one can recall that previous studies on a series of PhAs diluted in carbon tetrachloride (CCl_4) showed that they form nanoaggregates consisting of 2–3 molecules (independent of their molecular weight).⁷⁰ It should be noted that these results agree well with molecular dynamics computations, supported by X-ray diffraction, which revealed that PhAs organize into dimeric and trimeric H-bonded clusters, maintained by additional weak interactions.⁸⁶ Thus, it might indicate that the former scenario is valid. However, as the latter cannot be completely ignored, we decided to remove the ‘core’ molecules from the examined confined systems. For this purpose, the studied porous materials were heated to the chosen temperature ($T = 353\text{--}363 \text{ K}$) to evaporate the molecules that are not strongly interacting with the interface of membranes. Note that in the case of bulk compounds, the complete evaporation at those



temperatures was accomplished in less than one hour ($t = 40$ min; see Fig. S5†); thus, the same procedure was applied in the case of the examined incorporated MAs.

Fig. 2(a) and Fig. S7† show the FTIR spectra collected before ($t = 0$ min) and after ($t = 60$ min, longer than required to remove the bulk sample) the evaporation process of 2Ph1E infiltrated into native silica mesopores. Data for confined 3Ph1P are shown in Fig. S8.† As one can see, a systematic reduction of the intensity of all bands in the recorded spectra was detected upon evaporation. However, despite this fact, FTIR spectra collected after the evaporation revealed the presence of all three characteristic regions previously observed for both bulk and confined MAs (before the evaporation); however, with some differences. This finding might be shown in a better way in Fig. 3, where we compare all available FTIR spectra together. Note that data collected after the evaporation did not exhibit the presence of a sharp peak at ~ 3750 cm^{-1} , characteristic for an 'empty' native silica membrane, which clearly shows that molecules of examined alcohols are still present within the porous materials after the evaporation (Fig. 3). The same behavior was also observed in the case of PhAs within silica templates of $d = 8$ nm, please see Fig. S6.† Therefore, we assume that all changes observed within the examined porous materials after evaporation are solely related to the formation of the interfacial layer strongly bonded to the pore walls.

The most significant changes are observed in both ν_{OH} bonded and ν_{OH} free band ranges (Fig. 2(a) and Fig. S7†). In the case of the ν_{OH} bonded band, one can see a very broad structure of relatively small amplitude, whereas for the ν_{OH} free band, aside from broadening, a pronounced shift towards higher wavenumber can be observed as well. Interestingly, the same changes occurring within the 'residual' ν_{OH} band were previously also observed for MAs diluted in CCl_4 solution⁷⁰ (those data are included in Fig. 3). As can be observed, the ν_{OH} free bands in both spectra are located in a similar spectral range, which might imply that there are some non-H-bonded alcohol molecules present in the confined samples. This observation agrees with the results presented for water confined in periodic mesoporous (organo)silicas, which showed that in the adsorbed layer, non-bonded OH groups and van der Waals water-water interactions may still exist.⁸⁷ In this context, one can also assume that the observed very broad and blurred ν_{OH} bonded band of confined 2Ph1E after evaporation also somehow resembles the one recorded for dissolved PhAs, which was previously assigned to the dominant presence of small H-bonded alcohol aggregates.⁷⁰ Such complex character of the signal of evaporated samples provides direct evidence of the existence of different specific interactions occurring at the silica/alcohol interface, *i.e.*, O-H...O or O-H... π HBs.

In the next step, we focused on the ν_{CH} aromatic bands (located at 3100 – 3000 cm^{-1}), which were well visible in the

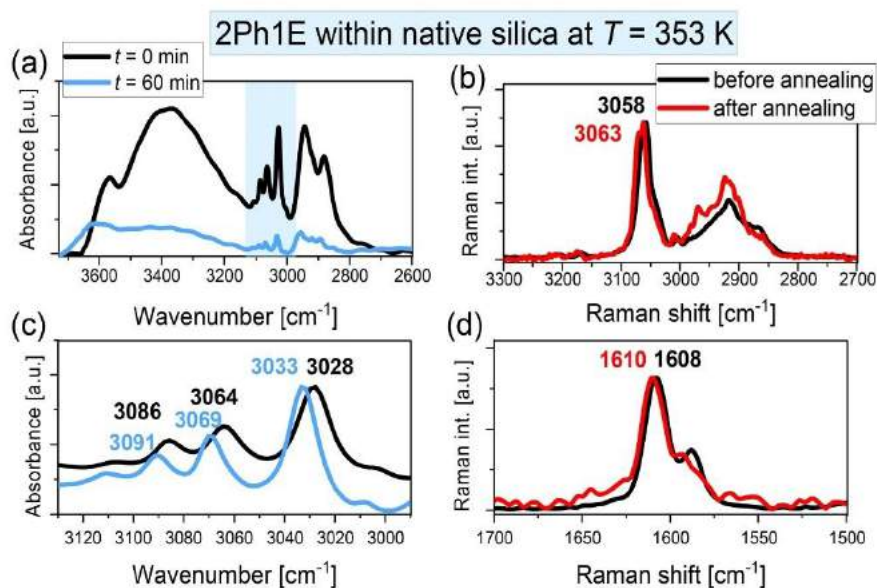


Fig. 2 (a and c) FTIR spectra before and after the evaporation process of 2Ph1E infiltrated into native silica mesopores ($d = 4$ nm) at $t = 0$ min and $t = 60$ min in the (a) 3730 – 2600 cm^{-1} and (c) 3130 – 2990 frequency regions. (b and d) Raman spectra of 2Ph1E within native silica nanopores at room temperature after evaporation at $T = 353$ K in the (b) 3300 – 2700 cm^{-1} and (d) 1700 – 1500 cm^{-1} spectral regions.



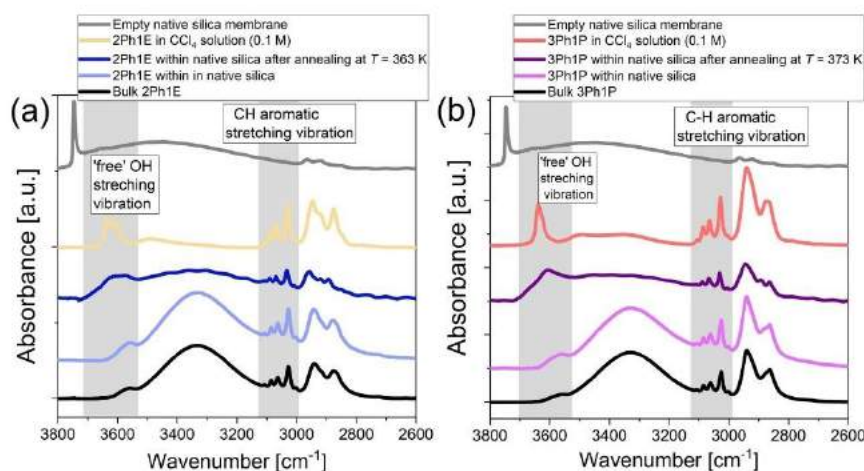


Fig. 3 Comparison of FTIR spectra recorded in the spectral region $3800\text{--}2600\text{ cm}^{-1}$ at $T = 297\text{ K}$ of bulk 2Ph1E (a) and 3Ph1P (b), MAs infiltrated into native silica mesopores of $d = 4\text{ nm}$ before and after evaporation, and bulk MAs within 0.1 M solution of CCl_4 . For comparison, in each case, the FTIR spectrum of an 'empty' native silica membrane is also included. Data for the bulk samples measured within 0.1 M solution of CCl_4 were taken from ref. 70. Data collected for PhAs within silica templates of $d = 8\text{ nm}$ are shown in Fig. S6.†

spectra after the annealing process and, interestingly, they shifted towards higher wavenumbers after evaporation for both confined MAs (Fig. 2(c) and S7(d)†). This also clearly proves two issues: (1) there are some molecules of alcohols present within porous materials after the performed evaporation (of duration longer than required for the bulk sample) and (2) these molecules have a different conformation from those observed for the freshly prepared samples due to the adsorption processes (of physical and/or chemical nature). Thus, this spectral region might be the fingerprint of the remaining IAL within the examined mesoporous matrices.

To identify the mechanism of the adsorption processes occurring at the silica/alcohol interface, *i.e.*, physisorption or chemisorption, we also performed Raman measurements on infiltrated 2Ph1E at room temperature ($T = 297\text{ K}$) before and after the annealing process. As shown in Fig. 2(b and d), the positions of the $\nu_{\text{CH aromatic}}$ peaks (the band at 3058 cm^{-1}) moved to a higher wavenumber (3063 cm^{-1}) after evaporation. Moreover, the change in the band's subtle structure located at $\sim 1610\text{ cm}^{-1}$ (the stretching vibrations of C=C groups) was also visible (Fig. 2(d)). On the other hand, no new/additional bands associated with creating a new type of bond, being the manifestation of the chemisorption process, were observed in the Raman spectra of infiltrated 2Ph1E after evaporation (Fig. S9†). These findings clearly indicate structural/conformational changes of MAs occurring in confinement after annealing. What is more, they are an effect of the adsorption processes of a physical nature (physical adsorption). In this context, it can be added that gravimetric studies conducted for aliphatic alcohols incorporated into MCM-41 mesoporous tem-

plates also indicated that the physisorption process occurs in confinement.⁸⁸

It should be highlighted that identical spectral effects were observed during the evaporation of both alcohols from silanized silica templates (Fig. S7(c, d) and S8(c, d)†). Surprisingly, in the case of silanized systems, the remaining signal in FTIR spectra originating from MA molecules was still detected after $t = 60\text{ min}$, just like for native templates (Fig. S6(c, d) and S7(c, d)†). Moreover, the $\nu_{\text{CH aromatic}}$ bands were also shifted for both MAs incorporated within silanized silica templates after evaporation. However, the intensity of the analyzed signals was smaller when compared to that coming from the untreated templates. For better clarity, a comparison of FTIR spectra for 2Ph1E within silanized membranes of $d = 4\text{ nm}$ is presented in Fig. S10.†

In order to gain deeper insight into the behavior of studied alcohols in pores, with special emphasis on the molecules directly interacting with the pore walls, MD simulations were carried out. In Fig. 4(c), the simulated model is shown. The initial model is composed of an 8 nm -length silica pore with a diameter of $d = 4\text{ nm}$ and additional reservoirs on both ends of the pore filled with the studied alcohol. The initial simulation was performed in the NPT at temperature $T = 293\text{ K}$ and pressure $p = 1\text{ bar}$, which was applied in the z direction (anisotropic) to obtain proper alcohol density inside the pore. As one can see in Fig. 4(c), after the equilibration, the 2Ph1E alcohol density in the pore is approximately 30% lower than in the reservoir outside the pore (0.67 g cm^{-3} versus 1 g cm^{-3}), where there is a typical bulk density. Importantly, this result agrees very well with the data reported in ref. 89, where it was shown



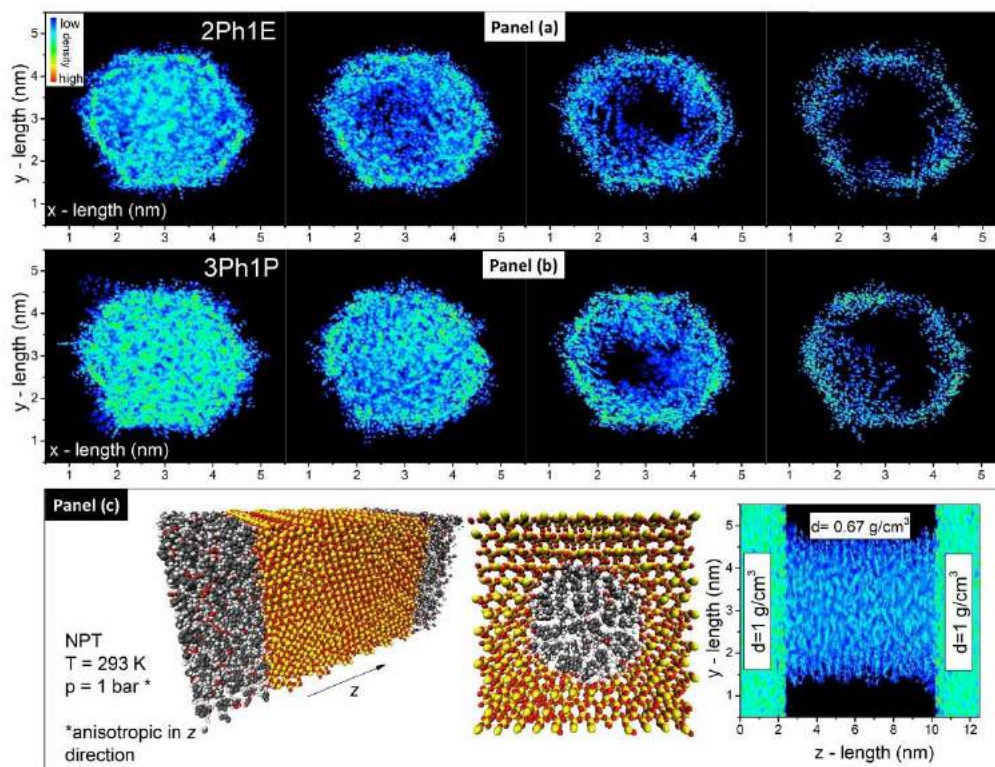


Fig. 4 (a) Density maps of 2Ph1E within pores of $d = 4$ nm in the xy plane. From left to right, maps for 100%, 75%, 50%, and 25% of the initial density are presented. (b) Density maps of 3Ph1P within pores of $d = 4$ nm in the xy plane. From left to right, maps for 100%, 75%, 50%, and 25% of the initial density are shown. (c) Silica pore filled with alcohol: model and density map for an equilibrated model in the xz plane with marked average density in the different zones.

that the free volume inside pores is higher with respect to the bulk material. After the initial NPT simulation, the box was limited to the pore only (without additional molecular reservoirs), and NVT production runs with constant volume were performed. In the last step, the evaporation of alcohol from the pore was simulated by performing NVT simulations with reduced alcohol density inside the pore with 75%, 50%, and 25% initial density. This procedure mimics the evaporation experiment described above. In Fig. 4(a) and (b), one can observe the xy plane cut through the center of the pore with the mapped alcohol density. It is clearly seen how the reduction of the amount of alcohol molecules from 100% to 25% is associated with the formation of an alcohol layer on the inner surface of the silica pore. Moreover, there are slight differences between 2Ph1E and 3Ph1P. In the case of 2Ph1E, the formation of the inner layer is more pronounced than in the case of 3Ph1P (its formation becomes visible at 75% of initial density). This is caused by the differences in the

H-bond interaction energies between alcohol molecules as well as between alcohol-silica molecules.

Moreover, the impact of the pore size on the formation of the alcohol layer at the silica pore interface was checked by performing additional MD simulations. The simulation was performed on the silica pore characterized by $d = 8$ nm filled with 2Ph1E molecules (see Fig. 5(a)). It was found that the elimination of alcohol molecules from the pore interior led to the formation of the same alcohol layer as in the case of the pore with a diameter $d = 4$ nm. Although the process of layer formation occurs in both systems, a significant difference in alcohol density inside different pores was found. In the case of $d = 4$ nm, the average alcohol density is equal to 0.67 g cm^{-3} , while it is equal to 0.86 g cm^{-3} in the case of $d = 8$ nm (versus 1 g cm^{-3} in the bulk system). The formation of the alcohol layer, as well as a comparison of alcohol density in the xy -plane for 2Ph1E for both systems filled with molecules at 25% of initial density, is shown in Fig. S11.†



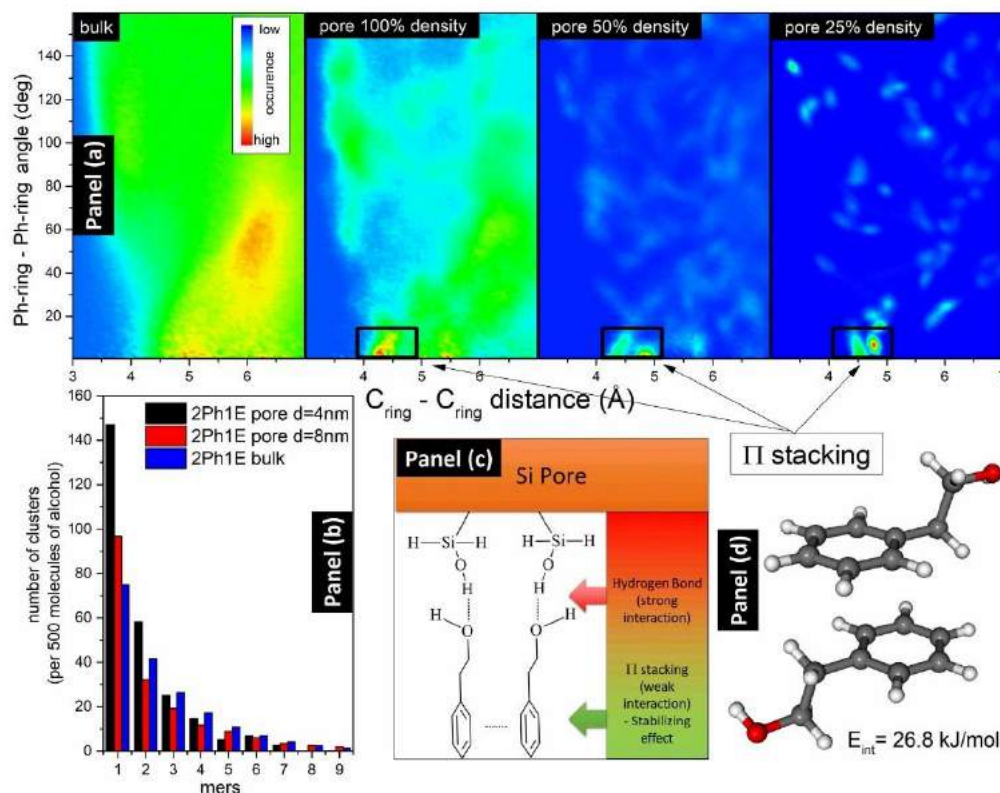


Fig. 5 (a) Maps of 2Ph1E presenting phenyl ring distance versus dihedral angle between phenyl rings in the pore system. The marked boxes are the areas of sandwich-type π -stacking interactions. (b) Histogram comparing the formation of clusters in the 2Ph1E alcohol in bulk and in pores with diameters $d = 4$ nm and $d = 8$ nm. (c) Model representing interactions at the pore-alcohol interface and the role of HBs and π - π interactions. (d) Energy of π -stacking interaction between two 2Ph1E molecules calculated in the DFT model.

MD simulations have also been used to obtain HB cluster distributions for 2Ph1E and 3Ph1P alcohols. In Fig. 5(b), a comparison of histograms for 2Ph1E in the bulk and pores with $d = 4$ nm and $d = 8$ nm is presented. As one can see, the alcohol molecules form the strongest clusters in the bulk system and the weakest in the small pore of $d = 4$ nm. The clustering ability of alcohol molecules in large pores of $d = 8$ nm diameter is between that in small pores of $d = 4$ nm and the bulk system. More distributions of clusters are presented in Fig. S12.† Interestingly, the distribution of self-assemblies formed by alcohol-alcohol interactions in the pores is similar to the distribution of clusters in a bulk system. However, the average cluster size is slightly lower in the pores for both alcohols. This result is quite consistent with the FTIR data that indicated a very small change in the position of the ν_{OH} bonded band in the pores with respect to the bulk sample. In the case of 2Ph1E, we have an average cluster size, α , equal to 3.7 mole-

cules in the bulk system and 3.2 molecules within the pores, which can be related to the 30% lower density. For 3Ph1P, the situation is similar, where $\alpha = 4.5$ molecules and $\alpha = 3.3$ molecules within bulk and pores, respectively. In bulk 3Ph1P, 20.6% of molecules are non-H-bonded (monomers), while in 2Ph1E, there are 14.9% monomers, which means a higher association degree of 2Ph1E than of 3Ph1P. The next comparison is related to all HBs in silica pores (*i.e.*, silica-silica, alcohol-alcohol, and alcohol-silica) with initial and reduced alcohol density (100% and 50%). 2Ph1E in both density scenarios (100% and 50%) has more clusters than 3Ph1P. For an initial 100% density, there are only 6.9% free OH groups in the entire 2Ph1E pore system, while this value is 22.2% for 3Ph1P. However, when we compare HBs existing only in the core region between alcohol molecules, the percentage of free OH groups is higher in the pores than in the bulk for both systems (30% free OH groups in 2Ph1E and 33% in 3Ph1P). This result

also agrees with the FTIR data, showing an increase in the $\nu_{\text{OH free}}$ band intensity for confined samples compared to bulk samples, thus the existence of a larger amount/number of monomers under confinement. When the density is reduced to 50% of the initial value, and we take into account all HBs (silica–silica, alcohol–alcohol, and silica–alcohol), there are 14% free OH groups in 2Ph1E, while 30% in 3Ph1P. During the reduction of alcohol density in the pores, the differences between 2Ph1E and 3Ph1P systems become smaller, which can indicate that the strength of the silica–alcohol bond and tendency to form layer are similar for both systems, while alcohol–alcohol HBs are much weaker in 3Ph1P. The same behavior was observed for 2Ph1E in the pore with diameter $d = 8$ nm. There are 10.6% free OH groups in the entire pore system, while 19.3% free OH groups in the core area (alcohol–alcohol). The data related to the average densities and amounts of free OH groups in all studied systems are presented in Table S1.†

The formation of the layer caused by the physisorption process is related to the H-bond interactions between hydroxyl groups from alcohol and silica. Therefore, in the next step, we performed an analysis of H-bond cluster formation in bulk alcohols and in pores fully filled with alcohol and after partial evaporation (50% of density). Moreover, we have used DFT calculations to obtain interaction energies between alcohol molecules and between alcohol and silica. It was found that the H-bond energy between silica and alcohol is higher than between two alcohol molecules, but only when the silica group is a donor and alcohol is an acceptor of the H-bond. The interaction energy, E_{int} , between two 2Ph1E molecules is equal to $E_{\text{int}} = 42.6 \text{ kJ mol}^{-1}$. When SiOH or SiO₂H₂ groups are donors and alcohol is the acceptor, the interaction energies are equal to $E_{\text{int,SiOH}} = 45.3 \text{ kJ mol}^{-1}$ and $E_{\text{int,SiO}_2\text{H}_2} = 50.2 \text{ kJ mol}^{-1}$, respectively. In the opposite situation, when the alcohol is a proton donor, and SiOH or SiO₂H₂ are acceptors, the interaction energies are equal to $E_{\text{int,SiOH}} = 30.5 \text{ kJ mol}^{-1}$ and $E_{\text{int,SiO}_2\text{H}_2} = 32.1 \text{ kJ mol}^{-1}$, respectively. This is a clear indication that from the energetic point of view, the most stable are connections of alcohol with the pore SiOH and SiO₂H₂ groups when the alcohol is an acceptor of hydrogen. In the aromatic alcohols, there are also present π -stacking interactions;^{90,91} thus, we have calculated the energies of two possible π -stacking formations. The first one is a sandwich type, which is slightly displaced, and the second one is a T-shape π -stacking. The energy of the sandwich-type interaction is equal to $E_{\text{int,sandwich}} = 26.8 \text{ kJ mol}^{-1}$, while the energy of the T-shape reaches $E_{\text{int,T-shape}} = 16.4 \text{ kJ mol}^{-1}$. The sandwich-type interaction is shown in Fig. 5(d). The energy of sandwich π -stacking is two times smaller than the energy of the H-bond. However, when alcohols are connected by HBs to the inner layer of silica pores, these interactions can stabilize energetically the layer. This effect was found during molecular dynamics study, where in simulations mimicking evaporation, sandwich π -stacking interactions are abundant (see Fig. 5(a)). Therefore, the stability of the inner layer is greatly enhanced by the strong HBs with silica and by the additional π -stacking

interactions of alcohols connected to the silica by HBs. The visualization of such stable connection of alcohol with silica surface is presented in Fig. 5(c). It should be noted that this finding correlates well with the results of FTIR measurements, i.e., these π -stacking interactions occurring between the studied MAs can be responsible for the shift of the $\nu_{\text{CH aromatic}}$ bands towards higher wavenumbers after evaporation of confined MAs. Hence, as observed from FTIR data and molecular dynamics simulations, the formation of the interfacial layer induces and strengthens π -stacking interactions between alcohols.

IV. Conclusions

In summary, we conducted FTIR measurements for two MAs infiltrated into native and silanized silica mesopores ($d = 4\text{--}8$ nm) to investigate any differences in the nature of interactions under these conditions (the impact of confinement on intermolecular interactions). Initially, the spectra of both systems (bulk vs. confinement) showed only little discrepancies, indicating that the 'core' layer of the molecule dominates in infiltrated MAs. Interestingly, this finding was well supported by the MD simulations that revealed the small impact of the nanoscale confinement on the association phenomenon in both alcohols. To remove the bulk-like fraction (core layer), we proposed a solvent-free approach depending on the evaporation process. In this way, the layer at the interface was revealed for the first time in 2D-constrained systems. Importantly, the obtained 'residual' band was characterized by a new subtle structure compared to that in the bulk and confined MAs. The changes especially observed in the high-frequency region of IR spectra suggested the differences in the arrangement of both free and associated OH groups. The source of the observed differences was the formation of a layer adsorbed on the interface (IAL). It should be noted that these changes were obtained regardless of the kind/type of silica templates used (non-treated/treated). What is more, the Raman spectra of 2Ph1E in native silica mesopores before and after annealing clearly indicate the formation of IAL due to the physisorption mechanism, not chemisorption. Importantly, these suppositions were further confirmed by MD simulations, which indicated the formation of the interfacial layer (considered as IAL due to its resistance to the evaporation process) attached to the silica pores that is stabilized by the effective H-bonds and enormously strong π -stacking interactions. In conclusion, we present a pioneering work with a novel approach to examining strongly bonded interfacial layers formed in pores of similar characteristics to IAL investigated in thin films or silica nanoparticles.

Data and materials availability

The ESI† file is available free of charge at <https://pubs.acs.org>. It contains additional figures and tables, including the sche-



matic structure of silica mesopore templates, IR spectra of bulk and infiltrated MAs at room temperature, IR spectra of bulk MAs before and after evaporation, IR spectra of MAs infiltrated into native silica pores ($d = 4$ nm and 8 nm) before and after annealing, IR spectra of empty silanized silica template, Raman spectra of bulk and 2Ph1E incorporated into nanopores before and after annealing at 297 K, distribution of 2Ph1E molecules in xy plane within $d = 8$ nm nanopore at different levels of initial density, the density of 2Ph1E molecules in the pore for the equilibrating NPT, schematic existence of strongly bonded alcohol layer at the silica interface for silica mesopores ($d = 4$ and 8 nm) obtained from molecular dynamics calculations, histograms comparing the formation of clusters in MAs in mesopores with $d = 8$ nm with 100% and 50% alcohol densities, and a table including average densities of alcohols, and the amounts of free OH groups in the studied systems.

Author contributions

N. S. – writing – original draft, investigation, formal analysis, visualization. M. T. – writing – original draft, conceptualization, funding acquisition. B. H. – formal analysis, methodology. P. W. – investigation, formal analysis. R. W. – investigation. M. H. – investigation. M. P. – methodology. K. K. – supervision, funding acquisition, writing – review & editing.

Conflicts of interest

The authors declare no competing financial interests.

Acknowledgements

The experimental part of this research was funded by National Science Centre, Poland [Dec. no 2019/33/B/ST3/00500]. MD simulations of this work were funded by the National Science Centre, Poland [Dec. no 2022/47/B/ST4/00236]. For the purpose of Open Access, the author has applied a CC-BY public copy-right licence to any Author Accepted Manuscript (AAM) version arising from this submission.

References

- 1 D. T. Limmer and D. Chandler, *J. Chem. Phys.*, 2012, **137**, 1841–1844.
- 2 P. Huber, *J. Phys.: Condens. Matter*, 2015, **27**, 103102.
- 3 L. Petychakis, G. Floudas and G. Fleischer, *Europhys. Lett.*, 1997, **40**, 685–690.
- 4 H. Duran, A. Gitsas, G. Floudas, M. Mondeshki, M. Steinhart and W. Knoll, *Macromolecules*, 2009, **42**, 2881–2885.
- 5 M. Krutyeva, A. Wischnewski, M. Monkenbusch, L. Willner, J. Maiz, C. Mijangos, A. Arbe, J. Colmenero, A. Radulescu, O. Holderer, M. Ohl and D. Richter, *Phys. Rev. Lett.*, 2013, **110**, 1–5.
- 6 C. L. Jackson and G. B. McKenna, *Chem. Mater.*, 1996, **8**, 2128–2137.
- 7 C. Alba-Simionesco, G. Dosseh, E. Dumont, B. Frick, B. Geil, D. Morineau, V. Teboul and Y. Xia, *Eur. Phys. J. E: Soft Matter Biol. Phys.*, 2003, **12**, 19–28.
- 8 W. Yan, V. K. S. Hsiao, Y. B. Zheng, Y. M. Shariff, T. Gao and T. J. Huang, *Thin Solid Films*, 2009, **517**, 1794–1798.
- 9 G. Jeon, S. Y. Yang and J. K. Kim, *J. Mater. Chem.*, 2012, **22**, 14814–14834.
- 10 A. Hashemi, M. Ezati, J. Mohammadnejad, B. Houshmand and S. Faghihi, *Int. J. Nanomed.*, 2020, **15**, 4471–4481.
- 11 S. Sotiropoulou, V. Vamvakaki and N. A. Chaniotakis, *Biosens. Bioelectron.*, 2005, **20**, 1674–1679.
- 12 S. P. Adiga, C. Jin, L. A. Curtiss, N. A. Monteiro-Riviere and R. J. Narayan, *Wiley Interdiscip. Rev.: Nanomed. Nanobiotechnol.*, 2009, **1**, 568–581.
- 13 M. Tarnacka, A. Chrobok, K. Matuszek, S. Golba, P. Maksym, K. Kaminski and M. Paluch, *ACS Appl. Mater. Interfaces*, 2016, **8**, 29779–29790.
- 14 A. Schönhals, F. Rittig and J. Kärger, *J. Chem. Phys.*, 2010, **133**, 094903.
- 15 M. Tarnacka, M. Wojtyniak, A. Brzózka, A. Talik, B. Hachuła, E. Kamińska, G. D. Sulka, K. Kaminski and M. Paluch, *Nano Lett.*, 2020, **20**, 5714–5719.
- 16 W. K. Kipnusu, M. M. Elmahdy, M. Elsayed, R. Krause-Rehberg and F. Kremer, *Macromolecules*, 2019, **52**, 1864–1873.
- 17 R. Renou, A. Szymczyk and A. Ghoufi, *J. Chem. Phys.*, 2014, **140**, 044704.
- 18 A. Panagopoulou, C. Rodríguez-Tinoco, R. P. White, J. E. G. Lipson and S. Napolitano, *Phys. Rev. Lett.*, 2020, **124**, 27802.
- 19 A. Talik, M. Tarnacka, M. Wojtyniak, E. Kaminska, K. Kaminski and M. Paluch, *J. Mol. Liq.*, 2020, **298**, 111973.
- 20 S. Napolitano and M. Wübbenhorst, *Nat. Commun.*, 2011, **2**, 260.
- 21 S. Napolitano, V. Lupaşcu and M. Wübbenhorst, *Macromolecules*, 2008, **41**, 1061–1063.
- 22 S. Napolitano, C. Rotella and M. Wübbenhorst, *ACS Macro Lett.*, 2012, **1**, 1189–1193.
- 23 C. Rotella, S. Napolitano, S. Vandendriessche, V. K. Valev, T. Verbiest, M. Larkowska, S. Kucharski and M. Wübbenhorst, *Langmuir*, 2011, **27**, 13533–13538.
- 24 P. Gin, N. Jiang, C. Liang, T. Taniguchi, B. Akgun, S. K. Satija, M. K. Endoh and T. Koga, *Phys. Rev. Lett.*, 2012, **109**, 1–5.
- 25 J. M. Y. Carrillo, S. Cheng, R. Kumar, M. Goswami, A. P. Sokolov and B. G. Sumpter, *Macromolecules*, 2015, **48**, 4207–4219.
- 26 S. Napolitano and D. Cangialosi, *Macromolecules*, 2013, **46**, 8051–8053.
- 27 D. Cangialosi, V. M. Boucher, A. Alegria and J. Colmenero, *J. Chem. Phys.*, 2011, **135**, 014901.



- 28 R. P. White and J. E. G. Lipson, *Macromolecules*, 2016, **49**, 3987–4007.
- 29 R. P. White and J. E. G. Lipson, *ACS Macro Lett.*, 2017, **6**, 529–534.
- 30 A. Debot, R. P. White, J. E. G. Lipson and S. Napolitano, *ACS Macro Lett.*, 2019, **8**, 41–45.
- 31 N. Bizmark, M. A. Ioannidis and D. E. Henneke, *Langmuir*, 2014, **30**, 710–717.
- 32 S. Milani, F. B. Bombelli, A. S. Pitek, K. A. Dawson and J. Rädler, *ACS Nano*, 2012, **6**, 2532–2541.
- 33 X. Li, O. Niitsoo and A. Couzis, *J. Colloid Interface Sci.*, 2014, **420**, 50–56.
- 34 Z. U. A. Arain, S. Al-Ansari, M. Ali, S. Memon, M. A. Bhatti, C. Lagat and M. Sarmadivaleh, *Petroleum*, 2020, **6**, 277–285.
- 35 M. Tarnacka, E. Kamińska, M. Paluch and K. Kamiński, *J. Phys. Chem. Lett.*, 2022, **13**, 10464–10470.
- 36 M. Tarnacka, E. Kamińska, K. Kaminski, C. M. Roland and M. Paluch, *J. Phys. Chem. C*, 2016, **120**, 7373–7380.
- 37 M. Tarnacka, O. Madejczyk, K. Kaminski and M. Paluch, *Macromolecules*, 2017, **50**, 5188–5193.
- 38 S. Zimny, M. Tarnacka, M. Geppert-Rybczyńska and K. Kamiński, *J. Phys. Chem. C*, 2023, **127**, 23034–23043.
- 39 K. Adrjanowicz and M. Paluch, *Phys. Rev. Lett.*, 2019, **122**, 176101.
- 40 M. Tarnacka, M. Dulski, M. Geppert-Rybczyńska, A. Talik, E. Kamińska, K. Kamiński and M. Paluch, *J. Phys. Chem. C*, 2018, **122**, 28033–28044.
- 41 M. F. Thees, J. A. McGuire and C. B. Roth, *Soft Matter*, 2020, **16**, 5366–5387.
- 42 N. Jiang, M. Sen, W. Zeng, Z. Chen, J. M. Cheung, Y. Morimitsu, M. K. Endoh, T. Koga, M. Fukuto, G. Yuan, S. K. Satija, J. M. Y. Carrillo and B. G. Sumpter, *Soft Matter*, 2018, **14**, 1108–1119.
- 43 C. Housmans, M. Sferrazza and S. Napolitano, *Macromolecules*, 2014, **47**, 3390–3393.
- 44 C. Jacob, J. R. Sangoro, P. Papadopoulos, T. Schubert, S. Naumov, R. Valiullin, J. Kärger and F. Kremer, *Phys. Chem. Chem. Phys.*, 2010, **12**, 13798–13803.
- 45 W. K. Kipnusu, W. Kossack, C. Jacob, M. Jasiurkowska, J. R. Sangoro and F. Kremer, *Z. Phys. Chem.*, 2012, **226**, 797–805.
- 46 S. Grimme, *Wiley Interdiscip. Rev.: Comput. Mol. Sci.*, 2011, **1**, 211–228.
- 47 F. Neese, *Wiley Interdiscip. Rev.: Comput. Mol. Sci.*, 2022, **12**, 1–15.
- 48 C. Bannwarth, E. Caldeweyher, S. Ehlert, A. Hansen, P. Pracht, J. Seibert, S. Spicher and S. Grimme, *Wiley Interdiscip. Rev.: Comput. Mol. Sci.*, 2021, **11**, 1–49.
- 49 F. Neese, *Wiley Interdiscip. Rev.: Comput. Mol. Sci.*, 2018, **8**, 1327.
- 50 F. Neese, *Wiley Interdiscip. Rev.: Comput. Mol. Sci.*, 2012, **2**, 73–78.
- 51 H. Bekker, H. J. C. Berendsen, E. J. Dijkstra, S. Achterop, R. van Drunen, D. van der Spoel, A. Sijbers and H. Keegstra, *et al.*, in *Physics computing 92*, ed. R. A. de Groot and J. Nadrechal, World Scientific, Singapore, 1993, pp. 252–256.
- 52 E. Lindahl, B. Hess and D. van der Spoel, *J. Mol. Model.*, 2001, **7**, 306–317.
- 53 D. Van Der Spoel, E. Lindahl, B. Hess, G. Groenhof, A. E. Mark and H. J. C. Berendsen, *J. Comput. Chem.*, 2005, **26**, 1701–1718.
- 54 B. Hess, C. Kutzner, D. van der Spoel and E. Lindahl, *J. Chem. Theory Comput.*, 2008, **4**, 435–447.
- 55 H. Kraus, J. Rybka, A. Hölzel, N. Trebel, U. Tallarek and N. Hansen, *Mol. Simul.*, 2021, **47**, 306–316.
- 56 K. Kanhaiya, M. Nathanson, P. J. in 't Veld, C. Zhu, I. Nikiforov, E. B. Tadmor, Y. K. Choi, W. Im, R. K. Mishra and H. Heinz, *J. Chem. Theory Comput.*, 2023, **19**, 8293–8322.
- 57 L. Martinez, R. Andrade, E. G. Birgin and J. M. Martinez, *J. Comput. Chem.*, 2009, **30**, 2157–2164.
- 58 M. Brehm and B. Kirchner, *J. Chem. Inf. Model.*, 2011, **51**, 2007–2023.
- 59 O. Hollóczki, M. Macchiagodena, H. Weber, M. Thomas, M. Brehm, A. Stark, O. Russina, A. Triolo and B. Kirchner, *ChemPhysChem*, 2015, **16**, 3325–3333.
- 60 M. Brehm, M. Thomas, S. Gehrke and B. Kirchner, *J. Chem. Phys.*, 2020, **152**, 164105.
- 61 W. Ren, Y. Li, Y. Tang, J. Xu, C. Zhang, O. K. C. Tsui and X. Wang, *ACS Macro Lett.*, 2023, **12**, 854–859.
- 62 C. Rodríguez-Tinoco, D. N. Simavilla, R. D. Priestley, M. Wübbenhorst and S. Napolitano, *ACS Macro Lett.*, 2020, **9**, 318–322.
- 63 S. Napolitano, *Soft Matter*, 2020, **16**, 5348–5365.
- 64 A. B. Unni, R. Mroczka, J. Kubacki and K. Adrjanowicz, *J. Mol. Liq.*, 2022, **368**, 120675.
- 65 A. B. Unni, R. Winkler, D. M. Duarte, K. Chat and K. Adrjanowicz, *J. Phys. Chem. B*, 2022, **126**, 8072–8079.
- 66 K. Randazzo, M. Bartkiewicz, B. Graczykowski, D. Cangialosi, G. Fytas, B. Zuo and R. D. Priestley, *Macromolecules*, 2021, **54**, 10224–10234.
- 67 Y. Qiang, K. T. Turner and D. Lee, *Macromolecules*, 2023, **56**, 122–135.
- 68 M. A. Khazaei, D. Bastani, A. Mohammadi and A. Kordzadeh, *Langmuir*, 2022, **38**, 12421–12431.
- 69 H. Li, X. Chen, D. Shen, F. Wu, R. Pleixats and J. Pan, *Nanoscale*, 2021, **13**, 15998–16016.
- 70 N. Soszka, B. Hachuła, M. Tarnacka, E. Kamińska, J. Grelska, K. Jurkiewicz, M. Geppert-Rybczyńska, R. Wrzalik, K. Grzybowska, S. Pawlus, M. Paluch and K. Kamiński, *Phys. Chem. Chem. Phys.*, 2021, **23**, 23796–23807.
- 71 A. Talik, M. Tarnacka, M. Geppert-Rybczyńska, B. Hachuła, R. Bernat, A. Chrzanowska, K. Kaminski and M. Paluch, *J. Colloid Interface Sci.*, 2020, **576**, 217–229.
- 72 J. R. Bailey and M. M. McGuire, *Langmuir*, 2007, **23**, 10995–10999.
- 73 M. Baum, F. Rieutord, F. Juranyi, C. Rey and D. Rébiscoul, *Langmuir*, 2019, **35**, 10780–10794.
- 74 S. A. Yamada, J. Y. Shin, W. H. Thompson and M. D. Fayer, *J. Phys. Chem. C*, 2019, **123**, 5790–5803.
- 75 S. Le Caër, S. Pin, S. Esnouf, Q. Raffy, J. P. Renault, J. B. Brubach, G. Creff and P. Roy, *Phys. Chem. Chem. Phys.*, 2011, **13**, 17658–17666.

- 76 X. F. Huang, Q. Wang, X. X. Liu, S. H. Yang, C. X. Li, G. Sun, L. Q. Pan and K. Q. Lu, *J. Phys. Chem. C*, 2009, **113**, 18768–18771.
- 77 R. Musat, J. P. Renault, M. Candelaresi, D. J. Palmer, S. Le Caër, R. Righini and S. Pommeret, *Angew. Chem., Int. Ed.*, 2008, **47**, 8033–8035.
- 78 S. A. Yamada, S. T. Hung, W. H. Thompson and M. D. Fayer, *J. Chem. Phys.*, 2020, **152**, 154704.
- 79 H. S. Senanayake, J. A. Greathouse, A. G. Ilgen and W. H. Thompson, *J. Chem. Phys.*, 2021, **154**, 104503.
- 80 A. Ghoufi, *J. Phys. Chem. B*, 2020, **124**, 11501–11509.
- 81 A. Ghoufi, I. Hureau, R. Lefort and D. Morineau, *J. Phys. Chem. C*, 2011, **115**, 17761–17767.
- 82 A. Ghoufi, I. Hureau, D. Morineau, R. Renou and A. Szymczyk, *J. Phys. Chem. C*, 2013, **117**, 15203–15212.
- 83 C. L. Jackson and G. B. McKenna, *J. Non-Cryst. Solids*, 1991, **131–133**, 221–224.
- 84 J. Y. Park and G. B. McKenna, *Phys. Rev. B: Condens. Matter Mater. Phys.*, 2000, **61**, 6667–6676.
- 85 K. Adrjanowicz, K. Kolodziejczyk, W. K. Kipnusu, M. Tarnacka, E. U. Mapesa, E. Kaminska, S. Pawlus, K. Kaminski and M. Paluch, *J. Phys. Chem. C*, 2015, **119**, 14366–14374.
- 86 J. Grelska, K. Jurkiewicz, A. Nowok and S. Pawlus, *Phys. Rev. E*, 2023, **108**, 024603.
- 87 B. Malfait, A. Moréac, A. Jani, R. Lefort, P. Huber, M. Fröba and D. Morineau, *J. Phys. Chem. C*, 2022, **126**, 3520–3531.
- 88 P. J. Branton, P. G. Hall and K. S. W. Sing, *Adsorption*, 1995, **1**, 77–82.
- 89 W. K. Kipnusu, M. Elsayed, W. Kossack, S. Pawlus, K. Adrjanowicz, M. Tress, E. U. Mapesa, R. Krause-Rehberg, K. Kaminski and F. Kremer, *J. Phys. Chem. Lett.*, 2015, **6**, 3708–3712.
- 90 T. Chen, M. Li and J. Liu, *Cryst. Growth Des.*, 2018, **18**, 2765–2783.
- 91 J. H. Deng, J. Luo, Y. L. Mao, S. Lai, Y. N. Gong, D. C. Zhong and T. B. Lu, *Sci. Adv.*, 2020, **6**, 1–9.



Chorzów, 10.04.2024

Dr hab. Barbara Hachuła, prof. UŚ
Instytut Chemii
Wydział Nauk Ścisłych i Technicznych
Uniwersytet Śląski w Katowicach
ul. Szkolna 9
40-006 Katowice

OŚWIADCZENIE

Oświadczam, że w pracy:

P1. N. Soszka, B. Hachuła, M. Tarnacka, E. Kamińska, J. Grelska, K. Jurkiewicz, M. Geppert-Rybczyńska, R. Wrzalik, K. Grzybowska, S. Pawlus, M. Paluch, K. Kamiński, **The Impact of the Length of Alkyl Chain on the Behavior of Benzyl Alcohol Homologues – the Interplay between Dispersive and Hydrogen Bond Interactions.** *Phys. Chem. Chem. Phys.* **2021**, 23 (41), 23796 – 23807.

mój udział polegał na opracowaniu koncepcji badań, nadzorowaniu przeprowadzonych analiz, dyskusji wyników, współtworzeniu i korekcy manuskryptu wraz z odpowiedziami na uwagi recenzentów;

P2. N. Soszka, B. Hachuła, M. Tarnacka, J. Grelska, K. Jurkiewicz, M. Geppert – Rybczyńska, R. Wrzalik, K. Grzybowska, S. Pawlus, M. Paluch, K. Kamiński, **Aromaticity Effect on Supramolecular Aggregation. Aromatic vs. Cyclic Monohydroxy Alcohols.** *Spectrochim. Acta – Part A Mol. Biomol. Spectrosc.* **2022**, 276, 121235.

mój udział polegał na opracowaniu koncepcji badań, nadzorowaniu przeprowadzonych analiz, analizie i dyskusji wyników, współtworzeniu i korekcy manuskryptu wraz z odpowiedziami na uwagi recenzentów;

P3. N. Soszka, M. Tarnacka, B. Hachuła, M. Geppert – Rybczyńska, K. Prusik, K. Kamiński, **The Impact of Interface Modification on the Behavior of Phenyl Alcohols within Silica Templates.** *J. Phys. Chem. C*, **2024**, (doi: 10.1021/acs.jpcc.3c08084)

mój udział polegał na nadzorowaniu przeprowadzonych analiz, dyskusji wyników oraz współtworzeniu i korekcy manuskryptu;

P4. N. Soszka, M. Tarnacka, B. Hachuła, P. Włodarczyk, R. Wrzalik, M. Hreczka, M. Paluch, K. Kamiński, The Existence of Strongly Bonded Layer in Associating Liquids within Silica Pores – the Spectral and Molecular Dynamics Study. *Nanoscale*, **2024**, 16, 6636-6647

mój udział polegał na nadzorowaniu przeprowadzonych analiz, dyskusji wyników oraz współtworzeniu i korekcji manuskryptu.

Barbara Hachuła

Chorzów, 10.04.2024

Dr hab. Magdalena Tarnacka, prof. UŚ
Instytut Fizyki im. Augusta Chełkowskiego
Wydział Nauk Ścisłych i Technicznych
Uniwersytet Śląski w Katowicach
ul. 75 Pułku Piechoty 1
41-500 Chorzów

OŚWIADCZENIE

Oświadczam, że w pracy:

P1. N. Soszka, B. Hachuła, M. Tarnacka, E. Kamińska, J. Grelska, K. Jurkiewicz, M. Geppert-Rybczyńska, R. Wrzalik, K. Grzybowska, S. Pawlus, M. Paluch, K. Kamiński,
The Impact of the Length of Alkyl Chain on the Behavior of Benzyl Alcohol Homologues – the Interplay between Dispersive and Hydrogen Bond Interactions.
Phys. Chem. Chem. Phys. **2021**, 23 (41), 23796 – 23807.

mój udział polegał na wykonaniu badań kalorymetrycznych, ich analizie i interpretacji, dyskusji otrzymanych wyników, współtworzeniu manuskryptu wraz z odpowiedziami na uwagi recenzentów oraz finansowaniu badań w ramach projektu NCN OPUS;

P2. N. Soszka, B. Hachuła, M. Tarnacka, J. Grelska, K. Jurkiewicz, M. Geppert – Rybczyńska, R. Wrzalik, K. Grzybowska, S. Pawlus, M. Paluch, K. Kamiński,
Aromaticity Effect on Supramolecular Aggregation. Aromatic vs. Cyclic Monohydroxy Alcohols. *Spectrochim. Acta – Part A Mol. Biomol. Spectrosc.* **2022**, 276, 121235.

mój udział polegał na wykonaniu badań dielektrycznych i kalorymetrycznych, ich analizie i interpretacji, dyskusji otrzymanych wyników, współtworzeniu manuskryptu wraz z odpowiedziami na uwagi recenzentów oraz finansowaniu badań w ramach projektu NCN OPUS;

P3. N. Soszka, M. Tarnacka, B. Hachuła, M. Geppert – Rybczyńska, K. Prusik, K. Kamiński, **The Impact of Interface Modification on the Behavior of Phenyl Alcohols within Silica Templates.** *J. Phys. Chem. C*, **2024**, (doi: 10.1021/acs.jpcc.3c08084)

mój udział polegał na opracowaniu koncepcji badań, wykonaniu pomiarów dielektrycznych i kalorymetrycznych, ich analizie i interpretacji, dyskusji wyników, współtworzeniu

manuskryptu wraz z odpowiedziami na uwagi recenzentów oraz finansowaniu badań w ramach projektu NCN OPUS;

P4. N. Soszka, M. Tarnacka, B. Hachuła, P. Włodarczyk, R. Wrzalik, M. Hreczka, M. Paluch, K. Kamiński, The Existence of Strongly Bonded Layer in Associating Liquids within Silica Pores – the Spectral and Molecular Dynamics Study. *Nanoscale*, **2024**, 16, 6636-6647

mój udział polegał na opracowaniu koncepcji badań, analizie danych, dyskusji wyników, współtworzeniu i korekcie manuskryptu wraz z odpowiedziami na uwagi recenzentów oraz finansowaniu badań w ramach projektu NCN OPUS.

*Magdalena
Tarnacka*

Chorzów, 10.04.2024

Prof. dr hab. Kamil Kamiński
Instytut Fizyki im. Augusta Chelkowskiego
Wydział Nauk Ścisłych i Technicznych
Uniwersytet Śląski w Katowicach
ul. 75 Pułku Piechoty 1
41-500 Chorzów

OŚWIADCZENIE

Oświadczam, że w pracy:

P1. N. Soszka, B. Hachuła, M. Tarnacka, E. Kamińska, J. Grelska, K. Jurkiewicz, M. Geppert-Rybczyńska, R. Wrzalik, K. Grzybowska, S. Pawlus, M. Paluch, K. Kamiński, **The Impact of the Length of Alkyl Chain on the Behavior of Benzyl Alcohol Homologues – the Interplay between Dispersive and Hydrogen Bond Interactions.** *Phys. Chem. Chem. Phys.* **2021**, 23 (41), 23796 – 23807.

mój udział polegał na nadzorowaniu przeprowadzonych analiz, dyskusji otrzymanych wyników oraz współtworzeniu i korekcji manuskryptu;

P2. N. Soszka, B. Hachuła, M. Tarnacka, J. Grelska, K. Jurkiewicz, M. Geppert – Rybczyńska, R. Wrzalik, K. Grzybowska, S. Pawlus, M. Paluch, K. Kamiński, **Aromaticity Effect on Supramolecular Aggregation. Aromatic vs. Cyclic Monohydroxy Alcohols.** *Spectrochim. Acta – Part A Mol. Biomol. Spectrosc.* **2022**, 276, 121235.

mój udział polegał na nadzorowaniu przeprowadzonych analiz, dyskusji otrzymanych wyników oraz współtworzeniu i korekcji manuskryptu;

P3. N. Soszka, M. Tarnacka, B. Hachuła, M. Geppert – Rybczyńska, K. Prusik, K. Kamiński, **The Impact of Interface Modification on the Behavior of Phenyl Alcohols within Silica Templates.** *J. Phys. Chem. C*, **2024**, (doi: 10.1021/acs.jpcc.3c08084)

mój udział polegał na nadzorowaniu przeprowadzonych analiz, dyskusji otrzymanych wyników oraz współtworzeniu i korekcji manuskryptu;

P4. N. Soszka, M. Tarnacka, B. Hachuła, P. Włodarczyk, R. Wrzalik, M. Hreczka, M. Paluch, K. Kamiński, The Existence of Strongly Bonded Layer in Associating Liquids within Silica Pores – the Spectral and Molecular Dynamics Study. *Nanoscale*, **2024**, 16, 6636-6647

mój udział polegał na nadzorowaniu przeprowadzonych analiz, dyskusji otrzymanych wyników, współtworzeniu i korekcji manuskryptu oraz finansowaniu badań w ramach projektu NCN OPUS.

Kamil Kamiński

Chorzów, 10.04.2024

dr hab. Monika Geppert-Rybczyńska, prof. UŚ
Instytut Chemii
Wydział Nauk Ścisłych i Technicznych
Uniwersytet Śląski w Katowicach
ul. Szkolna 9
40-006 Katowice

OŚWIADCZENIE

Oświadczam, że w pracy:

P1. N. Soszka, B. Hachuła, M. Tarnacka, F. Kamińska, J. Grelska, K. Jurkiewicz, M. Geppert-Rybczyńska, R. Wrzałik, K. Grzybowska, S. Pawlus, M. Paluch, K. Kamiński, **The Impact of the Length of Alkyl Chain on the Behavior of Benzyl Alcohol Homologues – the Interplay between Dispersive and Hydrogen Bond Interactions.** *Phys. Chem. Chem. Phys.* **2021**, 23 (41), 23796 – 23807.

mój wkład polegał na wykonaniu pomiarów napięcia powierzchniowego, entropii powierzchniowej oraz molowej entropii powierzchniowej i ich analizie, dyskusji otrzymanych wyników oraz współtworzeniu manuskryptu;

P2. N. Soszka, B. Hachuła, M. Tarnacka, J. Grelska, K. Jurkiewicz, M. Geppert – Rybczyńska, R. Wrzałik, K. Grzybowska, S. Pawlus, M. Paluch, K. Kamiński, **Aromaticity Effect on Supramolecular Aggregation. Aromatic vs. Cyclic Monohydroxy Alcohols.** *Spectrochim. Acta – Part A Mol. Biomol. Spectrosc.* **2022**, 276, 121235.

mój wkład polegał na pomiarów napięcia powierzchniowego, entropii powierzchniowej oraz molowej entropii powierzchniowej i ich analizie, dyskusji otrzymanych wyników oraz współtworzeniu manuskryptu;

P3. N. Soszka, M. Tarnacka, B. Hachuła, M. Geppert – Rybczyńska, K. Prusik, K. Kamiński, **The Impact of Interface Modification on the Behavior of Phenyl Alcohols within Silica Templates.** *J. Phys. Chem. C*, **2024**, (doi: 10.1021/acs.jpcc.3c08084)

mój wkład polegał na wykonaniu pomiarów kątów zwilżania.



Chorzów, 10.04.2024

dr hab. Roman Wrzalik, prof. UŚ
Instytut Fizyki im. Augusta Chełkowskiego
Wydział Nauk Ścisłych i Technicznych
Uniwersytet Śląski w Katowicach
ul. 75 Pułku Piechoty 1
41-500 Chorzów

OŚWIADCZENIE

Oświadczam, że w pracy:

P1. N. Soszka, B. Hachuła, M. Tarnacka, E. Kamińska, J. Grelska, K. Jurkiewicz, M. Geppert-Rybczyńska, R. Wrzalik, K. Grzybowska, S. Pawlus, M. Paluch, K. Kamiński,
The Impact of the Length of Alkyl Chain on the Behavior of Benzyl Alcohol Homologues – the Interplay between Dispersive and Hydrogen Bond Interactions.
Phys. Chem. Chem. Phys. **2021**, 23 (41), 23796 – 23807.

mój udział polegał na wykonaniu części pomiarów IR, przeprowadzenie obliczeń DFT oraz dyskusji wyników;

P2. N. Soszka, B. Hachuła, M. Tarnacka, J. Grelska, K. Jurkiewicz, M. Geppert – Rybczyńska, R. Wrzalik, K. Grzybowska, S. Pawlus, M. Paluch, K. Kamiński,
Aromaticity Effect on Supramolecular Aggregation. Aromatic vs. Cyclic Monohydroxy Alcohols. *Spectrochim. Acta – Part A Mol. Biomol. Spectrosc.* **2022**, 276, 121235.

mój udział polegał na wykonaniu części pomiarów IR oraz dyskusji wyników;

P3. N. Soszka, M. Tarnacka, B. Hachuła, P. Włodarczyk, R. Wrzalik, M. Hreczka, M. Paluch, K. Kamiński, The Existence of Strongly Bonded Layer in Associating Liquids within Silica Pores – the Spectral and Molecular Dynamics Study. *Nanoscale*, **2024**, 16, 6636-6647

mój udział polegał na wykonaniu części pomiarów IR.



Chorzów, 10.04.2024

Prof. dr hab. Sebastian Pawlus
Instytut Fizyki im. Augusta Chelkowskiego
Wydział Nauk Ścisłych i Technicznych
Uniwersytet Śląski w Katowicach
ul. 75 Pułku Piechoty 1
41-500 Chorzów

OŚWIADCZENIE

Oświadczam, że w pracy:

P1. N. Soszka, B. Hachuła, M. Tarnacka, E. Kamińska, J. Grelska, K. Jurkiewicz, M. Geppert-Rybczyńska, R. Wrzalik, K. Grzybowska, S. Pawlus, M. Paluch, K. Kamiński,
The Impact of the Length of Alkyl Chain on the Behavior of Benzyl Alcohol Homologues – the Interplay between Dispersive and Hydrogen Bond Interactions.
Phys. Chem. Chem. Phys. **2021**, 23 (41), 23796 – 23807.

mój udział polegał na dyskusji wyników, korekcji manuskryptu oraz finansowaniu badań w ramach projektu NCN OPUS;

P2. N. Soszka, B. Hachuła, M. Tarnacka, J. Grelska, K. Jurkiewicz, M. Geppert – Rybczyńska, R. Wrzalik, K. Grzybowska, S. Pawlus, M. Paluch, K. Kamiński,
Aromaticity Effect on Supramolecular Aggregation. Aromatic vs. Cyclic Monohydroxy Alcohols. *Spectrochim. Acta – Part A Mol. Biomol. Spectrosc.* **2022**, 276, 121235.

Mój udział polegał na dyskusji wyników, korekcji manuskryptu oraz finansowaniu badań w ramach projektu NCN OPUS.



Chorzów, 10.04.2024

dr inż. Karolina Jurkiewicz
Instytut Fizyki im. Augusta Chełkowskiego
Wydział Nauk Ścisłych i Technicznych
Uniwersytet Śląski w Katowicach
ul. 75 Pułku Piechoty 1
41-500 Chorzów

OŚWIADCZENIE

Oświadczam, że w pracy:

P1. N. Soszka, B. Hachuła, M. Tarnacka, E. Kamińska, J. Grelska, K. Jurkiewicz, M. Geppert-Rybczyńska, R. Wrzałik, K. Grzybowska, S. Pawlus, M. Paluch, K. Kamiński,
The Impact of the Length of Alkyl Chain on the Behavior of Benzyl Alcohol Homologues – the Interplay between Dispersive and Hydrogen Bond Interactions.
Phys. Chem. Chem. Phys. **2021**, 23 (41), 23796 – 23807.

mój udział polegał na wykonaniu badań dyfrakcyjnych i ich analizie, dyskusji otrzymanych wyników oraz współtworzeniu manuskryptu;

P2. N. Soszka, B. Hachuła, M. Tarnacka, J. Grelska, K. Jurkiewicz, M. Geppert –
Rybczyńska, R. Wrzałik, K. Grzybowska, S. Pawlus, M. Paluch, K. Kamiński,
Aromaticity Effect on Supramolecular Aggregation. Aromatic vs. Cyclic Monohydroxy Alcohols. *Spectrochim. Acta – Part A Mol. Biomol. Spectrosc.* **2022**, 276, 121235.

mój udział polegał na wykonaniu badań dyfrakcyjnych i ich analizie, dyskusji otrzymanych wyników oraz współtworzeniu manuskryptu.

Jurkiewicz

Chorzów, 10.04.2024

mgr Joanna Grelska
Instytut Fizyki im. Augusta Chełkowskiego
Wydział Nauk Ścisłych i Technicznych
Uniwersytet Śląski w Katowicach
ul. 75 Pułku Piechoty 1
41-500 Chorzów

OŚWIADCZENIE

Oświadczam, że w pracy:

P1. N. Soszka, B. Hachuła, M. Tarnacka, E. Kamińska, J. Grelska, K. Jurkiewicz, M. Geppert-Rybczyńska, R. Wrzalik, K. Grzybowska, S. Pawlus, M. Paluch, K. Kamiński,
The Impact of the Length of Alkyl Chain on the Behavior of Benzyl Alcohol Homologues – the Interplay between Dispersive and Hydrogen Bond Interactions.
Phys. Chem. Chem. Phys. **2021**, 23 (41), 23796 – 23807.

mój udział polegał na wykonaniu badań dyfrakcyjnych i ich analizie, dyskusji otrzymanych wyników oraz współtworzeniu manuskryptu;

P2. N. Soszka, B. Hachuła, M. Tarnacka, J. Grelska, K. Jurkiewicz, M. Geppert – Rybczyńska, R. Wrzalik, K. Grzybowska, S. Pawlus, M. Paluch, K. Kamiński,
Aromaticity Effect on Supramolecular Aggregation. Aromatic vs. Cyclic Monohydroxy Alcohols. *Spectrochim. Acta – Part A Mol. Biomol. Spectrosc.* **2022**, 276, 121235.

mój udział polegał na wykonaniu badań dyfrakcyjnych i ich analizie, dyskusji otrzymanych wyników oraz współtworzeniu manuskryptu.



Chorzów, 10.04.2024

dr Katarzyna Grzybowska, prof. UŚ
Instytut Fizyki im. Augusta Chełkowskiego
Wydział Nauk Ścisłych i Technicznych
Uniwersytet Śląski w Katowicach
ul. 75 Pułku Piechoty 1
41-500 Chorzów

OŚWIADCZENIE

Oświadczam, że w pracy:

P1. N. Soszka, B. Hachuła, M. Tarnacka, E. Kamińska, J. Grelska, K. Jurkiewicz, M. Geppert-Rybczyńska, R. Wrzalik, K. Grzybowska, S. Pawlus, M. Paluch, K. Kamiński,
The Impact of the Length of Alkyl Chain on the Behavior of Benzyl Alcohol Homologues – the Interplay between Dispersive and Hydrogen Bond Interactions.
Phys. Chem. Chem. Phys. **2021**, 23 (41), 23796 – 23807.

mój udział polegał na wykonaniu pomiarów współczynnika załamania światła oraz dyskusji otrzymanych wyników;

P2. N. Soszka, B. Hachuła, M. Tarnacka, J. Grelska, K. Jurkiewicz, M. Geppert – Rybczyńska, R. Wrzalik, K. Grzybowska, S. Pawlus, M. Paluch, K. Kamiński,
Aromaticity Effect on Supramolecular Aggregation. Aromatic vs. Cyclic Monohydroxy Alcohols. *Spectrochim. Acta – Part A Mol. Biomol. Spectrosc.* **2022**, 276, 121235.

mój udział polegał na wykonaniu pomiarów współczynnika załamania światła oraz dyskusji otrzymanych wyników.

Katarzyna Grzybowska

Chorzów, 10.04.2024

dr hab. Ewa Ozimina-Kamińska, prof. SUM
Katedra i Zakład Farmakognozji i Fitochemii
Wydział Nauk Farmaceutycznych w Sosnowcu
Śląskiego Uniwersytetu Medycznego w Katowicach
ul. Jagiellońska 4
41-200 Sosnowiec

OŚWIADCZENIE

Oświadczam, że w pracy:

N. Soszka, B. Hachula, M. Tarnacka, E. Kamińska, J. Grelska, K. Jurkiewicz, M. Geppert-Rybczyńska, R. Wrzalik, K. Grzybowska, S. Pawlus, M. Paluch, K. Kamiński,
The Impact of the Length of Alkyl Chain on the Behavior of Benzyl Alcohol Homologues – the Interplay between Dispersive and Hydrogen Bond Interactions.
Phys. Chem. Chem. Phys. **2021**, 23 (41), 23796 – 23807.

mój wkład polegał na wykonaniu badań dielektrycznych oraz dyskusji otrzymanych wyników.

Ewa Ozimina-Kamińska

Chorzów, 10.04.2024

Prof. dr hab. Marian Paluch
Instytut Fizyki im. Augusta Chełkowskiego
Wydział Nauk Ścisłych i Technicznych
Uniwersytet Śląski w Katowicach
ul. 75 Pułku Piechoty 1
41-500 Chorzów

OŚWIADCZENIE

Oświadczam, że w pracy:

P1. N. Soszka, B. Hachuła, M. Tarnacka, E. Kamińska, J. Grelska, K. Jurkiewicz, M. Geppert-Rybczyńska, R. Wrzalik, K. Grzybowska, S. Pawlus, M. Paluch, K. Kamiński, **The Impact of the Length of Alkyl Chain on the Behavior of Benzyl Alcohol Homologues – the Interplay between Dispersive and Hydrogen Bond Interactions.** *Phys. Chem. Chem. Phys.* **2021**, 23 (41), 23796 – 23807.

mój udział polegał na udziale w dyskusji wyników;

P2. N. Soszka, B. Hachuła, M. Tarnacka, J. Grelska, K. Jurkiewicz, M. Geppert – Rybczyńska, R. Wrzalik, K. Grzybowska, S. Pawlus, M. Paluch, K. Kamiński, **Aromaticity Effect on Supramolecular Aggregation. Aromatic vs. Cyclic Monohydroxy Alcohols.** *Spectrochim. Acta – Part A Mol. Biomol. Spectrosc.* **2022**, 276, 121235.

mój udział polegał na udziale w dyskusji wyników;

P3. N. Soszka, M. Tarnacka, B. Hachuła, P. Włodarczyk, R. Wrzalik, M. Hreczka, M. Paluch, K. Kamiński, **The Existence of Strongly Bonded Layer in Associating Liquids within Silica Pores – the Spectral and Molecular Dynamics Study.** *Nanoscale*, **2024**, 16, 6636-6647

mój udział polegał na udziale w dyskusji wyników.



Chorzów, 10.04.2024

dr Krystian Prusik
Instytut Inżynierii Materiałowej
Wydział Nauk Ścisłych i Technicznych
Uniwersytet Śląski w Katowicach
ul. 75 Pułku Piechoty 1A
41-500 Chorzów

OŚWIADCZENIE

Oświadczam, że w pracy:

P1.N. Soszka, M. Tarnacka, B. Hachuła, M. Geppert – Rybczyńska, K. Prusik, K. Kamiński, **The Impact of Interface Modification on the Behavior of Phenyl Alcohols within Silica Templates.** *J. Phys. Chem. C*, 2024 (doi: 10.1021/acs.jpcc.3c08084)

mój wkład polegał na wykonaniu badań mikroskopowych i analizie otrzymanych wyników.



Chorzów, 10.04.2024

dr Patryk Włodarczyk
Instytut Metali Nieżelaznych
Sieć Badawcza Łukasiewicz
ul. Sowińskiego 5
44-100 Gliwice

OŚWIADCZENIE

Oświadczam, że w pracy:

N. Soszka, M. Tarnacka, B. Hachuła, P. Włodarczyk, R. Wrzałik, M. Hreczka, M. Paluch,
K. Kamiński, The Existence of Strongly Bonded Layer in Associating Liquids within Silica
Pores – the Spectral and Molecular Dynamics Study. *Nanoscale*, **2024**, 16, 6636-6647

Mój wkład polegał na wykonaniu symulacji dynamiki molekularnej i analizie wyników oraz
współtworzeniu manuskryptu.

P. Włodarczyk

Chorzów, 10.04.2024

mgr Marek Hreczka
Instytut Metali Nieżelaznych
Sieć Badawcza Łukasiewicz
ul. Sowińskiego 5
44-100 Gliwice

Katedra Mechatroniki
Wydział Elektryczny
Politechnika Śląska
ul. Akademicka 10A
44-100 Gliwice

OŚWIADCZENIE

Oświadczam, że w pracy:

N. Soszka, M. Tarnacka, B. Hachuła, P. Włodarczyk, R. Wrzalik, M. Hreczka, M. Pałuch, K. Kamiński, The Existence of Strongly Bonded Layer in Associating Liquids within Silica Pores – the Spectral and Molecular Dynamics Study. *Nanoscale*, **2024**, 16, 6636-6647

Mój wkład polegał na wykonaniu symulacji dynamiki molekularnej i analizie wyników.



5. BIBLIOGRAFIA

- [1] L. Sobczyk, Wiązanie wodorowe - wybrane zagadnienia, *Wiadomości Chem.* 55 (2001) 596–611.
- [2] B. Hachuła, Efekty spektralne dynamicznych oddziaływań kooperatywnych w układach wiązań wodorowych w oparciu o spolaryzowane widma w podczerwieni modelowych kryształów molekularnych. Praca doktorska, (2009).
- [3] Y. Marechal, *The Hydrogen Bond and the Water Molecule*, 2007. <https://doi.org/10.1016/B978-0-444-51957-3.X5000-8>.
- [4] G. Desiraju, T. Steiner, *The Weak Hydrogen Bond*, 2010. <https://doi.org/10.1093/acprof:oso/9780198509707.001.0001>.
- [5] W. Dannhauser, Dielectric study of intermolecular association in isomeric octyl alcohols, *J. Chem. Phys.* 48 (1968) 1911–1917. <https://doi.org/10.1063/1.1668989>.
- [6] T. Böhmer, J.P. Gabriel, T. Richter, F. Pabst, T. Blochowicz, Influence of Molecular Architecture on the Dynamics of H-Bonded Supramolecular Structures in Phenyl-Propanols, *J. Phys. Chem. B.* 123 (2019) 10959–10966. <https://doi.org/10.1021/acs.jpcc.9b07768>.
- [7] M. Wikarek, S. Pawlus, S.N. Tripathy, A. Szulc, M. Paluch, How Different Molecular Architectures Influence the Dynamics of H-Bonded Structures in Glass-Forming Monohydroxy Alcohols, *J. Phys. Chem. B.* 120 (2016) 5744–5752. <https://doi.org/10.1021/acs.jpcc.6b01458>.
- [8] J. Grelska, K. Jurkiewicz, A. Burian, S. Pawlus, Supramolecular Structure of Phenyl Derivatives of Butanol Isomers, *J. Phys. Chem. B.* (2022) 3563–3571. <https://doi.org/10.1021/acs.jpcc.2c01269>.
- [9] A. Kudlik, C. Tschirwitz, S. Benkhof, T. Blochowicz, E. Rössler, Slow secondary relaxation process in supercooled liquids, *Europhys. Lett.* 40 (1997) 649–654. <https://doi.org/10.1209/epl/i1997-00518-y>
- [10] S. Bauer, K. Burlafinger, C. Gainaru, P. Lunkenheimer, W. Hiller, A. Loidl, R. Böhmer, Debye relaxation and 250 K anomaly in glass forming monohydroxy alcohols, *J. Chem. Phys.* 138 (2013) 094505. <https://doi.org/10.1063/1.4793469>.
- [11] Y. Gao, W. Tu, Z. Chen, Y. Tian, R. Liu, L.M. Wang, Dielectric relaxation of long-chain glass-forming monohydroxy alcohols, *J. Chem. Phys.* 139 (2013) 164504. <https://doi.org/10.1063/1.4825398>.
- [12] B. Hachuła, E. Kamińska, K. Koperwas, R. Wrzalik, K. Jurkiewicz, M. Tarnacka, D. Scelta, S. Fanetti, S. Pawlus, M. Paluch, K. Kamiński, A study of O-H...O hydrogen bonds along various isolines in 2-ethyl-1-hexanol. Temperature or pressure - which parameter controls their behavior?, *Spectrochim. Acta - Part A Mol. Biomol. Spectrosc.* 283 (2022) 121726. <https://doi.org/10.1016/j.saa.2022.121726>.
- [13] C.P. Johari, W. Dannhauser, Dielectric study of the pressure dependence of intermolecular association in isomeric octyl alcohols, *J. Chem. Phys.* 48 (1968) 5114–5122. <https://doi.org/10.1063/1.1668182>.
- [14] D. Fragiadakis, C.M. Roland, R. Casalini, Insights on the origin of the Debye process in monoalcohols from dielectric spectroscopy under extreme pressure conditions, *J. Chem. Phys.* 132 (2010) 144505. <https://doi.org/10.1063/1.3374820>.

- [15] S. Pawlus, M. Wikarek, C. Gainaru, M. Paluch, R. Böhmer, How do high pressures change the Debye process of 4-methyl-3-heptanol?, *J. Chem. Phys.* 139 (2013) 064501. <https://doi.org/10.1063/1.4816364>.
- [16] C. Gainaru, M. Wikarek, S. Pawlus, M. Paluch, R. Figuli, M. Wilhelm, T. Hecksher, B. Jakobsen, J.C. Dyre, R. Böhmer, Oscillatory shear and high-pressure dielectric study of 5-methyl-3-heptanol, *Colloid Polym. Sci.* 292 (2014) 1913–1921. <https://doi.org/10.1007/s00396-014-3274-0>.
- [17] C. Brot, Open and cyclic multimers in alcohol solutions. A quantitative model for the association and the permittivity, *J. Mol. Struct.* 250 (1991) 253–257. [https://doi.org/10.1016/0022-2860\(91\)85032-X](https://doi.org/10.1016/0022-2860(91)85032-X).
- [18] H. Nadolny, A. Volmari, H. Weingärtner, Orientational Dynamics of Hydrogen-Bonded Liquids- A Comparative Study of Dielectric and Nuclear Magnetic Relaxation in n-Butanol-Tetrachloromethane Mixtures, *Berichte Der Bunsengesellschaft/Physical Chem. Chem. Phys.* 102 (1998) 866–871. <https://doi.org/10.1002/bbpc.19981020612>.
- [19] O.E. Kalinovskaya, J.K. Vij, G.P. Johari, Mechanism of the major orientation polarization in alcohols, and the effects of steric hindrance-, and dilution-induced decrease on H-bonding, *J. Phys. Chem. A.* 105 (2001) 5061–5070. <https://doi.org/10.1021/jp0040695>.
- [20] M. Kwaśniewicz, M.A. Czarnecki, The Effect of Chain Length on Mid-Infrared and Near-Infrared Spectra of Aliphatic 1-Alcohols, *Appl. Spectrosc.* 72 (2018) 288–296. <https://doi.org/10.1177/0003702817732253>.
- [21] M.A. Czarnecki, Study on self-association of octanols by two-dimensional FT-NIR correlation spectroscopy, *Vib. Spectrosc.* 36 (2004) 237–239. <https://doi.org/10.1016/j.vibspec.2003.11.017>.
- [22] F. Palombo, P. Sassi, M. Paolantoni, A. Morresi, R.S. Cataliotti, Comparison of hydrogen bonding in 1-octanol and 2-octanol as probed by spectroscopic techniques, *J. Phys. Chem. B.* 110 (2006) 18017–18025. <https://doi.org/10.1021/jp062614h>.
- [23] P. Sassi, F. Palombo, R.S. Cataliotti, M. Paolantoni, A. Morresi, Distributions of H-bonding aggregates in tert-butyl alcohol: The pure liquid and its alkane mixtures, *J. Phys. Chem. A.* 111 (2007) 6020–6027. <https://doi.org/10.1021/jp071609q>.
- [24] P. Sillrén, A. Matic, M. Karlsson, M. Koza, M. MacCarini, P. Fouquet, M. Götz, T. Bauer, R. Gulich, P. Lunkenheimer, A. Loidl, J. Mattsson, C. Gainaru, E. Vynokur, S. Schildmann, S. Bauer, R. Böhmer, Liquid 1-propanol studied by neutron scattering, near-infrared, and dielectric spectroscopy, *J. Chem. Phys.* 140 (2014) 124501. <https://doi.org/10.1063/1.4868556>.
- [25] M. Iwahashi, M. Suzuki, N. Katayama, H. Matsuzawa, M.A. Czarnecki, Y. Ozaki, A. Wakisaka, Molecular self-assembling of butan-1-ol, butan-2-ol, and 2-methylpropan-2-ol in carbon tetrachloride solutions as observed by near-infrared spectroscopic measurements, *Appl. Spectrosc.* 54 (2000) 268–276. <https://doi.org/10.1366/0003702001949203>.
- [26] A.I. Brodskii, V.D. Pokhodenko, V.S. Kuts, Investigation of the association of alcohols and phenols by the NMR method, *Russ. Chem. Rev.* 39 (1970) 347.
- [27] K. Łucak, A.Z. Szeremeta, R. Wrzalik, J. Grelska, K. Jurkiewicz, N. Soszka, B. Hachuła, D. Kramarczyk, K. Grzybowska, B. Yao, K. Kamiński, S. Pawlus, Experimental and Computational Approach to Studying Supramolecular Structures in Propanol and Its Halogen Derivatives, *J. Phys. Chem. B.* 127 (2023) 9102–9110. <https://doi.org/10.1021/acs.jpcc.3c02092>.
- [28] P.W. Atkins, *Chemia fizyczna*, Wydawnictwo Naukowe PWN, Warszawa, 2012, n.d.

- [29] K. Pigoń, Z. Ruziewicz, *Chemia fizyczna*, tom II, (2005) 724.
- [30] M.E. Flores, T. Shibue, N. Sugimura, H. Nishide, F. Martínez, A.F. Olea, I. Moreno-Villoslada, N-Hexanol association in cyclohexane studied by NMR and NIR spectroscopies, *J. Mol. Liq.* 199 (2014) 301–308. <https://doi.org/10.1016/j.molliq.2014.09.012>.
- [31] T.K. Manojkumar, D. Kim, K.S. Kim, Theoretical studies on hydroquinone-benzene clusters, *J. Chem. Phys.* 122 (2005) 014305. <https://doi.org/10.1063/1.1824893>.
- [32] N.A. Seifert, A.S. Hazrah, W. Jäger, The 1-Naphthol Dimer and Its Surprising Preference for π - π Stacking over Hydrogen Bonding, *J. Phys. Chem. Lett.* 10 (2019) 2836–2841. <https://doi.org/10.1021/acs.jpcllett.9b00646>.
- [33] G.P. Johari, O.E. Kalinovskaya, J.K. Vij, Effects of induced steric hindrance on the dielectric behavior and H bonding in the supercooled liquid and vitreous alcohol, *J. Chem. Phys.* 114 (2001) 4634–4642. <https://doi.org/10.1063/1.1346635>.
- [34] A. Nowok, M. Dulski, J. Grelska, A.Z. Szeremeta, K. Jurkiewicz, K. Grzybowska, M. Musiał, S. Pawlus, Phenyl Ring: A Steric Hindrance or a Source of Different Hydrogen Bonding Patterns in Self-Organizing Systems?, *J. Phys. Chem. Lett.* 12 (2021) 2142–2147. <https://doi.org/10.1021/acs.jpcllett.1c00186>.
- [35] B. Hachuła, J. Grelska, N. Soszka, K. Jurkiewicz, A. Nowok, A.Z. Szeremeta, S. Pawlus, M. Paluch, K. Kamiński, Systematic studies on the dynamics, intermolecular interactions and local structure in the alkyl and phenyl substituted butanol isomers, *J. Mol. Liq.* (2021) 117098. <https://doi.org/10.1016/j.molliq.2021.117098>.
- [36] K. Jurkiewicz, S. Kołodziej, B. Hachuła, K. Grzybowska, M. Musiał, J. Grelska, R. Bielas, A. Talik, S. Pawlus, K. Kamiński, M. Paluch, Interplay between structural static and dynamical parameters as a key factor to understand peculiar behaviour of associated liquids, *J. Mol. Liq.* 319 (2020) 114084. <https://doi.org/10.1016/j.molliq.2020.114084>.
- [37] M. Beiner, G.T. Rengarajan, S. Pankaj, D. Enke, M. Steinhart, Manipulating the crystalline state of pharmaceuticals by nanoconfinement, *Nano Lett.* 7 (2007) 1381–1385. <https://doi.org/10.1021/nl0705081>.
- [38] M.T. Chevalier, J. Gonzalez, V. Alvarez, Biodegradable polymeric microparticles as drug delivery devices, *IFMBE Proc.* 49 (2015) 187–190. https://doi.org/10.1007/978-3-319-13117-7_49.
- [39] Y. Wang, F. Li, J. Xin, J. Xu, G. Yu, Q. Shi, Mesoporous Drug Delivery System: From Physical Properties of Drug in Solid State to Controlled Release, *Molecules.* 28 (2023) 3406. <https://doi.org/10.3390/molecules28083406>.
- [40] J. Ko, R. Berger, H. Lee, H. Yoon, J. Cho, K. Char, Electronic effects of nano-confinement in functional organic and inorganic materials for optoelectronics, *Chem. Soc. Rev.* 50 (2021) 3585–3628. <https://doi.org/10.1039/d0cs01501f>.
- [41] Y. Li, X. Yue, G. Huang, M. Wang, Q. Zhang, C. Wang, H. Yi, S. Wang, Li⁺ Selectivity of Carboxylate Graphene Nanopores Inspired by Electric Field and Nanoconfinement, *Small.* 17 (2021) 1–9. <https://doi.org/10.1002/sml.202006704>.
- [42] A.R. Brás, M. Dionísio, A. Schönhals, Confinement and surface effects on the molecular dynamics of a nematic mixture investigated by dielectric relaxation spectroscopy, *J. Phys. Chem. B.* 112 (2008) 8227–8235. <https://doi.org/10.1021/jp802133e>.
- [43] C. Gainaru, S. Schildmann, R. Böhmer, Surface and confinement effects on the dielectric

- relaxation of a monohydroxy alcohol, *J. Chem. Phys.* 135 (2011) 174510. <https://doi.org/10.1063/1.3655356>.
- [44] F. He, L.M. Wang, R. Richert, Dynamics of supercooled liquids in the vicinity of soft and hard interfaces, *Phys. Rev. B - Condens. Matter Mater. Phys.* 71 (2005) 1–10. <https://doi.org/10.1103/PhysRevB.71.144205>.
- [45] R. Richert, M. Yang, Surface induced glass transition in a confined molecular liquid, *J. Phys. Chem. B.* 107 (2003) 895–898. <https://doi.org/10.1021/jp022039r>.
- [46] A. Talik, M. Tarnacka, M. Wojtyniak, E. Kaminska, K. Kaminski, M. Paluch, The influence of the nanocurvature on the surface interactions and molecular dynamics of model liquid confined in cylindrical pores, *J. Mol. Liq.* 298 (2020) 111973. <https://doi.org/10.1016/j.molliq.2019.111973>.
- [47] S. Alexandris, P. Papadopoulos, G. Sakellariou, M. Steinhart, H.J. Butt, G. Floudas, Interfacial energy and glass temperature of polymers confined to nanoporous alumina, *Macromolecules.* 49 (2016) 7400–7414. <https://doi.org/10.1021/acs.macromol.6b01484>.
- [48] R. Winkler, W. Tu, M. Dulski, L. Laskowski, K. Adrjanowicz, Effect of the Surface Polarity, through Employing Nonpolar Spacer Groups, on the Glass-Transition Dynamics of Poly(phenyl methylsiloxane) Confined in Alumina Nanopores, *Macromolecules.* 54 (2021) 10951–10968. <https://doi.org/10.1021/acs.macromol.1c02145>.
- [49] H. Wang, K.L. Kearns, A. Zhang, A.A. Shamsabadi, Y. Jin, A. Bond, S.M. Hurney, C. Morillo, Z. Fakhraai, Effect of nanopore geometry in the conformation and vibrational dynamics of a highly confined molecular glass, *Nano Lett.* 21 (2021) 1778–1784. <https://doi.org/10.1021/acs.nanolett.0c04744>.
- [50] W.K. Kipnusu, M.M. Elmahdy, M. Elsayed, R. Krause-Rehberg, F. Kremer, Counterbalance between Surface and Confinement Effects As Studied for Amino-Terminated Poly(propylene glycol) Constraint in Silica Nanopores, *Macromolecules.* 52 (2019) 1864–1873. <https://doi.org/10.1021/acs.macromol.8b02687>.
- [51] W.K. Kipnusu, M. Elsayed, R. Krause-Rehberg, F. Kremer, Glassy dynamics of polymethylphenylsiloxane in one- and two-dimensional nanometric confinement - A comparison, *J. Chem. Phys.* 146 (2017) 203302. <https://doi.org/10.1063/1.4974767>.
- [52] J.Y. Park, G.B. McKenna, Size and confinement effects on the glass transition behavior of polystyrene/o-terphenyl polymer solutions, *Phys. Rev. B - Condens. Matter Mater. Phys.* 61 (2000) 6667–6676. <https://doi.org/10.1103/PhysRevB.61.6667>.
- [53] C.J. Ellison, R.L. Ruszkowski, N.J. Fredin, J.M. Torkelson, Dramatic reduction of the effect of nanoconfinement on the glass transition of polymer films via addition of small-molecule diluent, *Phys. Rev. Lett.* 92 (2004) 1–4. <https://doi.org/10.1103/PhysRevLett.92.095702>.
- [54] V.M. Boucher, D. Cangialosi, H. Yin, A. Schönhals, A. Alegría, J. Colmenero, Tg depression and invariant segmental dynamics in polystyrene thin films, *Soft Matter.* 8 (2012) 5119–5122. <https://doi.org/10.1039/c2sm25419k>.
- [55] A. Serghei, H. Huth, C. Schick, F. Kremer, Glassy dynamics in thin polymer layers having a free upper interface, *Macromolecules.* 41 (2008) 3636–3639. <https://doi.org/10.1021/ma702381t>.
- [56] D. Labahn, R. Mix, A. Schönhals, Dielectric relaxation of ultrathin films of supported polysulfone, *Phys. Rev. E - Stat. Nonlinear, Soft Matter Phys.* 79 (2009) 1–9. <https://doi.org/10.1103/PhysRevE.79.011801>.

- [57] H. Yin, S. Napolitano, A. Schönhals, Molecular mobility and glass transition of thin films of poly(bisphenol A carbonate), *Macromolecules*. 45 (2012) 1652–1662. <https://doi.org/10.1021/ma202127p>.
- [58] J.L. Keddie, R.A.L. Jones, R.A. Cory, Temperature in Thin Polymer Films, *Faraday Discuss.* (1994) 219–230.
- [59] C.J. Ellison, J.M. Torkelson, The distribution of glass-transition temperatures in nanoscopically confined glass formers, *Nat. Mater.* 2 (2003) 695–700. <https://doi.org/10.1038/nmat980>.
- [60] C. Yang, R. Onitsuka, I. Takahashi, Confinement effects on glass transition temperature, transition breadth, and linear expansivity: An ultraslow X-ray reflectivity study on supported ultrathin polystyrene films, *Eur. Phys. J. E.* 36 (2013) 1–8. <https://doi.org/10.1140/epje/i2013-13066-3>.
- [61] G.H. Findenegg, S. Jähnert, D. Akcakayiran, A. Schreiber, Freezing and melting of water confined in silica nanopores, *ChemPhysChem*. 9 (2008) 2651–2659. <https://doi.org/10.1002/cphc.200800616>.
- [62] P. Bampoulis, K. Sotthewes, E. Dollekamp, B. Poelsema, Water confined in two-dimensions: Fundamentals and applications, *Surf. Sci. Rep.* 73 (2018) 233–264. <https://doi.org/10.1016/j.surfrep.2018.09.001>.
- [63] A. Tinti, G. Camisasca, A. Giacomello, Structure and dynamics of water confined in cylindrical nanopores with varying hydrophobicity, *Philos. Trans. R. Soc. A Math. Phys. Eng. Sci.* 379 (2021). <https://doi.org/10.1098/rsta.2020.0403>.
- [64] D. Morineau, C. Alba-Simionesco, Does Molecular Self-Association Survive in Nanochannels?, *J. Phys. Chem. Lett.* 1 (2010) 1155–1159. <https://doi.org/10.1021/jz100132d>.
- [65] A. Ghoufi, I. Hureau, R. Lefort, D. Morineau, Hydrogen-bond-induced supermolecular assemblies in a nanoconfined tertiary alcohol, *J. Phys. Chem. C*. 115 (2011) 17761–17767. <https://doi.org/10.1021/jp205943p>.
- [66] A. Ghoufi, I. Hureau, D. Morineau, R. Renou, A. Szymczyk, Confinement of tert -Butanol Nanoclusters in Hydrophilic and Hydrophobic Silica Nanopores, *J. Phys. Chem. C*. 117 (2013) 15203–15212. <https://doi.org/10.1021/jp404702j>.
- [67] W.K. Kipnusu, M. Elsayed, W. Kossack, S. Pawlus, K. Adrjanowicz, M. Tress, E.U. Mapesa, R. Krause-Rehberg, K. Kaminski, F. Kremer, Confinement for More Space: A Larger Free Volume and Enhanced Glassy Dynamics of 2-Ethyl-1-hexanol in Nanopores, *J. Phys. Chem. Lett.* 6 (2015) 3708–3712. <https://doi.org/10.1021/acs.jpcllett.5b01533>.
- [68] A. Ananiadou, G. Papamokos, M. Steinhart, G. Floudas, Effect of confinement on the dynamics of 1-propanol and other monohydroxy alcohols, *J. Chem. Phys.* 155 (2021) 184504. <https://doi.org/10.1063/5.0063967>.
- [69] A. Górny, M. Tarnacka, S. Zimny, M. Geppert-Rybczyńska, A. Brzózka, G.D. Sulka, M. Paluch, K. Kamiński, Impact of Nanostructurization of the Pore Walls on the Dynamics of a Series of Phenyl Alcohols Incorporated within Nanoporous Aluminum Oxide Templates, *J. Phys. Chem. C*. 126 (2022) 18475–18489. <https://doi.org/10.1021/acs.jpcc.2c05446>.
- [70] M. Požar, J. Bolle, C. Sternemann, A. Perera, On the X-ray Scattering Pre-peak of Linear Monomers and the Related Microstructure from Computer Simulations, *J. Phys. Chem. B*. 124 (2020) 8358–8371. <https://doi.org/10.1021/acs.jpcc.0c05932>.
- [71] A. Ghoufi, Molecular origin of the prepeak in the structure factor of alcohols, *J. Phys. Chem. B*.

- 124 (2020) 11501–11509. <https://doi.org/10.1021/acs.jpcc.0c09302>.
- [72] N. Soszka, B. Hachuła, M. Tarnacka, E. Kaminska, S. Pawlus, K. Kaminski, M. Paluch, Is a Dissociation Process Underlying the Molecular Origin of the Debye Process in Monohydroxy Alcohols?, *J. Phys. Chem. B.* 125 (2021) 2960–2967. <https://doi.org/10.1021/acs.jpcc.0c10970>.
- [73] G. Williams, D.C. Watts, Non-symmetrical dielectric relaxation behaviour arising from a simple empirical decay function, *Trans. Faraday Soc.* 66 (1970) 80–85. <https://doi.org/10.1039/TF9706600080>.
- [74] R. Kohlrausch, Ueber das Dellmann'sche Elektrometer, *Ann. Phys.* 148 (1847) 353–405.
- [75] J.G. Kirkwood, The dielectric polarization of polar liquids, *J. Chem. Phys.* 7 (1939) 911–919. <https://doi.org/10.1063/1.1750343>.
- [76] S. Napolitano, M. Wübbenhorst, The lifetime of the deviations from bulk behaviour in polymers confined at the nanoscale, *Nat. Commun.* 2 (2011) 260. <https://doi.org/10.1038/ncomms1259>.
- [77] S. Napolitano, V. Lupaşcu, M. Wübbenhorst, Temperature dependence of the deviations from bulk behavior in ultrathin polymer films, *Macromolecules.* 41 (2008) 1061–1063. <https://doi.org/10.1021/ma702081w>.
- [78] C. Rotella, S. Napolitano, S. Vandendriessche, V.K. Valev, T. Verbiest, M. Larkowska, S. Kucharski, M. Wübbenhorst, Adsorption kinetics of ultrathin polymer films in the melt probed by dielectric spectroscopy and second-harmonic generation, *Langmuir.* 27 (2011) 13533–13538. <https://doi.org/10.1021/la2027779>.
- [79] S. Napolitano, C. Rotella, M. Wübbenhorst, Can thickness and interfacial interactions univocally determine the behavior of polymers confined at the nanoscale?, *ACS Macro Lett.* 1 (2012) 1189–1193. <https://doi.org/10.1021/mz300432d>.